UNIVERSITY OF TRENTO

Doctoral School in Civil, Environmental and Mechanical Engineering

Curriculum 1. Civil and Environmental Engineering

Mattia Carlin

The response of river bar topography to the hydrological flow regime

2021 - Doctoral thesis

Alternate bars are large-scale bedforms often rising in straight channelized rivers due to an instability mechanism. From an engineering point of view, due to their topographic expression and migration properties, alternate bars represent a problem in river management to the extent that they affect navigation and increase the flooding risk. On the other hand, they are fundamental for river biodiversity, being a suitable habitat for aquatic fauna and riparian vegetation.
While a vast literature is available for describing the equilibrium properties of alternate bars under steady flow conditions, much less information is available about the evolution of alternate bars subject to a complex, real flow series.
The purpose of this work is to provide a model for predicting the long-term average properties of alternate bars and for identifying the "bar-forming" discharge, which is a representative discharge value that, if applied steadily, is able to reproduce the same average topography of the flow regime.
To do that, a theoretical approach has been implemented by combining a morphodynamic model, which takes into account the main properties of alternate bars, with the hydrological characteristics of the flow regime. The model has been applied to four study cases with different morphological behaviours, obtaining satisfactory results in terms of the model capability to reproduce field observations, both qualitatively and quantitatively.

Mattia Carlin studied at the University of Trento, Italy, where he had a Master Degree in Environmental Engineering in 2017 with a thesis about river morphodynamics and alternate bars. The interest in this fascinating subject led him to start a PhD experience, also stimulated by the period spent at the IRSTEA research institute in Lyon during the master, where he deepened the topic by investigating the evolution of alternate bars by means of satellite images.
During the PhD he had the opportunity to be involved in a project about the integrated approach of river management, by taking into account both the hydraulic safety and the ecological and morphological trajectories of river evolution.

UNIVERSITY OF TRENTO - Italy
Department of Civil, Environmental and Mechanical Engineering

Doctoral School in Civil, Environmental and Mechanical Engineering
Topic 1. Civil and Environmental Engineering - XXXIII cycle 2017/2020

Doctoral Thesis - July 2021

Mattia Carlin

The response of river bar topography to the hydrological flow regime

Supervisors
Marco Tubino, University of Trento
Marco Redolfi, University of Trento

Credits of the cover image: Mattia Carlin (Isère River, France)

Contents on this book are licensed under a Creative Common Attribution
Non Commercial - No Derivatives
4.0 International License, except for the parts already published by other publishers.

University of Trento
Doctoral School in Civil, Environmental and Mechanical Engineering
http://web.unitn.it/en/dricam
Via Mesiano 77, I-38123 Trento
Tel. +39 0461 282670 / 2611 - *dicamphd@unitn.it*

ABSTRACT

Alternate bars are large-scale bedforms characterised by an ordered sequence of scour zones and depositional diagonal fronts alternating along channel banks, which are typical of straight channelized rivers. Due to their high relief and migration properties, they represent a problem in river management, because they affect navigation, increase the flooding risk and interact with instream structures. For this reason, in the last decades many studies took the challenge of defining suitable criteria able to describe their morphometric properties.

Theoretical, experimental and numerical works have clearly demonstrated that bar occurrence is a threshold process governed by the width-to-depth ratio of the channel, β. If this parameter exceeds a critical threshold, β_{cr}, an instability mechanism amplifies the riverbed perturbations occurring due to the effect of the turbulent flow on the cohesionless riverbed, leading to the spontaneous growth of finite amplitude bars. Under steady flow conditions, alternate bars achieve an equilibrium configuration, whose amplitude value is related to the difference $\beta - \beta_{cr}$.

Much less information is available to describe bar characteristics under variable flow conditions, when the width-to-depth ratio changes in time and the amplitude of bars evolves depending on the duration and the shape of the hydrograph. The effect of a single idealized flood on bar amplitude evolution was successfully described by the weakly nonlinear model of Tubino (1991), which was able to capture the trajectory of bar amplitude during different stages of the flood. Supported by experimental results, he found that the response of bars crucially depends on the ratio between the flood duration and the bar-growth timescale. Nevertheless, the effect of a complex flow regime, characterised by a sequence of flow events, is to a large extent unexplored. Specifically, (i) the definition of a criterion to predict the average response of alternate bars in a river reach subject to an hydrological flow regime and (ii) the quantification of bar

amplitude evolution due to a complex flow regime are still to a large extent unexplored.

The goals of this work are: (i) to investigate the dependence of bar properties to variable discharge conditions; (ii) to analyse the effect of flow unsteadiness in terms of duration and sequencing of flood events and derive the main hydrological characteristics that primarily control the average response of bar amplitude; (iii) to determine the long-term bar geometry and define the "bar-forming" discharge, which is the theoretical discharge that if maintained indefinitely would produce the same long-term bar response as the natural hydrograph; (iv) to analyse the effect that a sequence of flood events composing a complex flow series has on the evolution of bar amplitude.

To pursue these purposes, we adopted a methodology primary based on theoretical models, then supported and validated through the analysis of laboratory experiments and field data. The methodology and the key results for the different parts of this thesis can be summarized as follows:

1. First, the response of bar topography to different flow stages has been investigated both theoretically and through the analysis of experimental data, observing the dependence of alternate bars to peculiar threshold conditions. The validity of weakly nonlinear model of Colombini et al. (1987), originally defined in the neighborhood of the critical condition β_{cr}, has been extended taking into account the emersion of bars for low flows.

2. Subsequently, the average response of bars to idealized flow series has been analysed, exploring their dependence on the duration and sequencing of flood events. The probability density function has been found to be the essential hydrological information of the flow series required to determine the long-term response of bar amplitude, while the integral scale of flow sequence is a suitable metric to quantify the unsteadiness of a flow regime.

3. Then, an innovative approach has been introduced to define an occurrence criterion for alternate bars in straightened river reaches that accounts for the hydrological regime, and

to determine the average bar state, with the corresponding "bar-forming" discharge. The key novelty with respect to the classical methods adopted so far to predict the long-term equilibrium channel geometry is that in this case the morphodynamical work acted on river bars by relatively low-flow stages enhancing their formation can be reversed by high-flow stages that suppress them. Therefore, both the occurrence criterion and the average state are found from a balance between the cumulative effects of bar-forming and bar-suppressing events.

4. Finally, the weakly nonlinear model of Colombini et al. (1987), originally defined to predict the evolution of bars under steady flow conditions, has been extended to reproduce a natural flow series by considering the basic flow varying in time. This approach allows us to (i) statistically investigate the effect of flood magnitude and duration on the variations of bar amplitude and (ii) to simulate the morphological response of a river to alterations of the hydrological regime.

The long-term analysis of bar amplitude, as such as its evolution subject to the hydrological flow regime, have been applied to four different study cases, each of them characterised by a distinctive average bar response: two reaches of the Alpine Rhine River, upstream and downstream the confluence of the River Ill (Switzerland), respectively, the Adige River near Trento (Italy) and the Isère River near Montmèlian (France). The theoretical model is able to capture both qualitatively and quantitatively the observed bed response. Specifically, it predicts the occurrence of high-relief bars for the upstream reach of the Alpine Rhine River and for the Isère River, while a plane configuration is predicted for the Adige River. Also the intermediate response of the downstream reach of the Alpine Rhine River is reproduced, showing a predominant flat bed morphology with sporadic low-relief bars.

SOMMARIO

Le barre alternate sono forme di fondo di grandi dimensioni che si sviluppano tipicamente nei fiumi rettificati. Esse si presentano come una sequenza ordinata di zone di scavo alternate a fronti diagonali di deposito che si dispongono lungo le sponde dei corsi d'acqua. A causa della loro altezza e della capacità di migrare lungo il canale, le barre rappresentano un problema nella gestione dei corsi d'acqua; esse, infatti, interferiscono con la navigazione, aumentano il rischio idraulico e interagiscono con i manufatti presenti in alveo. Per questo motivo, negli ultimi decenni sono stati fatti molti studi volti a descriverne le proprietà morfometriche.

Molti lavori teorici, sperimentali e numerici hanno chiaramente dimostrato che la presenza di barre alternate nei corsi d'acqua è un processo a soglia governato dal parametro β, il quale esprime il rapporto tra la larghezza del canale e la profondità della corrente. Qualora tale parametro sia maggiore di un valore critico β_{cr}, un meccanismo di instabilità amplifica le perturbazioni di piccola ampiezza che si generano sul fondo del canale in seguito al campo di moto turbolento, portando allo sviluppo di barre alternate che crescono fino a raggiungere un valore di altezza ben definito. Nel caso in cui la portata sia costante, infatti, le barre raggiungono una configurazione di equilibrio, presentando un'altezza che dipende dalla differenza $\beta - \beta_{cr}$.

Al contrario, le caratteristiche che le barre alternate assumono nel caso in cui la portata sia variabile, ovvero quando il parametro β varia nel tempo e l'ampiezza evolve a seconda della durata e della forma dell'idrogramma di piena, sono meno conosciute. L'effetto che un singolo evento di piena ha sull'evoluzione dell'ampiezza delle barre è stato con successo descritto dal modello debolmente non lineare di Tubino (1991), il quale è in grado di predire la traiettoria evolutiva dell'altezza durante le diverse fasi della piena. Supportato da evidenze sperimentali, Tubino (1991) ha scoperto che la risposta delle barre dipende in modo sostanziale dal rapporto tra la durata della piena e il tempo scala delle

barre. Ciononostante, la descrizione dell'effetto che una serie idrologica caratterizzata da una complessa sequenza di eventi ha sulla morfologia di un corso d'acqua è tuttora un argomento di studio. Nello specifico, in letteratura non sono ancora disponibili modelli (i) per predire la risposta topografica media delle barre alternate in un tratto di fiume soggetto a un regime idrologico e (ii) per quantificare l'altezza che esse raggiungono in seguito alla sequenza naturale di eventi di piena.

Gli obiettivi della tesi sono: (i) studiare la dipendenza delle proprietà delle barre a diversi valori di portata; (ii) analizzare l'effetto della non stazionarietà della portata in termini di durata e sequenza degli eventi, al fine di determinare le principali caratteristiche del regime idrologico che controllano la risposta delle barre; (iii) determinare la risposta delle barre nel lungo periodo e definire una portata formativa per le barre, ovvero un valore rappresentativo di portata che, se mantenuto costante per un tempo sufficientemente lungo, produrrebbe la stessa topografia media della serie idrologica; (iv) analizzare gli effetti che una sequenza complessa di eventi di piena ha sull'evoluzione dell'altezza delle barre.

Per raggiungere tali obiettivi, è stata adottata una metodologia principalmente basata su modelli teorici, i quali sono stati successivamente validati da evidenze sperimentali e dati di campo. La metodologia adottata e i principali risultati della tesi possono essere così riassunti:

1. Per prima cosa è stata indagata la risposta topografica delle barre a differenti valori di portata, sia da un punto di vista teorico che analizzando risultati sperimentali, osservando la dipendenza delle barre da particolari valori soglia di portata. La validità del modello debolmente non lineare di Colombini et al. (1987), inizialmente definito in un intorno di β_{cr}, è stata estesa tenendo conto dell'emersione delle barre a basse portate.

2. Successivamente, è stata analizza la risposta media delle barre a diverse sequenze di piene ideali, esplorando la dipendenza dell'altezza dalla durata e dall'ordine degli eventi. La densità di probabilità della serie idrologica è risultata essere l'ingrediente essenziale per determinare la

risposta dell'altezza delle barre nel lungo periodo, mentre la scala integrale può essere considerata una metrica utile per quantificare la non stazionarietà della serie stessa.

3. Poi, un metodo innovativo è stato introdotto per stabilire un criterio di formazione delle barre in un fiume rettificato in base al regime idrologico, andando a predire l'altezza media nel lungo periodo e identificando un valore di portata formativa. L'elemento chiave del metodo rispetto agli approcci classici utilizzati per definire le caratteristiche geometriche di un corso d'acqua all'equilibrio consiste nel fatto che, nel caso delle barre, il lavoro morfologico svolto dalle piene moderate per formare le barre può essere capovolto dagli eventi più intensi fino a determinare una morfologia di fondo piano.

4. Infine, il modello debolmente non lineare di Colombini et al. (1987), inizialmente definito per descrivere l'evoluzione delle barre a portata costante, è stato esteso al caso di portata variabile e utilizzato per descrivere l'evoluzione morfologica delle barre nel tempo in seguito ad una complessa sequenza di eventi, considerando il moto base variabile. Ciò ha permesso di (i) effettuare un'analisi statistica per valutare l'effetto della durata e dell'intensità delle piene nel processo evolutivo dell'altezza delle barre e (ii) simulare la risposta morfologica di un corso d'acqua ad alterazioni del regime idrologico.

L'analisi dell'altezza delle barre nel lungo periodo, così come la sua evoluzione dovuta al regime idrologico, è stata effettuata su quattro differenti casi studio, ognuno dei quali caratterizzato da una particolare morfologia. Nel dettaglio, sono stati considerati due tratti del fiume Reno Alpino, rispettivamente a monte e a valle della confluenza con il fiume Ill (Svizzera), un tratto del fiume Adige nei pressi di Trento (Italia) e un tratto del fiume Isère vicino a Montmèlian (Francia). Il nostro modello è in grado di descrivere correttamente le caratteristiche morfologiche osservate nei corsi d'acqua, sia qualitativamente che quantitativamente. Nello specifico, esso è in grado di predire la presenza di barre alternate nel tratto di monte del Reno Alpino e nell'Isère, mentre

fornisce una morfologia di fondo piano nell'Adige. Inoltre, esso riproduce ragionevolmente la risposta intermedia del tratto di valle del Reno Alpino, nel quale la morfologia predominante di fondo piano è caratterizzata dalla presenza di sporadiche barre di piccola ampiezza.

ACKNOWLEDGMENTS

At the end of these three years of PhD I would like to thank many people I have had the pleasure of meeting or getting to know better.

First of all, a grateful thank goes to my supervisors, Prof. Marco Tubino and Dr. Marco Redolfi for their support in each moment and for the proficient scientific discussions that allowed for my professional growth.

I also would like to thank Professors Astrid Blom and Peter Nelson for their fruitful comments and suggestions about this PhD thesis, allowing for a significant improvement of the overall work.

Many thanks to my colleagues and friends Silvia D'Agostino and Josè Antonio Bonilla Porras (Pepe), who started such stimulating experience with me and shared joys and challenges that only a PhD is able to provide.

I cannot forget to thank my nice office mates, who enlightened the long working days in Mesiano.

Thanks to my family for always being present, especially in the moments of need. A special thought goes to my grandparents, if they could be here they would be proud of me.

Finally, I would like to express my gratitude to my beloved Benedetta, for being close to me at all times, both in the beautiful and the difficult ones.

CONTENTS

LIST OF FIGURES

The base physical quantities are here indicated as T (time), M (mass), L (length).

Latin

a	[—]	exponent equal to 3/2.
A	[—]	amplitude function of alternate bars.
A^*	[L]	dimensional amplitude of alternate bars.
a_0, a_1, a_2	[—]	coefficients of univariate and bivariate linear regression.
A_0	[—]	dimensionless initial value of bar amplitude.
A_0^*	[L]	dimensional initial value of bar amplitude.
A_{02}^*	[L]	dimensional form of the component $m = 0$ and $n = 2$ of bar amplitude.
A_{11}^*	[L]	dimensional form of the fundamental component of bar amplitude.
A_{20}^*	[L]	dimensional form of the component $m = 2$ and $n = 0$ of bar amplitude.
A_{22}^*	[L]	dimensional form of the component $m = 2$ and $n = 2$ of bar amplitude.
A_{as}^*	[L]	average state of bar amplitude.
$A_{as}'^*$	[L]	tentative value of bar amplitude.
A_{eq}	[—]	dimensionless equilibrium bar amplitude.
A_{eq}^*	[L]	dimensional equilibrium bar amplitude.

$\overline{A}_{eq}$	[–]	equilibrium bar amplitude (reference state).
A_f^*	[L]	final value of bar amplitude during flood events.
A_{fw}^*	[L]	fully-wet limited bar amplitude (for $Q < Q_{fw}$).
A_l	[L^2]	area of the reservoir.
A_{max}^*	[L]	bar amplitude corresponding to the fully-wet threshold Q_{fw}.
A_{min}^*	[L]	minimum value of bar amplitude during flood events.
A_T	[–]	equilibrium value of $\lvert A \rvert$ corresponding to the instantaneous flow characteristics.
A_{TF}	[–]	value of A_T at the end of the flow event.
b	[–]	exponent of a power low describing the flow rating curve.
b_1, b_2	[–]	coefficients of eq (2.37), see Fig. 5 of Colombini et al. (1987).
B	[L]	width of a rectangular weir.
BRI^*	[L]	bed relief index computed as the mean of BRI_{sec}^*.
BRI_{sec}^*	[L]	dimensional bottom standard deviation defined for each cross section.
c	[–]	friction coefficient.
C^*	[$L\,T^{-1}$]	dimensional wave celerity.
$\widehat{C}$	[–]	bar celerity scaled with respect to U_d^*.
c_0	[–]	friction coefficient (basic flow).
C_D	[–]	coefficient defined in eq. (2.48).
c_f	[–]	function modulating the climate change effect in a reference period.
c_Q	[–]	efflux coefficient $\simeq 0.41$.

c_ν	[—]	coefficient of variation of a flow series.
d_{50}	[L]	sediment diameter.
D	[—]	dimensionless depth-averaged flow depth.
D^*	[L]	dimensional depth-averaged flow depth.
D_0^*	[L]	uniform flow depth.
D_0	[—]	dimensionless uniform flow depth (basic flow).
$\overline{D}_0^*$	[L]	average uniform flow depth (reference state).
D_{00}, D_{02}, D_{20} D_{11}, D_{22}	[—]	components of D at various orders.
D_{01}	[—]	unsteady component of D_0.
D_1	[—]	perturbation of D for the linear solution.
D_i^*	[L]	water depth for $Q = Q_i$.
dQ	$[L^3\,T^{-1}]$	integral increment of discharge.
d_s	[—]	relative roughness.
$\overline{d}_s$	[—]	relative roughness (reference state).
dt_E	[—]	dimensionless increment of time in the Exner scale.
F	[—]	coefficient defined in eq. (2.58).
F_0	[—]	Froude number.
f_ξ		probability density function of variable ξ.
f_ξ^Υ		probability density function of variable ξ, scaled with the function Υ.
g	$[L\,T^{-2}]$	gravitational acceleration.
h	[L]	water level in the reservoir.
H_B^*	[L]	dimensional bar height computed as the maximum of H_{Bsec}^*.
$H_{B,a}^*$	[L]	mean value of cross sectional bar height along a wavelength.

H^*_{Bsec}	[L]	dimensional bar height defined for each cross section.
H_{BM}	[–]	dimensionless bar height (difference between maximum deposition and scour).
$\widehat{H}_{BM}$	[–]	dimensionless bar height with respect to the sediment size.
H^*_{BM}	[L]	dimensional bar height (difference between maximum deposition and scour).
i	[–]	imaginary unit equal to $\sqrt{-1}$.
j	[–]	index of discrete classes in numerical integration.
K	[T]	coefficient summarizing the characteristic of the reservoir.
k_1, k_2	[–]	coefficients of the analytical solution of the Landau-Stuart type equation.
L^*	[L]	bar length.
m	[–]	transverse mode of the harmonic components of the Fourier spectrum.
max, min, $mean$		maximum, minimum and mean operators.
max_{sec}, min_{sec}		maximum and minimum operators along individual cross section.
n	[–]	longitudinal mode of the Fourier spectrum components.
N	[–]	number of discharge values in the flow series.
N_f	[–]	number of flood events.
N_T	[–]	number of cycles required to achieve the equilibrium configuration of bar amplitude.
p	[–]	sediment porosity.
P_{form}	[–]	probability of bar formation.

P_{growth}	[—]	probability of growing for a bar with amplitude A'^{*}_{as}.
Q	$[L^3\,T^{-1}]$	dimensional flow discharge.
$\widehat{Q}$	[—]	dimensionless flow discharge scaled as in Parker et al. (2007).
$\overline{Q}$	$[L^3\,T^{-1}]$	dimensional flow discharge (reference state).
$\widehat{q} = \widehat{Q}/\widehat{W}$	[—]	dimensionless flow discharge per unit width (with respect to a d_{50} scale).
q_0	$[L^2\,T^{-1}]$	dimensional discharge per unit width.
$\overline{q}_0$	$[L^2\,T^{-1}]$	dimensional discharge per unit width (reference state).
q_{01}	[—]	unsteady component of q_0.
Q_2	$[L^3\,T^{-1}]$	discharge with a return time of 2 years.
Qc	$[L^3\,T^{-1}]$	mean value of discharge in the class ΔQ.
$\widehat{q}_{cr}$	[—]	dimensionless critical discharge for bar formation per unit channel width.
Q_{cr}	$[L^3\,T^{-1}]$	dimensional value of the critical discharge.
$Q_{d,IN}$, Q_d	[—]	dimensionless discharge values flowing input and output to the reservoir, respectively.
Q_{eff}	$[L^3\,T^{-1}]$	effective discharge (Wolman and Miller, 1960).
Q'_{eq}, Q'_{fw}	$[L^3\,T^{-1}]$	discharge values providing the equilibrium and the fully-wet limited bar amplitude equal to A'^{*}_{as}.
Q_{ev}	$[L^3\,T^{-1}]$	instantaneous fully-wet condition.
Q_{form}	$[L^3\,T^{-1}]$	bar-forming discharge.
Q_{fw}	$[L^3\,T^{-1}]$	fully-wet discharge.

$\widehat{q}_{fw}$	[–]	dimensionless fully-wet discharge per unit channel width.
q_i	$[L^2\,T^{-1}]$	discharge providing sediment for motion per unit channel width.
$\widehat{q}_i$	[–]	dimensionless discharge for sediment motion per unit channel width.
$\widehat{Q}_i$	[–]	dimensionless discharge for sediment motion.
Q_{IN}	$[L^3\,T^{-1}]$	input discharge in the reservoir.
Q_m	$[L^3\,T^{-1}]$	dimensional mean discharge.
Q_{max}	$[L^3\,T^{-1}]$	maximum discharge value in the flow series.
$\boldsymbol{q_s}$	[–]	dimensionless sediment flow rate vector per unit width.
Q_s^*	$[L^3\,T^{-1}]$	dimensional sediment discharge.
q_{sx}, q_{sy}	[–]	dimensionless longitudinal and transverse components of sediment flow rate per unit width.
q_{sx}^*, q_{sy}^*	[–]	dimensional longitudinal and transverse components of sediment flow rate per unit width.
$q_{sx,1}$, $q_{sy,1}$	[–]	perturbation of q_{sx} and q_{sy} for the linear solution.
r	[–]	empirical parameter of eq. (2.14).
$R = (\rho_s - \rho)/\rho$	[–]	submerged specific gravity of sediments.
R_{QQ}	[–]	Auto-correlation function.
S	[–]	channel slope.
std		standard deviation operator.
std_{sec}		standard deviation operator along individual cross section.
SD_ξ^*		dimensional standard deviation of variable ξ.
SK	[–]	skewness of the bed elevation η.
t^*	[T]	time.
t	[–]	dimensionless time.

T	$[-]$	slow time variable describing bar development.
t_1^*, t_2^*	$[T]$	different time values in which the auto-correlation of a signal is looked for.
T_{bar}	$[-]$	characteristic bar timescale.
T_{bar}^*	$[T]$	dimensional value of T_{bar}.
T_d^*	$[T]$	timescale related to the sediment size.
T_{df}	$[-]$	cumulative duration of flood events with respect to the total duration of activity.
T_E	$[-]$	dimensionless time scaled with T_{exn}^*.
T_{exn}	$[-]$	dimensionless Exner timescale.
T_{exn}^*	$[T]$	Exner timescale.
T_f	$[T]$	flood duration.
T_{flood}^*	$[T]$	characteristic flood timescale.
T_{flow}^*	$[T]$	characteristic timescale of a flow series.
$T_{f,r}$	$[T]$	Time required to reach the peak during flood events.
T_H^*	$[T]$	duration of the high flow phase (see Fig. 5.2).
T_r	$[T]$	return period.
T_R^*	$[T]$	reference time period.
U	$[-]$	dimensionless depth-averaged longitudinal component of velocity.
$\widehat{U}$	$[-]$	unsteadiness parameter of Tubino's (1991) model.
U_0^*	$[L\,T^{-1}]$	average flow velocity (basic flow).
$\overline{U}_0^*$	$[L\,T^{-1}]$	average flow velocity (reference state).
U_0	$[-]$	dimensionless instantaneous average flow velocity (basic flow).
U_{01}	$[-]$	unsteady component of U_0.

U_1	[–]	perturbation of U for the linear solution.
U_d^*	$[L\,T^{-1}]$	velocity scaling factor dependent to the sediment size.
V	[–]	dimensionless depth-averaged transverse component of velocity.
V_1	[–]	perturbation of V for the linear solution.
W	[L]	channel width.
$\widehat{W} = W/d_{50}$	[–]	dimensionless channel width (with respect to the grain size).
W_{cr}	[L]	critical channel width.
x^*	[L]	longitudinal coordinate.
x	[–]	dimensionless longitudinal coordinate.
y^*	[L]	transverse coordinate.
y	[–]	dimensionless transverse coordinate.

Greek

α	[–]	percentage of quantiles.
$\overline{\alpha}_0$, $\overline{\alpha}_1$, $\overline{\alpha}_2$	[–]	complex coefficients of eq. (2.50) (reference state).
$\overline{\alpha}_{0R}$, $\overline{\alpha}_{1R}$, $\overline{\alpha}_{2R}$	[–]	real part of coefficients $\overline{\alpha}_0$, $\overline{\alpha}_1$ and $\overline{\alpha}_2$.
$\overline{\alpha}_{0I}$, $\overline{\alpha}_{1I}$, $\overline{\alpha}_{2I}$	[–]	imaginary part of coefficients $\overline{\alpha}_0$, $\overline{\alpha}_1$ and $\overline{\alpha}_2$.
α_1, α_2	[–]	complex coefficients of eq. (2.28).
α_{1R}, α_{2R}	[–]	real part of coefficients α_1 and α_2.
α_{1I}, α_{2I}	[–]	imaginary part of coefficients α_1 and α_2.
β	[–]	width to depth ratio.
$\overline{\beta}$	[–]	average aspect ratio (reference state).
β_{cr}	[–]	critical aspect ratio.
$\beta_{cr,m}$	[–]	critical aspect ratio of mode-m.

β_{fw}	$[-]$	aspect ratio referred to the emersion condition.
$\overline{\gamma}_0$	$[T^2\,L^3]$	dimensional counterpart of coefficient $\overline{\alpha}_0$.
$\gamma_1, \overline{\gamma}_1$	$[T]$	dimensional counterpart of coefficients α_1 and $\overline{\alpha}_1$.
$\gamma_2, \overline{\gamma}_2$	$[T^{-1}\,L^{-2}]$	dimensional counterpart of coefficients α_2 and $\overline{\alpha}_2$.
δ	$[-]$	perturbation parameter of the unsteady component.
Δ	$[-]$	$\mathcal{O}(1)$ parameter.
ΔA	$[-]$	dimensionless variation of bar amplitude.
ΔA_{0m}	$[-]$	dimensionless variation of bar amplitude between the initial value and the minimum reached during the flood event.
ΔA^*_{0m}	$[L]$	dimensional counterpart of ΔA_{0m} scaled with A^*_{as}.
ΔA_{f0}	$[-]$	dimensionless variation of bar amplitude between the beginning and the end of a flood event.
ΔA^*_{f0}	$[L]$	dimensional counterpart of ΔA_{f0} scaled with A^*_{as}.
ΔA_{tot}	$[-]$	total variation of bar amplitude.
ΔQ	$[L^3\,T^{-1}]$	increment or class of water discharge.
$\widetilde{\Delta Q}$	$[-]$	dimensionless discharge defined in eq. (4.1).
$\widetilde{\Delta Q}_{max}$	$[-]$	random variable of the dimensionless peak discharges.
Δt^*	$[T]$	timestep increment.
$\widetilde{\Delta T}_f$	$[-]$	random variable of the dimensionless flood duration.
$\widetilde{\Delta T}_{f,r}$	$[-]$	random variable of the dimensionless duration needed to reach the flood peak.

ΔV_s	$[L^3]$	volume of sediment transported by the discharge class ΔQ.
ϵ	$[-]$	perturbation parameter.
$\overline{\epsilon}$	$[-]$	perturbation parameter (reference state).
ζ	$[-]$	dimensionless time variable associated with the basic unsteady flow.
η^*	$[L]$	dimensional bed elevation.
η	$[-]$	dimensionless bed elevation.
η_0	$[-]$	dimensionless initial bed elevation.
η_1	$[-]$	perturbation of η for the linear solution.
$\eta_{22}, \eta_{02}, \eta_{20}$	$[-]$	bed amplitudes of the second harmonics of η.
η^*_M	$[L]$	measure of the maximum scour.
θ	$[-]$	Shields parameter.
θ'	$[-]$	normalized Shields stress.
θ_0	$[-]$	Shields parameter (basic flow).
$\overline{\theta}_0$	$[-]$	Shields parameter (reference state).
θ_i	$[-]$	Shields parameter corresponding to the threshold for motion.
κ	$[T]$	integral scale of the flow regime.
λ	$[-]$	dimensionless bar wavenumber.
λ_1	$[-]$	perturbation of λ for the weakly nonlinear solution.
λ_{cr}	$[-]$	critical bar wavenumber.
λ_{max}	$[-]$	bar wavenumber of maximum amplification.
μ	$[-]$	residual terms of multiple linear regression.
ξ, Υ		dummy variables.
ρ_s, ρ	$[M\,L^{-3}]$	sediment and water density.
ρ_{QQ}	$[-]$	normalized auto-correlation function.

σ^*	$[T^{-1}]$	dimensional timescale of the flood event.
σ	$[-]$	dimensionless timescale of the flood event.
$\boldsymbol{\tau}$	$[-]$	dimensionless bed stress vector.
τ_x, τ_y	$[-]$	dimensionless longitudinal and transverse components.
$\tau_{x,1}$, $\tau_{y,1}$	$[-]$	perturbation of τ_x and τ_y for the linear solution.
τ^*	$[M\,L^{-1}\,T^{-2}]$	mean shear stress (basic flow).
Φ	$[-]$	equilibrium sediment transport rate.
Φ_0	$[-]$	equilibrium sediment transport rate (basic flow).
φ	$[-]$	angle between particle velocity and longitudinal direction.
ψ	$[-]$	pulse signal of the stochastic eq. (5.5).
ω	$[-]$	nonlinear angular frequency.
ω_0	$[-]$	linear angular frequency.
ω_1	$[-]$	phase of the complex function A, eq. (2.52).
ω_{cr}	$[-]$	linear angular frequency corresponding to the critical condition.
Ω	$[-]$	nonlinear bar growth rate.
Ω^*	$[T^{-1}]$	dimensional nonlinear bar growth rate.
Ω'^*	$[T^{-1}]$	nonlinear bar growth rate as a function of Q and A'^*_{as}.
Ω_0	$[-]$	linear bar growth rate.
Ω_0^*	$[T^{-1}]$	dimensional linear growth rate of bars.
$\overline{\Omega_0}$	$[-]$	weakly nonlinear approximation of the linear bar growth rate (reference state).

$\overline{\Omega}_0^*$	$[T^{-1}]$	dimensional linear bar growth rate (reference state).
$\widehat{\Omega}_0$	$[-]$	linear bar growth rate made dimensionless with T_d^*.
$\Omega_{0,m}^*$	$[T^{-1}]$	dimensional mean linear growth rate of bars.
$\Omega_{0,max}^*$	$[T^{-1}]$	maximum value of the linear bar growth rate with respect to the discharge.

Acronyms

BF	Bar-forming discharge method.
c.c.	complex conjugate of a complex number.
CPP	Compound Poisson Process.
CST	weakly nonlinear model of Colombini et al. (1987).
CST-SbS	weakly nonlinear model of Colombini et al. (1987) applied step-by-step to model the evolution of bar amplitude at varying discharge conditions.
DEM	Digital Elevation Model.
LHLH	Flow series built by interposing low and high triangular floods.
LLHH	Flow series built by interposing low and high triangular floods taken twice.
SWE	Shallow Water-Exner system of equations.
T91	weakly nonlinear model of Tubino (1991).

1 INTRODUCTION

1.1 CONTEXT

In the last few centuries many European rivers were regulated to increase land availability and industrial production, and to reduce the flooding risk (Dynesius and Nilsson, 1994; Nilsson et al., 2005; Molle, 2009). In particular, their course was often straightened and their width was typically restricted through the construction of embankments (Hohensinner et al., 2007; Diaz-Redondo et al., 2017; Serlet et al., 2018; Scorpio et al., 2018). Despite the fairly regular geometry that was artificially imposed, the riverbed often reacted by self-producing a sequence of scour and deposition zones, typically migrating downstream, called alternate bars (Fig. 1.1a,b). Such large-scale bedforms can be observed also in natural rivers, when the planform shape presents low sinuosity (e.g., Fig. 1.1c). Irregularities in the channel geometry of rivers, as bends or section narrowing, represent obstacles that are able to trigger the development of forced bars (e.g., Blondeaux and Seminara, 1985; Struiksma et al., 1985; Zolezzi and Seminara, 2001), which are nearly twice as long as free bars, do not migrate downstream and often interact with free bars (Seminara and Tubino, 1989).

From an engineering point of view, the occurrence of alternate bars represents one of the most problematic aspects in the management of regulated rivers. Indeed, due to their relatively high relief and their capability to modify the riverbed pattern, alternate bars may affect channel navigability and interact with structures. On the other hand, the presence of bars in rivers is important for increasing biodiversity, being a suitable habitat for aquatic fauna and riparian vegetation (e.g., Gilvear and Willby, 2006; Gilvear et al., 2007; Zeng et al., 2015).

As widely documented by theoretical (e.g., Parker, 1976; Fredsoe, 1978; Colombini et al., 1987; Nelson, 1990; Schielen et al., 1993; Federici and Seminara, 2006; Bertagni and Camporeale,

Figure 1.1. Examples of alternate bars in channelized (panels a and b) and natural (panel c) rivers. (a) Isère River (France), 45° 23′ N, 05° 59′ E; (b) Alpine Rhine River (Switzerland), 47° 10′ N, 09° 29′ E. (c) Cross River (Nigeria), 06° 03′ N, 08° 28′ E. From Google Earth, 3D web version (2020). Flow is from bottom to top in upper panels and from right to left in the bottom panel.

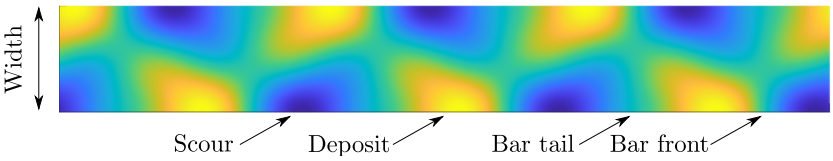

Figure 1.2. Configuration of alternate bars resulting from the analytical model of Colombini et al. (1987) in a straight, rectangular channel. Flow is from left to right.

2018), numerical (e.g., Defina, 2003; Crosato et al., 2012; Siviglia et al., 2013; Qian et al., 2017), and laboratory investigations (e.g., Ikeda, 1984; Jaeggi, 1984; Lanzoni, 2000b,a; Knaapen et al., 2001; Crosato et al., 2012; Redolfi et al., 2020), migrating alternate bars spontaneously develop in straight channels (e.g., see the ideal channel in Fig. 1.2) due to a riverbed instability mechanism, which occurs when the channel width-to-depth ratio, β, exceeds a threshold value, β_{cr}. Under constant discharge conditions, alternate bars grow until they attain a regime state, where they almost maintain the same average properties (height, wavelength and shape), while migrating downstream, although long-term fluctuations are possible (Crosato et al., 2012). Conversely, under unsteady flow conditions alternate bars evolve by varying their morphometric properties depending on the intensity and duration of flood events (e.g. Tubino, 1991; Welford, 1994; Hall, 2004; Eekhout et al., 2013). Specifically, since the variation of discharge implies a consequent variation of the channel aspect ratio, during flood events high discharge stages can provide values of the aspect ratio lower than the critical threshold. Therefore, during a single flood event a channel that typically form alternate bars can experience the condition of channel stability (i.e. related to the flat bed) when the peak of the flood event occurs.

In general, for given river geometry (i.e. channel width, longitudinal slope and sediment size), the threshold condition for bar formation corresponds to a specific discharge value, and therefore the hydrological regime may include both bar-forming and bar-suppressing stages. However, existing studies on bar response to variable discharge (e.g. Jaballah et al., 2015; Adami et al., 2016; Nelson and Morgan, 2018; Jourdain et al., 2020) mainly focussed on the effect of a individual flow event, and therefore not much

information exists about the expected properties of alternate bars as a result of the complex sequence of events that characterise the hydrological regime. The questions then arise of (i) how to define a criterion to determine how likely alternate bars are to be present in a river reach and to predict their long-term average properties, or, alternatively, a "*bar-forming*" discharge value associated with such average conditions, and (ii) how to quantify the effect that a complex flow series is able to produce on the bar amplitude.

Finally, once the dependence of bar properties on flow unsteadiness is found, a more general aspect about the response of alternate bars to a longer timescale can be investigated. Indeed, having a method to predict the average behaviour of alternate bars allows us to forecast how such long-term response can change once an alteration of the hydrological regime occurs, for example due to human pressures or climate changes.

1.2 THE CONCEPT OF DOMINANT DISCHARGE

Defining the average response of a river reach to the hydrological regime and identifying a suitable metric (i.e. a specific discharge value) that controls such response are very common issues in river morphodynamics. To address these issues the concept of "*formative*" or "*dominant*" discharge was first introduced by Inglis (1949) as the discharge value that produces the same effect on river morphology as the whole hydrological series. Since then, various methods have been proposed in the literature (see Blom et al., 2017) to define the formative conditions for specific river properties (e.g., channel width, longitudinal slope, bed surface texture), such as the bankfull discharge (Inglis, 1949; Leopold and Wolman, 1957; Andrews, 1980; Emmett and Wolman, 2001) or the discharge value associated to a fixed recurrence interval ($1.5 - 2$ year flood, see Pickup and Warner, 1976; Williams, 1978; Nash, 1994, for example).

The concept of "dominant" event is often connected with that of geomorphic *effectiveness* (Lisenby et al., 2018), as for the "effective discharge" method proposed by Wolman and Miller (1960) in which the solid transport is considered the main driver of morphological evolution (Benson and Thomas, 1966; Andrews,

1980). The method considers as "dominant" the discharge that moves the largest volume of sediments over a period of time. It combines the magnitude of the hydrological events with their frequency of occurrence, taking the product between the duration curve of the flow series and the solid transport rate, which is commonly modeled by deterministic transport predictors. Similarly, the half-yield discharge, for which the dominant discharge is associated with the stage discriminating the 50 % of sediments cumulatively yielded by the flow series (e.g. Prins, 1969; Soar and Thorne, 2001; Vogel et al., 2003), and the discharge associated with the 75th percentile of cumulative sediment yield (Copeland et al., 2005) were introduced as alternative metrics of the Wolman and Miller's (1960) magnitude-frequency approach.

The effective discharge method has been extensively employed in the case of sandy streams, due to easier availability of sediment transport data (i.e. Benson and Thomas, 1966; Ashmore and Day, 1988; Crowder and Knapp, 2005; Ferro and Porto, 2012). However, many applications to gravel bed rivers are also documented in the literature, in which the sediment transport rate is quantified by means of both theoretical bedload predictors (Pickup and Warner, 1976; Andrews, 1980; Barry et al., 2008) and field data (Carling, 1988; Emmett and Wolman, 2001; Goodwin, 2004; Downs et al., 2016). In the case of coarse and natural rivers, predicted formative values are in fairly good agreement with those obtained with the alternative definitions of bankfull discharge or $1.5 - 2$ year flood (Andrews, 1980; Emmett and Wolman, 2001; Doyle et al., 2007), while they substantially differ in regulated-channelized rivers (Doyle et al., 2007) and flashy systems (Pickup and Warner, 1976). Recently, Sholtes and Bledsoe (2016) found that the half-yield discharge provides slightly better results than the effective discharge when compared with the bankfull discharge, both in fine and coarse alluvial reaches. Although little theoretical argument are available to strength the validity of the half-yield discharge, authors suggest that it can be considered as "an index discharge of intermediate magnitude, derived from process-based sediment yield analysis", able to well predict the bankfull discharge.

Despite the various attempts to define a generally-valid concept of formative discharge, it clearly appears that its definition

needs to be related to the specific morphodynamic aspect under investigation (e.g., Church and Ferguson, 2015; Lisenby et al., 2018), as "no single steady discharge can affect all characteristics of channel geometry in a similar manner as the varying flow rate" (Blom et al., 2017). Furthermore, other variables affect the morphodynamical response of rivers to the hydrological regime, such as the catchment area, the climate characteristics of the region, the nature of sediment transport and the river pattern. For example, small basins tend to be controlled by catastrophic events (Ashmore and Day, 1988), even more so when they are located in semi-arid regions (Baker, 1977; Selby, 1974), and the formative processes that governs channel morphology are different in the case of braided rivers (Surian et al., 2009) or mountain streams (Vianello and D'Agostino, 2007; Bunte et al., 2014).

1.3 DISTINCTIVE CHARACTERISTICS OF ALTERNATE BAR BEHAVIOUR

Why do we need a novel, specific approach to determine the long-term average bar response to the hydrological regime in straight channelized rivers? Analysing the method proposed by Wolman and Miller (1960), which is one of the most implemented in literature, we can identify four main assumptions that are implicitly posed: (i) the morphodynamical work increases with the sediment transport, and therefore with flow discharge; (ii) increasing the flow discharge, the timescale of bed evolution gets shorter according to the Exner equation, and therefore the river response gets faster; (iii) all the flow stages above the threshold of incipient sediment motion work in the same direction, their effect increasing monotonically with flow discharge; (iv) the response of sediment transport to flow variability is instantaneous.

However, the observed behaviour of alternate bars does not perfectly fit any of these assumptions, making it necessary to introduce a new approach accounting for the distinctive response of alternate bars. Indeed, as discharge increases, the width-to-depth ratio decreases and so does the equilibrium amplitude of bars (Redolfi et al., 2020). Moreover, the growth rate of bars (that is the reciprocal of their timescale) increases to a maximum value and then drops at higher discharge, until it becomes nega-

tive. Therefore, besides the threshold for sediment motion, such particular behaviour sets a second, upper threshold (the critical discharge for bar formation) that discriminates bar-forming from bar-suppressing flow stages, being the discharge value for which the channel aspect ratio equals the critical one. From this consideration a key property of bar behaviour derives: the morphodynamic work that relatively low-flow stages (below the critical threshold) produce to form river bars can be reversed by high-flow stages (above the critical threshold), making the average response of the channel dependent on the competition between such flow conditions. It is worth noticing that an analogous opposite response to low and high flows was also found by Blom et al. (2016, 2017) in their model of the equilibrium channel slope. However, in this case an equlibrium slope is always achieved, independently of the magnitude of the channel-forming discharge, while alternate bars do not necessarily form if suppressing events predominate over forming ones. Finally, the time scale of bar amplification/decay is often comparable with that associated with flood events. Therefore, bar adaptation to flow variability is not instantaneous (Tubino, 1991; Welford, 1994), which implies that bar height may not attain at each flow stage the corresponding equilibrium value. In Tab. 1.1 these peculiarities of alternate bars are synthesized and compared with the classical assumptions of the effective discharge method.

The need for a specific representative discharge for alternate bars have been already highlighted by Blondeaux and Seminara (1985) and Jaballah et al. (2015), while Crosato and Mosselman (2009), in the absence of a suitable estimate, used the bankfull discharge to define a criterion for the occurrence of bars. Such need is also supported by the few available field observations, which suggest that bar topography is mainly determined by specific flow conditions, such as the tails of flow hydrographs (Welford, 1994) or the "bar-full" stage (Biedenharn and Thorne, 1994).

1.4 RESEARCH QUESTIONS

The present PhD work is devoted to analyse the long-term effect of a complex flow regime on the morphometric properties

Table 1.1. Summary of the distinctive characteristics of alternate bars for which the classical approach of the effective discharge method is not suitable to determine the formative conditions for bars.

	Effective discharge method	**Bar response**
(i)	The morphological work increases with the discharge	The amplitude of bars decreases with the discharge
(ii)	The river timescale gets shorter for increasing discharge values, which makes the morphological evolution faster	The bar timescale exhibits a maxiumum near the critical discharge, so that the speed of bar evolution does not increase monotonically with the discharge
(iii)	Flow stages larger than the threshold for sediment motion work in the same direction	High discharge values can reverse the work made by moderate flows to form bars
(iv)	The response of sediment transport to discharge variations is instantaneous	Bar response to discharge variations is delayed

of alternate bars. To address this purpose we approached the problem by steps, answering the following questions:

1. How do equilibrium bar properties respond to discharge variations and to what extent they can be predicted by means of theoretical models?

2. Which characteristics of the complex flow series mainly determine the evolution of the bar amplitude?

3. To what extent do the properties of bars depend on the timescale of a flow series and how can we define the timescale of a flow series?

4. Is it possible to develop a method for predicting the average bar amplitude observed in a river reach (i.e. determined by the flow regime) and the corresponding discharge value that can be considered as formative?

5. How do alternate bars evolve during flood events with respect to the average morphology?

6. How does the long-term bar amplitude in a river reach change by modifying the hydrological forcing?

1.5 OUTLINE OF THE THESIS

The work is organized within 8 Chapters:

- in Chapter 2 the key results from the theoretical works of Colombini et al. (1987) and Tubino (1991) are presented and extensively discussed;

- in Chapter 3 the equilibrium response of bars to different discharge stages is analysed from a theoretical point of view, defining peculiar threshold values of discharge that characterise bar behaviour;

- in Chapter 4 the theoretical prediction of bar properties to discharge variations is compared with experimental observations, providing an approximate solution for bar amplitude when the emersion condition occurs;

- in Chapter 5 the average effect determined by different simplified flow sequences on bar amplitude is investigated for a test case, finding that the required hydrological information to describe the long-term bar properties is given by the probability density function;

- in Chapter 6 we propose an innovative approach to compute the average bar height in a river reach, by providing the corresponding "bar-forming" discharge;

- in Chapter 7 we extend the applicability of Colombini et al. (1987) to variable flow conditions, analysing the effect of magnitude and duration of flood events to bar amplitude

with attention on the response of bars to alteration of the hydrological regime;

- in Chapter 8 we provide a response of the research questions by summarizing the main results of this work.

Two appendices complete the work:

- Appendix A provides a statistical interpretation of the effective discharge method, suitable to describe the parallelism with our model to define the bar-forming discharge;
- Appendix B compares the equilibrium properties of bars predicted by the weakly nonlinear models of Colombini et al. (1987) and Tubino (1991).

2

ALTERNATE BARS: THEORETICAL FRAMEWORK

2.1 INTRODUCTION

From a mathematical point of view, the stability of river channels has been investigated since the sixties of the last century, with the approach proposed by Callander (1969). The possibility to predict the development of bars in rivers and prevent potential risks related to their evolution with an almost negligible computational time promoted the development of several bar theories in the next decades (e.g. Parker, 1976; Fredsoe, 1978; Colombini et al., 1987; Crosato and Mosselman, 2009; Bertagni and Camporeale, 2018), through an approximate representation of the flow field by means a two-dimensional Saint Venant-Exner shallow water system of equations, which was analytically or semi-analytically solved (Tubino et al., 1999).

One of the most implemented techniques consists of approaching the problem by linearizing the governing equations assuming small the perturbation that triggers the instability mechanism. Under steady flow conditions the linear analysis allows to quantify the wavelength of bars and their migration rate, but no information is provided about their amplitude, for which the nonlinear interactions must be accounted for. Indeed, weakly nonlinear approaches provide an estimate of the equilibrium bar amplitude achieved by the perturbation after a certain time.

Specifically, for a given flow discharge, Q, the depth-averaged flow field is computed for a straight domain of constant width, W, slope, S, and uniform grain size, d_{50}, by considering the sediment supply sufficiently large to allow for transport capacity condition. These assumptions of theoretical approaches do not reflect the real heterogeneity of rivers, characterised by non uniform channel geometry, sediment sorting and an unsteady flow regime. Lanzoni and Tubino (1999) included grain sorting into the framework of a linear stability analysis, finding an increasing

reduction of bar instability with sediment heterogeneity. Furbish (1998) focussed on steep rough channels characterised by strong variations in channel width and bed elevation within short distances, observing similar instability mechanisms affecting purely alluvial rivers in forming free bars. Nelson and Seminara (2012) provided a stability analysis in straight bedrock channels not uniformly covered by sediments, finding that a bar-like pattern can spontaneously occur and Nelson et al. (2014) extended the analysis including the effect of channel curvature in their nonlinear asymptotic theory. Tubino (1991) implemented a weakly nonlinear approach to investigate the response of bar amplitude to unsteady flow discharge by linearizing a flood event around a reference state. The main output of the theory concerns the ratio between the bar timescale and the flood timescale, which should be of the same order of magnitude to allow for bottom evolution during the flood event.

In this chapter the theories of Colombini et al. (1987) (Section 2.2) and Tubino (1991) (Section 2.3) for free bars are exhaustively explained, since they constitute the main foundation in this work.

2.2 ALTERNATE BAR THEORY UNDER STEADY FLOW CONDITIONS

The theoretical framework of this work is based on the Colombini et al. (1987) weakly nonlinear theory, which is partially explained below following the approach of Adami (2016). To be consistent with the literature, dimensional variables that will be made dimensionless through appropriate scale quantities (e.g., flow velocity and water depth) are written with an asterisk (*).

2.2.1 *Hypothesis and assumptions*

Colombini et al.'s (1987) theory considered an infinite straight channel with erodible bottom and a constant width W, characterised by non-erodible banks, and solves the two-dimensional Shallow Water-Exner system of equations (SWE) by means a perturbation approach. The shallow water assumption allows the depth-averaged formulation of the problem, assuming negligible (i) the vertical acceleration respect to gravity and (ii) the

effect of flow separation, which was found rather weak by flume experiments (Jaeggi, 1984). The channel has constant slope S and it is fed by a constant discharge which provides a bed-load sediment transport of particles with a uniform grain size d_{50} in equilibrium with the transport capacity.

The definition of these parameters determines a reference uniform flow state (hereinafter identified by the subscript '$_0$') related to a channel with rectangular cross section and initial flat bed. This reference state can be assumed as the scale quantity providing the order of magnitude of the variables of the formulated problem, which in this way can be set in a dimensionless form. There are three key parameters and they are explained below.

The first dimensionless parameter is the aspect ratio of the channel, β, defined for the half cross section as:

$$\beta = \frac{W}{2D_0^*}, \tag{2.1}$$

where D_0^* is the uniform water depth.

The second dimensionless parameter is the Shields stress parameter, θ, which can be expressed as:

$$\theta = \frac{\tau^*}{(\rho_s - \rho) g d_{50}}, \tag{2.2}$$

where τ^* is the mean shear stress exerted by the flow on the bottom, ρ_s and ρ are the density of the sediment and of the water respectively and $g = 9.81\,m\,s^{-2}$ is the gravitational acceleration.

The last dimensionless parameter is the relative roughness, d_s, measuring the magnitude of the bottom roughness with respect to the uniform flow depth:

$$d_s = \frac{d_{50}}{D_0^*}. \tag{2.3}$$

2.2.2 *Mathematical model*

The mathematical model of alternate bar morphodynamics in a single-thread channel with constant width, slope and grain size is represented by the previously-mentioned SWE system of equations. Considering the Cartesian coordinate system (x, y)

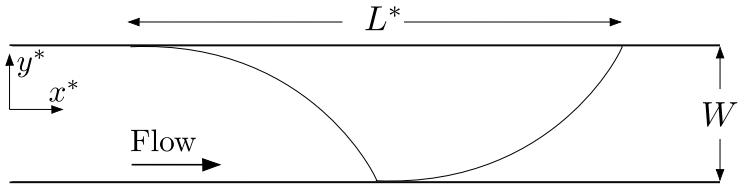

Figure 2.1. Planform sketch representing channel geometry and system of reference. The curved lines indicate the position of the bar front.

shown in Fig. 2.1, in which the longitudinal and transverse coordinates (x^*, y^*) have been scaled with half the channel width $W/2$, the dimensionless SWE system is defined as follow:

$$U\frac{\partial U}{\partial x} + V\frac{\partial U}{\partial y} + \frac{1}{F_0^2}\frac{\partial(\eta + D)}{\partial x} + \beta\frac{\tau_x}{D} = 0 \tag{2.4}$$

$$U\frac{\partial V}{\partial x} + V\frac{\partial V}{\partial y} + \frac{1}{F_0^2}\frac{\partial(\eta + D)}{\partial y} + \beta\frac{\tau_y}{D} = 0 \tag{2.5}$$

$$\frac{\partial(UD)}{\partial x} + \frac{\partial(VD)}{\partial y} = 0 \tag{2.6}$$

$$\frac{\partial \eta}{\partial t} + Q_0\left[\frac{\partial q_{sx}}{\partial x} + \frac{\partial q_{sy}}{\partial y}\right] = 0. \tag{2.7}$$

where eqs. (2.4) and (2.5) represent the momentum balance in the x and y directions respectively and eqs. (2.6) and (2.7) are the continuity equations for water and sediments respectively. The system (2.4−2.7) presents four unknowns: the components of the flow velocity U and V in the longitudinal and transverse directions respectively, made dimensionless with the uniform flow velocity U_0^*, the local water depth D and the bottom elevation η, scaled with the reference water depth D_0^*. The time t^* for the bottom evolution is made dimensionless by means the hydrodynamics timescale $W/(2U_0^*)$. Finally, F_0 is the Froude number of the uniform flow, which occurs due to the dimensionless form of the system, defined as:

$$F_0 = \frac{U_0^*}{\sqrt{gD_0^*}}, \tag{2.8}$$

and Q_0 is the ratio between the scale of sediment discharge and the flow rate:

$$Q_0 = \frac{d_{50}\sqrt{gRd_{50}}}{(1-p)U_0^*D_0^*}, \tag{2.9}$$

in which p is the sediment porosity and R is the relative submerged weight of sediments defined as $(\rho_s - \rho)\rho^{-1}$.

The mathematical problem requires two closure relations for the shear stress $\boldsymbol{\tau} = (\tau_x, \tau_y)$ and the sediment transport discharge for unit width $\boldsymbol{q_s} = (q_{sx}, q_{sy})$. The shear stress $\boldsymbol{\tau}$ is usually defined as a function of the friction coefficient c, as:

$$\boldsymbol{\tau} = (\tau_x, \tau_y) = (U, V)\sqrt{U^2 + V^2}\, c, \tag{2.10}$$

where for the friction coefficient several expressions are available in literature, such as the Einstein (1950) formula:

$$c = 6 + 2.5 \ln\left(\frac{D}{2.5\, d_s}\right), \tag{2.11}$$

for the skin friction, in which the roughness parameter is set equal to $(2.5\, d_{50})$ following the formulation proposed by Engelund and Hansens (1967), or the Engelund and Hansens (1967) formula for a dune-covered bed:

$$c = \left(\frac{0.06 + 0.4\,\theta^2}{\theta}\right)^{\frac{1}{2}} \left[6 + 2.5 \ln\left(\frac{0.06 + 0.4\,\theta^2}{2.5\, d_s\, \theta}\right)\right]. \tag{2.12}$$

The sediment is assumed to be transported mainly as bed-load and the effect of the slope in the transverse direction is modelled on the direction and intensity of the bed-load, associating the local variation of sediment transport with an average direction of the particle trajectories driven by the gravity, as suggested by Engelund (1981). In a dimensionless form it becomes:

$$\boldsymbol{q_s} = (q_{sx}, q_{sy}) = (\cos\varphi, \sin\varphi)\Phi, \tag{2.13}$$

where φ, assumed as a small angle, is defined as:

$$\sin\varphi = V\sqrt{U^2 + V^2} - \frac{r}{\beta\sqrt{\theta}}\frac{\partial \eta}{\partial y}. \tag{2.14}$$

Eq. 2.14 models the trajectory of sediment particles along an inclined bed accounting for the transverse deviation due to gravity, in which the parameter r is an empirical constant that assumes typical values in the range $0.3 - 0.6$ (Engelund, 1981; Olesen, 1983). The larger the parameter r, the greater the deviation of

particle trajectory from the direction of the inclined bed, resulting in a greater difficulty of the riverbed to form bars. The sediment flux can be reconstructed by scaling the dimensionless variables (q_{sx}, q_{sy}) as follow:

$$(q^*_{sx}, q^*_{sy}) = d_{50}\sqrt{R\,g\,d_{50}}(q_{sx}, q_{sy}). \tag{2.15}$$

Finally, Φ represents the intensity of the sediment transport rate, which can be expressed by means of several relations. In this PhD thesis we focus on the following transport relations:

1. Meyer-Peter and Muller (1948):

$$\Phi = 8(\theta - \theta_i)^{\frac{3}{2}}, \tag{2.16}$$

in which the critical value of the Shields parameter, θ_i, representing the incipient value of sediment motion, is equal to 0.047.

2. Parker (1978):

$$\Phi = 11.2\,\theta^{\frac{3}{2}}\left(1 - \frac{\theta_i}{\theta}\right)^{\frac{9}{2}}, \tag{2.17}$$

with $\theta_i = 0.03$.

3. Parker (1990):

$$\Phi = 0.00218\,\theta^{\frac{3}{2}}\,H(\theta'), \tag{2.18}$$

in which $\theta' = \theta/\theta_i$ is the normalized Shields stress with $\theta_i = 0.0386$, and the function $H(\theta')$ is given by:

$$H(\theta') = \begin{cases} 5474\left(1 - \dfrac{0.853}{\theta'}\right)^{\frac{9}{2}} & \text{if: } \theta' > 1.59 \\ \exp\left[14.2(\theta' - 1) - 9.28(\theta' - 1)^2\right] & \text{if: } \theta' > 1 \\ \theta'^{14.2} & \text{otherwise} \end{cases}. \tag{2.19}$$

Notice that for $\theta' > 1.59$ the formula almost coincides with Parker's (1978) relation.

In this chapter, accordingly with the original formulation of Colombini et al. (1987), the Meyer-Peter and Muller (1948) relation is used.

2.2.3 *Linear theory*

The linear solution of the governing system (2.4—2.7) is found by means of a perturbation approach, which consists of introducing a small initial bed perturbation having the form of a three-dimensional, double-sinusoidal bed deformation, assumed "small", and investigating the stability of the system.

Before going into detail with the linear solution we must specify the boundary conditions. In particular, the system of eqs. (2.4—2.7) is defined for a straight channel with constant width and slope and uniform grain size, upstream fed by constant water discharge and solid discharge in equilibrium with the transport capacity. The infinite length of the channel allows for considering the solution as periodic. In the transverse direction we have to impose the vanishing of the flux of water and sediments at the channel banks, namely $V = q_{sy} = 0$ when $y = \pm 1$.

The trivial solution is given by the uniform flow and the initial flat bed, which in the dimensionless form reads:

$$\begin{cases} U = U_0 = 1 \\ V = 0 \\ D = D_0 = 1 \\ \eta = \eta_0(x) \end{cases} . \tag{2.20}$$

A non trivial solution can be found by considering a perturbation of order ϵ, which depends on temporal t and spatial (x, y) coordinates, as follow:

$$\begin{cases} U = U_0 + \epsilon U_1(x, y, t) \\ V = 0 + \epsilon V_1(x, y, t) \\ D = D_0 + \epsilon D_1(x, y, t) \\ \eta = \eta_0(x) + \epsilon \eta_1(x, y, t) \end{cases} \tag{2.21a}$$

$$\begin{cases} \tau_x = c_0 + \epsilon \tau_{x,1}(x, y, t) \\ \tau_y = 0 + \epsilon \tau_{y,1}(x, y, t) \\ q_{sx} = \Phi_0 + \epsilon q_{sx,1}(x, y, t) \\ q_{sy} = 0 + \epsilon q_{sy,1}(x, y, t) \end{cases} , \tag{2.21b}$$

in which variables characterised by the subscript '$_1$' have the same order of magnitude of the respective uniform ones, but

reduced to infinitesimal perturbations by means the parameter ϵ. It is worth noticing that, at the first order of approximation, i.e. $\mathcal{O}(1)$, only the longitudinal components of the shear stress and the sediment discharge per unit width are different from zero, due to the basic uniform flow. Specifically, the dimensionless shear stress equals the uniform friction coefficient, while the sediment discharge is given by Φ_0, being $\cos\varphi = 1$.

Such definition of the unknowns (eq. 2.21) allows to rewrite the system (2.4–2.7) in a linear form (i.e. neglecting nonlinear terms), which provides the following solution for the water depth in a complex formulation (for all the unknowns the shape of the solution is the same):

$$D(x, y, t) = D_0 + \left[\epsilon \exp(\Omega_0 t) E_1 S_1 + \text{c.c.}\right] \tag{2.22a}$$

$$= D_0 + \left[\epsilon \exp(\Omega_0 t) S_1 \cos(\lambda x - \omega_0 t) + \text{c.c.}\right] \tag{2.22b}$$

where we define

$$S_1 = \sin\left(\frac{\pi}{2} y\right), \quad E_m = \exp mi(\lambda x - \omega_0 t) \tag{2.23a,b}$$

with $m = 1$ identifies the bar mode related to alternate bars. The structure of the solution expressed in eq. (2.22a) represents a wave propagating in space and time. Indeed, being linear systems satisfied by wave-like solutions, the perturbation term, D_1, is posed equal to $\exp(\Omega_0 t) E_1 S_1$, providing one of the possible solutions of the system that is expressive for alternate bars. Eq. (2.22b) is derived by the Euler's rule ($\exp(i\alpha) = \cos\alpha + i\sin\alpha$), which is often implemented in bar theories to simplify the algebraic calculations leading to the analytical solution. The parameter λ is the bar wavenumber, easily related to the dimensionless bar wavelength L^*/W (see Fig. 2.1 for the definition of bar length, L^*) by:

$$\lambda = \frac{\pi W}{L^*}. \tag{2.24}$$

In eq. (2.22b) the parameters Ω_0 and ω_0 are real quantities representing the amplification rate and the angular frequency respectively, and c.c. is the *complex conjugate* of a complex number. By substituting the solution for each variable in the form of eq. (2.22) into the system (2.4–2.7), an algebraic form can be found, providing the following stability condition:

$$\frac{dA}{dt} = \Omega_0 A, \tag{2.25}$$

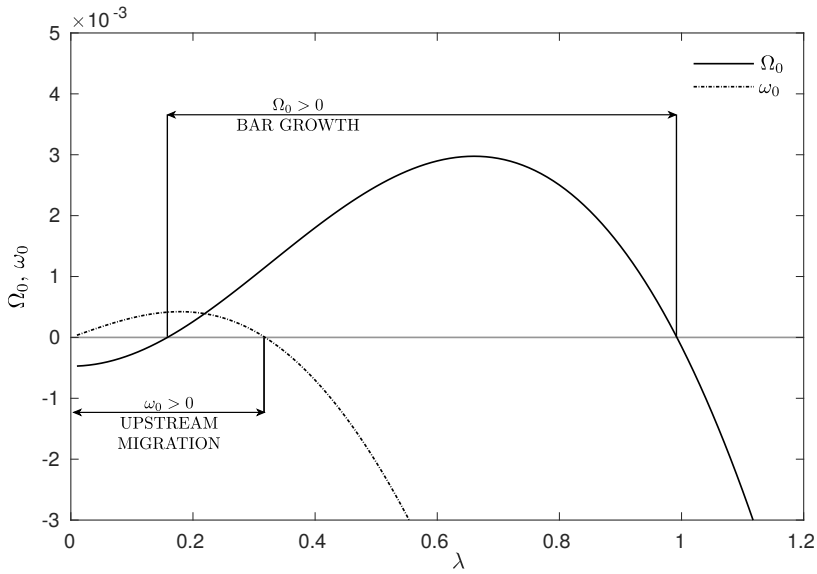

Figure 2.2. The growth rate Ω_0 and the angular frequency ω_0 versus the wavenumber for alternate bars, with $\theta_0 = 0.1$, $\beta = 30$ and $d_s = 0.07$. The preferred wavenumber to be amplified corresponds to peak of the Ω_0 function.

which gives an exponential growth of bars in time $A(t) = \exp(\Omega_0 t)$. Depending on the sign of the amplification factor Ω_0, two different responses of the riverbed can be found on the initial, small, bar wave: if $\Omega_0 < 0$ the initial wave is damped and the bottom is flattened (stable condition), otherwise, if $\Omega_0 > 0$ the wave is amplified and the bar grows (unstable condition).

The quantification of the amplification factor Ω_0 and the angular frequency ω_0 with respect to the bar wavenumber λ, for given values of the uniform flow parameters θ_0, β and d_s (i.e. for a given flow discharge) is shown in Fig. 2.2. It is evident that any discharge stage is able to amplify only a restricted range of wavelengths. In particular, the preferred wavelength can be identified considering the maximum of the growth rate Ω_0. A similar reasoning is valid for the angular frequency, which discriminates the bar wavelengths for which a downstream migration is possible.

Increasing the aspect ratio β, the amplification region widens, while, on the contrary, for low values of β the amplification factor is always negative. The neutral curve can be found varying

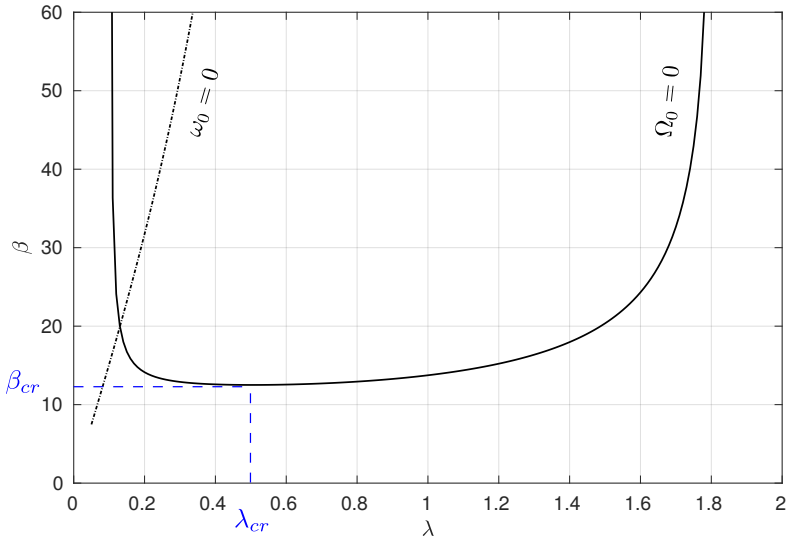

Figure 2.3. Neutral curves in the plane (λ, β) with $\theta_0 = 0.1$ and $d_s = 0.01$. Alternate bars are expected to form the region above the curve $\Omega_0 = 0$, which represents the unstable region, when an upstream or downstream migration is delimited by the $\omega_0 = 0$ curve.

the aspect ratio and selecting the wavenumbers for which the growth rate Ω_0 is equal to 0, identifying the bar configurations that are not amplified (see Fig. 2.3, where the neutral curve is computed for given values of θ_0 and d_s). In the plane (λ, β) alternate bars can be expected to form only in the unstable region above the neutral curve $\Omega_0 = 0$, while below the growth rate is always negative and all the states lead invariably to a flat bed. The curve $\omega_0 = 0$ identifies the condition of not migrating bars. Therefore, in the unstable region we can distinguish bars characterised by different signs of the angular frequency, namely negative on the right and positive on the left of the curve $\omega_0 = 0$ respectively. From a physical point of view, the different sign of the angular frequency identifies two opposite directions of bar migration in the channel: when the angular frequency is positive, the migration occurs downstream, conversely it occurs upstream. This latter condition is rarely observed in rivers, but it can be numerically reproduced (e.g. Siviglia et al., 2013).

The minimum of the neutral curve $\Omega_0 = 0$ represents the so-called "critical" condition corresponding to a critical value of the

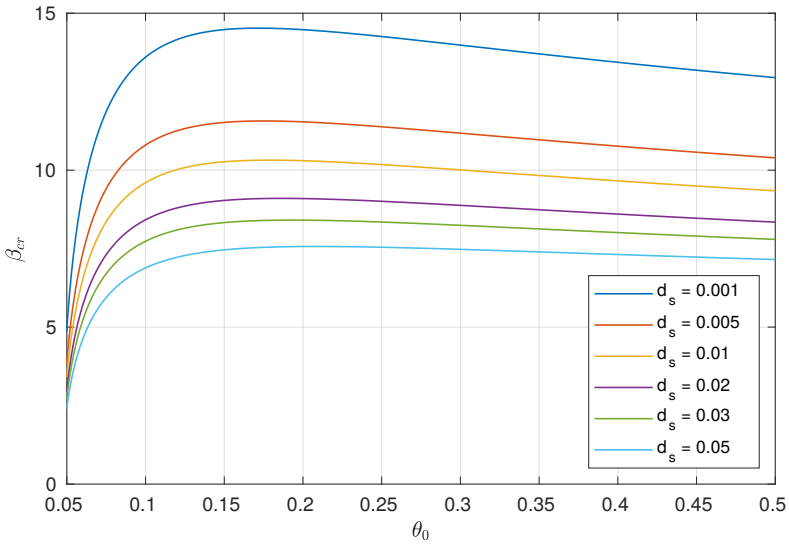

Figure 2.4. Critical aspect ratio for alternate bars as function of the Shields parameter θ_0 for different values of d_s (plane bed, $r = 0.3$).

aspect ratio, β_{cr} and a critical value of the bar wavenumber, λ_{cr}. By the shape of the neutral curve, it is evident that the channel aspect ratio is the key parameter in the stability analysis of a channel. More precisely, bars are expected to form when the aspect ratio of the channel is larger than the critical threshold, letting us suppose that narrow channels are reluctant to amplify bottom perturbations. While the critical aspect ratio has a well defined limit, the critical wavenumber is less selective, because for $\beta \simeq \beta_{cr}$ a range of λ between $0.3 - 0.7$ is close to marginal stability conditions. In Fig. 2.4 the trend of β_{cr} with respect to the Shields parameter θ_0 is reported for different values of d_s. A sharp decrease of the critical aspect ratio can be found for low values of the Shields parameter close to the threshold for motion, due to the strong reduction of the sediment transport. Furthermore, the instability of the channel is found to become larger for coarser channels, being the critical aspect ratio lower for increasing values of the relative roughness. Despite the physical explanation of this behaviour is still an open issue, we can suppose that the role of destabilizing effects gets stronger when friction increases (Seminara, 2010).

The stability of the channel is mainly determined by gravity, whose role is taken into account by the parameter r, already defined in eq. (2.14). Low values of r reduce the stability region, with the limit case of $r = 0$ for which a small perturbation of the riverbed inexorably grows. Conversely, for larger values of r the stable region widens and bars tend to be suppressed. The calibration of the parameter r depends on the choice of friction and bed load formulas, but values ranging between $0.3 \div 0.6$ typically allows for good predictions of laboratory experiments.

The linear stability analysis is strictly valid for small-amplitude bar perturbation and provides useful information about bar formation and wavelength. However, no information is provided about the bar amplitude, due to the exponential growth of bars in time resulting from eq. (2.25), which can be representative only for the fist stages of bar growth. To have a measure of the amplitude of the resulting bar, fixed geometrical and discharge information, nonlinear effects must be taken into account.

2.2.4 *Weakly nonlinear theory*

Colombini et al. (1987) proposed a weakly nonlinear approach to overcome the lack of information about the expected bar amplitude. Indeed, laboratory investigations suggested that for steady flow conditions an equilibrium amplitude is achieved by bars, with an order of magnitude of the water depth (e.g. Ikeda, 1984). It is evident that bar amplitude cannot be fitted by the exponential growth resulting from eq. (2.25).

The weakly nonlinear approach consists in looking for a solution of bar amplitude in the neighborhood of the critical conditions,

$$\beta = \beta_{cr}(1 + \epsilon), \quad \lambda = \lambda_{cr} + \epsilon\lambda_1 \tag{2.26a,b}$$

where ϵ is assumed to be small. Defining the channel aspect ratio by eq. (2.26a) means that the channel width can slightly vary around the critical condition, by keeping fixed the channel slope and the uniform water depth. Moreover, eq. (2.26b) implies that also the wavenumber can be slightly perturbed with respect to the critical value λ_{cr}.

At this point, the problem is approached considering a multiple-scale technique, based on the idea that the characteristic timescale

of amplitude evolution T is much smaller than the hydrodynamic timescale. Mathematically, the two timescales are related by the perturbation parameter ϵ, namely $T = \epsilon t$, which determines:

$$\frac{\partial}{\partial t} \to \frac{\partial}{\partial t} + \epsilon \frac{\partial}{\partial T}. \tag{2.27}$$

The new nonlinear terms generate high order harmonics, both in the longitudinal and in the transverse directions. Following the same procedure described for the linear case, the solution can be found writing the fundamental unknowns, eq. (2.22b), at third order. The amplitude relation presents the same linear structure, but with a new nonlinear term:

$$\frac{dA}{dT} = \alpha_1 A + \alpha_2 A|A^2|, \tag{2.28}$$

in which α_1 and α_2 are complex coefficients, functions of θ_0 and d_s, and α_1 is the measure of the approximated linear bar growth rate by the relation:

$$\Omega_0 = \epsilon \alpha_{1R}, \tag{2.29}$$

(hereinafter the subscripts '$_R$' and '$_I$' denote the real and imaginary parts of a complex number, respectively). Eq. (2.28) is of the Landau-Stuart type and presents the following properties:

1. neglecting the nonlinear term the exponential behaviour of bar amplitude is found;
2. an analytical solution is available, which assumes the following general form:

$$A(T) = \left[-\frac{k_2}{k_1} + \left(A_0^{-2} + \frac{k_2}{k_1} \right) \exp(-2k_1 T) \right]^{-\frac{1}{2}}, \tag{2.30}$$

   depending exclusively on the initial bar amplitude A_0, where $k_1 = \alpha_{1R}$ and $k_2 = \alpha_{2R}$ for eq. (2.28);
3. the nonlinear term inhibits bar growth and allows for an equilibrium amplitude when $T \to \infty$, even though α_{1R} and α_{2R} have opposite sign (see Figs. 2.5 and 2.6 where α_{1R} and α_{2R} are plotted as function of θ_0 for different values of d_s).

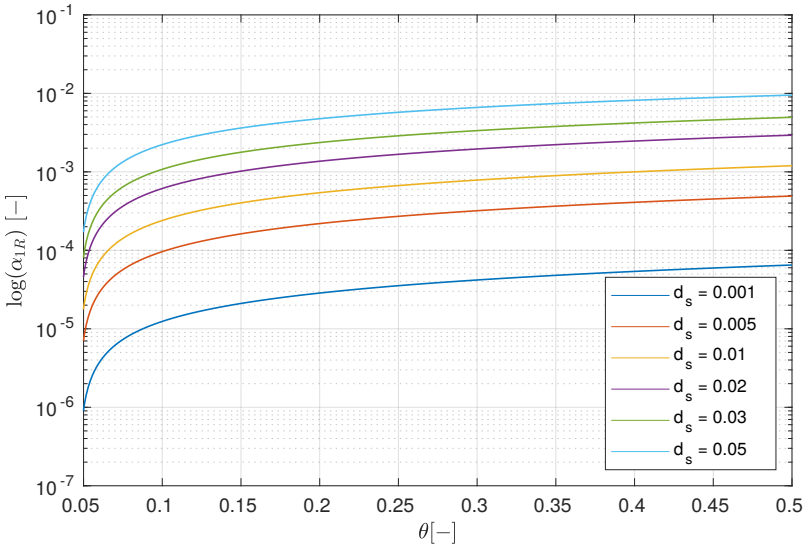

Figure 2.5. Real part of the coefficient α_1 as function of the Shields parameter θ_0 for different values of d_s (plane bed, $r = 0.3$).

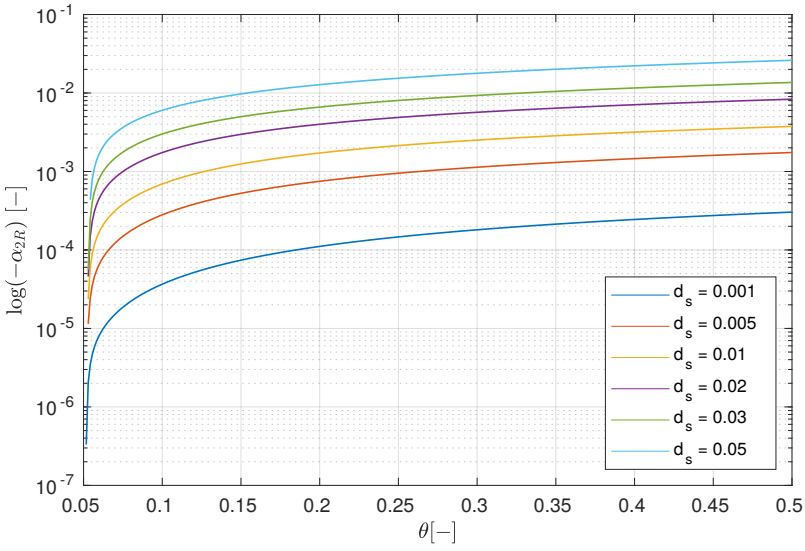

Figure 2.6. Real part of the coefficient α_2 as function of the Shields parameter θ_0 for different values of d_s (plane bed, $r = 0.3$).

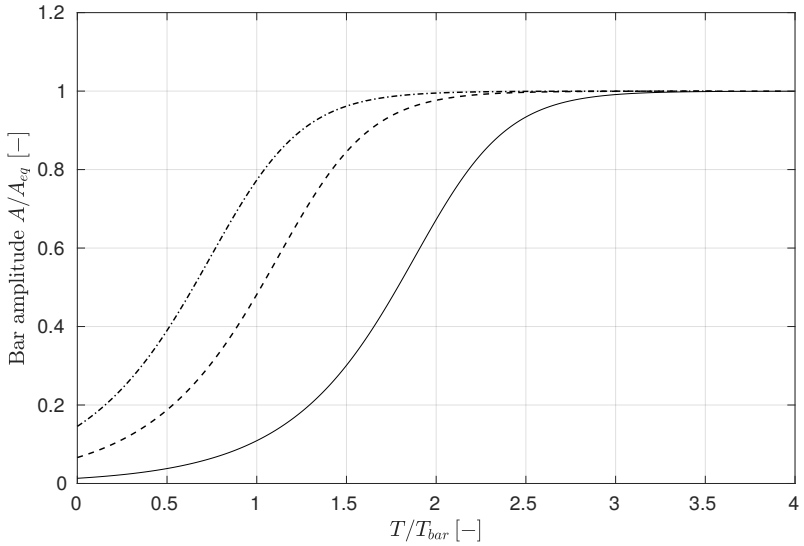

Figure 2.7. Evolution of bar amplitude in time for different values of the initial amplitude A_0 (plane bed, $\beta = 23.7$, $\theta_0 = 0.07$ and $d_s = 0.011$).

The equilibrium amplitude A_{eq} corresponds to the condition in which the temporal variation of bar amplitude vanishes, namely:

$$\alpha_1 A + \alpha_2 A|A^2| = 0, \tag{2.31}$$

which gives the following non trivial solution:

$$A_{eq} = \sqrt{-\frac{\alpha_{1R}}{\alpha_{2R}}}. \tag{2.32}$$

An example of bar amplitude evolution in time, with respect to the equilibrium value, is shown in Fig. 2.7 for different values of initial bar amplitude. The lower the initial value of bar amplitude, the longer the time required to reach the equilibrium configuration.

Once the system is solved, the solution at the equilibrium stage can be found for the system unknowns by neglecting higher order terms (i.e. $\mathcal{O}(\epsilon^2)$ terms). For example, we report the expressions for the flow depth:

$$\begin{aligned} D(x,y) = 1 &+ \epsilon^{1/2}\left[A_{eq}\, D_{11}\, S_1\, E_1 + c.c.\right] \\ &+ \epsilon\left[A_{eq}^2 (D_{22} C_2 + D_{02}) E_2 + c.c.\right], \\ &+ \epsilon\left[A_{eq}^2 (D_{20} C_2 + D_{00})\right] \end{aligned} \tag{2.33}$$

and the bed topography η, from which the bar height can be measured:

$$\begin{aligned}\eta(x,y) =& \epsilon^{1/2} A_{eq}\, S_1\, \exp(i\,\lambda_{cr}\, x) \\ &+ \epsilon A_{eq}^2 \left[\eta_{22} C_2 \exp(i\,2\lambda_{cr}\, x)\right] \\ &+ \epsilon A_{eq}^2 \left[\eta_{02} \exp(i\,2\lambda_{cr}\, x) + \eta_{20}\, C_2\right] + \text{c.c.}\end{aligned} \quad , \tag{2.34}$$

where:

$$C_2 = \cos(\pi\, y), \tag{2.35}$$

and D_{11}, D_{22}, D_{02}, D_{20}, D_{00}, η_{22}, η_{02} and η_{20} are complex or real coefficients defining the different orders of harmonics. Following the definition proposed by Ikeda (1984), the bar height H_{BM}^* is given as the difference between the maximum and minimum of bed elevation:

$$H_{BM}^* = D_0^* \big(\max(\eta) - \min(\eta) \big) \tag{2.36}$$

Moreover, a simple expression for the bar height can be derived:

$$H_{BM}^* = D_0^* \left[b_1 \left(\frac{\beta - \beta_{cr}}{\beta_{cr}} \right)^{\frac{1}{2}} + b_2 \left(\frac{\beta - \beta_{cr}}{\beta_{cr}} \right) \right], \tag{2.37}$$

neglecting the third order terms in the bar amplitude solution and considering $\beta < 2\beta_{cr}$. The two coefficients b_1 and b_2 are complicated functions of θ_0 and d_s, although their dependence on these parameters is relatively smooth. The trend of b_1 and b_2 with respect to θ_0 and d_s can be found in the Fig. 5 of Colombini et al. (1987).

Relation (2.37) shows that the equilibrium bar height scales with the channel water depth, D_0^*, as observed in the field. Moreover, the bar height is related with the difference between the channel aspect ratio and the critical threshold β_{cr}.

The difference between maximum and minimum of bed elevation is a suitable metric to quantify the magnitude of the bar wave when the purpose is to estimate the maximum scour occurring in the channel, η_M^*, defined by Colombini et al. (1987) as:

$$\eta_M^* = 0.57\, H_{BM}^*, \tag{2.38}$$

but it presents limitations if you must compare theoretical predictions with field measurements, due to the difficulty to individuate the sections of maximum scour in real rivers. In Chapter. 4 a more extensive discussion about the analysis of suitable metrics to quantify the height of bars is proposed.

Finally, the weakly nonlinear approach allows for the approximation of the linear migration speed:

$$\omega_0 = \omega_{cr} - \epsilon\alpha_{1I} \tag{2.39}$$

and for the definition of the nonlinear one, by including the nonlinear correction by means of the A_{eq}^2 term:

$$\omega = \omega_{cr} - \epsilon\left[\alpha_{1I} + A_{eq}^2\,\alpha_{2I}\right] \tag{2.40}$$

where ω_{cr} is the linear migration rate computed in the critical conditions.

2.3 ALTERNATE BAR THEORY UNDER UNSTEADY FLOW CONDITIONS

The evolution of alternate bar amplitude under unsteady flow can be predicted by means of the weakly nonlinear theory of Tubino (1991), which solves the 2D SWE system of equations in a straight channel with erodible bottom, for given values of the channel width W, downstream gradient S and grain size d_{50}. This model is an extension of the above-described weakly nonlinear model for steady flow conditions of Colombini et al. (1987) to an individual flood event. Discharge variations are accounted for analytically through a perturbation approach, linearizing the flood around a reference discharge value $\overline{q}_0$ (hereinafter overlined variables are related to the reference state). The reference state uniquely identifies the average speed and flow depth $\overline{U}_0^*$ and $\overline{D}_0^*$, which allow the computation of the instantaneous average speed U_0^* and flow depth D_0^* as:

$$U_0^* = \overline{U}_0^*\,U_0(\zeta), \quad D_0^* = \overline{D}_0^*\,D_0(\zeta) \tag{2.41a,b}$$

in which ζ is the dimensionless time variable describing the flow variations within an individual flood event, defined as:

$$\zeta = \sigma^*\,t^*, \tag{2.42}$$

where σ^* represents the characteristic dimensional timescale of the flood event. The characteristic time of the unsteady basic state implies the dependence of β, θ_0 and d_s to ζ; in particular β decreases during the rising stage of the flood, making the system decreasingly unstable. In sight of this, it can happen that this parameter falls in the stable region close to the peak, returning to the unstable state during the decreasing stage.

In a dimensionless form, the flood timescale is given by:

$$\sigma = \frac{\sigma^* W}{2\,\overline{U}_0^*}, \tag{2.43}$$

which represents the ratio between the average time required by the flood wave to move along the channel and its period and can be assumed much smaller than 1.

The weakly nonlinear approach, similarly to the steady case of Colombini et al. (1987), provides the perturbation of the average aspect ratio $\overline{\beta}$ in the neighborhood of the critical conditions β_{cr}, related to the reference state, by means of a small amplitude ϵ:

$$\overline{\beta} = \beta_{cr}(\overline{\theta}_0, \overline{d}_s)(1+\epsilon). \tag{2.44}$$

Assuming also the unsteadiness to be weak ($\delta \ll 1$), the flow discharge per unit width can be written as:

$$\frac{q_0(\zeta)}{\overline{q}_0} = \left[1 + \delta q_{01}(\zeta)\right]. \tag{2.45}$$

where q_{01} is the unsteady component of q_0 with respect to the reference state $\overline{q}_0$.

The above assumptions allow for an analytical solution of the problem, by means the linearization of the basic flow variables into steady and unsteady components:

$$U_0 = 1 + \delta U_{01}(\zeta) + \mathcal{O}(\delta^2) \tag{2.46a}$$

$$D_0 = 1 + \delta D_{01}(\zeta) + \mathcal{O}(\delta^2) \tag{2.46b}$$

with the unsteady components given by:

$$U_{01} = \left(1 - \frac{2}{3 - C_D}\right) q_{01}, \qquad D_{01} = \frac{2}{3 - C_D}\, q_{01} \tag{2.47a,b}$$

in which:

$$C_D = \left[\frac{1}{c}\frac{\partial c}{\partial D}\right]_{\overline{d}_s} \tag{2.48}$$

represents the variation of the friction coefficient with respect to the water depth at the reference state.

Relations (2.46a,b) allow to calculate the variation of the aspect ratio β during the flood event as:

$$\beta \simeq \overline{\beta}\left[1 - \delta D_{01}(\zeta)\right] + \mathcal{O}(\delta^2). \tag{2.49}$$

The solution must be expanded in power series of the two parameters $\epsilon^{1/2}$ and δ, similarly to eq. (2.22). Following the same procedure implemented for the steady case of Colombini et al. (1987), substituting the solution of unknowns into the equation system (2.4−2.7), a solubility condition, similar to 2.32, can be found:

$$\frac{dA}{dT} = A\left[\overline{\alpha}_1 + \overline{\alpha}_0 \Delta q_{01}(\zeta)\right] + \overline{\alpha}_2 A|A^2|, \tag{2.50}$$

where $\overline{\alpha}_0$ is an additional complex parameter with respect to eq. (2.28) expressing the unsteadiness effect of the basic flow and $\Delta \sim \mathcal{O}(1)$ is the ratio between δ and ϵ. Here, the coefficients $\overline{\alpha}_0$, $\overline{\alpha}_1$ and $\overline{\alpha}_2$ must be referred to the reference state, hence they are function of $\overline{\theta}_0$ and $\overline{d}_s$ only. It is worth noticing that the coefficient of the first order term of eq. (2.50) provides a measure of the linear bar growth rate of bars, Ω_0, which can be defined as:

$$\Omega_0 = \overline{\epsilon}\left[\overline{\alpha}_1 + \overline{\alpha}_0 \Delta q_{01}(\zeta)\right] = \overline{\Omega}_0 + \overline{\epsilon}\,\overline{\alpha}_0 \Delta q_{01}(\zeta), \tag{2.51}$$

where $\overline{\Omega}_0$ is the weakly nonlinear approximation of the growth rate (eq. 2.29) computed at the reference state and $\overline{\epsilon} = \epsilon(\overline{\theta}_0, \overline{d}_s)$.

The amplitude function can be written in the form:

$$A = |A(T)| \exp\left[i\omega_1(T)\right], \tag{2.52}$$

where ω_1 represents the phase. By eq. (2.52) we can rewrite eq. (2.50) as function of the dimensionless time ζ:

$$\frac{d|A|}{d\zeta} = \frac{1}{\widehat{U}}\left\{\left[1 + \Delta\frac{\overline{\alpha}_{0R}}{\overline{\alpha}_{1R}} q_{01}(\zeta)\right]|A| + \frac{\overline{\alpha}_{2R}}{\overline{\alpha}_{1R}}|A|^3\right\} \tag{2.53}$$

and compute the angular frequency:

$$\frac{d\omega_1}{d\zeta} = \frac{1}{\widehat{U}}\left[\frac{\overline{\alpha}_{11}}{\overline{\alpha}_{1R}} + \Delta\frac{\overline{\alpha}_{01}}{\overline{\alpha}_{1R}}q_{01}(\zeta) + |A|^2\frac{\overline{\alpha}_{21}}{\overline{\alpha}_{1R}}\right] \tag{2.54}$$

The unsteadiness parameter $\widehat{U}$ represents the ratio between the time scale of the flood and the time scale of the bar growth, computed at the reference state:

$$\widehat{U} = \frac{\sigma}{\overline{\Omega}_0}. \tag{2.55}$$

The main result of the model is that the effect of the flood on the bar amplitude depends exclusively on the parameter $\widehat{U}$, which classifies three different situations:

- $\widehat{U} \gg 1$: the flood timescale is too short to allow for bar evolution, therefore:

$$\frac{d|A|}{d\zeta} \simeq 0. \tag{2.56}$$

- $\widehat{U} \ll 1$: the flood timescale is sufficiently long to allow for bars to achieve the equilibrium amplitude configuration given by:

$$|A| = A_T = A_{eq}\left[1 - \Delta F\, q_{01}\right]^{\frac{1}{2}}, \tag{2.57}$$

  where A_{eq} is computed as eq. (2.32) with coefficients referred to the reference state and:

$$F(\overline{d}_s, \overline{\theta}_0) = -\frac{\overline{\alpha}_{0R}}{\overline{\alpha}_{1R}}. \tag{2.58}$$

- $\widehat{U} \sim \mathcal{O}(1)$: the bar and flood timescales have the same order of magnitude, so that bars can evolve during the flood event, but the equilibrium configuration is not achieved. Below the solution for this case is briefly explained.

The procedure proposed by Tubino (1991) can be summarized in the following steps, starting from the portion of hydrograph that exceeds the threshold for motion, defined as q_i. Variables are made dimensionless considering a reference basic state ($\overline{U}_0^*$ and

$\overline{D}_0^*$) and an error procedure is used for satisfying the following two conditions:

$$\overline{\epsilon} = \frac{\overline{\beta} - \beta_{cr}(\overline{\theta}_0, \overline{d}_s)}{\beta_{cr}(\overline{\theta}_0, \overline{d}_s)} = \delta \tag{2.59}$$

to identify the reference discharge value:

$$\overline{q}_0 = \frac{q_i}{1-\delta}, \tag{2.60}$$

which allows the computation of the q_{01} function, needed to quantify the growth rate of bars:

$$q_{01} = \frac{\frac{q_0}{\overline{q}_0} - 1}{\delta}. \tag{2.61}$$

At this point, computing the unsteadiness parameter $\widehat{U}$, the parameter F and the final value A_{TF} of the equilibrium amplitude, by substituting $\Delta = 1$ and $q_{01} = -1$ in eq. (2.57), the actual amplitude of the perturbation is given by:

$$|A| = A_{TF}\left\{\frac{\exp\left[\int_0^\zeta G(\xi)d\xi\right]}{2\widehat{U}^{-1}(1+F)\left[\int_0^\zeta \exp\left[\int_0^\Upsilon G(\xi)d\xi\right]d\Upsilon\right] + A_0^{-2}}\right\}^{\frac{1}{2}} \tag{2.62}$$

with $G(\xi) = 2\widehat{U}^{-1}(1-F)\,q_{01}(\xi))$ and ξ and Υ are dummy variables. Alternatively, the actual bar amplitude can be computed numerically, by integrating eq. (2.53).

Following the Tubino (1991) theory, the nonlinear bar migration speed of eq. (2.40) is modified as follow:

$$\omega = \omega_{cr}(\overline{\theta}_0, \overline{d}_s) - \overline{\epsilon}\left[\overline{\alpha}_{11} + q_{01}\overline{\alpha}_{01} + A_{TF}^2\,\overline{\alpha}_{21}\right] \tag{2.63}$$

in which coefficients are computed at the reference state.

2.4 CONCLUSIONS

The analytical theories of Colombini et al. (1987) and Tubino (1991) provide, among other, well-established methods for modelling the evolution of alternate bars under steady and unsteady flow conditions respectively. In this PhD thesis we take advantage of these models to investigate the response of alternate bars

to actual flow series, by considering the effect that a wide range of discharges have in modifying the pattern of bars.

In the following chapters, we will provide an innovative interpretation of theoretical results by analysing the model response to the complex flow sequencing that characterises the natural forcing of the flow regime in rivers.

3

EQUILIBRIUM RESPONSE OF ALTERNATE BARS TO DISCHARGE VARIATIONS

3.1 INTRODUCTION

The weakly nonlinear theory of Colombini et al. (1987) is able to provide a good representation of equilibrium bar properties under steady flow conditions. However, the steady flow assumption is a too strong approximation if the purpose is to investigate the response of alternate bars in rivers, since the flow discharge varies in time, mainly depending on the rainfall or the snow-melting process. The unsteadiness of the flow regime poses an open issue concerning the formative discharge related to alternate bars, whose definition cannot be separated from the analysis of bar response to discharge variations. Indeed, once a large range of discharges is explored by the river, the application of the weakly nonlinear theories requires to carefully consider some aspects. First, the values of the channel aspect ratio can highly vary up to values for which the theoretical model is pushed at its limit (i.e. far from the critical condition). Specifically, for increasing values of the channel aspect ratio, the nonlinear effects tend to be progressively more important (Colombini and Tubino, 1991), requiring a deeper analysis to correctly interpret the weakly nonlinear results. Second, the competition of alternate bars with higher modes can also occur, with a consequent potential development of central or multiple bars (e.g., Rodrigues et al., 2015).

For this reason, in this chapter the theory of Colombini et al. (1987) is applied to a channel with fixed geometry for different discharge conditions, in order to describe the variation of equilibrium properties. It is worth noting that the purpose of the following analysis is not to analyse the unsteady response of alternate bars to a single flood event as proposed by Tubino (1991), but rather to investigate the equilibrium response to the different stages of typical flood events.

3.2 DEFINITION OF NEW DIMENSIONLESS PARAMETERS

The investigation of alternate bars in straight channels depends on the average properties of the flow field and sediment transport, whose characterisation requires the definition of three dimensionless parameters. The classical approach, as followed by Colombini et al. (1987), considers β, θ_0 and d_s as the suitable dimensionless parameters to describe the main properties of bars depending on the discharge conditions (see Chapter 2 for further details). However, to analyse how the equilibrium bar properties of alternate bars vary with the discharge in a real study case, in which channel width and slope and median grain size can be reasonably fixed, it is convenient to define different dimensionless quantities, since in the definition of β, θ_0 and d_s the hydraulic parameters (which depend on the discharge) are mixed with geometrical quantities and grain size. Therefore, we introduce:

$$\widehat{W} = \frac{W}{d_{50}}, \qquad S, \qquad \widehat{Q} = \frac{Q}{\sqrt{g\, d_{50}^5}}, \tag{3.1a-c}$$

representing the channel width $\widehat{W}$, scaled with the sediment size, the channel slope S and the discharge $\widehat{Q}$ made dimensionless as in Parker et al. (2007). In this way, the dependence of the water discharge is isolated in $\widehat{Q}$, while $\widehat{W}$ and S does not depend to the hydraulic conditions and are uniquely defined for a given channel. Typical values of these parameters in gravel bed rivers are $\widehat{W} = 10^2 - 10^4$, $S = 10^{-2} - 10^0$ % and $\widehat{Q} = 10^2 - 10^7$ (e.g., Parker et al., 2007).

In many cases it is useful to consider the dimensionless discharge per unit channel width, namely:

$$\widehat{q} = \frac{Q}{W\sqrt{g\, d_{50}^3}}, \tag{3.2}$$

in order to reduce the variability in a range $10 - 10^4$. The two definitions of eqs. (3.1c) and (3.2) are related trough the dimensionless channel width as $\widehat{Q} = \widehat{W}\,\widehat{q}$.

The above definition of dimensionless parameters in eq. (3.1) allows us to investigate the dependence of classical parameters

β, θ_0 and d_s with respect to the discharge variation. Rodrigues et al. (2015) computed these parameters for a specific case in the Loire River, while here we generalize the analysis with respect to the new dimensionless parameters. In general, the dependence of the classical parameters to $\widehat{W}$, S and $\widehat{q}$ can be summarized as:

$$\beta = f(\widehat{W}, S, \widehat{q}), \tag{3.3a}$$

$$\theta = f(S, \widehat{q}), \tag{3.3b}$$

$$d_s = f(S, \widehat{q}), \tag{3.3c}$$

where f identifies a generic function. Specifically, by applying the uniform flow condition, we can compute eq. (3.3) as:

$$\beta = \frac{\widehat{W}}{2}\left(\frac{c_0\sqrt{S}}{\widehat{q}}\right)^{\frac{2}{3}}, \tag{3.4a}$$

$$\theta = \frac{1}{R}\left(\frac{\widehat{q}\,S}{c_0}\right)^{\frac{2}{3}}, \tag{3.4b}$$

$$d_s = \left(\frac{c_0\sqrt{S}}{\widehat{q}}\right)^{\frac{2}{3}}. \tag{3.4c}$$

which can be made explicit by expressing the resistance coefficient c_0 with a power law (i.e. not with the logarithmic relation of eq. 2.11). Figs. 3.1 and 3.2 show the dependence of the classical parameters β, θ_0 and d_s on the discharge per unit width, considering the uniform flow conditions for a rectangular cross section channel.

The increment of discharge implies that the uniform Shields parameter θ_0 increases (Fig. 3.1a), while the relative roughness decreases because of the increment of the flow depth (Fig. 3.1b). Moreover, increasing the channel slope has the twofold effect of increasing the bed shear stress and reducing the water depth, such that both θ_0 and d_s increase.

The main parameter that controls the response of alternate bars to discharge variations is the aspect ratio, which invariably decreases with respect to the water discharge (Fig. 3.2). Therefore, increasing the water discharge enhances the stability of the channel, due to the reduction of the aspect ratio. Conversely, for given discharge conditions (i.e. at fixed $\widehat{q}$), β increases by increasing both $\widehat{W}$ and S. However, the response of bars depends on the

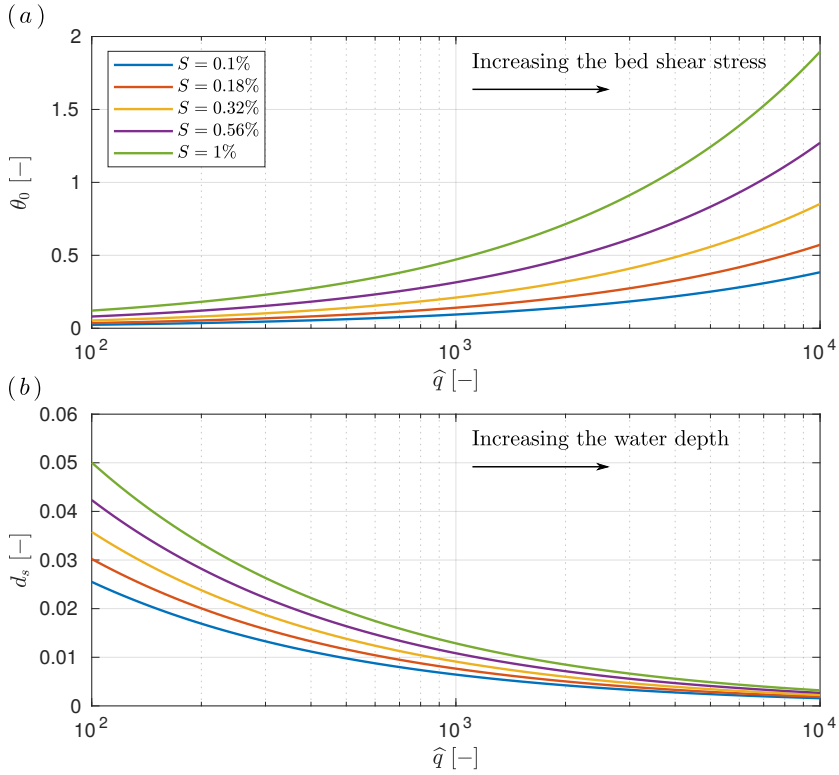

Figure 3.1. Variation of classical parameters θ_0 (a) and d_s (b) with respect to the discharge for different values of channel slope.

difference $\beta - \beta_{cr}$ rather than on the absolute value of the aspect ratio. Therefore, in the following we provide the variation of the critical aspect ratio and the difference $\beta - \beta_{cr}$ with respect to the water discharge. It is worth noticing that the critical threshold is a function of θ_0 and d_s (Colombini et al., 1987), hence it depends only of S and $\hat{q}$ (see eq. 3.3).

Fig. 3.3 reveals a general increasing trend of β_{cr} with flow discharge, thus supporting the increasing stability of the channel with increasing water discharge, though at large $\hat{q}$ values β_{cr} reaches a maximum and then starts decreasing. The role of the channel slope differs for low or high discharge values. Specifically, for high discharge values, the higher the slope, the lower the value of β_{cr}, while for low discharge values the opposite trend occurs, due to the fact that the higher channel slope allows for sediment motion at lower discharge values. The difference

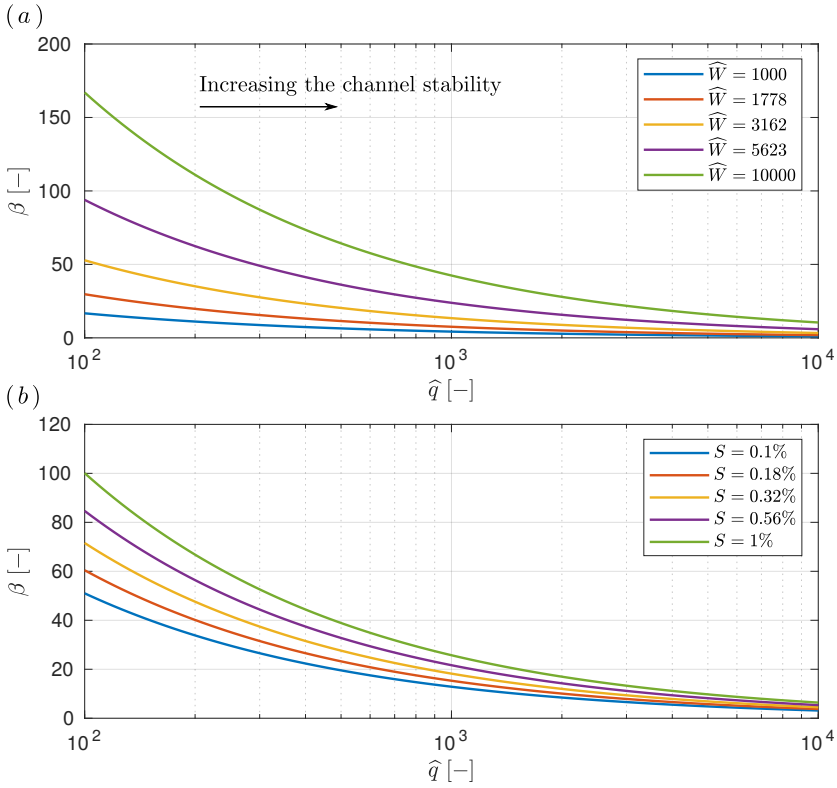

Figure 3.2. Variation of β with respect to the flow discharge for different values of $\widehat{W}$ (a) and S (b). We consider S = 0.25 % in panel (a) and $\widehat{W} = 4000$ in panel (b).

$\beta - \beta_{cr}$, shown in Fig. 3.4, is a decreasing function with respect to the water discharge, meaning that the propensity of the channel to form bars decreases. Indeed, once the channel aspect ratio becomes smaller than the critical one, bar formation is not allowed according with Colombini et al. (1987) theory, although the riverbed is not necessarily plane (in Chapter 4 we briefly discuss about diagonal bars).

In the next section we provide an interpretation of the main characteristics of alternate bars (i.e. bar height, bar growth rate and bar celerity) with respect to the dimensionless discharge $\widehat{q}$.

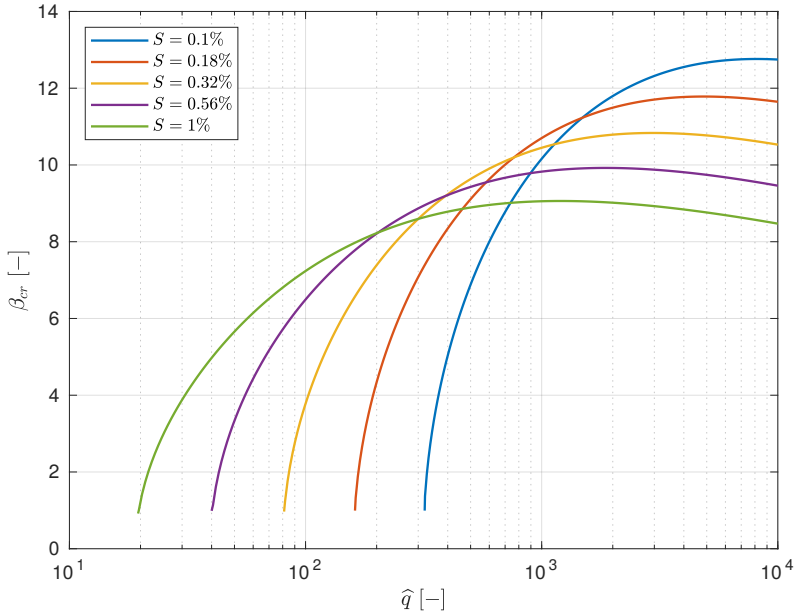

Figure 3.3. Critical aspect ratio β_{cr} with respect to the discharge for different values of the channel slope.

3.3 BAR CHARACTERISTICS

3.3.1 *Bar height*

According to the weakly nonlinear theory of Colombini et al. (1987), the dimensionless bar height, scaled with the mean flow depth, mainly depends on the perturbation parameter ϵ defined as:

$$\epsilon = \frac{\beta - \beta_{cr}}{\beta_{cr}}, \tag{3.5}$$

since the bed configuration is derived by the superimposition of harmonics computed at different orders (i.e. $\mathcal{O}(\epsilon^{1/2})$ and $\mathcal{O}(\epsilon)$ in eq. 2.34).

From the curves of $\beta - \beta_{cr}$ reported in Fig. 3.4 it is evident that the perturbation parameter is a decreasing function of flow discharge. Since the critical aspect ratio is at the denominator of the ratio, we expect that ϵ tends to infinity for low discharge values.

Bar height has been computed accordingly with the definition proposed by Ikeda (1984) as the difference between maximum

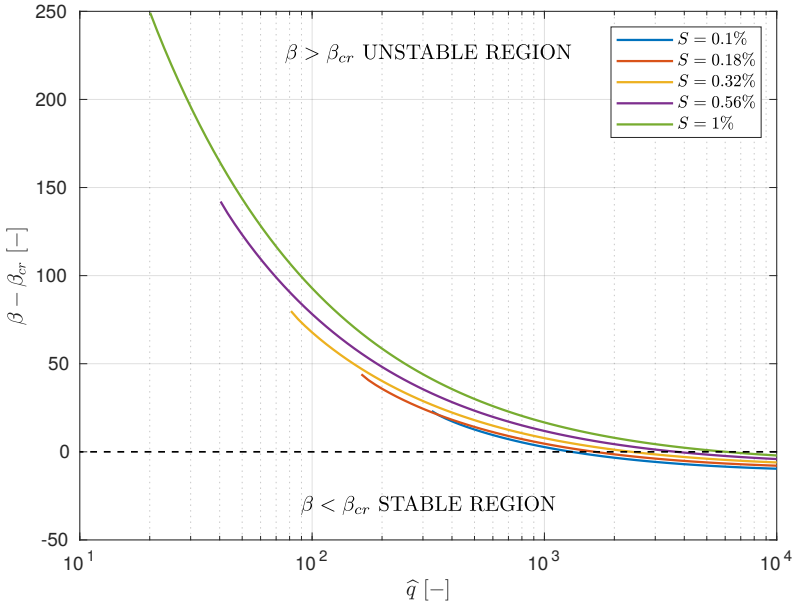

Figure 3.4. Difference between β and β_{cr} with respect to the discharge for different values of the channel slope. Such quantity, which divided by β_{cr} represents the perturbation parameter ϵ, provides a measure of the amplitude of bars.

deposit and minimum scour in the bed topography (see eq. 2.37) and scaled with respect to the median grain size, to be consistent with the new dimensionless parameters. Specifically:

$$\widehat{H}_{BM} = \frac{H^*_{BM}}{d_{50}} = \frac{H_{BM}}{d_s}. \tag{3.6}$$

In Fig. 3.5 the variation of the equilibrium bar height with the discharge is reported for different values of $\widehat{W}$ (panel a) and S (panel b). Curves are truncated at values of discharge corresponding to $\epsilon = 2$, accordingly with the consideration of Colombini et al. (1987) for which the theory is convergent for $\epsilon \sim \mathcal{O}(1)$, despite the strict definition of validity for $\epsilon \ll 1$.

The decreasing trend of bar height with increasing values of discharge allows us to identify a particular condition of discharge for which bar height vanishes, hereinafter called *critical discharge for bar formation* or simply *critical threshold*, $\widehat{q}_{cr}$. This discharge value corresponds to the condition for which $\beta = \beta_{cr}$ (i.e. $\epsilon = 0$) and it is properly discussed in Section 3.4.2.

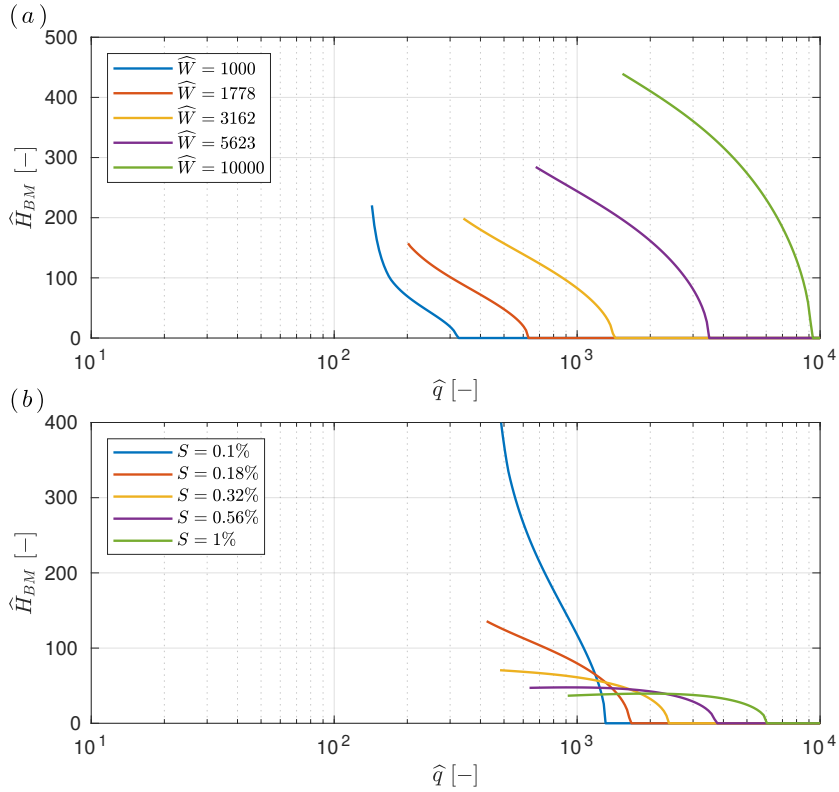

Figure 3.5. Equilibrium height of bars predicted by the Colombini et al. (1987) weakly nonlinear theory for different values of $\widehat{W}$ (a) and S (b). We consider S = 0.25 % in panel (a) and $\widehat{W} = 4000$ in panel (b).

From Fig. 3.5a it is evident that the larger the channel width, the larger the critical threshold, and, consequently, the larger the range of discharges for which alternate bars have an equilibrium amplitude. Moreover, this aspect suggests that by increasing the width of the channel, the propensity of the river bed to organize itself in alternating pattern also increases, being high the expected topographic expression and large the range of discharges for which alternate bars are expected to form.

A similar response can be found also increasing the channel slope (Fig. 3.5b), since the larger the channel slope, the larger the range of discharges for which the equilibrium bar height is theoretically predicted. However, curves of $\widehat{\mathrm{H}}_{\mathrm{BM}}$ computed at different slopes present a less regular trend. Specifically, they (i)

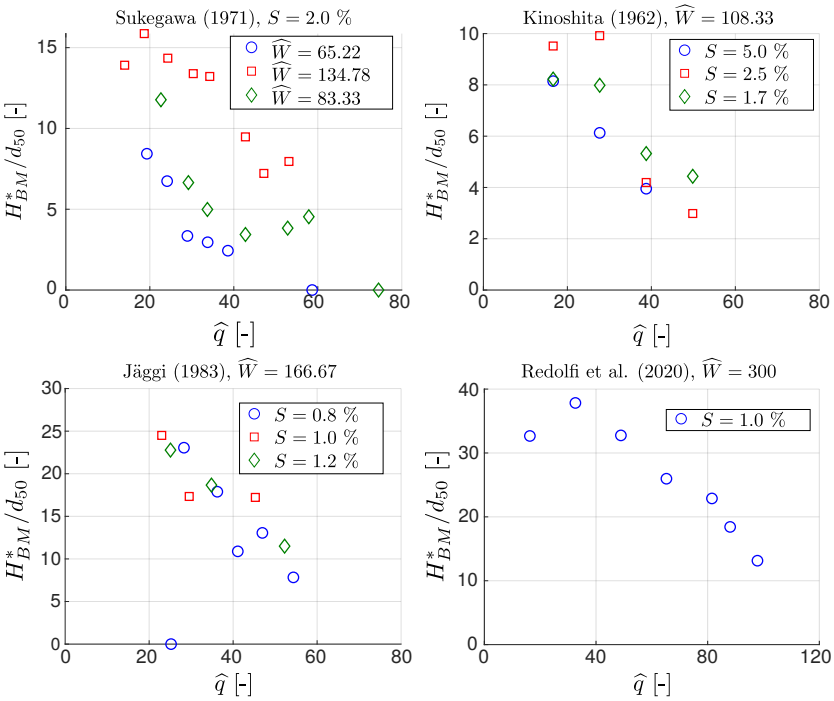

Figure 3.6. Relationship between the equilibrium bar height and the unit discharge resulting from the laboratory experiments of Kinoshita (1961), Sukegawa (1971), Jäggi (1983) and Redolfi et al. (2020) for a wide range of dimensionless channel width $\widehat{W}$ and slope S.

cross for low discharges and (ii) show a general non-monotonic response by increasing the value of channel slope. Such trend is probably due to the high values of the Shields parameter achieved for steep channels.

To qualitatively confirm the theoretical result, we performed a reanalysis of existing laboratory experiments (see Fig. 3.6) for which the equilibrium bar properties (H^*_{BM}) are available for different geometrical characteristics of the channel and flow conditions. These data have been processed as follows:

- we have grouped experiments having the same channel width and sediment size, and a similar slope (with maximum deviation from the median value of 20 %); each group is represented in Fig. 3.6, in terms of $\widehat{W}$ and S parameters, with a different marker;

- we have only considered groups that encompassed at least three distinct discharge values.

For almost all groups of experiments reported in Fig. 3.6 a relatively sharp decline of bar height with increasing flow discharge is displayed, accordingly with the shape of theoretical curves of bar height. At this stage, a direct comparison between experimental data and theoretical results is not performed, being the purpose of this chapter to investigate the essential response of Colombini et al.'s (1987) theory to discharge variation. A theoretical prediction of experimental observations is provided in Chapter 4.

The aforementioned decreasing trend of bar height with respect to the water discharge highlights a first peculiarity in alternate bar response to discharge variations, which differentiates bar behaviour from other morphological characteristics. Indeed, increasing the discharge value, the topographical response of alternate bars reduces until vanishing at the critical threshold, above which alternate bars are not expected to form (if discharges are applied steadily for a sufficient long time). Hence, in the definition of a formative discharge for alternate bars we must take into account that relatively large discharge values are mainly responsible for providing a channel flat bed configuration rather than of developing alternate bar patterns. Conversely, classical approaches in determining the formative conditions of a river in terms of its equilibrium geometry, tend to attach great importance to discharge values sufficiently large to model the morphology of the channel due to the nonlinear relationship between water discharge and sediment discharge (e.g., the bankfull discharge, Pickup and Warner, 1976).

3.3.2 *Bar growth rate*

A key parameter to determine the effectiveness of a given discharge value to produce alternate bar pattern is the linear bar growth rate, Ω_0, whose reciprocal provides the dimensionless timescale of bar evolution, T_{bar}:

$$T_{bar} = \frac{1}{|\Omega_0|}. \tag{3.7}$$

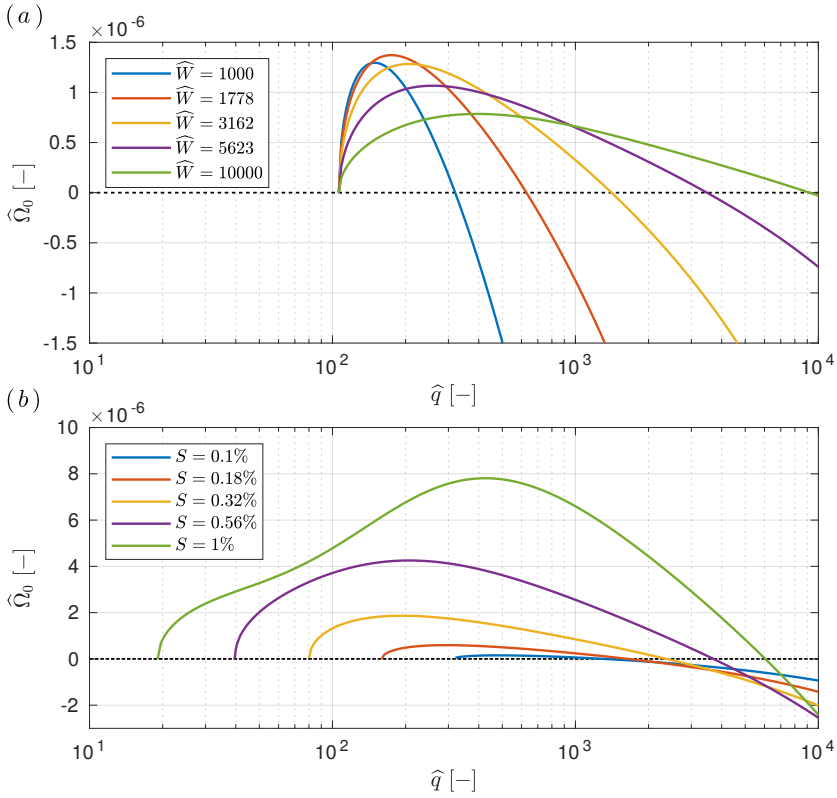

Figure 3.7. The linear growth rate of free alternate bars as a function of water discharge for different values of $\widehat{W}$ (a) and S (b). The critical threshold $\widehat{q}_{cr}$ discriminates between bar-forming ($\widehat{\Omega}_0 > 0$) and bar-suppressing ($\widehat{\Omega}_0 < 0$) flow conditions. We consider $S = 0.25\,\%$ in panel (a) and $\widehat{W} = 4000$ in panel (b).

Here we consider the growth rate associated to the wavenumber of maximum amplification, λ_{max}, (i.e. corresponding to the peak of Ω_0 in Fig. 2.2). Similarly to the bar height, a timescale, T_d^*, related to the sediment size has been used to scale the growth rate, specifically $T_d^* = \sqrt{d_{50}\, g^{-1}}$. Hence:

$$\widehat{\Omega}_0 = \Omega_0 \frac{2\,\widehat{q}\,d_s}{\widehat{W}}. \tag{3.8}$$

As illustrated in Fig. 3.7, the growth rate $\widehat{\Omega}_0$ shows a non-monotonic dependency on water discharge, with a peak value that strongly depends on both the channel width $\widehat{W}$ and slope S. We note that the growth rate vanishes at two precise flow

conditions: (i) at the threshold for sediment motion (i.e. $\widehat{q} = \widehat{q}_i$), discriminating the discharge values which can produce morphological activity and (ii) at the critical threshold (i.e. $\widehat{q} = \widehat{q}_{cr}$), where the tendency to spontaneously form alternate bars becomes very weak. Trends described above are overall observed both varying $\widehat{W}$ and S. Nevertheless, the dependence of the growth rate with respect to the slope is twofold, since the larger S, the larger both (i) the range of discharges with positive growth rate and (ii) the absolute value of the peak of the curve, while the larger $\widehat{W}$ the larger the discharge range, but not the peak value.

While the threshold for motion is a common parameter appearing in most river morphodynamic processes, the critical threshold for bar formation is a specific characteristic of free alternate bars, due to their instability mechanism. The key role of the critical threshold is that it distinguishes two different responses of the riverbed to discharges lower or larger than the threshold. In particular, for discharge values larger than the critical threshold the growth rate is negative and the riverbed tends to be stabilized, because of the damping of small amplitude waves that can rise from flow disturbances. This result underlines that discharge stages can have two opposite effects on bar evolution, depending on their position with respect to the critical threshold.

With the decreasing trend of bar height, this second characteristic of bar growth rate is peculiar of alternate bars, which are not primarily governed by the timescale of the sediment transport, T^*_{exn}, (i.e. determined by the Exner equation and exclusively influenced by the threshold for motion), but have a proper evolution timescale governed by the instability mechanism of formation (eq. 3.7). Indeed, the timescale of sediment transport becomes shorter for increasing discharge values, while bar timescale tends to infinity in the neighborhood of the critical threshold (i.e. the growth rate tends to zero). The Exner timescale, which represents the time required by the sediment transport to form a deposit of depth equal to D^*_0 over an area of $W \times W$ (see Garcia Lugo et al., 2015, for a similar definition), is given by:

$$T^*_{exn} = \frac{W D^*_0 (1-p)}{\Phi_0 \sqrt{g R d^3_{50}}}. \tag{3.9}$$

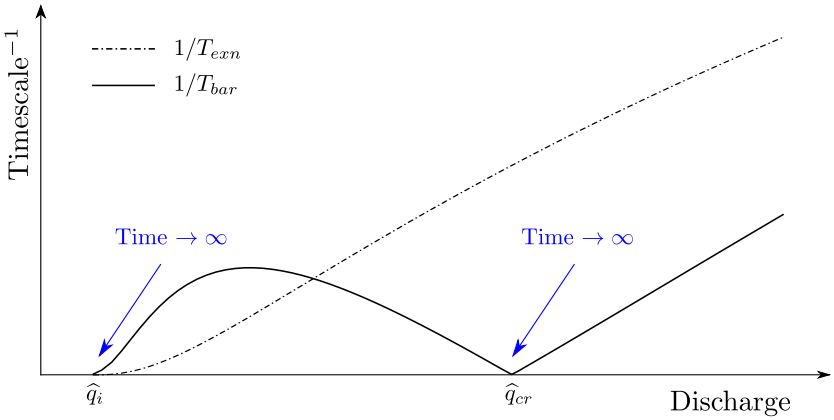

Figure 3.8. Qualitative comparison between the linear growth rate of bar and the reciprocal of the Exner timescale, typical of the sediment transport process. While increasing the discharge value, the timescale of sediment transport becomes shorter, the timescale of bar evolution tends to infinity in the neighborhood of the critical threshold.

The difference between the Exner and the bar timescales is qualitatively shown in Fig. 3.8, where the linear growth rate of bars is compared with the reciprocal of the sediment transport timescale. The Exner timescale is made dimensionless through the hydrodynamic timescale $W\,(2\,U_0^*)^{-1}$.

3.3.3 *Bar migration rate*

The migration of free bars represents one of the main problems affecting river management in terms of navigation and interaction with instream structures. The linear analysis of Colombini et al. (1987) provides the quantification of the angular frequency, ω_0, which is further approximated by the weakly nonlinear model (eq. 2.39) and corrected taking into account the nonlinear effects (eq. 2.40). Similar to the bar growth rate, we consider the angular frequency associated with the wavenumber of maximum amplification, λ_{max}. Considering the scaling factor for the velocity dependent on the sediment diameter, $U_d^* = \sqrt{g\,d_{50}}$, we can write the dimensionless bar celerity as:

$$\widehat{C} = \frac{\omega_0}{\lambda_{max}}\,\widehat{q}\,d_s. \tag{3.10}$$

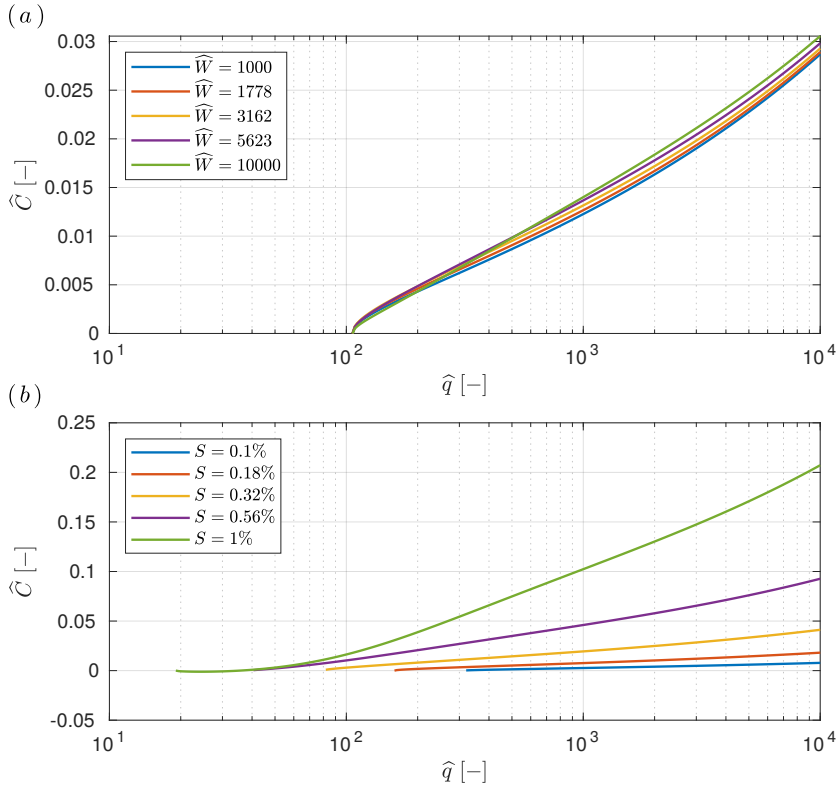

Figure 3.9. The linear migration rate of free alternate bars as a function of water discharge for different values of $\widehat{W}$ (a) and S (b). Negative values of celerity identify the upstream migration of bars. We consider S = 0.25 % in panel (a) and $\widehat{W} = 4000$ in panel (b).

In Fig. 3.9 the dimensionless bar celerity is computed for different values of $\widehat{W}$ and S in panels (a) and (b) respectively, providing an increasing trend in both cases. Moreover, we can notice that the celerity of bars is almost independent of the channel width, while it strongly depends of the channel slope. This is due to the fact that bar celerity depends of the bed shear stress, which is a function of the channel slope (i.e. it increases by increasing the channel slope), but not of the channel width. In panel (b), for the largest values of slope the celerity becomes slightly negative when the discharge approaches the incipient condition, being the angular frequency negative too. Specifically, a negative angular frequency identifies the condition of upstream migration of alternate bars as the most unstable. However, upstream migrat-

ing bars are rarely observed in rivers because such condition of negative angular frequency usually occurs under flow stages for which other effects could become dominant, as, for example, the emersion of bars.

3.4 THRESHOLD VALUES OF DISCHARGE

From the above considerations, it is evident that the response of alternate bars strongly depends on the values of flow discharge being smaller or larger than specific threshold values. Specifically, in this section we investigate the trend of the aforementioned threshold for motion and critical threshold with respect to different channel characteristics $\widehat{W}$ and S. In addiction, considering that the height of bars tends to increase when the flow discharge gets smaller, we introduce a third threshold value of discharge corresponding to the condition of bar height for which the emersion occurs (i.e. the local value of water depth vanishes). Finally, some considerations about other distinctive characteristics of bars are briefly reported.

3.4.1 *Incipient motion*

The sediment motion in gravel bed rivers is a threshold process, which requires a minimum bed shear stress to start the particle transport. It is evident that all the morphological processes are influenced by this threshold value, including alternate bars, since no sediment transport occurs for lower values of discharge. The quantification of the threshold value θ_i is not trivial, being dependent on many variables related for example to grain properties, flow field strength and bed armouring (Johnson, 2016), but it is fundamental to describe the sediment transport rate by means of deterministic relations as Meyer-Peter and Muller (1948); Parker (1978); Wong and Parker (2006). However, the variety of grain shape and size, and the particle clustering that spontaneously form in the riverbed complicate the application of empirical relations calibrated on the basis of laboratory experiments (Brayshaw, 1985), since the threshold for motion is not uniquely determined.

Nevertheless, for the purpose of this work we consider the incipient discharge, $\widehat{Q}_i$, as the value of discharge providing a

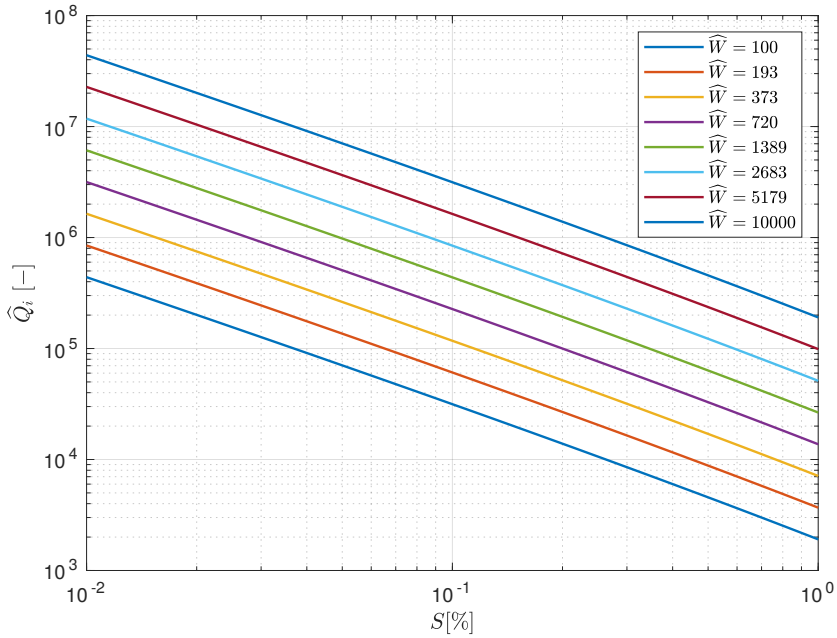

Figure 3.10. Dimensionless discharge corresponding to the threshold for motion $\widehat{Q}_i$ with respect to the channel slope S for different values of $\widehat{W}$.

Shields parameter in a rectangular channel equal to the incipient condition, given by:

$$\widehat{Q}_i = \widehat{W}\left[6 + 2.5\log\left(\frac{\theta_i R}{2.5 S}\right)\right]\frac{(\theta_i R)^{\frac{3}{2}}}{S}. \tag{3.11}$$

It is worth noticing that the dimensionless discharge per unit width is independent on $\widehat{W}$, meaning that $\widehat{Q}_i = \widehat{W}\,\widehat{q}_i$.

The variation of the threshold for motion has been computed with respect to the channel slope for a typical range of the dimensionless channel width $\widehat{W}$ as shown in Fig. 3.10. We can notice an opposite trend: increasing the channel slope the minimum flow discharge required for the incipient motion decreases while increasing the channel width the threshold for motion increases too.

We note that the behaviour of alternate bars in the neighborhood of the threshold for motion is hard to model with the Colombini et al. (1987) theory, due to the strong variation of

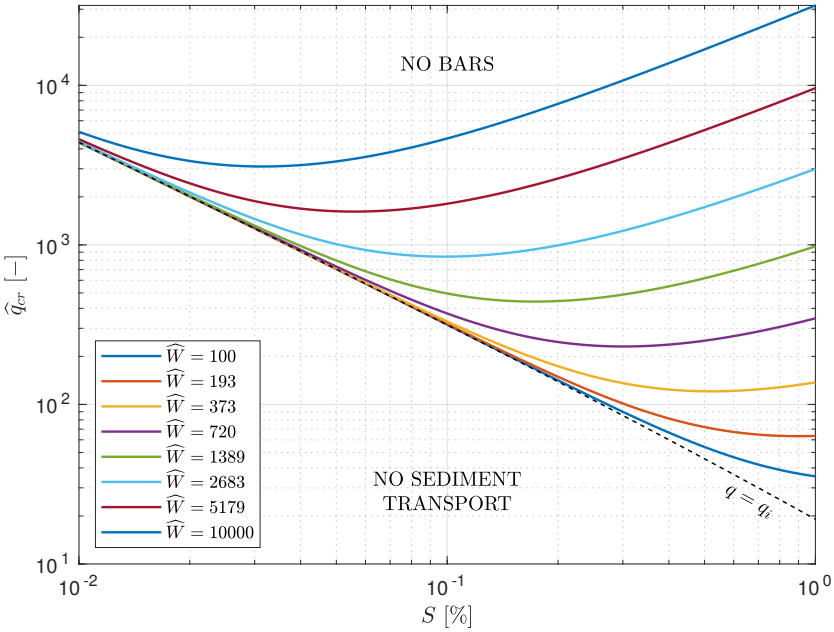

Figure 3.11. Critical threshold for bar formation $\widehat{q}_{cr}$, expressed per unit channel width, with respect to the channel slope S for different values of $\widehat{W}$ (plane bed, $r = 0.3$).

parameters α_{1R} and α_{2R} that determine the amplitude of bars. In particular, both the coefficients tend sharply to zero and nonlinear effects become predominant, reducing the validity of the weakly nonlinear theory.

3.4.2 *Critical discharge for bar formation*

The critical discharge associated with bar formation, $\widehat{q}_{cr}$, is a key parameter to investigate the response of alternate bars to discharge variations, since it identifies the maximum water discharge able to provide bar evolution if steadily applied in a channel with rectangular section.

To analyse the effect of channel slope and width to the critical threshold, we consider the same range of S and $\widehat{W}$ implemented for the threshold for motion, obtaining the plot of Fig. 3.11. As we can expect, as the channel slope gets smaller all the curves tend to the asymptotic condition represented by the threshold for

motion $\widehat{q}_i$, which is the lowest limit to have morphological evolution. A non-monotonic trend characterises the critical threshold, which presents a minimum significantly close to the incipient discharge value. This aspect can be explained considering the trend of the critical aspect ratio β_{cr} with respect to the Shields parameter θ_0 (Fig. 2.4), which sharply decreases approaching the threshold for motion. This means that the difference between β and β_{cr} increases, as well as the propensity of the channel to form bars. Since the relation between the channel slope and the uniform Shields parameter is of linear proportionality (i.e. $\theta = S\,D^*/(R\,d_{50})$, the trend of Fig. 3.11 is reasonable.

We can suppose that the closer the critical threshold to the threshold for motion, the lower the propensity of the channel to form alternate bars, being narrow the discharge range for which the equilibrium bar height is expected.

3.4.3 *Fully-wet condition*

As already mentioned, the perturbation parameter ϵ is a measure of the magnitude of bar height, which must be small due to the weakly nonlinear assumption of small perturbation (Colombini et al., 1987). However, it was found that this assumption is not so strict and the weakly nonlinear theory provides a good agreement with experimental results also for $\epsilon \sim \mathcal{O}(1)$ (e.g., Colombini et al., 1987). Nevertheless, it appears evident that for low discharge values (close to the threshold for sediment motion), the theory predicts a bar height that progressively tends to infinity, due to the strong increment of the perturbation parameter. This prediction is totally devoid of physical foundation, since it is proved that bars achieve a finite height also for low flows (see for example experimental results of Fig. 3.6). Moreover, bars can evolve only if sediment transport is allowed, meaning that the cross section must be at least completely wet. Therefore, the physical emersion of bars, whose modelling is far from trivial (Siviglia et al., 2013; Adami et al., 2016), cannot be treated by means of the weakly nonlinear model of Colombini et al. (1987), since the domain on which the theory is defined becomes unconnected.

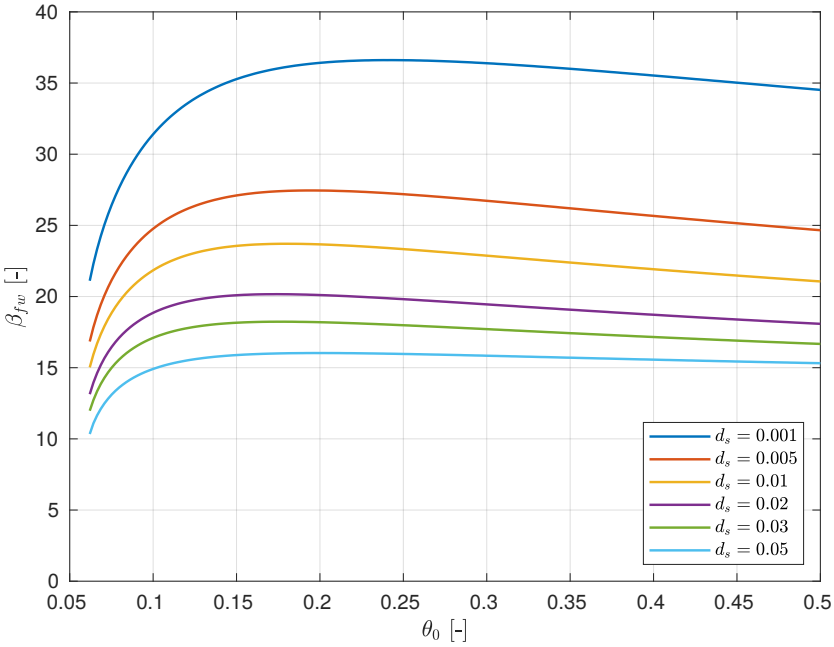

Figure 3.12. Aspect ratio corresponding to the condition of emersion as function of the Shields parameter θ_0 for different values of the relative roughness d_s.

Interpreting this condition in terms of the classical parameters of the Colombini et al. (1987) theory consists of the computation of the aspect ratio corresponding to the emersion conditions, β_{fw}, as function of the Shields parameter θ_0 for different values of roughness d_s (see also Vignoli and Tubino, 2004). From result shown in Fig. 3.12 we note that the emersion condition is almost independent on the Shields parameter and it decreases by increasing the relative roughness. This inverse dependence of β_{fw} with respect to the relative roughness and the non-monotonic trend are found also for the critical aspect ratio β_{cr} (see Fig. 2.4), but β_{fw} is always larger than β_{cr}.

Here we investigate the emersion condition in terms of the new dimensionless parameters, specifically by means of the discharge per unit width, hereinafter called *fully-wet* threshold, $\widehat{q}_{fw}$, identifying the minimum discharge value for which bars are always submerged and can evolve according to the weakly nonlinear theory of Colombini et al. (1987). In Fig. 3.13 the trend

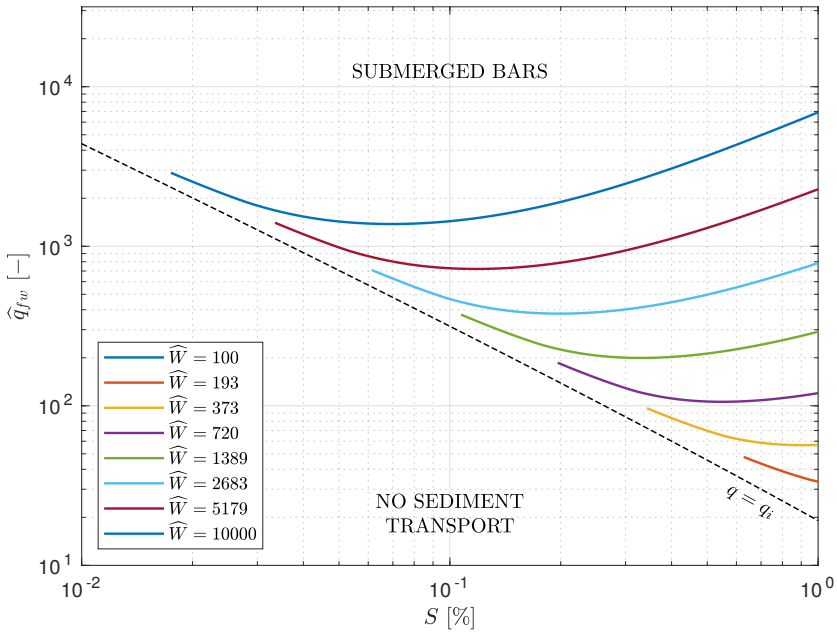

Figure 3.13. Fully-wet threshold, $\widehat{q}_{fw}$, defining the emersion condition, expressed per unit channel width, with respect to the channel slope S for different values of $\widehat{W}$.

of the fully-wet discharge per unit channel width is plotted versus the channel slope S for different widths $\widehat{W}$. It is evident that the fully-wet threshold is defined in the range between the threshold for motion and the critical discharge. The larger the channel width, the larger the minimum water discharge required to always submerge bars.

Differently from the critical threshold, curves in Fig. 3.13 do not reach the threshold for motion, because such values of $\widehat{W}$ and S represent conditions in which bars are always emerged. This is the reason for which the fully-wet discharge referred to $\widehat{W} = 100$ never occurs for the investigated range of slopes.

The fully-wet threshold highlights the incapability of the Colombini et al. (1987) theory to predict a reasonable value of bar amplitude for discharges between the threshold for motion and the fully-wet threshold. Specifically, it poses a lower limit for the validity of the Colombini et al. (1987) theory, which allows for the definition of bar height in the range of discharges between $\widehat{q}_{fw}$ and $\widehat{q}_{cr}$. It is worth noticing that the aforementioned lower

limit could not be strict, being the bedform evolution during the emersion conditions affected by mechanisms that exceed theoretical assumptions, including for example the absence of wet and dry algorithms in the model formulation and the non-vanishing bar amplitude. Nevertheless, such fully-wet threshold allows for identifying a limiting condition in the range of parameters (i.e. $\widehat{W}$, S and $\widehat{q}$) for which the theoretical prediction can be reasonably used, providing a useful criterion to critically analyse theoretical results.

The importance of this instrument becomes evident considering that approaching the problem of alternate bars at a river reach scale means that for the most of the year a typical alpine river experiences low flow conditions, usually of the order of magnitude of the incipient threshold. Therefore, it is important (i) to identify the discharge value over that the theoretical prediction is far to be good and (ii) to quantify the response of riverbed in terms of bar amplitude also in the range of discharge in which the theory is not strictly valid, at most in an approximate way. The latter purpose will be treated in Chapter 4.

3.4.4 *Considerations about thresholds*

The response of bars is found to be characterised by specific threshold values (i.e. the critical threshold for bar formation and the fully-wet threshold) that make the analysis different from that of other river properties, such as the average width or slope.

A further consideration is needed with respect to the mechanism of competition among higher order bar modes with alternate bars (Tubino et al., 1999), usually occurring for large values of the channel aspect ratio (i.e. for low discharge values, reasonably in the range between the threshold for motion and the fully-wet threshold). For example, Jaballah et al. (2015) found that central bars are predominant in the Arc River at low flow stages with respect to alternate bars. Although a clear threshold to distinguish the most unstable bar mode is not provided here, we discuss this aspect in Chapter 6 by proposing a criterion to predict when multiple bars are preferred to alternate bars in the morphological pattern of a river.

Finally, it is worth noticing that various theories for river bars and meandering have highlighted the important role played by the so-called *resonant threshold* in discriminating between different styles of planform evolution of meandering rivers (Seminara et al., 2001; Lanzoni and Seminara, 2006; Frascati and Lanzoni, 2009; Zolezzi et al., 2009; Monegaglia et al., 2019) as well as between prevailing upstream or downstream development of steady bars due to localized perturbations of channel geometry (Zolezzi and Seminara, 2001; Mosselman et al., 2006). The term "resonant" refers to the resonant behaviour of the linear solution for flow and bed topography in meanders with periodic curvature distribution that was originally discovered by Blondeaux and Seminara (1985). Such condition represents a point of convergence between river bars and meanders, because at resonance the curvature of the channel axis excites a natural alternate-bar mode of oscillation of bed topography, the main difference between the two phenomena being that meander point bars are quasi-steady. The interaction between free and forced bars and the role of resonance in their competition has been widely discussed in the literature (e.g., Nelson, 1990; Tubino and Seminara, 1990; Garcia and Niño, 1993). However, this aspect goes beyond the purpose of the present work, which is mainly focussed on the development of migrating bars in regulated river reaches.

3.5 CONCLUSIONS

The analysis of the equilibrium response of bar properties at different discharge states allows to highlight some distinctive characteristics of alternate bars:

1. The response of the equilibrium bar height to increasing flow discharge is described by a curve that sharply decreases to zero. This aspect highlights a first difference of bar behaviour with respect to other morphological characteristics of a river as the equilibrium slope or width of the channel. Indeed, increasing the discharge value, the topographic expression of the riverbed reduces until vanishing at the critical threshold, $\widehat{q}_{cr}$ (i.e. the discharge value for which β equals β_{cr}).

2. The critical threshold for bars, $\widehat{q}_{cr}$, is a key parameter for defining the upper discharge value for which alternate bars are expected to form accordingly with the Colombini et al. (1987) weakly nonlinear model. For discharge values larger than the critical threshold the instability mechanism governing bar occurrence is inhibited.

3. The characteristic timescale of bar evolution, provided by the linear bar growth rate, underlines a different role played by discharges lower or larger than the critical threshold for bar formation, which respectively amplify or damp the perturbation waves triggered in the channel. Therefore, the height of a bar can be modified by the sequences of flood events occurring in the hydrological history of the channel.

4. The fully-wet threshold, $\widehat{q}_{fw}$, identifies the lower limit for which the Colombini et al. (1987) theory is strictly valid. The typically large frequency of occurrence of low flows in rivers (i.e. discharge values lower than the fully-wet threshold) requires the estimation of a reasonable bar amplitude in the range of discharges between $\widehat{q}_i$ and $\widehat{q}_{fw}$.

4

MORPHOMETRIC PROPERTIES OF ALTERNATE BARS AND WATER DISCHARGE

This chapter is based on the paper: Redolfi, M., M. Welber, M. Carlin, M. Tubino, and W. Bertoldi (2020), Morphometric properties of alternate bars and water discharge: a laboratory investigation, Earth Surface Dynamics, 8(3), 789–808, https://doi.org/10.5194/esurf-8-789-2020.

4.1 INTRODUCTION

A number of investigations (e.g. Kinoshita, 1961; Sukegawa, 1971; Parker, 1976; Fredsoe, 1978; Fujita and Muramoto, 1982; Siviglia et al., 2013) demonstrated that bar occurrence is a spontaneous phenomenon due to an instability mechanism of the cohesionless bed. Due to this autogenic formation mechanism, this kind of bed morphology is often referred as "free bars" (Seminara and Tubino, 1989). The Colombini et al. (1987) theory, described in Section 2.2, provides the quantification of equilibrium properties of bars under steady flow conditions if the width-to-depth ratio of the channel, β, is larger than the critical threshold β_{cr}. Conversely, if the channel is relatively narrow (i.e. $\beta < \beta_{cr}$), gravitational effects tend to damp the small, periodic perturbation of the riverbed, inhibiting bar formation.

However, the critical threshold β_{cr} does not represent a sharp distinction between equilibrium bar pattern and plane bed, since other bed features may result from other instability mechanisms. Specifically, Colombini and Stocchino (2012) described diagonal bars as short, shallow, and fast-migrating three-dimensional bedforms that are easily confused with alternate bars due to their diagonal fronts.

Although the equilibrium properties of alternate bars were long investigated, a systematic description of how these properties depend on the water discharge is still to a certain extent unexplored. From a theoretical point of view, as shown in Chapter 3 the governing parameters of the theoretical formulation

depend on the water discharge, making the flow discharge a crucial ingredient to describe changing in riverbed response. Moreover, three particular values of discharge (i.e. the threshold for motion, the critical threshold and the fully-wet condition) are fundamental to physically interpret theoretical results. The purpose of this chapter is to investigate the equilibrium response of Colombini et al. (1987) theory to discharge variations, providing the interpretation of theoretical predictions by means of experimental results performed at different discharge conditions. Specifically, the approach presented in Chapter 3 for interpreting the Colombini et al.'s (1987) theory has been tested with a set of laboratory experiments.

4.2 METHOD

The theory of Colombini et al. (1987) has been applied to a set of laboratory experiments conducted in a 24 m long flume with constant geometrical characteristics at the Hydraulics Lab of the University of Trento. Theoretical predictions have been compared with experimental results in terms of bar height (by means of different metrics), bar shape and bar migration rate.

For the present analysis, we considered the Parker (1978) relation for the sediment transport and the logarithmic friction formula of Engelund and Fredsoe (1982), as in the original formulation of Colombini et al. (1987). Sediment porosity was set to the typical value of 0.40 while the empirical parameter r of eq. (2.14) was calibrated by minimizing the difference between experimental and analytical values of H^*_{BM}, resulting in a value of 0.27.

To highlight the dependence of bar properties to the characteristic thresholds previously mentioned, a new dimensionless discharge has been defined:

$$\widetilde{\Delta Q} = \frac{Q - Q_{cr}}{Q_{cr} - Q_i}, \tag{4.1}$$

so that values from -1 to 0 cover the entire range of bar formation from the threshold for sediment motion Q_i to the critical threshold Q_{cr}.

4.2.1 *Experimental configuration*

The physical model consisted in a straight channel of width $W = 0.305\,\mathrm{m}$, with vertical banks built out of plywood covered by a thick plastic tarp. Uniform sand with a median diameter of $d_{50} = 1.01\,\mathrm{mm}$ was used as feed and bed material. A set of 16 steady flow runs was performed, with discharge ranging from $Q = 0.5$ to $4.2\,\mathrm{l\,s^{-1}}$, to ensure a sufficiently wide range of channel aspect ratio. At the beginning of each run the flume bottom was graded to a slope $S = 0.01$.

The experimental results used for the comparison with theoretical predictions have been obtained as follows:

- The bed topography was detected at the end of each run by means of laser surveys (vertical accuracy of $0.1\,\mathrm{mm}$ and spatial resolution of $50\times5\,\mathrm{mm}$, longitudinal and transverse directions, respectively) and the resulting Digital Elevation Model (DEM) was detrended by subtracting the average longitudinal slope.

- To allow for the comparison of bar shape, in order to filter out the relatively small differences of single bar units, the spatial coordinates of each bar DEM were scaled by the bar wavelength and the channel width, and then re-sampled in a regular grid of 64×64 points, which allowed the definition of the "ensemble bar" of the channel as the average bar topography. The ensemble bars computed for each discharge value were used to compare the different metrics of bar height and bar shape resulting from the theory.

- The migration rate of the alternate bars was estimated by tracking the position of up to 15 individual bar fronts at fixed time intervals.

The main characteristics of the experiments are summarized in Table 4.1.

4.2.2 *Metrics on bar height*

The magnitude of bars can be measured in different ways, depending on the available instruments and the purpose of the

Table 4.1. Summary data from the laboratory experiments. Channel width, slope, and median grain size are constant and equal to $W = 0.305\,\mathrm{m}$, $S = 1.0\,\%$, and $d_{50} = 1.01\,\mathrm{mm}$, respectively. The water depth, Froude number, Shields number, and aspect ratio are computed by assuming uniform flow conditions over a plane bed and considering the friction formula in eq. (2.11).

Experiment #			1	2	3	4	5	6	7	8	9
Discharge	Q	$[\mathrm{ls}^{-1}]$	0.5	1.0	1.5	2.0	2.5	2.7	3.0	3.4	4.2
Dimensionless discharge	$\widetilde{\Delta Q}$	[–]	−0.94	−0.81	−0.68	−0.55	−0.42	−0.36	−0.28	−0.18	0.03
Water depth	D_0^*	[cm]	0.72	1.06	1.34	1.58	1.79	1.87	1.99	2.14	2.42
Froude number	F_0	[–]	0.86	0.96	1.02	1.06	1.09	1.10	1.12	1.13	1.17
Shields number	θ_0	[–]	0.043	0.064	0.080	0.095	0.108	0.113	0.120	0.129	0.145
Aspect ratio	β	[–]	21.3	14.4	11.4	9.7	8.5	8.1	7.7	7.1	6.3
Critical aspect ratio	β_{cr}	[–]	2.6	4.1	4.8	5.3	5.7	5.8	6.0	6.1	6.4

investigation. For example, if the DEM is available as the output of laboratory investigation, the difference between the maximum and minimum elevation within a bar unit can be easily computed after removing the mean bed slope (i.e. the definition of H^*_{BM} proposed by Ikeda, 1984). Conversely, the same measure of bar height in a channelized river can hardly be made, due to the difficulty of identifying the section with the maximum scour, which is usually not aligned with the top of the bar. For this reason, different metrics can be found in literature and in the following we deal with it in detail. A dimensional notation is implemented.

Fujita and Muramoto (1985), similarly to Ikeda (1984), proposed a definition of bar height based on the difference between the maximum and minimum elevation along transverse cross sections (H^*_{Bsec}) in a bar wavelength. The corresponding value of bar height is given by the maximum value obtained among the individual cross sectional measures (H^*_B). This definition can be synthesized by the following notation:

$$H^*_{Bsec} = \max_{sec}(\eta^*) - \min_{sec}(\eta^*) \tag{4.2a}$$

$$H^*_B = \max\left(H^*_{Bsec}\right) \tag{4.2b}$$

where $\max_{sec}$ and $\min_{sec}$ denote the maximum and minimum elevation along individual cross sections.

In spite of their clear physical meaning, the above definitions are based on the extreme elevation values, and therefore they are susceptible to measurement errors and outliers. For this reason, it is sometimes convenient to analyse the topography of bars through different metrics, considering the relief rather than the height of bars. To do that, we can compute the standard deviation (here termed std) of the elevation distribution:

$$SD^*_\eta = std(\eta^*), \tag{4.3}$$

or the bed relief index BRI^* (e.g. Hoey and Sutherland, 1991; Lièbault et al., 2013):

$$BRI^*_{sec} = std_{sec}(\eta^*) \tag{4.4a}$$

$$BRI^* = mean(BRI^*_{sec}), \tag{4.4b}$$

where std_{sec} and BRI^{*}_{sec} denote the standard deviation and the bed relief index of a single cross section of the elevation map respectively.

4.2.3 *Bar shape and migration rate*

As shown in Section 2.2, the weakly nonlinear solution of the riverbed is determined by superimposing first and second order harmonics and considering their respective spatial lag. The analysis of single components provides the spatial arrangement of the bedform, and allows us to quantify the dominant harmonic of the pattern (in general the first harmonic, which identifies the alternate pattern).

To obtain synthetic information about the spatial structure of experimental topographies, the elevation maps have been analysed through the two-dimensional Fourier transform (e.g., Garcia and Niño, 1993; Zolezzi et al., 2005), determining the amplitude of the first and second harmonics.

A further method to quantify the shape of the bed topography in terms of the asymmetry of the bed elevation distribution is via the skewness parameter (SK), which provides information on the relative proportion of high and low areas within a bar. Riverbed elevation maps often show negative skewness, with deep, narrow channels carved into large, higher-elevation bars (e.g., Bertoldi et al., 2011; Garcia Lugo et al., 2015).

Finally, the migration rate of bars, C^{*}, is computed by dividing the weakly nonlinear solution for the angular frequency (see eq. 2.40) with the critical wavenumber, λ_{cr}.

4.3 RESULTS

4.3.1 *Bar height*

The values of the equilibrium bar height predicted by the weakly nonlinear theory with respect to the water discharge are reported in Fig. 4.1. We note that the decreasing trend of bar height experimentally observed is reproduced by the theory. Bar height vanishes for a discharge value of $4.11\,\mathrm{l\,s^{-1}}$, which

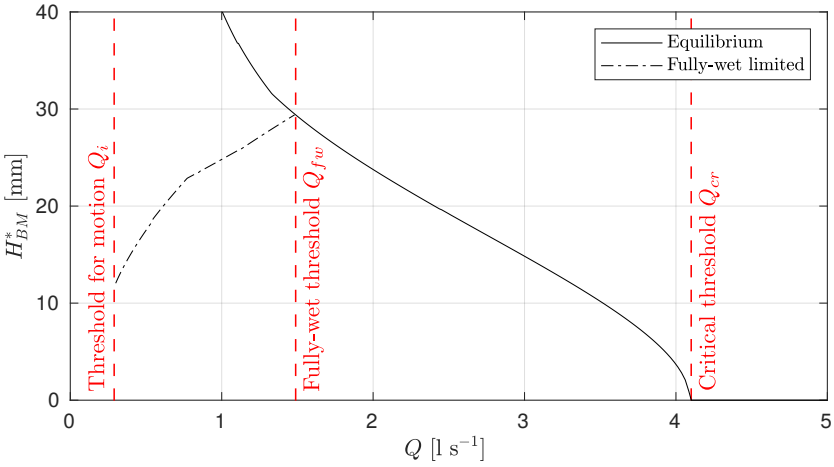

Figure 4.1. Bar amplitude as function of water discharge according to the Colombini et al. (1987) theory, with the solid lines indicating equilibrium conditions and the dash-dot lines representing the bar height limited by the fully-wet condition. The discharge for incipient motion, the fully-wet condition and the critical threshold are highlighted by vertical dashed lines.

represents the critical threshold, Q_{cr}, above that bars are not expected to form.

As discussed in Chapter 3, the weakly nonlinear theory is formally valid near the critical conditions, although the comparison with experimental data suggests its applicability within a wider range of conditions (Colombini et al., 1987; Lanzoni, 2000a). Therefore, we identified the fully-wet discharge, $Q_{fw} = 1.49\,\mathrm{l\,s^{-1}}$, which represents the lower limit at which the theory can provide a reasonable prediction of the equilibrium bar height. For lower values of discharge the system cannot achieve the equilibrium configuration of bar height, but it is limited to the emersion condition. The simplest and practical solution to this problem, in the absence of a suitable analytical solution, is to limit the amplitude of bar to the value at which it is submerged. This value of bar amplitude can be computed through a bisection method by seeking for conditions at which the minimum depth along the bar, as resulting from the weakly nonlinear model (eq. 2.33), is zero. This condition of emersion-limited bar height is represented by the dash-dot line in Fig. 4.1, which shows an

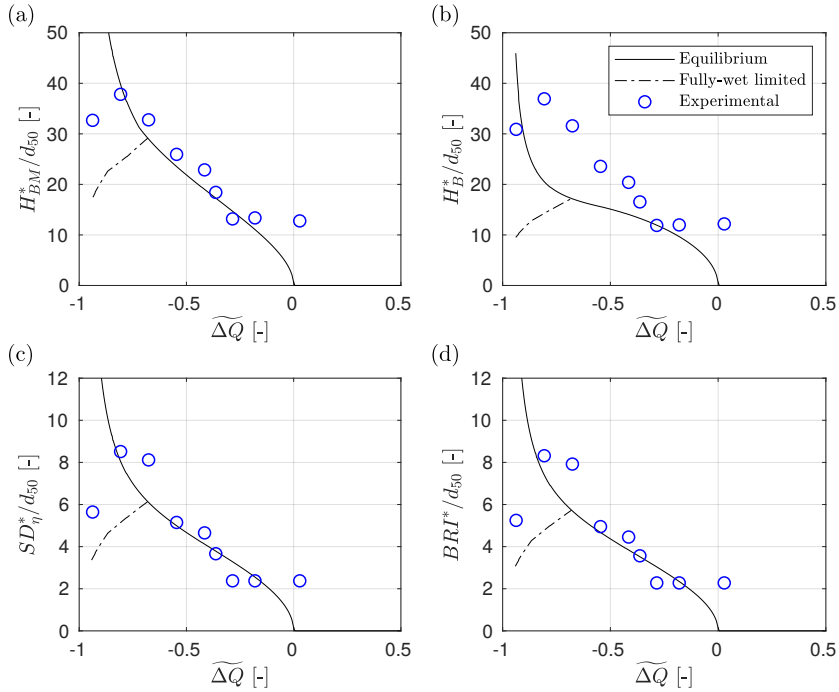

Figure 4.2. Dimensionless bar height as a function of the scaled discharge from theory (lines) and experiments (markers) for the different metrics. (a, b) Bar height and (c, d) bar relief of bed elevation distribution (scaled with the median grain size d_{50}), with the solid lines indicating equilibrium conditions and the dash–dot lines representing the bar height limited by the fully-wet condition.

increasing trend with respect to the discharge from the threshold for sediment motion ($Q_i = 0.26\,l\,s^{-1}$) to the fully-wet threshold.

The analytical model reproduces all the metrics implemented to quantify the height of alternate bars remarkably well (Fig. 4.2). Furthermore, we can notice that for discharges lower than the fully-wet threshold, Q_{fw}, the theoretical estimate of the emersion-limited bar height provides a reasonable prediction for the trend of the first two experimental points ($Q = 0.5\,l\,s^{-1}$ and $Q = 1.0\,l\,s^{-1}$, corresponding to $\widetilde{\Delta Q} = -0.94$ and $\widetilde{\Delta Q} = -0.81$ respectively), in spite of a slight underestimation. A major difference between predicted and measured value is obtained for the cross sectional bar height H^*_B, for which the theory provides a smoother decreasing trend with respect to the experiments, resulting in a underestimation of the metric.

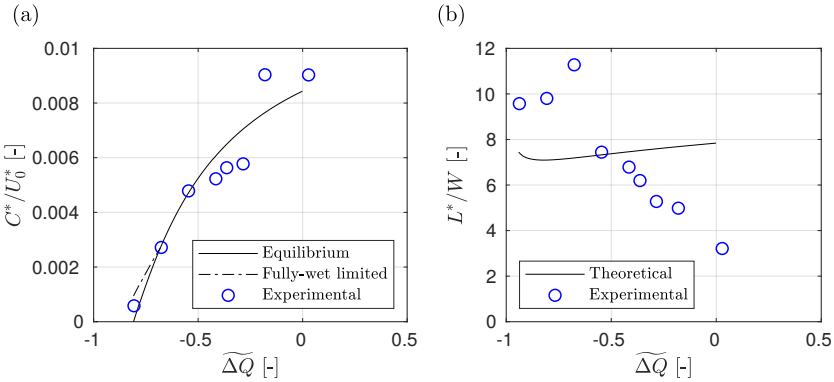

Figure 4.3. Dimensionless bar migration rate (a) and wavelength (b) as a function of the scaled discharge from theory (lines) and experiments (markers). Quantities are scaled with the flow velocity U_0^* and the channel width W, respectively.

4.3.2 *Bar migration and wavelength*

The migration rate of bars, scaled with the uniform flow velocity U_0^*, is reported in Fig. 4.3a. A good agreement between theoretical prediction and experimental values can be observed for both the overall trend and the absolute values, but for a slight overestimation of the observed values corresponding to $Q = 2.7\,l\,s^{-1}$ and $Q = 3.0\,l\,s^{-1}$ (i.e. $\widetilde{\Delta Q} = -0.36$ and $\widetilde{\Delta Q} = -0.28$ respectively) and a slight underestimation for the last two points. Moreover, approaching the condition of sediment motion, the predicted migration of bars tends to zero, in agreement with experimental results for discharges lower than $1.0\,l\,s^{-1}$ (i.e. $\widetilde{\Delta Q} = -0.81$). Similarly to the bar height, also for the migration rate the fully-wet limitation provides a good prediction of the experimental results, both quantitatively and qualitatively.

Furthermore, the theory properly predicts the wavelength of bars only for intermediate values of discharge (see Fig. 4.3b), while it does not capture the overall decreasing trend and therefore sharply underestimates the length of bars observed in the three runs with $Q \leqslant 1.5\,l s^{-1}$ ($\widetilde{\Delta Q} \leqslant -0.68$). This aspect is due to the fact that the weakly nonlinear model of Colombini et al. (1987) does not provide an equation for describing the evolution of bar wavelength, but it only considers the most unstable wavelength.

The gap in the model is supported by the fact that the marginal curve (see Fig. 2.3) is flat in the neighborhood of the critical conditions, highlighting how the choice of the actual length of bars is not a selective process (see for example Fig. 4 in Colombini et al., 1987, where theoretical bar wavelength is compared with a large database of experimental measurements). Therefore, the criterion of considering the wavenumber of maximum amplification is not necessarily representative for the channel, being the range of wavenumber corresponding to the critical conditions relatively large.

As mentioned before, for discharge values larger than the critical threshold (i.e. $\widetilde{\Delta Q} > 0$), the Colombini et al. (1987) theory predicts no bars in the flume, therefore the definition of bar celerity and wavelength is meaningless.

4.3.3 *Diagonal bars*

From the analysis of bar height and bar migration rate (Figs. 4.2 and 4.3 respectively) we can notice that bars observed in experiments performed at $3.4\,\mathrm{l\,s^{-1}}$ and $4.2\,\mathrm{l\,s^{-1}}$ (i.e. $\widetilde{\Delta Q} = -0.18$ and $\widetilde{\Delta Q} = 0.03$ respectively) are anomalous for three reasons: (i) they occur in the neighborhood of the limit of the region of bar formation (i.e., at $Q \simeq Q_{cr}$), (ii) they exhibit a much faster migration rate with respect to experiments performed at lower discharge, and (iii) their wavelength is much shorter with respect to the typically observed values ($L^* = 5 - 12\,W$; see Tubino et al., 1999). This type of bedforms closely resembles the diagonal bars described by Jaeggi (1984) as three-dimensional mesoforms characterised by a wavelength of around 3 times the channel width, limited relief, symmetrical elevation distribution, and the presence of shallow pools. These bedforms were observed at Froude numbers close to 1 and did not match the region for alternate bar formation. Experimental observations by Jaeggi (1984) suggested that diagonal bars can be considered intermediate bedforms associated with the transition of dunes from two- to three-dimensional configuration. This idea was confirmed by the theoretical work of Colombini and Stocchino (2012), which provided an interpretation of diagonal bars as three-dimensional oblique dunes, clearly distinct from alternate bars. Herein, we

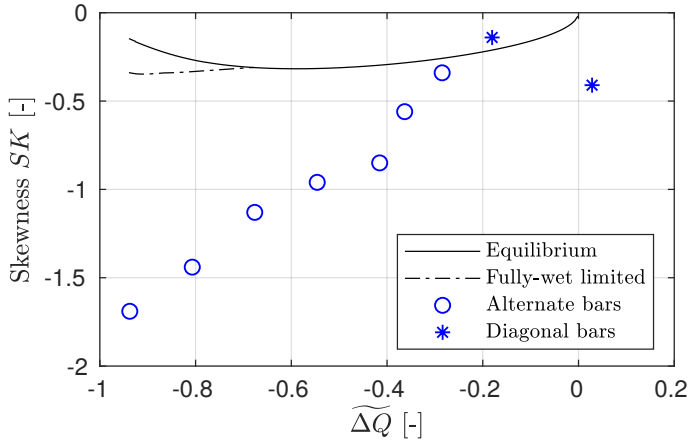

Figure 4.4. Skewness of the bed elevation distribution as a function of the scaled discharge. Markers indicate the skewness of the experimental ensemble bars; lines illustrate results from the weakly nonlinear theory, with the dash-dot line referring to the solution obtained by limiting the bar growth to the fully-wet condition.

will therefore refer to bars observed at $\widetilde{\Delta Q} \simeq 0$ as "diagonal bars", reserving the term "alternate bars" for the remaining cases.

4.3.4 *Bar shape*

We analysed the equilibrium response of the bar shape at different discharge stages by computing the skewness and the Fourier components of the predicted bar topographies for each discharge value, in order to quantify the bed asymmetry and the predominant harmonics (i.e. intended as the the harmonics in which the system allocates the highest quantities of energy).

Fig. 4.4 shows that the skewness, which has been computed starting from the mean and standard deviation values of the distribution of bar topographies, is always negative, indicating a left-tailed bed elevation distribution. Except for the lowest discharge values, the skewness has an overall trend that progressively increases with the flow discharge from -0.4 to almost vanishing values (i.e., nearly symmetrical bed elevation distribution) when approaching the critical condition for bar formation (i.e., $\widetilde{\Delta Q} \simeq 0$). Comparing the theoretical curve with the experiments, we observe a qualitative agreement since the trend is

captured by the theoretical model, but the measured topography is much more asymmetric than the predicted one (i.e. in absolute value the measured skewness is almost three times larger, matching typical values observed for wandering and braided channels, Garcia Lugo et al., 2015), highlighting the limited capability of the theoretical model to fully represent the complex, highly nonlinear morphodynamic processes (see Colombini et al., 1987). It is interesting to note that, differently from the equilibrium solution, the fully-wet limitation has a monotonic trend, providing an increment of the bed topography asymmetry for the lowest discharge values (i.e. the absolute value of the skewness is larger).

The weakly nonlinear theory of Colombini et al. (1987) resolves the first 2×2 modes of the Fourier spectrum, providing the first four harmonic components (see Fig. 4.5), identified by their transverse (m) and longitudinal (n) mode. In this representation, $m = 1$ indicates half a wave period in one channel width, while $n = 1$ indicates a complete sinusoidal period in one bar wavelength. Harmonic components with $m = 0$ and $n = 0$ are constant along the y and x axis, respectively.

Results in Fig. 4.5 clearly show that alternate bars are dominated by the fundamental component A^*_{11} (panel a), representing a double sinusoidal bed deformation, whose amplitude is larger than each component of the second order harmonic for all discharge values. Theoretical predictions reproduce fairly well experimental observations, at least for values of the flow discharge in the neighborhood of the critical threshold Q_{cr}. However, an overall underestimation of experimental results is found, mainly for discharge values in the neighborhood of the fully-wet threshold (i.e. $Q = 1.0$ and $1.5\,l\,s^{-1}$). Similarly to the metrics of bar height, the fully-wet limited curve is able to capture the experimental trend of the first two points.

The second order harmonic is given by the superimposition of three components, A^*_{20}, A^*_{02} and A^*_{22}. Specifically, (i) the component A^*_{20}, with longitudinal mode $n = 0$, is a sinusoidal symmetric bed deformation that is constant in x^*, see Fig. 2.1 for the reference system, (ii) the component A^*_{02}, with a transverse mode $m = 0$, is a purely longitudinal bed deformation and (iii)

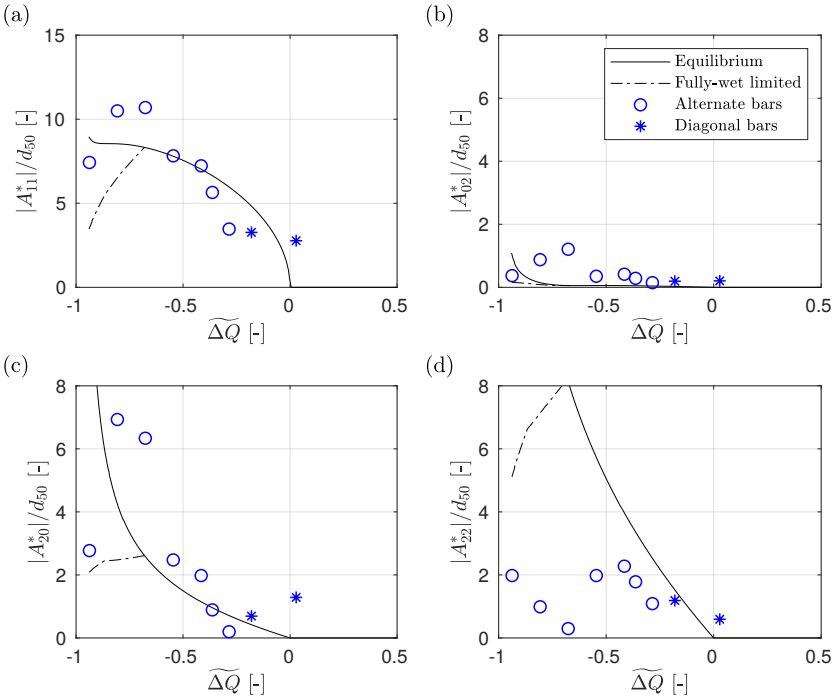

Figure 4.5. Amplitude of the first four Fourier components depending on the scaled discharge from theory (lines) and experiments (markers). (a) Amplitude of the fundamental component A^*_{11} scaled with the grain size d_{50}. (b, c, d) Amplitude of the individual second order components A^*_{02}, A^*_{20} and A^*_{22} scaled with the grain size d_{50}. The solid lines indicate theoretical results at equilibrium, while the dash-dot lines indicate theoretical results obtained by limiting the bar growth to the fully-wet condition.

A^*_{22} is a symmetric bed deformation that completes two periods in one bar wavelength.

From Fig. 4.5b we obtain that the predicted component A^*_{02} is much smaller than the others and turns out to be negligible, showing that the transversely averaged bed elevation is nearly zero for all the cross sections. Experimental observations confirm the theoretical predictions. Conversely, the two components A^*_{20} and A^*_{22} (panels c and d) are significantly larger than the component A^*_{02}, showing a very similar trend, with the component A^*_{22} almost the double of A^*_{02}.

Comparing the theoretical predictions with the observed values, we can see that the component A^*_{22} does not fit values in the

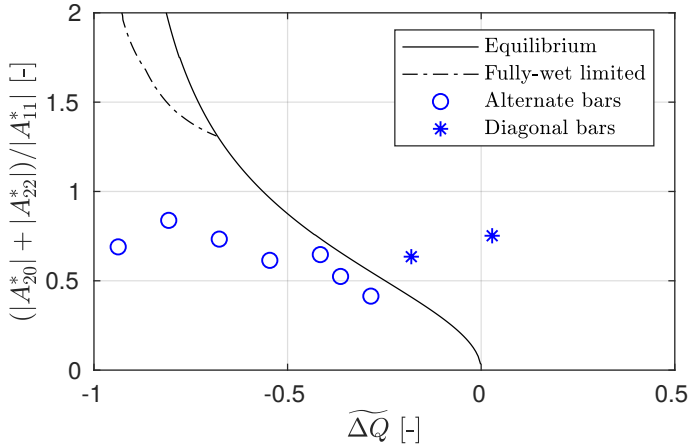

Figure 4.6. Sum of the $m = 2$ components A^*_{20} and A^*_{22} scaled with $|A^*_{11}|$ from theory (lines) and experiments (markers). The solid lines indicate theoretical results at equilibrium, while the dash-dot lines indicate theoretical results obtained by limiting the bar growth to the fully-wet condition.

neighborhood of the fully-wet condition, since measured values are much smaller than the predicted ones. Conversely, in the same range of discharges close to the fully-wet condition, the component A^*_{20} is found to be larger than A^*_{22} and the theoretical prediction better mimic the overall decreasing trend. Such results reveal that the mode-2 component is not dominated by the presence of regular, periodic central bars, as suggested by the theory, but it is mainly associated with a bell-shaped distortion of the average cross section (Fujita and Muramoto, 1985).

To investigate the overall importance of the $m = 2$ components (i.e. considering the dominant terms of the second harmonic) with respect to the fundamental one, we analyse the sum of the absolute values of the coefficients A^*_{20} and A^*_{22} scaled with the amplitude of the fundamental harmonic A^*_{11}. Fig. 4.6 shows that the theory provides a decreasing trend approaching zero near critical conditions (i.e. $\widetilde{\Delta Q} = 0$), which quite-well reproduces the general response of $m = 2$ observed components, despite its limited capability to quantify fully nonlinear interactions. Nevertheless, differently from theoretical predictions, experiments do not vanish when approaching the critical threshold. From a morphological point of view this implies that for $Q \to Q_{cr}$,

while "theoretical" bars tend to become purely sinusoidal (A^*_{11} component only) as the solution approaches its linear limit, observed bars retain a certain degree of nonlinearity, showing a $m = 2$ component that derives from the presence of clear diagonal fronts (i.e. diagonal bars). It is worth noticing that the theory underestimates the second harmonic and overestimates the first one (Fig. 4.5a), highlighting the alternate structure of bar pattern. In general, by considering the fully-wet limitation we observe a large overestimation of experimental results at low discharge values, despite the mitigation of extremely large values at the equilibrium.

4.4 DISCUSSION

4.4.1 *Discharge and bar height*

The decreasing trend of bar height with respect to the discharge, extensively discussed in Chapter 3, is confirmed by experimental observations, which are well reproduced by the weakly nonlinear theory both qualitatively and quantitatively. The inverse correlation with the sediment transport rate, which increases for increasing discharges, implies that the highest bars are formed by moderate floods, large enough to move sediments but sufficiently lower than the critical threshold Q_{cr}.

The capability of the theoretical model to reproduce the decreasing trend of bar height is a significant result, despite the calibration of the parameter r. It is worth noticing that experimental results show a non-monotonic variation of bar height with the discharge, since the first point ($Q = 0.5\,l\,s^{-1}$) is always lower than the second one ($Q = 1.0\,l\,s^{-1}$) for all the metrics considered. This behaviour can be fairly-well reproduced by the theoretical model if the emersion condition is accounted for and the fully-wet limitation of bar amplitude is computed. In spite of its approximate derivation, the fully-wet limitation can be considered a useful tool to extend the validity of the Colombini et al. (1987) model to discharge values lower than the fully-wet threshold.

4.4.2 *Discharge and bar shape*

The analysis of the harmonics composing the riverbed solution of the theoretical model shows that (i) the fundamental component A_{11}^* dominates the overall shape of bars and (ii) the component A_{22}^* dominates the second order harmonic. Therefore, the alternate pattern we find for moderate discharge values tends to be modified in a central bar pattern for low flows, as reported also in Crosato and Mosselman (2009). The analysis of the Fourier spectrum of measured topographies confirms the dominance of the fundamental harmonic A_{11}^*, but shows larger values of A_{20}^* component with respect to A_{22}^*. This aspect allows us to conclude that for low flows the system promotes a topography in which deposition occurs near the centre of the bars and deep pools are mainly concentrated near the banks rather than with scour and deposition equally distributed between the centre of the channel and the area near the banks. This response of riverbed can be explained taking into account nonlinear effects, which become progressively predominant when the channel aspect ratio increases (Colombini and Tubino, 1991). Nevertheless, the overall shape of bars is reproduced by the weakly nonlinear model, although with larger degree of symmetry, as proved by the trend of the skewness parameter.

4.4.3 *Suitable metrics for quantifying bar height and relief*

The laboratory dataset used for this work allowed for the comparison of a number of methods and metrics to characterise bar height and relief. Historically, interest in the quantification of bar height arose from the influence of bars on human activities and interaction with artificial structures (Jaeggi, 1984). Therefore, maximum scour and deposition were the most relevant parameters utilized to evaluate the risk of levee instability and levee overtopping, respectively. From an analytical point of view, metrics of bar height based on maxima and minima (H_{BM}^* and H_B^*) clearly identify the amplitude of the bar wave propagating in the channel. However, if applied to field or laboratory data, they are highly sensitive to measurement errors and uncertainties that may derive from the presence of vegetation on the bar top and

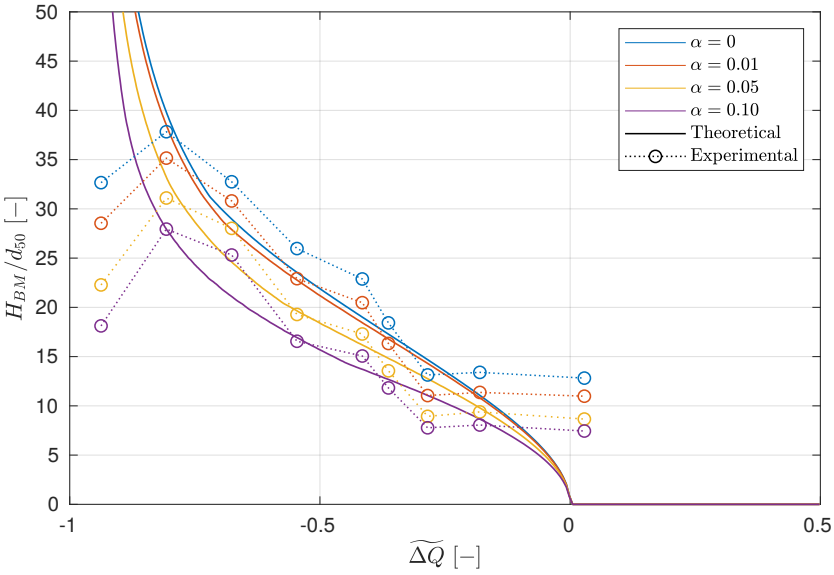

Figure 4.7. Bar height computed by excluding extreme values in the topography of bars in different percentages α. Theoretical predictions (lines) are compared with experimental measures (dot-circle lines).

from the difficulty of measuring the bottom elevation in deep pools. A suitable method to avoid the interference of outliers is to exclude the extreme values of the sample filtering a given percentage α equally distributed in both tails of the sample. Fig. 4.7 shows the predicted bar height H^*_{BM} computed by excluding maxima and minima of the bed elevation η^* in the percentages α equal to 0.01, 0.05 and 0.10. As we can expect, resulted curves of bar height reduce in magnitude (see the reference curve computed for $\alpha = 0$). Theoretical curves differ significantly among each other for moderate-low flows, while they tend to coincide in the neighborhood of the critical threshold. Conversely, experimental bar height decreases of an almost constant value for all discharge values, providing almost parallel curves. The effect of outliers is much more significant for experimental topographies rather than for theoretical ones, due to the greater complexity of actual bar shapes. Nevertheless, theoretical prediction provides a good qualitative and quantitative agreement also excluding extreme values of bar topography.

A further limitation of maxima and minima metrics is that the estimation of both H^*_{BM} and H^*_B requires the identification of individual bar units, which introduces potential sources of uncertainties and limits its application to bed configurations in which a dominant longitudinal wavelength is clearly recognizable.

Comparatively, SD^*_η and BRI^* are robust indices that do not depend on extreme values of elevation but on the entire bed elevation distribution. Moreover, these bed relief metrics can be applied to a range of different morphologies, thus allowing for comparisons between bars and other bedforms. Since SD^*_η and BRI^* show the same trend observed for H^*_{BM} and H^*_B, the former can provide better data when the purpose is not to quantify the maximum scour and deposition but rather to measure morphological trajectories and to compare study cases with experimental and numerical simulations.

It is also important to note that metrics based on the comparison of elevation values at different longitudinal positions (i.e., H^*_{BM} and SD^*_η) require detrending the bed elevation by removing the average slope that is often not obvious to define. Our experiments show that results are very similar when instead considering the cross-section-based indices H^*_B and BRI^*, with the advantage that they are fully independent of how the average slope is detrended. This similarity is linked to the presence of deep, small pools and large, flat bar tops. Cross-sectional relief is more strongly influenced by the former, and the maximum elevation along the cross section where the location of the lowest point is not very different from the highest point of the entire bar.

4.5 CONCLUSIONS

In this chapter we investigated the response of alternate bars to discharge variation, supporting theoretical prediction with laboratory experiments. The quantification of bar properties in terms of height, shape and migration rate has been successfully performed for a flume with constant width, slope and uniform grain size, allowing us to draw the following conclusions.

1. The decreasing trend of bar height is confirmed by laboratory observations and well reproduced by the equilibrium conditions predicted with the weakly nonlinear model of Colombini et al. (1987).

2. The limitation of bar amplitude to the emersion condition (i.e. for discharge values lower than the fully-wet threshold Q_{fw}) provides a good agreement both qualitatively and quantitatively with experimental observations.

3. The shape of bars can be qualitatively predicted by the theoretical approach, especially for low flows, where the mode-2 components become increasingly important. The actual shape of bars at low flow cannot be satisfactorily predicted by the Colombini et al. (1987) model due to the increasingly dominance of nonlinear effects.

4. Different metrics can be implemented to investigate the height of bars, based on maxima and minima values or on the relief of bar topography. The presence of outliers in measured data can be mitigated by excluding a certain percentage of the extreme values in the bed topography.

5

EFFECT OF FLOW UNSTEADINESS ON THE LONG-TERM EVOLUTION OF ALTERNATE BARS

This chapter is mainly based on the paper: Carlin, M., M. Redolfi, and M. Tubino (2020), Effect of flow unsteadiness on the long-term evolution of alternate bars, in Proceedings of River Flow 2020, edited by CRC Press, pp. 539–547, https://doi.org/10.1201/b22619-76.

In this chapter we analyse how the long-term average properties of bars respond to variations of flow regime in terms of flood duration and sequencing. For this purpose, we applied the weakly nonlinear model of Tubino (1991) to two types of simplified flow series, built (i) by composing in three different ways triangular flood events or (ii) by means of the Compound Poisson Process, a robust method that allows us to well reproduce flow regimes typical of the Alpine Region (e.g., Bertagni et al., 2018). For each method the probability density function was kept constant for all duration and sequencing considered. Results reveal that the average bar amplitude is primarily controlled by the flow probability density function, with the other hydrological parameters playing a secondary role. Conversely, the modification of the bar amplitude in single events and the time needed by rivers to recover from extreme events strongly depend on flood duration and sequencing.

5.1 INTRODUCTION

The investigation of bar properties under variable flow conditions is limited to few theoretical models (Tubino, 1991; Hall, 2004), experimental or field investigations (Welford, 1994; Eekhout et al., 2013) and numerical works (Defina, 2003). Considering that alternate bar properties are governed by the width-to-depth ratio β (see Chapter 2), the crucial aspect differentiating variable flow to steady flow conditions is that β changes in time, and therefore bar amplitude evolves in time depending on the magnitude and

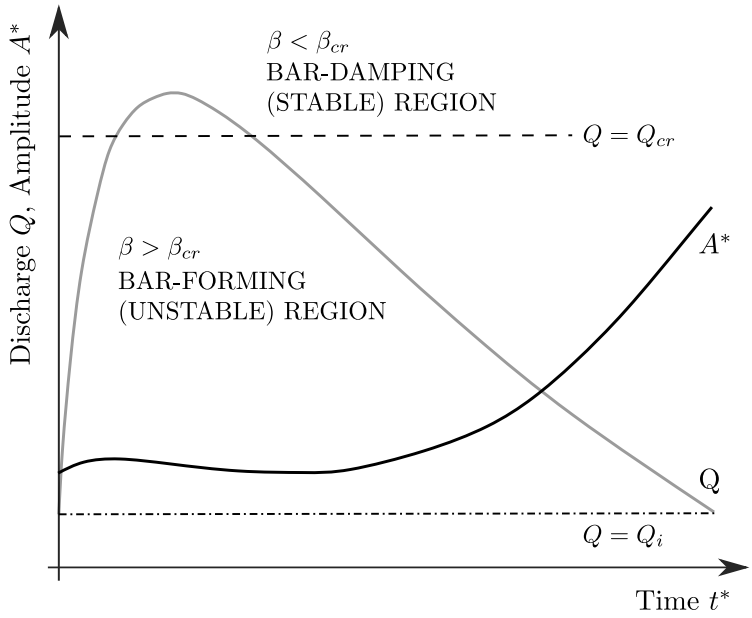

Figure 5.1. Evolution of the bar amplitude during an idealized flood event, according to the model of Tubino (1991). The dash-dotted line identifies the threshold for sediment motion, Q_i, while the dashed line indicates the critical threshold for bar formation: when discharge exceeds the critical value Q_{cr} the aspect ratio β is lower than the critical value β_{cr} and bar amplitude is damped, while for lower discharge values bar growth is promoted.

duration of the hydrograph. Fig. 5.1 provides an example of bar amplitude response to a single idealized flood event, as predicted by the analytical model of Tubino (1991). Such theory suggested that the evolution of bar amplitude crucially depends on the ratio between the timescale of bar growth and the timescale of the flood event, which was measured by means of the unsteadiness parameter $\widehat{U}$ (see Section 2.3 for more details). The main result revealed that relatively fast events (large values of $\widehat{U}$) do not affect bar amplitude, while longer floods (small values of $\widehat{U}$) allow bar amplitude to adapt to variable flow conditions. Moreover, it was found that the typically longer falling limb of the hydrograph has a major effect in determining the final topographical expression of bars, as reported in Welford (1994) and Eekhout et al. (2013).

However, existing studies mainly focussed on individual events, while the role of the entire hydrological regime on bar response

is still to a large extent unexplored. The question then arises whether the different magnitude and sequence of flood events are able to affect the long-term response of alternate bars, in order to define which properties of the flow series primarily control such average response. The definition of such key hydrological parameters is a prerequisite to properly investigate the issue of "dominant" or "formative" discharge for river bars, whose definition is still missing in literature (Jaballah et al., 2015). Therefore, beyond the investigation of the effect that the hydrological forcing produces on the evolution of bar amplitude, we are looking for a synthetic hydrological indicator able to summarize the complexity of the flow regime, as such as the probability density function for the effective discharge method proposed by Wolman and Miller (1960).

To address this question, we applied the weakly nonlinear theory of Tubino (1991) to two types of idealized flow sequences built (i) by composing in three different ways triangular floods and (ii) by applying the Compound Poisson Process, a stochastic algorithm allowing us to predict flow series statistically similar to actual, complex sequences. During each simulation, the probability density function is kept constant for both the typologies of flow series, while the duration and sequencing of flood events is varied.

The work is organized as follows: an explanation of the evolutionary model is reported in Section 5.2, the setting of numerical simulations is explained in Section 5.3, the main results are illustrated in Section 5.4 and discussed in Section 5.5.

5.2 MODELLING MORPHOLOGICAL EVOLUTION

The evolution of alternate bar amplitude under unsteady flow can be predicted by means of the weakly nonlinear theory of Tubino (1991), which solves the two-dimensional shallow water equations coupled with the Exner equation (SWE) in a straight channel with erodible bottom, for given values of the channel width, downstream gradient and grain size (see Section 2.3 for further details). Discharge variations are accounted for analytically through a perturbation approach, linearizing the flood

around a reference discharge value $\overline{Q}$, for which the steady model of Colombini et al. (1987) is solved.

The resulting Landau-Stuart type equation that governs the evolution of bar amplitude A^* in time can be written in the following dimensional form:

$$\frac{dA^*}{dt^*} = \overline{\Omega}_0^* A^* + \overline{\gamma}_2 A^{*3}, \tag{5.1}$$

where t^* is time and $\overline{\Omega}_0^*$ represents the linear growth rate of bars, analogously to eq. (2.28). Linearization of the flow hydrograph around a reference state implies that $\overline{\Omega}_0^*$ changes with the flow discharge Q as follows:

$$\overline{\Omega}_0^* = \overline{\gamma}_1 + \overline{\gamma}_0 (Q - \overline{Q}). \tag{5.2}$$

The coefficients $\overline{\gamma}_0$, $\overline{\gamma}_1$ and $\overline{\gamma}_2$ depend on the reference discharge, and can be easily computed from their dimensionless counterparts $\overline{\alpha}_0$, $\overline{\alpha}_1$ and $\overline{\alpha}_2$ as defined in Tubino (1991) (see eq. 2.51).

The sign of the growth rate $\overline{\Omega}_0^*$ defines the tendency of the flow-bottom interaction to promote ($\overline{\Omega}_0^* > 0$) or to damp ($\overline{\Omega}_0^* < 0$) bar amplitude. Therefore, the critical conditions for bar formation (i.e. $\beta = \beta_{cr}$) can be found by imposing $\overline{\Omega}_0^* = 0$ in eq. (5.2), which gives:

$$Q_{cr} = \overline{Q} - \frac{\overline{\gamma}_1}{\overline{\gamma}_0}. \tag{5.3}$$

We note that the growth rate of bars decreases with flow discharge (see also Fig. 5.1), and therefore γ_0 is negative.

In the steady case ($Q = const$), both $\overline{\Omega}_0^*$ and $\overline{\gamma}_2$ are constant, and therefore eq. (5.1) can be solved in the analytical form of eq. (2.30) proposed in Section 2.2, in which parameters k_1 and k_2 assume values of $\overline{\Omega}_0^*$ and $\overline{\gamma}_2$ respectively.

5.3 METHOD

We refer to an ideal, prototype channel of width $W = 60\,m$ and downstream gradient $S = 0.2\,\%$, with the bottom composed by cohesionless material of median grain size of $d_{50} = 5\,cm$ and density $\rho_s = 2650\,kg/m^3$. In the present analysis we choose the logarithmic friction formula of Engelund and Fredsoe (1982) and

the sediment transport formula of Parker (1990), and we set to $r = 0.6$ the parameter that accounts for the gravitational effect of the lateral bed slope on sediment transport (Ikeda, 1982, see eq. 2.14). In these conditions, the critical discharge resulting from eq. (5.3) is $Q_{cr} = 605\,m^3\,s^{-1}$.

To evaluate the effect of the flood sequencing, we employ two different types of flow series: the first is given by the composition of symmetric triangular floods following three different orders, the second is formed by a sequence of floods occurring randomly and with a random magnitude, accordingly with the Compound Poisson Process, proposed by Bertagni et al. (2018) as a good approximation of natural flow series. Details of the two methods are explained in the following.

5.3.1 *Triangular flow series*

We implement three different sequences of triangular flood events in order to have the same probability density function f_Q for all of them (see Fig. 5.2a,c). Specifically, we consider a range of discharge from $Q_{cr} - \Delta Q$ to $Q_{cr} + \Delta Q$, where a relatively small discharge variation ($\Delta Q = 100\,m^3\,s^{-1}$) is chosen to fall in the optimal range of validity of the weakly nonlinear model.

The three flow series are obtained by composing in different ways two distinct building blocks:

- the "high flow" (H) phase, characterised by a triangular variation between Q_{cr} and $Q_{cr} + \Delta Q$, and a duration T_H^*;
- the "low flow" (L) phase, characterised by a triangular variation between $Q_{cr} - \Delta Q$ and Q_{cr}, and having twice the duration of the high flow stage ($2\,T_H^*$).

We choose a longer duration of the low flow phase to better mimic the typical flow regime, but also to obtain a system where bar-forming states ($Q < Q_{cr}$) are more frequent than bar-damping states ($Q > Q_{cr}$). Specifically, the first two flow series are obtained by repeating a sequence of low flow and high flow phases in the following way: LHLH (first sequence, see Fig. 5.2b); LLHH (second sequence, see Fig. 5.2d). Finally, the third case is built by randomly composing low flow and high flow phases. In order

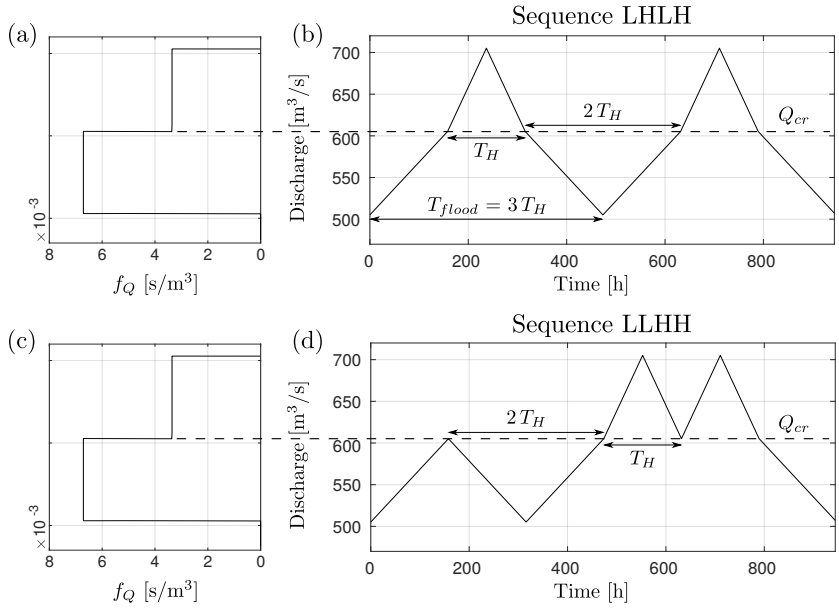

Figure 5.2. Representation of the first two flow series, having identical probability density function f_Q (panels a and c), but different sequencing of low (L) and high (H) flow phases: LHLH sequence (b) and LLHH sequence (d). The timescale of the flood, T^*_{flood}, is defined as three times the duration of the high flow phase, T^*_H.

to filter out the effect of random variability, numerical simulations for the random sequence have been repeated 1000 times, by computing results as ensemble means.

For each flow series, a set of simulations is performed, maintaining the same sequences but varying their timescale. Specifically, the parameter T^*_H is varied from 0.5 hours to 18 days. Each simulation is started by assuming an initially-small bed deformation of amplitude $A^*_0 = 0.01$ m.

Consistently with Tubino (1991), we quantify the unsteadiness parameter $\widehat{U}$ (i.e. the ratio between bar and flood timescales as defined in eq. 2.55), by taking T^*_{bar} as the dimensional counterpart of eq. (3.7). Therefore, we obtain that bar timescale is the inverse of the reference growth rate ($\overline{\Omega}^*_0 = \overline{\gamma}_1$), and define the flood timescale, T^*_{flood}, as $3\,T^*_H$ (i.e. as the period of the simplest, LHLH sequence):

$$\widehat{U} = \frac{T^*_{bar}}{T^*_{flood}} = \frac{1/\overline{\gamma}_1}{3\,T^*_H}. \tag{5.4}$$

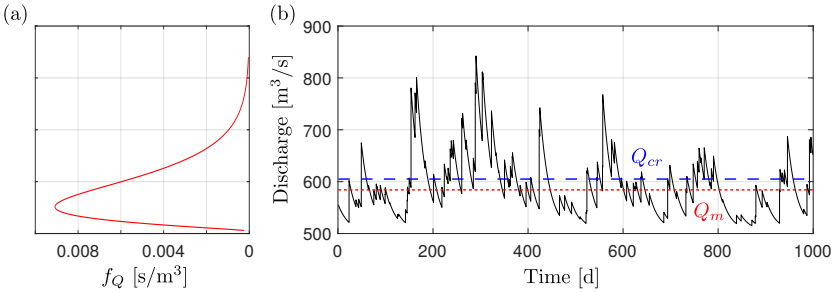

Figure 5.3. Representation of a stochastic flow series, characterised by a Gamma-distributed probability density function (a), computed by means of the Compound Poisson Process by integrating eq. (5.5) (b).

Since the parameter $\overline{\gamma}_1$ is the same for all the simulations, the analysed variations of the unsteadiness parameter $\widehat{U}$ only depend on the flood duration ($\widehat{U} \sim const/T^*_{flood}$).

5.3.2 *Stochastic flow series*

The Compound Poisson Process (CPP) is a parsimonious and robust strategy to model stochastically the flow variability (Botter et al., 2013; Bertagni et al., 2018). This approach addresses the composition of a flow series by means of the superimposition of pulses driven by precipitation, whose magnitude and frequency of occurrence are described by an exponential distribution. The sequence of events, see Fig. 5.3b, is computed integrating the following three-parameter stochastic equation:

$$\frac{dQ}{dt^*} = \psi(t^*) - \frac{Q}{\kappa}, \tag{5.5}$$

where κ represents the integral scale of the flow series (i.e. the integral of the auto-correlation function of Q) and $\psi(t^*)$ is the pulse signal, whose average period and magnitude are equal to κc_v^2 and $Q_m c_v^2$ respectively. Q_m is the average discharge of the flow series and c_v is the coefficient of variation of the flow series. The stochastic process defined by eq. (5.5) has a fixed Gamma-

distributed probability density function (Fig. 5.3a), which can be described by the following analytical expression:

$$f_Q(Q) = \frac{\Gamma\left(\frac{1}{c_v^2}\right)^{-1}}{Q_m\, c_v^2}\left(\frac{Q}{Q_m\, c_v^2}\right)^{\frac{1}{c_v^2}-1} \exp\left(-\frac{Q}{Q_m\, c_v^2}\right) \tag{5.6}$$

in which $\Gamma(\xi)$ is the Gamma function of argument ξ.

In order to obtain results of the same order of magnitude of the triangular flow series, the mean value of the stochastic flow series was chosen equal to $83\,m^3\,s^{-1}$ and the resulting flow sequence has been added to a basic state equal to $505\,m^3\,s^{-1}$. Nevertheless, being the intensity of pulses as their occurrence randomly distributed, the extreme values of discharges (i.e. maxima and minima values of the flow series) can be significantly different from the ones of the triangular flow series, which are limited in the interval $[Q_{cr} - \Delta Q, Q_{cr} + \Delta Q]$. The coefficient of variation was set equal to 0.663, which is a typical value of Alpine gravel-bed rivers (see Bertagni et al., 2018).

In this case, the timescale of the flow series, T^*_{flood}, has been chosen proportional to the integral time scale of the flow series κ. Specifically, we considered the average period of pulse occurrence, which is given by $\kappa\, c_v^2$. Therefore, the unsteadiness parameter is given by:

$$\widehat{U} = \frac{T^*_{bar}}{T^*_{flood}} = \frac{1/\overline{\gamma}_1}{\kappa\, c_v^2}. \tag{5.7}$$

For the stochastic flow series the duration is accounted for by varying the integral scale κ between 3.0 h to 90 days, in order to have similar values of T^*_{flood} of the triangular flow series. As well as for the random sequence of triangular floods, the effect of randomness was filtered out by repeating the numerical simulations 1000 times, to obtain a statistically robust calculation of results. Finally, as for the triangular flow series, the initial bed deformation is set to $A^*_0 = 0.01$ m.

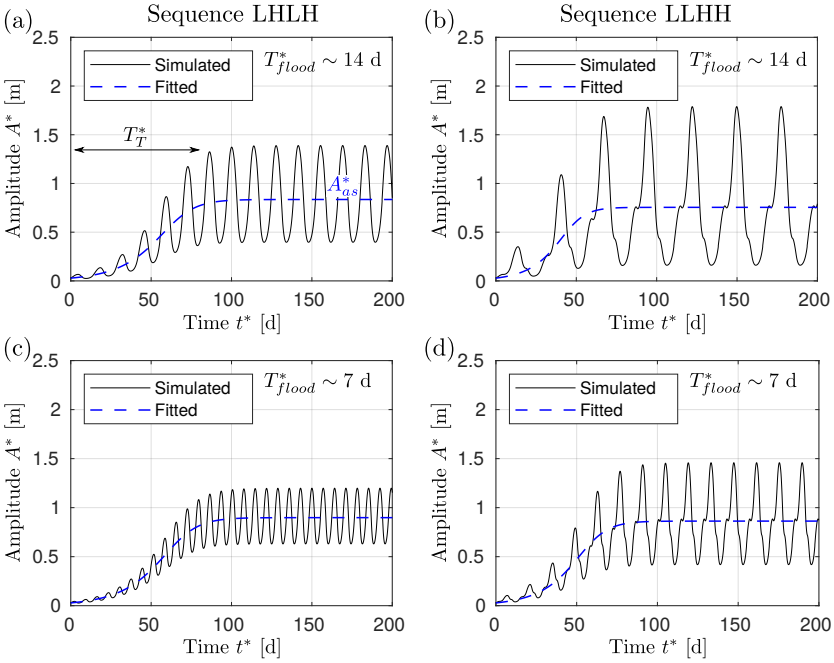

Figure 5.4. Effect of duration and sequencing of flood events on the evolution of bar amplitude. Left panels: LHLH sequence; right panels LLHH sequence. Upper panels: $T^*_{flood} \sim 14$ days; lower panels: $T^*_{flood} \sim 7$ days. The dashed curve is obtained by fitting the model results with a curve having the structure of eq. (2.30), which is used for computing the mean amplitude, A^*_{as}, and the transitory time, T^*_T.

5.4 RESULTS

5.4.1 *Time evolution of bar amplitude*

Fig. 5.4 illustrates results of the application of Tubino's (1991) model to four test cases by considering the two ordered sequences LHLH and LLHH as hydrological regime. Starting from nearly-flat initial conditions, the amplitude of alternate bars tends to increase, showing significant oscillations due to the periodic alternation of different discharge states (i.e. lower and larger than the critical threshold Q_{cr}). After the initial transitory phase, the system attains a limiting cycle, where the amplitude oscillates around an average state A^*_{as}.

By comparing the different test-cases, it seems that A^*_{as} does not vary significantly either with the duration of the floods or by changing the flood sequence from LHLH to LLHH. Similarly, the time needed to complete the initial transitory phase, T^*_T, seems approximately constant. Conversely, the magnitude of the amplitude oscillation significantly decreases when reducing the duration of the flood (e.g., Fig. 5.4a,c), while it increases with the complexity of the flow series (i.e. from LHLH to LLHH sequence, see Fig. 5.4a,b). Nevertheless, the above speculations are not necessarily overall valid, but require a more detailed analysis based on a larger variability in flood duration.

To quantify the magnitude of the amplitude oscillation we computed the standard deviation of the bar amplitude (SD^*_A), excluding the initial transitory phase. On the contrary, to capture the evolution of the average bar amplitude, filtering out its oscillations, we fit the model results with a curve having the structure of eq. (2.30), i.e. by assuming that time growth of the average amplitude is similar to that obtained in a steady flow case, but with calibrated values of model parameters. The resulting curves (dashed lines of Fig. 5.4) well reproduce the essential features of the average bar growth, from the initial amplitude A^*_0 to the asymptotic average value. From this curve we can easily calculate the mean amplitude A^*_{as} as the value for $t^* \to \infty$, and we can define the transitory time T^*_T as the time needed to reach an amplitude $A^* = 0.99\, A^*_{as}$.

5.4.2 *Long-term bar amplitude and standard deviation*

To systematically quantify the role of flood duration and sequencing on bar evolution the theoretical model of Tubino (1991) was applied to a wide range of T^*_{flood} (corresponding to $\widehat{U}$ ranging between 0.1 to 100). For each flow sequence the average bar amplitude, A^*_{as}, the magnitude of amplitude oscillations, SD^*_A, and the time required to complete the transitory phase, T^*_T, were computed and plotted with respect to the different duration as shown in Figs. 5.5 and 5.6, related to the triangular flow series and the stochastic process respectively.

Analysing the effect of the triangular flow sequences on bar evolution, we observe that the mean amplitude tends to increase

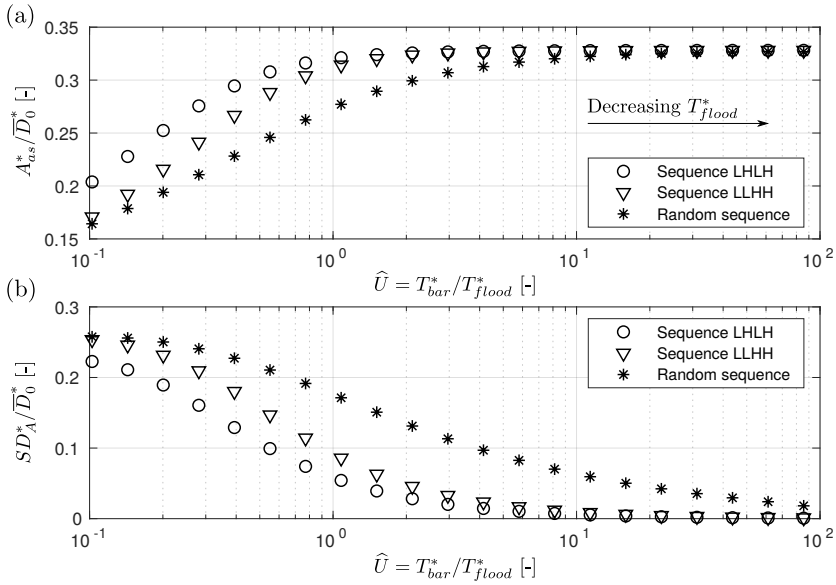

Figure 5.5. Average state of bar amplitude (a) and the standard deviation (b), scaled with the uniform water depth at the reference state, $\overline{D}^*_0$, as function of the unsteadiness parameter $\widehat{U}$, for the three triangular flow sequences. When decreasing the flood timescale T^*_{flood} the equilibrium bar amplitude A^*_{as} tends to approach a constant value, while the standard deviation SD^*_A invariably decreases. For both the equilibrium bar amplitude and the standard deviation, the data series tends to be shifted to the right when moving from the basic LHLH sequence to the more complex LLHH and random sequences.

with the unsteadiness parameter, until it attains a constant value that is nearly the same ($A^*_{as} \simeq 0.33\,\overline{D}^*_0$) for all the three flow series (see Fig. 5.5a). This indicates that when $\widehat{U}$ is sufficiently large the mean amplitude becomes essentially independent of both the duration and the sequencing of floods.

Conversely, the magnitude of the amplitude oscillation systematically decreases with the unsteadiness parameter $\widehat{U}$, as illustrated in Fig. 5.5b. Specifically, for relatively long floods the standard deviation SD^*_A shows the same order of magnitude as the mean amplitude A^*_{as}, while for relatively flashy floods the oscillations become very small. This behaviour is also evident when computing the coefficient of variation of the amplitude of bars, which decreases with $\widehat{U}$ from $1-1.3$ for $\widehat{U} = 0.1$ to almost vanish (i.e. $\mathcal{O}(10^{-2})$) for $\widehat{U} = 100$.

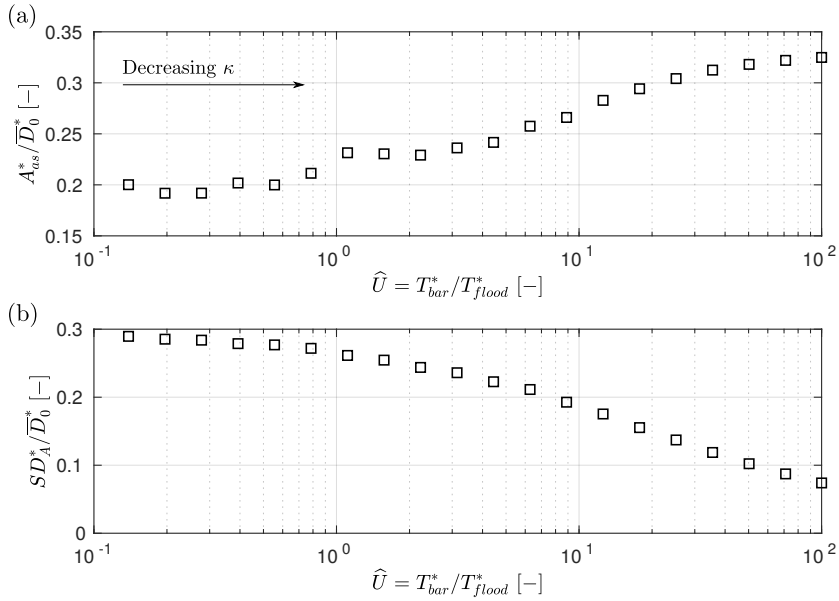

Figure 5.6. Average state of bar amplitude (a) and the standard deviation (b), scaled with the uniform water depth at the reference state, $\overline{D}^*_0$, as function of the unsteadiness parameter $\widehat{U}$, for the stochastic flow sequences. Trends are similar to the triangular flow series, but tend to shifted to the right of the random sequence reported in Fig. 5.5.

When comparing the results of the three different flow sequences, it appears that the data series of A^*_{as} and SD^*_A follow a very similar trend, but with a shift along the x-axis. Specifically, points of the sequence LLHH are very similar to those of the LHLH sequence, but with a nearly double value of the $\widehat{U}$ parameter. Similarly, the random sequence shows similar values of both A^*_{as} and SD^*_A, computed as ensemble means of repeated simulations, but with an unsteadiness parameter that is nearly an order of magnitude larger. This aspect indicates that the definition of the unsteadiness parameter $\widehat{U}$ is not sufficient to synthesize the variability of the flow sequence. The variation of bar amplitude increases with the complexity of the flood sequence and, consequently, the average state results in a lower value.

The above considerations can be overall valid also for results obtained by the stochastic process and shown in Fig. 5.6, although the two implemented methods to build the flow series

are not directly comparable due to the differences in the probability density function and the magnitude of floods.

Nevertheless, for the average state of bar amplitude, (i) an increasing trend of A^*_{as} is observed, despite a slight scatter for the lowest values of $\widehat{U}$ (i.e. the flow series with longest integral scale), and (ii) an asymptotic state is achieved, meaning that the magnitude and sequencing of flood events does not affect the long-term bar amplitude also for complex flow sequences with low values of T^*_{flood}. It is interesting to note that the average state of bar amplitude assumes values ranging between 0.15 to 0.35 times the reference water depth, which is the same range of values found for the triangular flow sequences. Therefore, despite the differences between the two methods, a similar response of alternate bars can be observed in the long-term and the same asymptotic ratio between A^*_{as} and $\overline{D}^*_0$ is found.

Moreover, as for the triangular flow series, the standard deviation shows a decreasing trend with respect to the unsteadiness parameter, but in absolute terms it is overall larger and it does not achieve null values for the shortest floods. Such behaviour is also displayed by the random sequence, whose values of standard deviation are always larger than for the ordered sequences. Nevertheless, the coefficient of variation of bar amplitude does not tend to zero for large values of $\widehat{U}$, but attains a value around 0.24, as if the characteristic timescale of the stochastic flow sequence was larger than its counterpart of the triangular flow series.

5.4.3 *Transition time*

We now analyse the effect that the duration and sequencing of flood events has on the transitory time T^*_T, namely how rapidly the system is able to reach the average state by considering the different hydrological series. In Fig. 5.7 the transitory time computed for the triangular flow series is expressed as the number of cycles required to achieve the average state, N_T, defined as the ratio between T^*_T and the flood timescale T^*_{flood}. Results show that for relatively large values of the parameter $\widehat{U}$ (nearly larger than 1), the transitory time is almost constant and values follow the straight 1 : 1 line in the bi-logarithmic plane (dashed line of Fig. 5.7), independently of the sequence of floods. As a

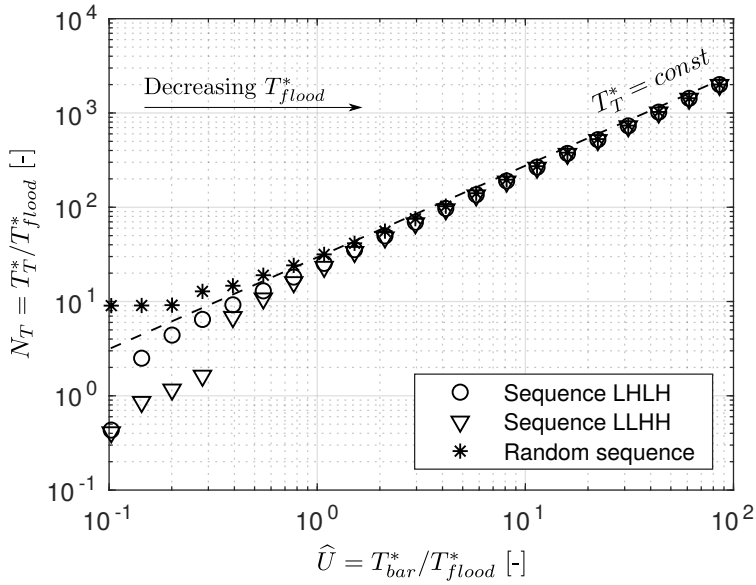

Figure 5.7. Ratio between the transitory time T^*_T and the flood duration T^*_{flood}, representing the number of floods needed to reach the regime conditions. Results for the three flow sequences as a function of the dimensionless parameter $\widehat{U}$. For relatively short flood duration, all the points tend to follow the dashed line, which is obtained by assuming T^*_T to be constant.

consequence, N_T turns out to be directly proportional to $\widehat{U}$, since the ratio T^*_T/T^*_{floods} depends exclusively on T^*_{floods} when T^*_T is constant.

On the other hand, for small values of the parameter $\widehat{U}$ the transitory time T^*_T is not constant and it highly depends on the specific sequencing of the flood events at the initial stages of bar development, increasing the scatter for all the sequences.

In the case of the stochastic process we provide the same scaling performed for the triangular flow series, dividing the transitory time T^*_T by T^*_{flood} (i.e. the average period of flood occurrence), obtaining results shown in Fig. 5.8. Also for the stochastic process N_T represents the average number of flood events required to complete the transitory phase. It is evident that the transitory time is almost independent of the duration of flood events, being points in Fig. 5.8 displayed along the straight line in the bi-logarithmic plane. Differently from the scenarios

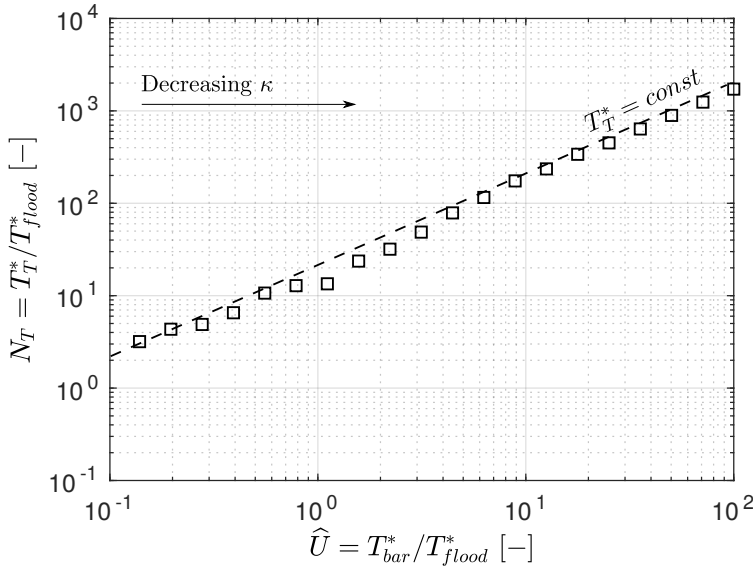

Figure 5.8. Ratio between the transitory time T_T^* and the flood timescale of the flow series, T_{flood}^*, which is defined as the averege periode of flood pulses in the stochastic process. The dotted line represents the straight 1 : 1 line in the bi-logarithmic plane, representing the condition for which the transitory time T_T^* is constant.

of triangular flow sequences, a low scatter is observed also for large values of T_{floods}^*.

5.4.4 *Characterisation of the timescale of the flow series for bar investigations*

Our analysis highlights that the unsteadiness parameter calculated on the basis of the individual flood events is not sufficient to explain the average bar state in a river, as an important role is also played by the actual sequencing of the flow events. This is evident considering that curves reproducing the average bar properties (i.e. A_{as}^* and SD_A^* with respect to $\widehat{U}$) provide similar values for different values of $\widehat{U}$. This suggests that our definition of T_{flood}^*, based on the period of flood occurrence, is not able to characterise the variability of the flow series, making necessary a more explanatory definition of the unsteadiness parameter. The

definition of such a parameter is not trivial and in the following we provide a possible metric.

To look for a representative timescale for a flow series we start from the integral scale described in the CPP stochastic process, which is proposed as a parameter required to statistically reproduce the characteristics of real flow series. Therefore, we compute the auto-correlation function for the triangular flow sequences, R_{QQ}, to evaluate how the sequences are correlated in time. To do that, we correlate the sequences with a delayed copy of the sequence itself as a function of the delay:

$$R_{QQ}(t_1^*, t_2^*) = E\Big[Q(t_1^*) - Q_m, Q(t_2^*) - Q_m\Big], \tag{5.8}$$

where t_1^* and t_2^* represent two different time in which the correlation is looked for, and normalize it with the value obtained when $t_1^* = t_2^*$ ($R_{QQ}(t_1^*, t_1^*)$).

$$\rho_{QQ}(t_1^*, t_1^*) = \frac{R_{QQ}(t_1^*, t_2^*)}{R_{QQ}(t_1^*, t_1^*)}. \tag{5.9}$$

It is evident that the definition of the integral scale is far to be significant for the ordered sequences LHLH and LLHH, since they present a strong correlation being composed by repeating identical building blocks (see Fig. 5.9a,b). Therefore, we perform the calculation exclusively for the random series, observing that after a certain time the auto-correlation of the sequence vanishes (Fig. 5.9c).

Being dt^* the timestep of the flow series, the integral scale is defined as:

$$\kappa = \int_0^\infty \rho_{QQ}(t_1^*, t_1^*) dt^*. \tag{5.10}$$

Nevertheless, for the computation of κ we considered the area below the curve that provides the best fitting of the auto-correlation function.

At this point, a new definition of the unsteadiness parameter is proposed, by considering the integral scale as the characteristic timescale of the flow series, T^*_{flow}:

$$\widehat{u} = \frac{T^*_{bar}}{T^*_{flow}} = \frac{1/\gamma_1}{\kappa}. \tag{5.11}$$

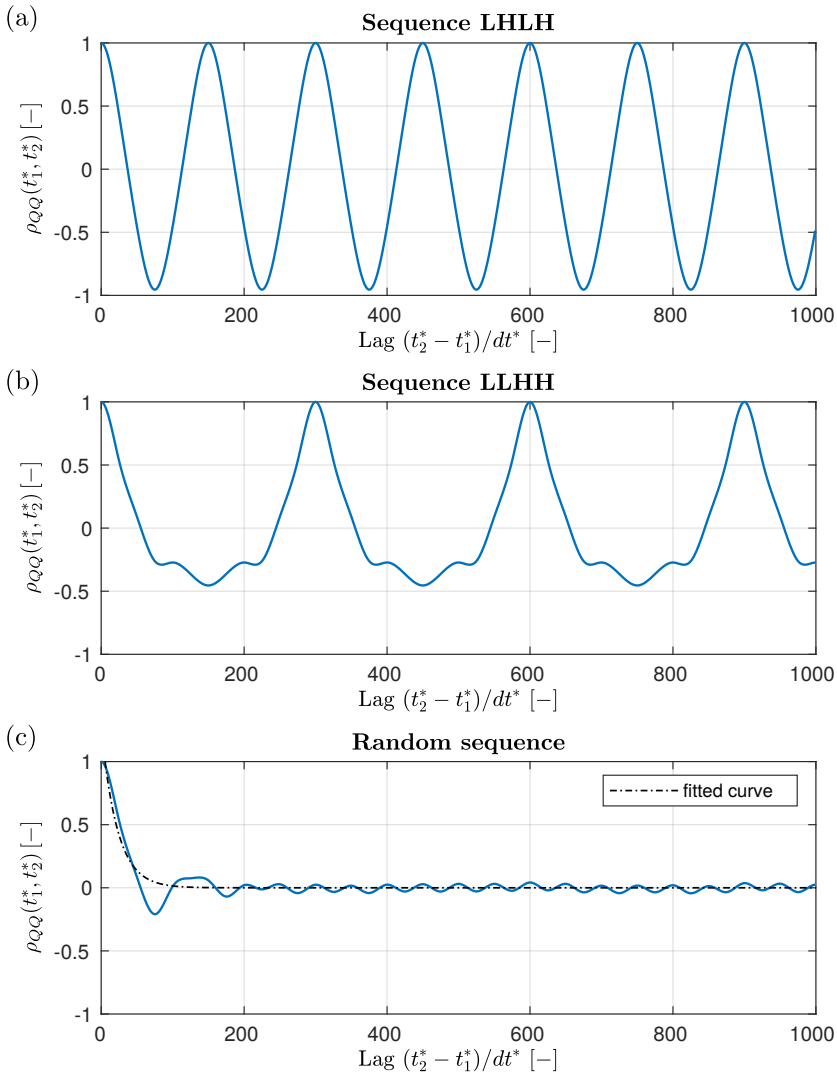

Figure 5.9. Normalized auto-correlation function with respect to the lag, $\rho_{QQ}(t_1^*, t_1^*)$, for the three triangular flow series. Specifically, sequences LHLH (a) and LLHH (b) show a strong correlation due to the order in the flood repetition, while the random sequence (c) markedly loses correlation after a certain number of timesteps. The integral scale for the random sequence is computed as the area of the fitting curve (dash-dotted line).

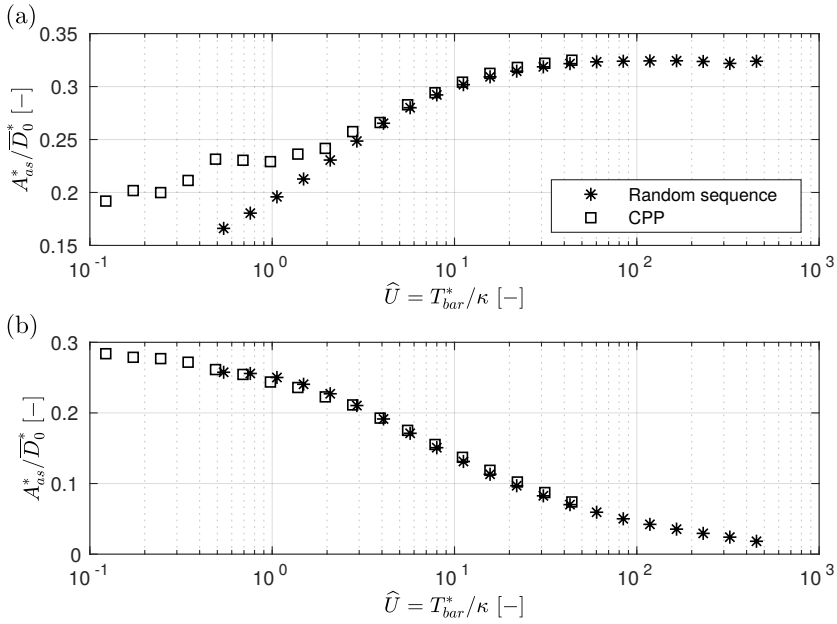

Figure 5.10. Comparison of average bar amplitude (a) and standard deviation (b) for the triangular sequences and the CPP stochastic process, by computing the unsteadiness parameter with the hydrological timescale of the flow series, T^*_{flow}, equal to the integral scale.

For the specific case of the random sequence, the integral scale is almost 5 times lower than T^*_{flood}.

The comparison of curves of average bar amplitude and standard deviation of Figs. 5.5 and 5.6, for the random sequence and the stochastic process respectively, are shown in Fig. 5.10 with respect to the new definition of the unsteadiness parameter (eq. 5.11). A good overlapping is overall observed for both the average bar amplitude and the standard deviation, although for the former quantity a scatter is observed for values of $\widehat{U}$ lower than ~ 2. Such discrepancy can be explained considering that for the flood sequences with long duration of events (i.e. large values of the integral scale), the average state is influenced by the sequencing of flood events and it is not independent of the probability density function, which is different for the two methods. The definition of the unsteadiness parameter by considering the integral scale as the suitable timescale to account for the sequenc-

ing of hydrological events allows us to compare the long-term bar amplitude produced by different hydrological regimes.

5.5 DISCUSSION AND CONCLUSIONS

5.5.1 *Summary of main results*

In the present analysis we investigate the effect that different hydrological regimes have on the long-term response of alternate bars. To address this question, we applied the Tubino (1991) model to predict the evolution of bar amplitude in time in a rectangular channel affected by varying discharge conditions. Specifically, we built different types of flow sequencing (i) by composing in different ways triangular flow series and (ii) by applying the stochastic approach of the CPP process.

Results reveal that for relatively short duration floods (i.e. for comparatively large values of the unsteadiness parameter $\widehat{U}$) the asymptotic, regime value of the average bar amplitude, A^*_{as}, is nearly independent of the duration and sequencing of the floods. This suggests that, under such conditions, the essential hydrological information needed to predict the average bar style are entirely contained in the flow probability density function, which represents a fundamental precondition for a possible definition of an equivalent, formative discharge for alternate bars. Starting from this result, in Chapter 6 we propose an innovative approach to quantify the long-term properties of bars and the corresponding formative conditions in real rivers, considering that a similar approach (i.e. based on the probability density function) was implemented by Blom et al. (2017) for defining an analytical solution for the channel-forming discharge.

Variations of bar amplitude during individual flow events turn out to depend mainly on the duration and sequencing of the floods. Specifically, long periods of moderate discharge (i.e. sufficiently high to transport sediments but significantly lower than the critical threshold Q_{cr}) can strongly increase the bar height, while periods of higher discharge tend to significantly reduce the amplitude of bars, eventually leading to their disappearance. It is worth noticing the analogy with Arkesteijn et al. (2019), who found that the probability density function of the flow regime is

responsible of the average equilibrium channel slope, while the sequencing of floods determines the instantaneous evolution of the riverbed. From an engineering point of view, the oscillation of bar amplitude is an important aspect to be accounted for in river management, since large variations with respect to the average state can affect navigation and flooding risk. A statistical analysis about the effect of real floods on the bar amplitude evolution is investigated in Chapter 7.

Analysis of the transitory time reveals that the shorter is the duration of the single flow events, the larger is the number of floods required to achieve a regime state. This implies that fluvial systems characterised by relatively long flow events are able to rapidly recover from catastrophic events or human interventions that may alter the bar state. Conversely, rivers characterised by a relatively flashy flood regime (or, more precisely, by small values of the unsteadiness parameter $\widehat{U}$) require a much higher number of floods to accumulate the time T_T^* that is needed to complete any transitory phase from highly disturbed conditions to an ordinary state.

Results obtained by implementing the stochastic flow series, which is able to mimic a complex conditions of real cases, are comparable with those obtained by the simplified flow sequences both in terms of average state and amplitude oscillations. Therefore, we can assume overall valid the above considerations also for natural rivers.

5.5.2 *Limitations and future perspectives*

The analysis of the evolution of bar amplitude in time by means of the theoretical model of Tubino (1991) represents a first, exploratory work to bridge the expected amplitude of bars in a river reach and the hydrological regime. Specifically, since the morphological model has been applied to a prototype channel forced by idealized flow sequences, results are significant to the extent of they need to be validated by appropriate experiments. Nevertheless, the response of the ideal channel to the simplified flow conditions is reasonable by considering the current knowledge about alternate bar characteristics. Indeed, (i) the existence of an equilibrium configuration around that the system oscillates

and (ii) the capability of bars to approach the "steady" equilibrium configuration when the duration of flood is sufficiently long (i.e. providing large oscillations of bar amplitude during each individual flood event) are reasonable extensions of the steady response of Colombini et al. (1987).

Therefore, two questions arise in order to extend this analysis and provide suitable results for the practical management of rivers:

1. Is it possible to identify a threshold value of the unsteadiness parameter in order to assume reasonable the prediction of the average value of bar amplitude by means of a model based on the probability density function (as, for example, the bar-forming discharge method proposed in Chapter 6)?

2. How does the unsteadiness parameter, computed by the channel characteristics and the hydrological forcing, can be bridged with the expected value of the average bar amplitude?

For now, a clear and documented answer to the above questions is not available, because the definition of the unsteadiness parameter for a complex flow series is not straightforward. Nevertheless, from the outcomes of this PhD work we can try to draw back some qualitative answers to the above questions.

The suitability of a probability density function-based model to predict the average bar amplitude can be ascertained by comparing the resulting value with the long-term mean value computed at each time step of the complex flow series (see for example the model proposed in Chapter 7). Considering the study cases depicted in Chapter 6, our analysis suggests that a pdf-based model is sufficient to reproduce the bar response to the hydrological regime for the upstream reach of the Alpine Rhine River and the Isère River, while large oscillations of bar amplitude are obtained when the unsteady model is applied to the downstream reach of the Alpine Rhine River, which implies that the morphological response can be also affected by the duration and sequencing of floods.

This finding introduces a further element of complexity in the definition of the timescale of a flow series, because the two

reaches of the Alpine Rhine River have a similar hydrological regime. Indeed, the effectiveness of the flow regime to form alternate bars depends not only on the duration of significant events, but also on their "distance" from the critical conditions for bar formation. Therefore, a simple relationship between the unsteadiness parameter and the average bar amplitude is not easy to determine, due to the various factors affecting the response of river bars.

In conclusion, the definition of a characteristic timescale of the hydrological flow regime suitable to describe such response is still an open issue, with respect to which the integral scale could represent a reasonable starting point.

6

THE LONG-TERM RESPONSE OF ALTERNATE BARS TO THE HYDROLOGICAL REGIME

This chapter is based on the paper: Carlin, M., M. Redolfi, and M. Tubino (2021), The long-term response of alternate bars to the hydrological regime, Water Resources Research, 57, e2020WR029314, https://doi.org/10.1029/2020WR029314.

In this chapter we analyse the long-term, average characteristics of alternate bars subject to a complex flow regime. Starting from the state-of-the-art theoretical models of bar dynamics, we propose a novel methodology to determine the long-term bar response to the hydrological river regime and the associated "bar-forming" discharge that, if applied steadily, would produce the same morphological response. We derive a generalized criterion to define whether bars are expected to form and to estimate the long-term bar topography, depending on flow probability density function and channel characteristics (width, slope and sediment size). Our procedure differs from the classical methods to define formative discharge, inasmuch as it accounts for the specific and reversible response of bar topography to the different flow stages that compose the hydrological regime. Application to four different gravel bed reaches in the Alpine region shows the capability of the procedure to interpret remarkably well different riverbed morphologies and to provide a reasonable prediction of the observed bar height, thus suggesting its potential to analyse long-term morphological trajectories following hydrological alterations and river restoration projects.

6.1 INTRODUCTION

The formation of migrating bars is one of the most studied topics in river morphodynamics. The large number of laboratory observations and theoretical results produced so far provides a consistent picture of the dependence of bar properties (morphol-

ogy, migration rate) on flow and sediment characteristics and highlights the role of the channel aspect ratio β as the main controlling parameter of bar instability (e.g Fredsoe, 1978; Colombini et al., 1987; Tubino et al., 1999; Siviglia et al., 2013; Bertagni and Camporeale, 2018).

Despite the large amount of literature, no much information is available about the investigation of long-term properties of alternate bars subject to a flow regime. Indeed, existing studies are focussed on individual flood events (Tubino, 1991; Welford, 1994; Eekhout et al., 2013) or consider simplified flow series (Carlin et al., 2020), not providing a suitable criterion to quantify the average bar height we can observe in a straight channelized river.

The purpose of this chapter is to investigate how bar amplitude responds to a complex flow regime, coupling the main evidences on bar behaviour explored in the previous chapters with the classical approach implemented in river morphodynamics to define the formative conditions of a typical fluvial phenomenon. The need of a new approach is motivated by a number of peculiar characteristics of the bar adaptation to varying flow: (i) the topographic expression of bars reduces with increasing discharge, (ii) the response of bars to flow variability is not instantaneous and bar evolution is allowed only if flood duration is sufficiently long with respect to bar timescale, and (iii) the critical threshold, Q_{cr}, discriminates bar-forming and bar-suppressing events. Classical approaches of formative discharge are based on the idea that (i) the larger the sediment transport rate, the larger the morphological work of the channel, (ii) the response of sediment transport to flow variability is instantaneous and (iii) all the flow stages larger than the threshold for sediment motion work in the same direction to determine the investigated phenomenon.

In this chapter we propose a new method to define an occurrence criterion for alternate bars in channelized river reaches that accounts for the hydrological regime. We then derive an estimate of the bar-forming discharge, defined as the discharge whose corresponding bar height coincides with the average value resulting from the hydrological cycle. The method is based on the statistical distribution of flow events and on the response of free alternate bars obtained from the weakly nonlinear Colombini

et al. (1987) model. The occurrence criterion and the bar-forming discharge arise from a balance between bar-forming and bar-suppressing flow stages, which represents a key difference with respect to the classical concept of effective discharge. The procedure has been applied to different gravel bed river reaches, the Alpine Rhine River (Switzerland), the Isère River (France), and the Adige River (Italy), for which long flow records were available, each of them characterised by a distinctive average bed response.

The chapter is organized as follows. In Section 6.2 we briefly summarize previous results on free alternate bars (see Chapters 3 and 4), highlighting their dependence on flow discharge. A general description of the study cases is proposed in Section 6.3. The new model is formulated in Section 6.4 and applied to the different study cases in Section 6.5. In Section 6.6 we discuss the main implications and limitations of the proposed approach; finally, we draw some conclusions in Section 6.7.

6.2 MAIN PROPERTIES OF ALTERNATE BARS

As discussed in previous chapters, bars exhibit some distinctive aspects that must be accounted for to describe their long-term properties in straight channels. Here we provide a summary of the most important characteristics of bars reported in Section 3 that we considered to develop our model.

In single thread channels the actual value of the aspect ratio changes significantly with water discharge. Specifically, being β inversely proportional to water depth, its value typically decreases with increasing flow discharge, as sketched in Fig. 6.1a, and so does the equilibrium bar height. The decreasing trend of bar height with the water discharge, qualitatively reported in Fig. 6.1b, is the first aspect differentiating alternate bars to other morphodynamic processes, whose evidence is driven by the magnitude of sediment transport. A key discharge value for alternate bars is given by the critical threshold for free bars formation, Q_{cr}, defined as the value corresponding to the condition $\beta = \beta_{cr}$.

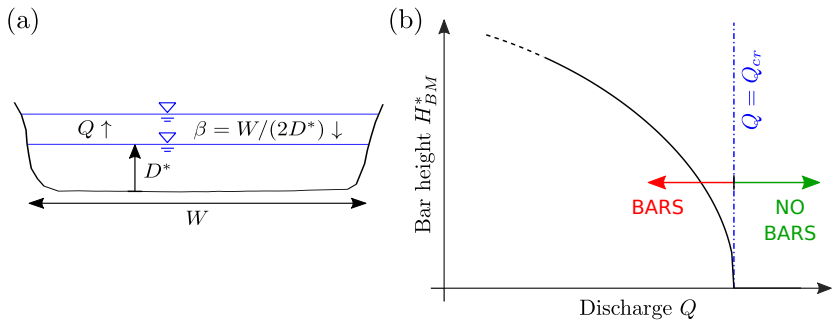

Figure 6.1. Equilibrium response of alternate bars to discharge variations: (a) the effect of increasing discharge, which leads to a decrease of the channel aspect ratio β; (b) the dependence of equilibrium bar height on flow discharge resulting from the Colombini et al. (1987) weakly nonlinear theory.

A second, specific aspect that characterises the response of river bars to different flow stages is the rate of change of their amplitude, which is defined as:

$$\Omega^* := \frac{1}{A^*}\frac{dA^*}{dt^*}, \tag{6.1}$$

where the generic symbol A^* is used here to encompass the various metrics proposed in the literature to measure the bar height. As extensively discussed in Chapter 3, Ω^* is the reciprocal of the time scale of the process and therefore represents a key ingredient to determine the effectiveness of a given flow stage to produce a morphodynamical response.

In general terms, the speed of riverbed evolutionary processes is set by the Exner continuity equation, and therefore it increases with sediment transport intensity, whence with flow discharge. However, bar instability exhibits a remarkably different behaviour (see Section 3.3.2), since the growth rate vanishes not only in correspondence to the threshold for motion, but also at the critical condition for bar formation. Fig. 6.2 summarizes this peculiarity of bar response to discharge variation, highlighting the expected tendency of a given flow stage to form ($Q < Q_{cr}$) or to suppress bars ($Q > Q_{cr}$), playing an opposite role depending on its position relatively to the critical threshold. It is worth noticing that the linear estimate of the bar growth rate is overall valid if the amplitude of bars is small, strictly infinites-

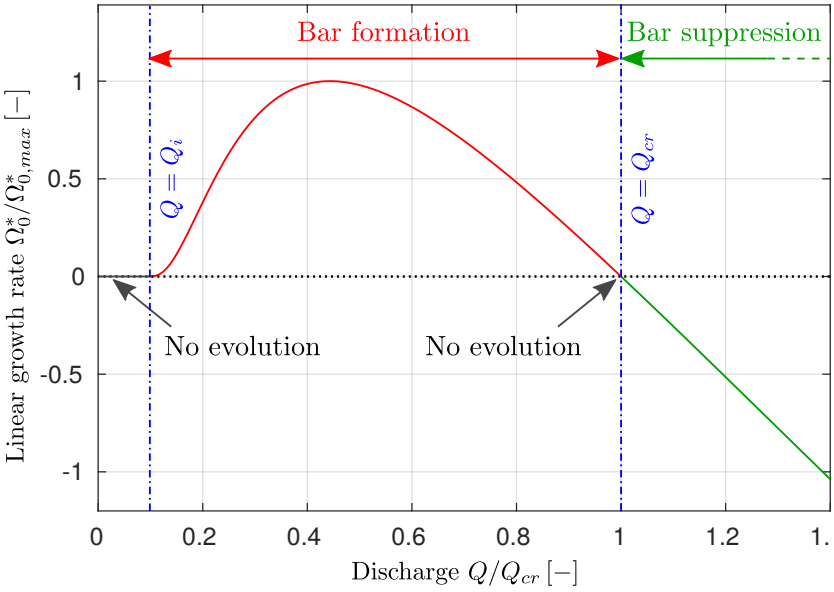

Figure 6.2. The linear growth rate of free alternate bars, scaled with its maximum value $\Omega^*_{0,max}$, as a function of water discharge. The critical threshold Q_{cr} discriminates between bar-forming ($\Omega^*_0 > 0$) and bar-suppressing ($\Omega^*_0 < 0$) flow conditions. When discharge is lower than the threshold of incipient sediment motion, Q_i, the growth rate vanishes and bar evolution is inhibited.

imal. In actual situations flood events are likely to rework an already existing bar topography, which requires also to account for finite amplitude effects on bar growth. In Section 6.4 we discuss how the scenario depicted in Figure 6.2 changes when the weakly nonlinear estimate of (Colombini et al., 1987) for the growth rate is adopted.

The above description of bar response to variable flow discharge can be readily extended to higher-order transverse modes (i.e., central or multiple-row bars). Their critical threshold (say, for mode m) is related to β_{cr} through the relationship $\beta_{cr,m} = m\,\beta_{cr}$, and therefore higher-order modes require large values of width-to-depth ratio to form, the corresponding values of the critical discharge being much smaller than Q_{cr}. However, in relatively wide channels favourable conditions for their growth can be frequently encountered at low flow stages that are still capable of transporting sediment (e.g, Rodrigues et al., 2015). In

the following sections we will focus our attention on the alternate bars mode $m = 1$. However, we will discuss about the limitations and potential extension of our approach to higher-order modes at the end of Section 6.6.

6.3 STUDY REACHES

We applied our model to investigate the riverbed response to the hydrological regime to four study reaches located in three channelized rivers of the alpine region: the Alpine Rhine River, the Isère River and the Adige River. Figure 6.3 shows the location of the study reaches, whose lengths range from 5 to 15 km, while Tab. 6.1 summarizes the reach-averaged values of river properties, as adopted in our analysis, as well as the relevant morphological and hydrological information. Channel width values refer to the morphodinamically active part of the river section, which has been taken to coincide with the bottom width.

The Rhine River, with a catchment area of about 190 000 km^2 and a length of 1326 km is one of the largest rivers in Europe, flowing from the Swiss Alps to the North Sea. The first 93 km of the river, from the confluence between Vorderrhein and Hinterrhein and the Lake of Constance, form the so-called Alpine Rhine. The Alpine sub-basin of the Rhine River covers the whole territory of Liechtenstein, the western part of Austria and the eastern part of Switzerland, draining an area of 6123 km^2. In the 19^{th} and 20^{th} century the Alpine Rhine River was heavily channelized, drastically simplifying the complex multi-thread morphology (Adami et al., 2016). We have focussed our analysis on two reaches located upstream and downstream the confluence of the Ill River (located near Eichenwies), which are representative of two different morphological responses of the riverbed to channelization. In particular, as shown in Figure 6.3a, the wider upstream reach presents a continuous sequence of alternate bars, while the narrower downstream reach displays a simpler morphology without evident bedforms. For this reason, the Alpine Rhine River can be considered an optimal morphodynamic laboratory, where two opposite bed responses manifest themselves, despite the very similar hydrological and sedimentological conditions. The flow regime is pluvio-nival, with significant snow-melt

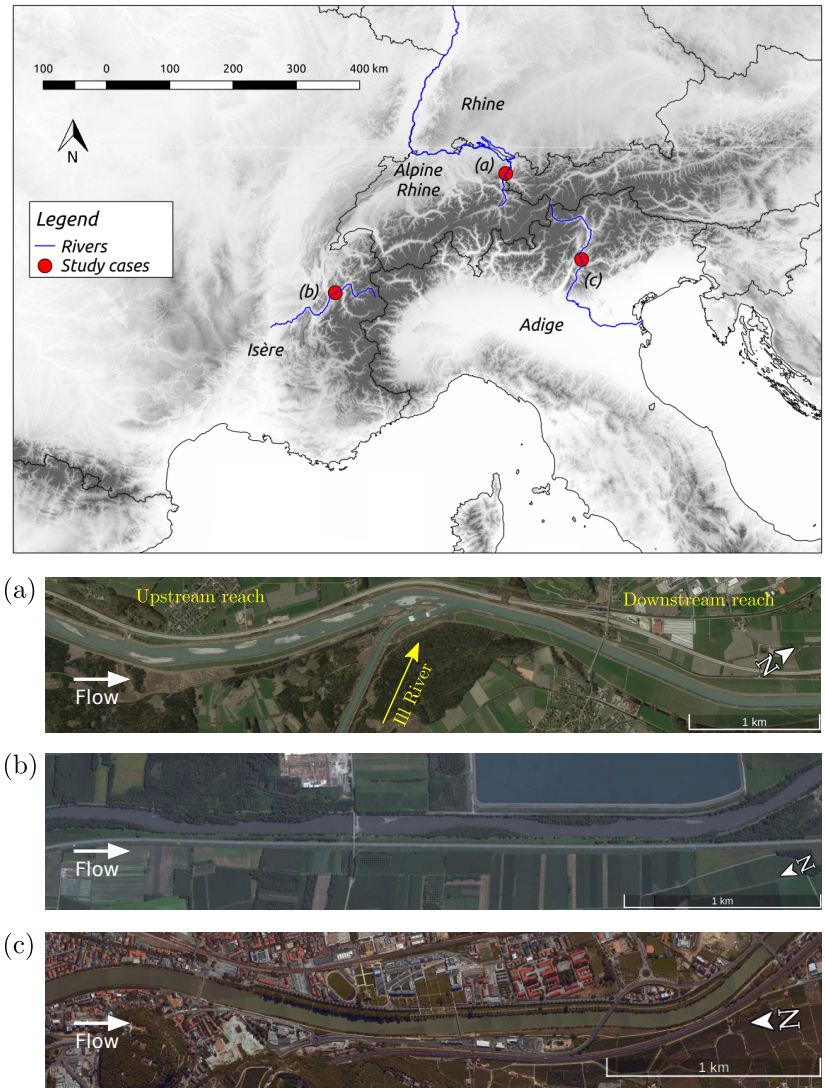

Figure 6.3. Location of the study cases in the alpine region. (a) Two reaches of the Alpine Rhine River, upstream and downstream the confluence of the Ill River, showing a transition from a clear alternate bar pattern to no evident bedforms; 09-Jul-2016, 47° 17′ N, 09° 33′ E; (b) Isère River with stable, vegetated bars, 28-Aug-2014, 45° 23′ N, 05° 59′ E; (c) Adige River with a flat bed morphology, 19-Jul-2015, 46° 03′ N, 11° 06′ E. From Google Earth, Digital Globe (2019).

in spring and summer and larger floods mainly in autumn. Discharge data recorded at intervals of 10 min are available from the Swiss station of Diepoldsau from 1984 to 2010.

The Isère River is 286 km long, flowing from the Graian Alps of Savoia (south-eastern France) to the Rhône River near Valence. The catchment area is about 12 000 km^2. In the 19^{th} century the river was channelized and straightened, causing the modification of riverbed morphology from braided to single-thread with alternate bars (Serlet et al., 2018). After the channelization, an intensive exploitation of the river basin resources for hydropower production began, with the construction of several dams in the early 20^{th} century and two inter-basin transfers. Our study reach is located near Montmèlian, downstream the confluence of the Arc River. The human pressures have strongly impacted on the natural nivo-glacial flow regime and the sediment supply, determining nowadays a very stable sequence of bars, mostly vegetated (see Serlet et al., 2018), as shown in Figure 6.3b. Hourly discharge data are available for the Montmèlian station from 1988 to 2015.

The Adige River, with a catchment of about 12 200 km^2 and an approximate length of 410 km, is the second longest river in Italy, flowing from the central-eastern Alps to the Adriatic Sea. Some sporadic works on channel banks have been carried out since the Middle Age, while a strong channelization was realized in the 19^{th} century. Our study reach is near the city of Trento, where the channel has a bottom width of about 70 m. Sediment samples collected at low flow stages in a recent field survey (Scorpio et al., 2018) have highlighted the presence of a pronounced armoring that is likely to persist over typical floods (Wilcock and DeTemple, 2005). A surface-based estimate provides a value of the median grain size of 53 mm. The bed morphology of the whole channelized part of the river is almost flat, without river bedforms (see Scorpio et al., 2018), as shown in Figure 6.3c. The original flow regime was nivo-glacial, characterised by the minimum flow in winter and larger floods in autumn due to long-lasting cyclonic fronts. Nowadays, the Adige River basin is one of the most exploited in Italy for hydropower production, with a large number of dams built along its tributaries, which have heavily modified the flow regime and filtered the sediment

supply. Discharge data recorded at intervals of 30 min are available for the gauging station of Trento-San Lorenzo from June 1994.

6.4 A METHOD TO DETERMINE THE RESPONSE OF ALTERNATE BARS TO THE HYDROLOGICAL FORCING

In this section we introduce a novel methodology to evaluate the long-term bar response to the river hydrograph, accounting for the key factors that characterise the response of bars to variations of flow discharge. We employ the case of the Alpine Rhine River, where two consecutive reaches exhibit similar hydrological and sedimentological characteristics, but a different bed configuration, as an optimal example to illustrate our procedure and to highlight the difference with respect to the classical method of the effective discharge (Wolman and Miller, 1960).

We assume a rectangular cross section and we compute uniform-flow parameters (i.e. water depth, velocity and associated dimensionless parameters) at different levels of discharge by considering the Engelund and Fredsoe (1982) friction formula. Moreover, we estimate the sediment rating curve through the Parker (1978) transport formula, assuming a relative submerged weight of sediment $R = 1.65$. Sensitivity of model results to the adopted transport predictor is tested in Section 6.6 (see Tab. 6.2), where Meyer-Peter and Muller (1948) formula is also employed. Bar properties are evaluated through the analytical model of Colombini et al. (1987), where the empirical coefficient r that measures the effect of gravity on transverse transport has been set equal to 0.6.

To introduce our procedure, we first consider the application of the effective discharge method to the "upstream" reach of the Alpine Rhine River as reported in Fig. 6.4a: the effective discharge, around $Q = 405\,m^3\,s^{-1}$, is calculated as the peak value of the product between the flow probability density function, f_Q, and the sediment rating curve, $Q_s^*(Q)$. The significance of this value is clear: it represents the discharge that on average gives the maximum contribution to the annual sediment transport (for details, see Appendix A).

Table 6.1. Summary of data for the four study reaches, with the respective references. Q_m and Q_{max} indicate the mean and the maximum discharge, respectively, Q_2 is the discharge value having a return period of two years and c_v is the coefficient of variation (i.e. the ratio between the standard deviation and the mean) of the entire flow series.

		Alpine Rhine[1]		Isère[2]	Adige[3]
		Upstream	Downstream		
Geometry					
Channel slope	[%]	0.13	0.10	0.19	0.08
Channel width	[m]	106	63	92	70
Median grain size	[mm]	25	25	35	53
Flow regime					
Q_m	$[m^3 s^{-1}]$	166	231	121	205
Q_2	$[m^3 s^{-1}]$	1075	1231	463	754
Q_{max}	$[m^3 s^{-1}]$	2399	2666	791	1885
c_v	[-]	0.74	0.68	0.53	0.61
Bar morphology		High-relief bars	Low-relief bars	Vegetated bars	No bars

[1] Adami et al. (2016), Mähr et al. (2014).
[2] Vautier (2000).
[3] Scorpio et al. (2018).

A complementary interpretation of the geomorphic significance of the above procedure can be obtained by considering that the morphodynamical efficacy of each flow stage, which is assumed to increase proportionally with the sediment transport rate, can be equivalently defined in terms of the timescale of the evolutionary process. Specifically, the timescale of the associated geomorphic changes, T^*_{exn}, as defined in eq. (3.9), presents an inversely proportional relation with the sediment transport rate Q^*_s:

$$T^*_{exn} \propto \frac{1}{Q^*_s}. \tag{6.2}$$

We then express the time in terms of T^*_{exn} units, defining a dimensionless time, t_E, whose increments are defined as:

$$dt_E = \frac{dt^*}{T^*_{exn}}. \tag{6.3}$$

Plotting the flow series as a function of t_E gives a reshaped hydrograph $Q(t)$, whose probability density function can be calculated as follows:

$$f_Q^{Q^*_s} = \frac{f_Q \, Q^*_s}{\int_0^\infty f_Q \, Q^*_s \, dQ}, \tag{6.4}$$

which coincides with the definition proposed by Blom et al. (2017) in their Equation (35). The scaled probability density function (6.4) provides a different interpretation of the effective discharge value as the most frequent flow state in the *"time of the sediment transport"*.

6.4.1 *A criterion for the alternate bars formation*

To apply a similar concept to the case of alternate bars, it is crucial to consider that the speed of bar adaptation is not simply proportional to the sediment transport rate, but it rather depends on the growth rate (here we consider the dimensional form of the linear value Ω^*_0). Therefore, it follows the non-monotonic curve represented in Fig. 6.2, which vanishes at both the threshold for incipient sediment motion and at the critical threshold for bar formation.

Considering the characteristic timescale of bars T^*_{bar}, as the dimensional form of eq. (3.7) to scale the time, we then obtain

a reshaped hydrograph that is associated with the following probability density function:

$$f_Q^{\Omega_0^*} = \frac{f_Q \left|\Omega_0^*\right|}{\int_0^\infty f_Q \left|\Omega_0^*\right| \, dQ}, \tag{6.5}$$

which represents the probability of observing a given discharge Q in the *"time of bar adaptation"*. The interpretation of $f_Q^{\Omega_0^*}(Q)$ is again very clear, as it indicates the effectiveness of each discharge state in forming ($\Omega_0^* > 0$) or suppressing ($\Omega_0^* < 0$) alternate bars.

As illustrated in Fig. 6.4b, this probability is basically obtained as the (scaled) product between the flow probability density function, f_Q, and the linear growth rate of bars, Ω_0^*. Similar to the approach of Wolman and Miller (1960), in this case the peak of the histogram gives the value of discharge that is more effective in forming bars, which turns out to be slightly lower than the effective discharge value of Fig. 6.4a.

We note that in the case of the upstream reach of the Rhine River the predicted critical discharge value for bar formation is quite large, approximately $Q_{cr} = 1500\,m^3\,s^{-1}$, and therefore the contribution of the extremely rare bar-suppressing stages ($\Omega_0^* < 0$) is not appreciable. In other words, within this reach bar formation is enhanced at almost all flow stages above the threshold for sediment motion Q_i. Under these circumstances, the information obtained through eq. (6.5) does not differ substantially from that resulting from the effective discharge method, but for the shift of the peak discharge towards lower values.

The difference between the two approaches becomes more evident when applying the same procedure to the downstream reach of the Alpine Rhine River, for which the predicted critical discharge for bar formation is much smaller, approximately $Q_{cr} = 467\,m^3\,s^{-1}$, and then the product of the probability density function and the linear growth rate provides the bi-modal distribution reported in Fig. 6.5. The two peaks still identify two discharge values of maximum effectiveness; however, their meaning is different, as events with $Q < Q_{cr}$ work to *form* the bars, while events with $Q > Q_{cr}$ work to *suppress* them. Hence, Fig. 6.5 highlights the important consequence of bars being a threshold process: different discharge states are not only characterised by different effectiveness, but they can also play in

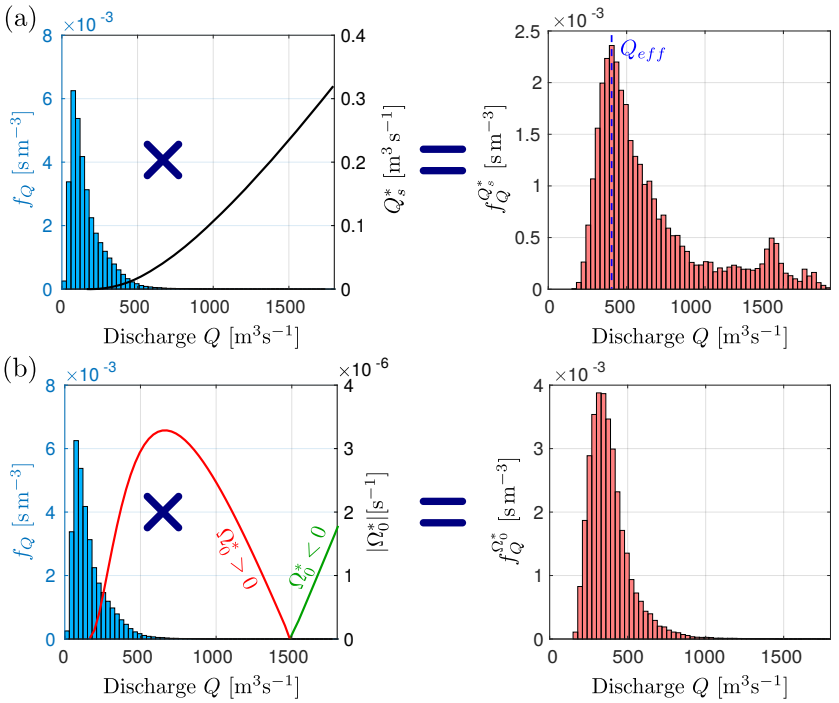

Figure 6.4. (a) The method of Wolman and Miller (1960) applied to the Rhine River reach upstream the confluence of the Ill River. The effective discharge, Q_{eff}, is the peak of $f_Q^{Q_s^*}$ (right panel), obtained by multiplying (left panel) the flow probability density function, f_Q, and the sediment rating curve, $Q_s^*(Q)$. (b) For the same river reach, the probability density function of flow stages, scaled with the timescale of bar adaptation, $f_Q^{\Omega_0^*}$ (right panel), which is obtained by multiplying (left panel) the flow probability density function, f_Q, by the absolute value of the linear growth rate, Ω_0^*.

opposite directions. Even though the slight preeminence of the red area suggests that bar-forming flow events tend to prevail in the downstream reach, we expect the height of bars to be much smaller than that in the upstream reach.

The recognition that bar topography can be continuously reworked by the counteracting effect of different flow stages suggests that the average bar response to the hydrological cycle, rather than being associated to a most effective discharge value, ultimately results from the cumulative effect of the entire range of discharge states. Specifically, it depends on the competition

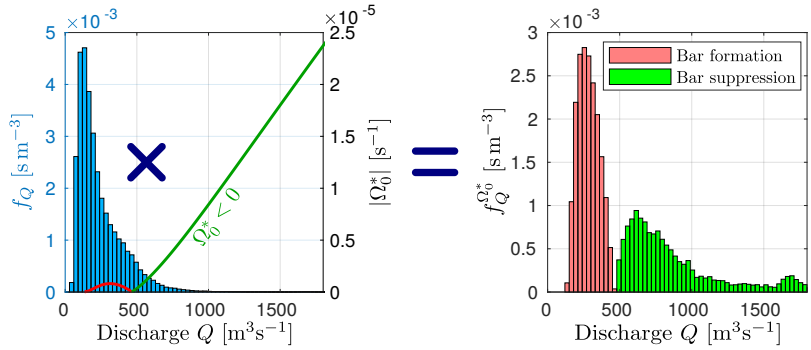

Figure 6.5. The Rhine River reach downstream the confluence of the Ill River: the probability density function of flow stages, scaled with the timescale of bar adaptation, $f_Q^{\Omega_0^*}$ (right panel), which is obtained by multiplying (left panel) the flow probability density function, f_Q, by the absolute value of the linear bar growth rate, $|\Omega_0^*|$. Colors identify bar-forming ($\Omega_0^* > 0$) and bar-suppressing ($\Omega_0^* < 0$) flow stages, depending on discharge being lower or higher than the critical threshold Q_{cr}.

between bar-forming and bar-suppressing events, whose overall effectiveness can be measured as the area of the histogram $f_Q^{\Omega_0^*}$, which represents a probability.

We then define the probability of bar formation in the following form:

$$P_{form} = P^0(Q < Q_{cr}) = \int_0^{Q_{cr}} f_Q^{\Omega_0^*} \, dQ, \tag{6.6}$$

while its complement, $1 - P_{form}$, represents the probability of bars to be suppressed. Therefore, an occurrence criterion for alternate bars that accounts for the hydrological regime can be obtained in the following simple form:

$$P_{form} > 0.5, \tag{6.7}$$

which also corresponds to the condition that the mean growth rate is positive, namely:

$$\Omega_{0,m}^* = \int_0^{\infty} \Omega_0^* \, f_Q \, dQ > 0. \tag{6.8}$$

The above criterion is obviously not strict, as different sources of uncertainties exist in the evaluation of lower and upper threshold discharges, Q_i and Q_{cr}. Furthermore, it refers to the average

state, and therefore indicates a preference for a particular morphodynamic style. Specifically, the probability P_{form} provides a measure of "how likely alternate bars are expected to form in a river reach".

6.4.2 *Definition of the bar-forming discharge and the associated bar height*

When the criterion (6.7) is satisfied, and then alternate bars are likely to form, a further question arises: what is the expected average bar height in the long-term?

To address this question, we propose the idea that the long-term average state of bars should correspond to the condition in which, accounting for the entire range of flow stages, the probability of growth and decay are balanced. In this perspective, we need to quantify the speed of bar height evolution, for the different flow stages.

In this case the information that comes from the linear growth rate Ω_0^* is no longer sufficient, because the tendency of *already-formed* bars to grow or decay is significantly different from that displayed in the early stage of bar formation. This is clear when analysing the behaviour of bar height with time under steady flow conditions, resulting from the weakly nonlinear theory of Colombini et al. (1987) (see Fig. 6.6). When the amplitude is relatively small, bars grow according to the linear growth rate Ω_0^*. However, as the amplitude increases, the bar growth gradually slows down, until the amplitude attains an equilibrium state. Furthermore, if the amplitude exceeds the equilibrium value, bars tend to decay, even under bar-forming conditions (i.e. $Q < Q_{cr}$).

In general, bar evolution can be quantified by means of the growth rate Ω^* (see Fig. 6.6), whose absolute value specifies the rate of change of the bar amplitude, while its sign indicates whether bars tend to grow ($\Omega^* > 0$) or decay ($\Omega^* < 0$). Theoretical works suggest that the time evolution of the bar amplitude, for a given discharge value, follows a Landau-Stuart equation, in which the linear growth rate is multiplied by a correction term that depends on the square of the amplitude, namely:

$$\Omega^* := \frac{1}{A^*}\frac{dA^*}{dt^*} = \Omega_0^* \left[1 - kA^{*2}\right], \tag{6.9}$$

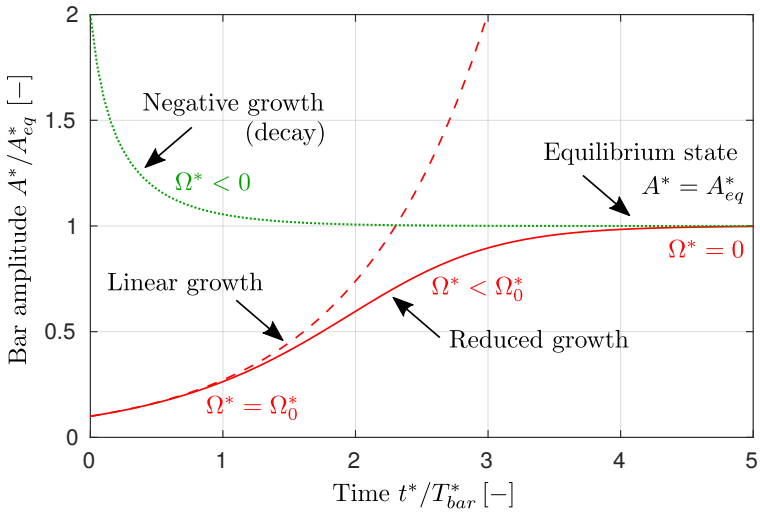

Figure 6.6. Evolutionary trajectories of bar amplitude, scaled by its equilibrium value A^*_{eq}, for a steady discharge $Q < Q_{cr}$ (i.e. under bar-forming conditions), as predicted by the weakly nonlinear theory of Colombini et al. (1987). When $A^* \ll A^*_{eq}$ bar amplitude increases according to the linear growth rate Ω^*_0 (dashed line), while the growth rate gradually decreases when the amplitude approaches its equilibrium value. If $A^* > A^*_{eq}$ the growth rate is negative, and then bars tend to return to their equilibrium state. Time is scaled with the characteristic time of bar growth T^*_{bar}.

where the coefficient k is a function of discharge that can be estimated by means of nonlinear analyses (Colombini et al., 1987; Bertagni and Camporeale, 2018).

It is useful to remember at this stage that bar topography resulting from nonlinear theories can be represented as the superimposition of harmonic components in longitudinal and transverse directions, from which the different metrics adopted to quantify bar height are readily derived, such as the elevation difference within a bar unit, H^*_{BM}, or the maximum value of the elevation differences calculated along individual cross-sections, H^*_B (see also Redolfi et al., 2020). The function A^* appearing in eq. (6.9) represents the amplitude of the dominant, first order, component of bed topography.

When $\Omega_0^* > 0$ (i.e. under bar-forming conditions), the coefficient k is determined by the equilibrium condition $\Omega^* = 0$, which gives:

$$k = A_{eq}^{*-2}, \tag{6.10}$$

so that eq. (6.9) can be expressed as:

$$\Omega^*(Q, A) := \frac{1}{A^*}\frac{dA^*}{dt^*} = \Omega_0^* \left[1 - \left(\frac{A^*}{A_{eq}^*}\right)^2\right]. \tag{6.11}$$

The term in square brackets in eq. (6.11) is always smaller than 1 and simply depends on the ratio between the current bar state and the equilibrium condition, and is always smaller than 1, eventually becoming negative when $A > A_{eq}$. Conversely, when $\Omega_0^* < 0$ (i.e. under bar-suppressing conditions) the parameter k is negative. This implies that $\Omega^* < \Omega_0^*$, which means that finite-amplitude bars tend to decay more rapidly than small-amplitude bedforms.

The resulting scenario of evolutionary trajectories of bars, for the different values of flow discharge characterising the hydrological cycle, is depicted in Fig. 6.7. As highlighted in Chapters 3 and 4, the equilibrium amplitude A_{eq}^* is a decreasing function of flow discharge that vanishes at the critical threshold Q_{cr}. Hence, bar amplitude decays above such threshold and, for $Q < Q_{cr}$, when its actual value is larger than A_{eq}^*. However, the threshold limit set by A_{eq}^* does not cover the full range of discharge states above the critical threshold Q_i. In fact, when the discharge is smaller than the so-called fully-wet threshold Q_{fw} (see Adami et al., 2016) the theoretical estimate of the equilibrium amplitude is no longer meaningful, because the theory predicts bars whose top elevation, at equilibrium, would exceed the water surface level (which is not compatible with the fundamental model assumptions). To circumvent this limitation, here we follow the approach suggested in Chapter 4, assuming that within this range of discharges the bar growth is bounded by the fully-wet value A_{fw}^*, which corresponds to the theoretical estimate of the amplitude when bars are at the onset of emerging from the water surface. Therefore, when $Q < Q_{fw}$, the growth rate follows the same trend described by eq. (6.11), but with A_{fw}^* representing the asymptotic limit. The fully-wet amplitude A_{fw}^* increases

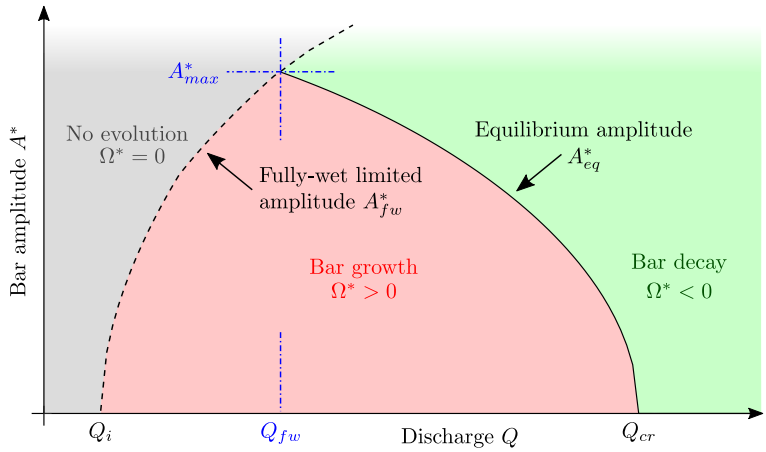

Figure 6.7. Morphological trajectory of alternate bars (defined by the sign of the growth rate Ω^*) depending on discharge and bar amplitude. Different regions (shaded areas) are delimited by the equilibrium amplitude (solid line) and the fully-wet limited amplitude (dashed line), depending on discharge being higher or lower than the fully-wet threshold Q_{fw} (see Redolfi et al., 2020). The point where the two lines intersect identifies the maximum bar amplitude A^*_{max}.

with the water discharge as illustrated in Fig. 6.7 and sets the left margin of the region of bar growth. Beyond this limit, as for values of $Q < Q_i$, we assume a vanishing growth rate, which implies that low flow stages are unable to substantially rework already-formed bars whose crests emerge from the water surface.

In summary, depending on the actual values of bar amplitude and discharge, three distinct regions can be identified, as illustrated in Fig. 6.7: (i) no evolution region, where the growth rate vanishes; (ii) bar growth region, where Ω^* is positive; (iii) bar decay region, where Ω^* is negative.

The above findings set the conceptual framework to define the average state of bars within a given river reach. With reference to Fig. 6.8a, let us assume a tentative value of the average bar amplitude, A'^*_{as}, and compute the corresponding growth rate of bars for the different flow stages:

$$\Omega'^* := \Omega^*(Q, A'^*_{as}). \tag{6.12}$$

Moving from low to high flows at a fixed value of bar amplitude we cross the three regions highlighted in Fig. 6.8a, which reflects

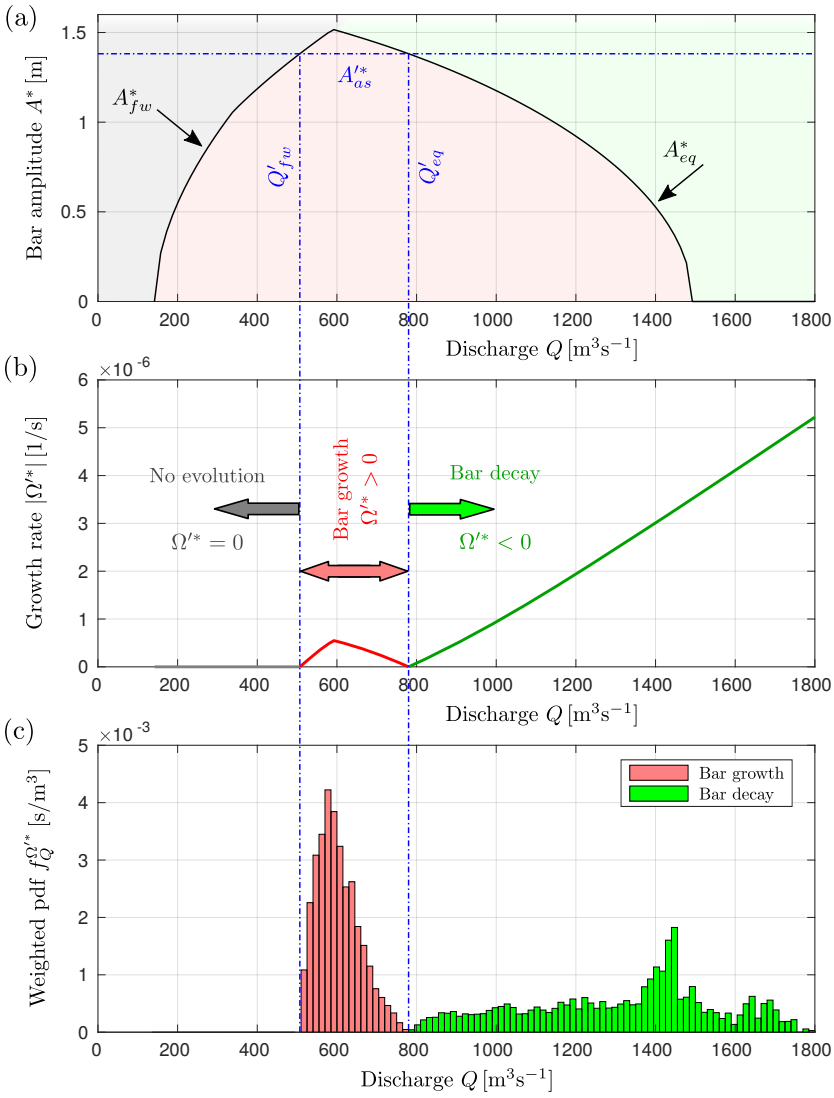

Figure 6.8. Illustration of the procedure for the evaluation of the average bar state: example of the upper reach of the Alpine Rhine River. (a) The regions of growth and decay, for a given value of the average bar amplitude A'^*_{as}. (b) The corresponding values of the growth rate Ω'^* for bars of amplitude A'^*_{as}. (c) Frequency of the flow events, weighted with the growth rate Ω'^*, which measures the effectiveness of the different flow states. Bars are assumed to be in long-term equilibrium when the probability of bar growth (i.e. red area) equals the probability of bar decay (i.e. green area).

on the resulting curve represented in Fig. 6.8b. Specifically, if we denote by Q'_{fw} and Q'_{eq} the discharge corresponding to the intersections with the fully-wet threshold, A^*_{fw}, and the equilibrium amplitude, A^*_{eq} (see Fig. 6.8a), the growth rate is positive when $Q'_{fw} < Q < Q'_{eq}$, otherwise it is either negative or vanishing.

We then define, as before, the scaled probability:

$$f_Q^{\Omega'^*} = \frac{f_Q\,|\Omega'^*|}{\int_0^\infty f_Q\,|\Omega'^*|\;dQ}, \tag{6.13}$$

which represents the effectiveness of the different discharge states in producing bar growth or decay, depending on the sign of Ω'^*. The cumulative effectiveness of the events with positive Ω'^* (i.e. the red area of Fig. 6.8c),

$$P_{growth}(A'^*_{as}) = P(Q'_{fw} < Q < Q'_{eq}) = \int_{Q'_{fw}}^{Q'_{eq}} f_Q^{\Omega'^*}\,dQ, \tag{6.14}$$

defines the probability of bars with the given amplitude A'^*_{as} to grow, while its complement, $(1 - P_{growth})$, measures the tendency to decay.

If $P_{growth} > 0.5$, bars of amplitude A'^*_{as} are likely to experience a long-term growth, while the opposite tendency is expected when $P_{growth} < 0.5$. Therefore, we can assume that a long-term equilibrium is attained when:

$$P_{growth} = 0.5. \tag{6.15}$$

This condition implicitly defines the value of the long-term average bar amplitude A^*_{as}. In practice, this value can be obtained by varying A'^*_{as} until the condition (6.15) is met, i.e. when the red and the green areas of Fig. 6.8a become equal.

Once the long-term average bar amplitude has been determined, we then compute the average-state bar topography and the associated bar height, through the weakly nonlinear solution of Colombini et al. (1987), and we define a bar-forming discharge, Q_{form}, as the value of discharge $\widehat{Q}_{eq}$ associated with the resulting average bar amplitude. Therefore, Q_{form} is the discharge that if maintained indefinitely would produce the same long-term bar topography as the river hydrograph (see the analogy with the channel-forming discharge proposed by Blom et al., 2017).

6.5 RESULTS

We now apply the methodology developed in Section 6.4 to the four study cases described in Section 6.3: a summary of model results is reported in Table 6.2. The procedure is based on two steps.

1. We first provide a criterion for evaluating whether bars are likely to form, which is based on the idea that this depends on how long the river stays in bar-forming conditions with respect to bar-suppressing conditions. The key novelty is that the duration of different flow stages is measured *in the time of the bars*, rather than in *absolute time*. This is accomplished by multiplying the flow probability density function by the linear bar growth rate, and comparing the weight of the resulting distributions that falls above or below the critical threshold for bar formation, Q_{cr}.

2. We then provide a criterion for estimating the long-term bar topography, which is based on the idea that the average state of bars corresponds to conditions for which the probabilities of bar growth and decay are equal. The key ingredient is that the effectiveness of the different discharge states not only depends on the discharge value, but also on bar amplitude, as suggested by nonlinear bar theories. Specifically, the higher is the bar, the wider is the range of discharge states for which bar amplitude tends to decay.

6.5.1 *The two cases of the Alpine Rhine River*

In the case of the upstream reach of the Alpine Rhine River, the value of probability resulting from eq. (6.6) is very high ($P_{form} = 0.99$, see Table 6.2), which indicates that alternate bars are very likely to form. Conversely, in the downstream reach the probability is around 50 % ($P_{form} = 0.58$), which reveals that the total work of bar-forming and bar-suppressing events (red and green area of Figure 6.5) almost balances. Therefore, the average state is close to the limiting conditions for bar formation,

Table 6.2. Summary of model results for the four study cases, as obtained with the transport formulas of Parker (1978) (P78) and Meyer-Peter and Muller (1948) (MPM). Q_{eff} is the effective discharge value (Wolman and Miller, 1960), Q_i and Q_{cr} are the critical values for incipient sediment motion and for bar formation, respectively, Q_{fw} is the fully-wet threshold, P_{form} is the probability of bar-forming events, $\Omega^*_{0,max}$ is the maximum bar growth rate, $H^*_{B,a}$ the average bar height and Q_{form} the corresponding bar-forming discharge. T_r indicates the return period of the reported discharge values.

		Alpine Rhine				Isère		Adige	
		Upstream		Downstream					
		P78	MPM	P78	MPM	P78	MPM	P78	MPM
Q_{eff}	$[m^3s^{-1}]$	405	435	465	465	330	350	1387	1388
$T_r(Q_{eff})$	[y]	1	1	1	1	1.19	1.26	16.37	16.43
Q_i	$[m^3s^{-1}]$	142	304	116	246	130	278	494	1048
Q_{cr}	$[m^3s^{-1}]$	1493	1278	467	456	1326	1136	938	1248
$T_r(Q_{cr})$	[y]	5.05	3.06	1	1	> 200	> 200	3.45	9.93
Q_{fw}	$[m^3s^{-1}]$	585	615	255	345	530	550	788	1213
$T_r(Q_{fw})$	[y]	1.06	1.08	1	1	2.87	3.23	2.19	8.77
P_{form}	[%]	99.9	99.8	57.9	56.8	100.0	100.0	11.4	16.7
$\Omega^*_{0,max}$	$[d^{-1}]$	0.284	0.461	0.070	0.196	0.578	0.952	0.005	0.050
$H^*_{B,a}$	[m]	2.4	2.5	0.49	0.53	2.6	2.7	0	0
Q_{form}	$[m^3s^{-1}]$	778	717	442	421	602	602	-	-
$T_r(Q_{form})$	[y]	1.25	1.17	1	1	4.45	4.45	-	-

in which bars that might possibly form would attain an almost vanishing amplitude.

We then compute the average-state bar topography and the associated bar height, through the weakly nonlinear solution of Colombini et al. (1987). Being based on extreme elevation values, the above-mentioned metrics H^*_{BM} and H^*_B are difficult to derive from field data, as different sources of measurement uncertainty exist and available cross-sectional data do not necessarily comprise the points of maximum and minimum elevation. Therefore, for comparison with field data we compute the mean value of the cross-sectional elevation differences in a bar wavelength, $H^*_{B,a}$. Results illustrated in Tab. 6.2 reveal that the estimated long-term bar height $H^*_{B,a}$ in the upstream reach of the Alpine Rhine River is about 2.4 m for both the tested sediment transport relations, while a much smaller value ($H^*_{B,m} \simeq 0.5$ m) is obtained for the downstream reach. This is in overall agreement with field measurements based on cross-sectional elevation data. Specifically, data for the upstream reach reported in Adami et al. (2016) (see their Figure 9) display cross-sectional elevation differences in the range from 2.5 to 4.0 m, while for the downstream reach we observe low-relief, submerged bars with an average height of about 0.4 m. It is worth noticing that the predicted value of bar height H^*_B for the upstream reach turns out to be 3.7 m, very close to the maximum values measured in the field. This comparison highlights the potential of our methodology to evaluate the long-term bar topography, though the theoretical estimates slightly overestimate the observed values of $H^*_{B,a}$. This difference can be easily corrected by tuning the empirical coefficient r that measures the effect of the lateral bed slope on bed-load transport. It is worth noticing that the proposed procedure provides a sound interpretation of the different bed response exhibited by two consecutive reaches of the Alpine Rhine River, upstream and downstream the confluence of the Ill River.

As reported in Table 6.2, the resulting values of the bar-forming discharge, Q_{form}, for the upstream reach of the Rhine River range from 720 to 780 $m^3\,s^{-1}$, depending on the transport formula used, and the associated return period is only slightly longer than one year. For the downstream reach the discharge value is very close to the critical threshold, which confirms the

river's weak propensity to form alternate bars. We note that the value of the bar-forming discharge is larger than that of effective discharge Q_{eff} in the upstream reach, while the opposite occurs in the downstream reach.

Results reported in Tab. 6.2 show that the proposed criterion for bar occurrence, which is based on P_{form}, and the predicted values of the average bar height and bar-forming discharge are almost independent of the adopted sediment transport formula. They also suggest that the different behaviour displayed by the downstream reach is mainly a consequence of the reduction of the critical bar threshold, and of the corresponding return period, due to its smaller channel width. Therefore, while bar-suppressing stages are extremely rare in the upstream reach, they become much more frequent in the downstream reach, which results in a barely visible bar pattern. Furthermore, the maximum positive value of the growth rate $\Omega^*_{0,max}$ (see Tab. 6.2) is larger for the upstream reach. We note that $\Omega^*_{0,max}$ provides an estimate of the timescale required for bar evolution, which is of the order of a few days for the upstream reach of the Rhine River. Such estimate, when combined with the resulting value of the return period of the bar forming discharge Q_{form}, suggests that bar topography in the upper Rhine may undergo significant changes during yearly recurring flood events.

6.5.2 *The cases of the Adige and the Isère River*

The study reach of the Adige River is characterised by an almost flat bed morphology and therefore represents a sort of limit case of the downstream Alpine Rhine River reach. Bar-suppressing events dominate over the bar-forming counterparts, as illustrated in Fig. 6.9a. Therefore, the resulting probability P_{form} is well below 0.5, as reported in Tab. 6.2, which implies that the formation of bars is very unlikely. We note that the presence of an armored bed surface, with a relatively large sediment size, produces a twofold effect: (i) the threshold for sediment motion Q_i is quite large and gets closer to the critical value Q_{cr}, which makes the flow events able to mobilize the riverbed relatively rare, while narrowing the range of bar-forming events; (ii) the maximum positive value of the growth rate $\Omega^*_{0,max}$ (see Tab.

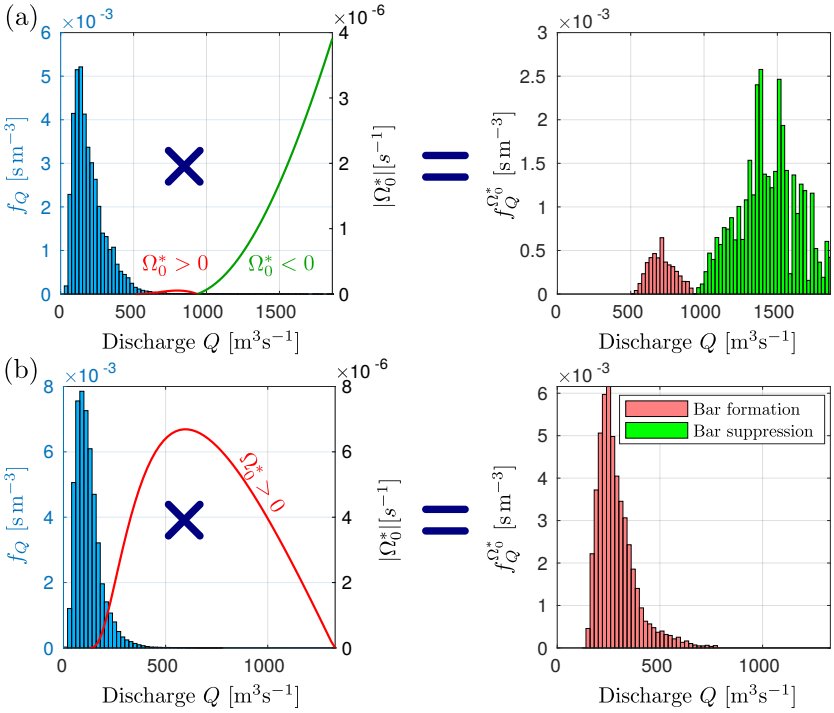

Figure 6.9. The scaled probability function for the Adige River (a) and for the Isère River (b), obtained by multiplying the flow probability density function f_Q (histogram) by the absolute value of linear bar growth rate $|\Omega_0^*|$ (solid line). The resulting histogram on the left panels represents the effectiveness of different flow states to form (red area) and to suppress (green area) alternate bars.

6.2) is quite small, say one-two orders of magnitude smaller than for the Rhine River, meaning that the process of bar formation is very slow. This implies that bar-forming events in the Adige River are not only less effective than bar-suppressing events, but they are also characterised by a very low effectiveness in *absolute* terms. A flood event lasting tens/hundreds of days within the formative range ($Q_i < Q < Q_{cr}$) would be required to allow a significant bar growth.

The case of the Isère River represents an opposite situation with respect to the Adige River, as the study reach displays a stable sequence of high-relief vegetated bars, whose average height $H_{B,m}$ is about 3.5 m. The river width is such that the threshold value Q_{cr} is very high, the return period being above

200 years, and therefore bar-suppressing events are extremely unlikely. The scaled probability function reported in Fig. 6.9b closely resembles that of the upper Rhine River. However, the return period of both the resulting bar-forming discharge Q_{form}, which is about 600 $m^3\ s^{-1}$, and of the fully-wet threshold Q_{fw} is much longer. This implies that flood events able to substantially rework the bar topography are relatively rare in the Isère River, which provides a favourable condition for vegetation development. The above findings are confirmed by the results of the numerical investigations of Jourdain et al. (2020), who analysed the influence of large events on bar dynamics in the Isère River, accounting for the role of riparian vegetation, and found that the actual equilibrium morphology of bars and vegetation cover can be associated with large floods, with a peak value of 800 $m^3\ s^{-1}$. We also note that the predicted average bar height $H_{B,a}$ resulting from our procedure, about 2.7 m, is in reasonable agreement with field measurements.

6.6 DISCUSSION

In this section, we emphasize the main difference between our definition of bar-forming discharge and the classical concept of formative discharge, and provide a generalized criterion for bar occurrence, depending on river and flow characteristics. Finally, we discuss the main limitations of the proposed methodology.

6.6.1 *Effective and bar-forming discharge*

The novel concept of bar-forming discharge proposed in this work significantly differs from the classical definition of effective discharge in terms of its dependence on river characteristics. To highlight this difference, we assume for simplicity that the probability density function of flow events can be represented by a two parameters distribution, so that it can be specified by fixing the mean discharge Q_m and the coefficient of variation c_v. Specifically, we consider a log-normal distribution (often implemented in engineering applications e.g. Castellarin et al., 2004; Bowers et al., 2012), which has been proven to effectively

reproduce the flow frequency distribution in the Rhine River (see Bertagni et al., 2018).

Under this hypothesis, the dependence of the bar-forming and effective discharge on flow and river parameters can be given in the following functional form:

$$\{Q_{form}, Q_{eff}\} = f\left(\underbrace{Q_m, c_v}_{\text{Flow parameters}} , \underbrace{S, W, d_{50}, g, \rho, \rho_s}_{\text{River parameters}} \right), \quad (6.16)$$

where ρ and ρ_s are water and sediment density, and g is the gravitational acceleration. The above relationship can be conveniently expressed in dimensionless form:

$$\left\{ \frac{Q_{form}}{Q_i}, \frac{Q_{eff}}{Q_i} \right\} = f\left(\frac{Q_m}{Q_i}, c_v, S, \frac{W}{d_{50}}, R \right), \quad (6.17)$$

where the threshold value for incipient sediment motion (Q_i) is used as scaling discharge.

In the case of the effective discharge, the functional relationship (6.17) can be reduced to a much simpler form. Specifically, assuming that the flow rating curve follows a power law with exponent b gives the following expression for the Shields parameter:

$$\frac{\theta}{\theta_i} = \frac{SD^*/(Rd_{50})}{SD_i^*/(Rd_{50})} = \frac{D^*}{D_i^*} = \left(\frac{Q}{Q_i} \right)^{1/b}. \quad (6.18)$$

Consequently, the response of the dimensionless sediment transport flux to variations of Q/Q_i is substantially independent of channel width, slope and sediment density, so that the scaled effective discharge merely depends on flow distribution relative to the threshold for sediment motion, namely:

$$\frac{Q_{eff}}{Q_i} = f\left(\frac{Q_m}{Q_i}, c_v \right). \quad (6.19)$$

Conversely, the bar-forming discharge retains an explicit dependence on river parameters as expressed by eq. (6.17). To analyse this dependence, we imagine an ideal experiment where channel width is increased and the mean discharge is proportionally increased (i.e $Q_m \propto W$), while maintaining constant slope, grain size and coefficient of variation. As illustrated in Fig.

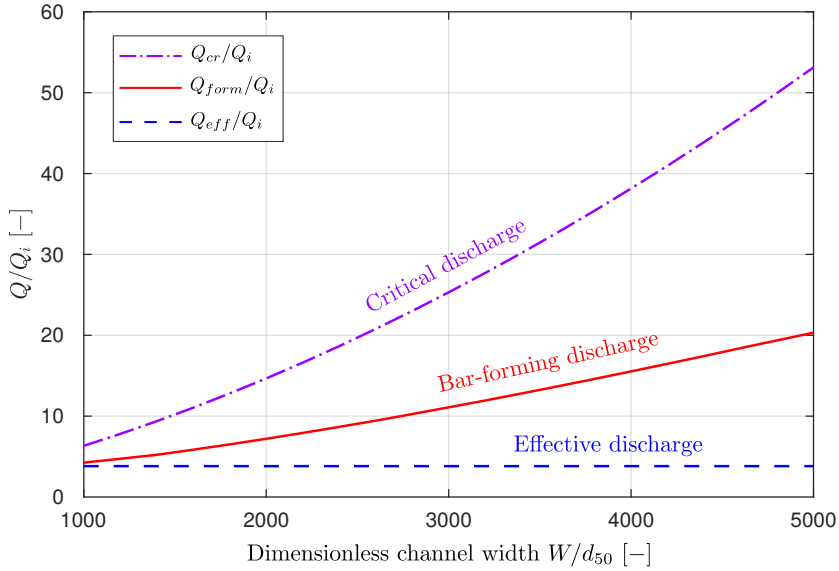

Figure 6.10. Effective (dashed line), bar-forming (solid line) and critical (dash-dot line) discharge (normalized with the incipient sediment motion discharge Q_i) as a function of the dimensionless channel width, illustrating the remarkable different response of the bar-forming discharge and the effective discharge to variations of river parameters. Example with channel slope $S = 0.30\,\%$, coefficient of variation $c_v = 0.7$, relative submerged weight of sediment $R = 1.65$, and $Q_m/Q_i = 2$.

6.10 the scaled bar-forming discharge increases with the channel width, and so does the scaled critical discharge, while Q_{eff}/Q_i remains constant. An analogous behaviour is obtained when changing the channel slope. This highlights the sensitivity of the bar-forming discharge to river parameters, and marks a clear difference with respect to the effective discharge, which depends on river characteristics only through changes of the threshold discharge Q_i.

6.6.2 *A criterion for bar formation under unsteady flow conditions*

The criterion for bar formation defined by eq. (6.7) can be generalized by plotting marginal curves that identify the regions of bar occurrence in the space of the key controlling parameters. In particular, for given values of flow and river parameters it is possible to identify a threshold channel width, W_{cr}, which

discriminates channels where alternate bars are likely to form from cases where no bars are expected. This enables for building bar existence diagrams, such as that illustrated in Fig. 6.11, where values of parameters typical of gravel bed rivers have been considered.

The critical width increases with the mean discharge, for given values of slope and grain size. This is because at higher flow values the mean duration of bar-suppressing events expands, so that wider channels are needed to allow for bar formation. The effect of channel slope and grain size variations is more complex, as it depends on the associated changes of the threshold discharge values, Q_i and Q_{cr}, that define, for given Q_m, the lower and upper limits of the range of bar-forming stages.

On one hand, increasing the channel slope lowers the threshold for incipient sediment motion Q_i, and therefore the region of bar occurrence widens, the more so because the critical threshold Q_{cr} generally increases with the channel slope. As a result the critical width W_{cr} gets smaller. However, at relatively low values of the Shields parameter θ the critical discharge displays an opposite, decreasing trend with the channel slope, which reflects the sharp increase with θ of the critical width-to-depth ratio β_{cr} predicted by bar theories (see Figure 6 of Colombini et al., 1987). This implies that the effect of slope variation becomes weaker (and possibly reverses). For more details about the dependence of the critical discharge with respect to the channel slope see Section 3.4.2, in which Fig. 3.11 displays the above explanation.

We note that, in terms of the parameters employed in Fig. 6.11, the Shields parameter gets smaller when both the mean discharge and the channel slope are relatively low and the sediment is coarser (dashed lines of Fig. 6.11). On the other hand, increasing the grain size leads to contrasting effects on bar formation, because Q_i gets larger and also Q_{cr} generally increases (see again Figure 6 of Colombini et al., 1987). The net effect of the competition between these two factors leads to an overall increase of the critical width as the sediment gets coarser, except for relatively low values of mean discharge and channel slope. Moreover, the effect of grain size reduces when raising the channel slope, becoming practically irrelevant for $S > 0.5\,\%$.

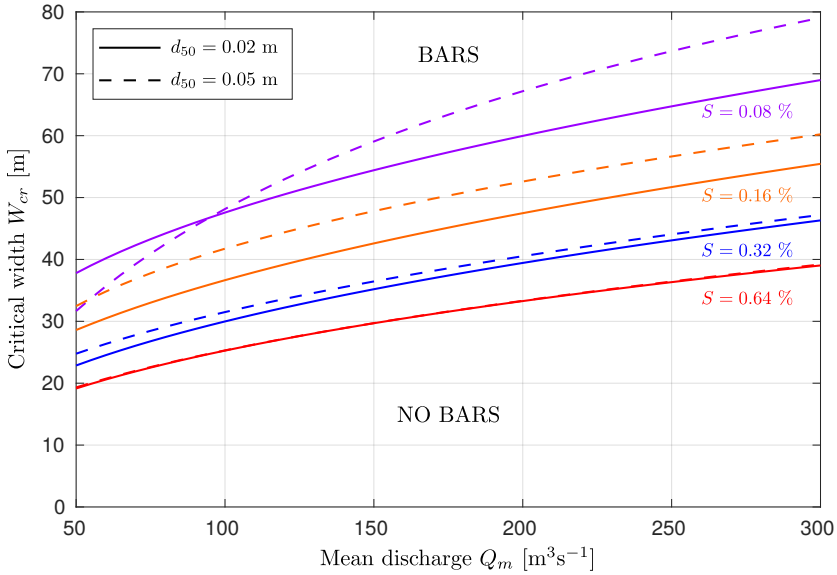

Figure 6.11. Critical channel width as a function of the mean discharge, for different values of channel slope (S) and median grain size (d_{50}), with dashed lines indicating the coarser bed material. Alternate bars are expected to form when the channel width exceeds the critical threshold W_{cr}. Example with fixed coefficient of variation $c_v = 0.7$.

6.6.3 *Limitations and future perspectives*

The procedure outlined in Section 6.4 to define the long-term bar height, and the corresponding formative discharge, is based on the assumption that the bar state can be represented by the average amplitude A^*_{as}, so that the long term bar evolution merely depends on the expected frequency of the different discharge states. Specifically, eq. (6.12) accounts for the effect of discharge changes on the growth rate, while it neglects the role of bar amplitude variations with respect to the average state, which may occur during individual flow events. These fluctuations can produce a net effect on the average growth rate, and therefore on the average bar height. However, as demonstrated by Carlin et al. (2020), their role is usually negligible when bar adaptation to changing discharge is comparatively slow (see Tubino, 1991), to such an extent that individual flow events are not capable to produce strong modifications of bar height. Conversely, the dependence of bar growth on the instantaneous bar amplitude

becomes relevant when the characteristic duration of flood events is long enough to heavily rework bar topography. In this case one should resort to different metrics to fully characterise, in a statistical sense, the flow regime, because the definition of the average state of bars would require to take into account the duration and sequencing of the individual flow events, an information that is not contained in the flow probability density function.

In our analysis we have assumed that the alternate mode, $m = 1$, is the dominant transverse mode of bar topography, as it is often the case of channelized river reaches. However, higher-order modes (e.g. central bars) can also develop in relatively wide channels, specifically at low flow stages, i.e at large width-to depth ratio values, provided their respective critical discharge exceeds the threshold for incipient sediment motion. The proposed methodology can be readily extended to determine the conditions for the possible formation of higher modes. For example, to assess whether central (i.e., $m = 2$) bars may form, we can compute their linear growth rate $\Omega_0^*(m = 2)$ and repeat the same procedure outlined in Section 6.4 to obtain the associated probability $P_{form}(m = 2)$. We note, however, that in this case the condition (6.7) is no longer sufficient, because both the alternate and central bar modes are simultaneously unstable, and therefore an additional criterion is required to determine the dominant mode resulting from their competition. Ultimately, a fully nonlinear, numerical solution would be required to determine the outcome of such competition. However, a common, albeit approximate, criterion is based on selecting the mode that displays the higher linear growth rate for a given discharge (e.g., Fredsoe, 1978; Seminara and Tubino, 1989). A straightforward way to extend this criterion to the entire river hydrograph is to compute the mean growth rate, defined as in eq. (6.8), and to compare the resulting values for the two modes. Two out of the four study cases analysed in Section 6.5 return a value of $P_{form}(m = 2)$ higher than 0.5, namely (and not surprisingly) the upstream reach of the Alpine Rhine River and the Isère River, suggesting that central bars might potentially form, especially at low flow stages. However, in both cases we obtain $\Omega_0^*(m = 1) > \Omega_0^*(m = 2)$, which implies that the alternate bar mode dominates. A detailed validation of this procedure

is beyond the scope of the present work, as it would require the analysis of more comprehensive data set, along with a comparison with alternative criteria based on the amplification of non-migrating bars (e.g., Crosato and Mosselman, 2009).

Finally, it is worth highlighting that in this paper we focus on gravel bed rivers, or at least on cases where most of the sediment is transported as bedload. However, our methodology can be naturally extended to rivers dominated by suspended sediment transport, provided that growth rate and equilibrium amplitude are suitably computed (e.g., by means of the three-dimensional, weakly non linear theory of Bertagni and Camporeale, 2018). In this case, even more attention is probably needed to investigate the competition among different unstable modes (Tubino et al., 1999) and the possible interaction between bars and migrating dunes (Colombini and Stocchino, 2012).

6.7 CONCLUSIONS

In this chapter we have investigated the response of bar topography to the hydrological regime, coupling the information derived from the statistical distribution of flow events with the theoretical predictions obtained from the weakly nonlinear model of Colombini et al. (1987). On the basis of the results of our study and the analysis of four gravel bed river reaches, we can draw the following conclusions:

1. We propose a novel criterion for determining whether free alternate bars are expected to form in a river reach, which depends on channel characteristics and on the probability distribution of flow events. The criterion is not merely based on the time spent by the river in bar-forming and bar-suppressing conditions, but also considers the effectiveness of the different discharge states, as measured by the linear bar growth rate.

2. The above criterion entails the definition of a threshold channel width W_{cr} that sets the transition between two different morphological styles. Modelling the response of bar topography by means of a theoretical model allows for

analysing the dependence of the threshold width on the key physical parameters.

3. When the river width is larger than W_{cr}, we propose a procedure for estimating the average bar height, which results from a long-term balance between the enhancing effect of moderate flow events and the opposite effect of more intense flood events.

4. The long-term average bar state allows us to define a bar-forming discharge as the value that, if applied steadily, would give the same bar amplitude as the hydrological regime. Differently from the effective discharge (Wolman and Miller, 1960), the bar-forming discharge is highly sensitive to variations of river characteristics, primarily the channel width.

The proposed method provides a sound interpretation of the markedly distinct bed configurations displayed by different gravel bed river reaches, along with a reasonable estimate of the long-term bar height resulting from a complex sequence of flow events. Therefore, the procedure could be suited to various applications, such as the analysis of long-term morphological trajectories following different scenarios of hydrological alterations (e.g. climate change, hydropower exploitation) and river engineering interventions (e.g., channel widening).

7

THE EFFECT OF FLOOD EVENTS ON THE ALTIMETRIC RESPONSE OF RIVER ALTERNATE BARS

7.1 INTRODUCTION

In Chapter 6 we investigated how the long-term, average properties of bars respond to changes of the hydrological regime. This average state represents the overall result of a multitude of flood events, each of them producing a different morphological alteration. However, a systematic description of how changes of bar properties depend on the characteristics of the individual floods is still missing, as existing studies are limited to a small number of flood events, not sufficient to make a statistical description of the riverbed response (e.g., Welford, 1994; Eekhout et al., 2013).

In this chapter, we aim at studying the time evolution of the bar amplitude in the relatively straight, channelized reaches of study cases presented in Section 6.3 (i.e. two reaches of the Alpine Rhine River upstream and downstream to the confluence with Ill River, the Adige River near Trento and the Isère River near Montmèlian), for which a detailed and long record of flow stages is available. This is accomplished by modelling the bed evolution through the theoretically-based model of Colombini et al. (1987), here applied by considering a time-varying basic flow and numerically integrating the bar amplitude. Compared with classical approaches based on numerically solving the two-dimensional shallow-water equations, our procedure allows for calculating the bar response over long periods of time with a very low computational cost.

This method enables to statistically analyse the expected impact that the flow regime has on bar evolution, investigating the effect produced from each flood event to the amplitude of bar. Focussing on the upstream reach of the Alpine Rhine River, which is a perfect laboratory to investigate bar evolution, and assuming that bars cannot evolve when the flow is too low to fully

submerge the bar crests (Redolfi et al., 2020), we identify more than 200 morphologically-active flood events, covering about 1.1 % of the total duration of the flow series. Model results reveal that moderate flow events tend to increase the bar amplitude, while larger floods reduce the bar height. However, the value of the peak discharge alone is not sufficient to explain the morphological changes, as an important (and opposite) role is also played by the duration of the events. Specifically, longer floods tend to promote an increase of the bar height during the receding phase, which implies that a strong reduction of the bar amplitude requires intense, but relatively short flood events. Furthermore, such analysis allows for a qualitative classification of flood events on the basis of their effect in modifying the amplitude of bars.

Finally, the model allows for simulating how the response of alternate bars in a river reach is affected by modification of the hydrological flow regime. Specifically, we model two scenarios of hydrological alteration representing the construction of a reservoir and the effect of future climate changes.

7.2 METHOD

7.2.1 *Morphological model for bar amplitude evolution*

The weakly nonlinear model of Tubino (1991) provides an analytical solution to describe how bar amplitude changes during a flood event by approaching the problem thorough a perturbation method. Specifically, this model extended the Colombini et al. (1987) theory to unsteady flow conditions, by linearizing the flow variability with respect to a reference discharge value, assuming weak such flow variability.

As a result of this linearized approach, the growth rate of bars linearly varies with the discharge, limiting the model applicability when discharge values do not largely depart from the reference conditions. This is a limitation in applying the Tubino (1991) model to actual flow series, since the range of discharge variation is almost 2 orders of magnitude wide. An evidence of such limitation can be observed by steadily comparing the linear bar growth rate predicted by the two models of Colombini et al. (1987) and Tubino (1991) as reported in Appendix B (see Fig. B.4).

We observe a large overestimation of the capability of low flows (i.e. in the neighborhood of the threshold for motion) to allow for bar evolution.

In this chapter we apply the weakly nonlinear model of Colombini et al. (1987) by modelling the flow variability as a sequence of steady-states. The overall idea is to assume the discharge constant in each temporal step and to compute the increment of bar amplitude accordingly with the Landau-Stuart type equation that describes the evolution of bar amplitude in time. Let us explain the method following a dimensional approach.

The model of Colombini et al. (1987) solves the two-dimensional Shallow Water Equations coupled with the Exner equation for sediment transport continuity in a infinite-long, straight, rectangular channel with constant width (W) and longitudinal gradient (S) and a uniform sediment size (d_{50}). We know that, for a given discharge value (Q), bar amplitude (A^*) can evolve until it achieves the equilibrium condition if the flowing discharge is maintained for a sufficient long time. This equilibrium configuration corresponds to a specific amplitude value A^*_{eq} if the discharge value is lower than the critical threshold for bar formation, Q_{cr}, or zero if the flowing discharge is larger (see Redolfi et al., 2020, for further details). In both cases, the growth of bars, under steady flow conditions, is governed by eq. 2.28, here reported in a dimensional form:

$$\frac{d|A^*|}{dt^*} = \gamma_1 |A^*| + \gamma_2 |A^*|^3, \tag{7.1}$$

in which γ_1 and γ_2 are coefficients that can be easily computed by their dimensionless counterpart α_{1R} and α_{2R} defined in Colombini et al. (1987) as:

$$\gamma_1 = \frac{2\, U_0^*\, \epsilon\, \alpha_{1R}}{W}, \qquad \gamma_2 = \frac{2\, U_0^*\, \alpha_{2R}}{W\, D_0^{*2}}, \tag{7.2a,b}$$

in which D_0^* and U_0^* are the uniform water depth and velocity and ϵ is the perturbation parameter.

Here, we extend the Colombini et al. (1987) model to variable flow conditions, obtaining the evolution of bar amplitude in time by integrating eq. (7.1). Specifically, we consider a real flow series $Q(t^*)$ and identify with Q_j the j-th value of discharge measured

at time t_j^*. Let us define $Qc(t^*)$ the vector of mean values of discharge Qc_j in each temporal interval $\Delta t_j^* = t_{j+1}^* - t_j^*$:

$$Qc_j = \frac{Q_j + Q_{j+1}}{2}, \tag{7.3}$$

with $j \subset [1, N-1]$ and N is the number of elements in the flow series.

The above discretization allows us to define a vector with uniform flow depth, $D_0^*(t^*)$, for all values of $Qc(t^*)$. At this point we can compute the corresponding coefficients $\gamma_1(t^*)$ and $\gamma_2(t^*)$ of the weakly nonlinear model of Colombini et al. (1987). To obtain the evolution of bar amplitude in time it is sufficient to compute the increment of bar amplitude at each timestep Δt_j^* by integrating eq. (7.1). The initial value of bar amplitude is the value computed at the previous step, which required to be computed in a dimensional form to have a continuous function of bar amplitude.

An important aspect must be considered, since the weakly nonlinear model of Colombini et al. (1987) is strictly valid when the flow conditions in the channel provide a value of the aspect ratio β in the neighborhood of the critical value, β_{cr}. Nevertheless, as reported in Chapter 3, the lower limit of the Colombini et al. (1987) theory can be fixed at the fully-wet threshold, Q_{fw}, which identifies the emersion condition for bars. As already highlighted, the absence of an analytical model to provide the equilibrium amplitude of bars for discharges lower than the fully-wet threshold is a problem when we investigate the response of bars to a real flow regime, since the most frequent stages of discharge in alpine rivers are typically low and close to the threshold for sediment motion (i.e. below the fully-wet threshold). To overcome this limitation we implement the method proposed by Redolfi et al. (2020) to provide a solution of bar amplitude also outside the range of validity of the model. As shown in Carlin et al. (2021) this approximation of bar amplitude is crucial to determine the actual growth rate of bars given the initial bar amplitude A_0^* and the discharge condition Q. Hence, in the present formulation if the discharge value Qc_j occurs when the amplitude of bars in the channel is larger than the maximum value of bar amplitude allowed by Qc_j (herein the instantaneous fully-wet threshold),

no evolution of bars is possible since the emersion condition is overcome.

In the present work we assume Engelund and Fredsoe (1982) friction formula, we estimate the sediment rating curve by means of Parker (1978) transport formula, with a relative submerged weight of sediment $R = 1.65$ and we set equal to 0.6 the empirical coefficient r that measures the effect of gravity on transverse transport.

7.2.2 *Hydrological variations of flow regime*

The evolutionary model of bar amplitude allows us to investigate the response of a river reach to variations in the flow regime, by quantifying how much the evolution of predicted bar amplitude A^* changes by changing the input discharge. Specifically, we build two realistic scenarios: the first assumes the construction of a reservoir with the purpose of flood lamination and the second simulates the effect of the climate change. In both cases the effects of hydrological variations on the slope of the channel (e.g. Zema et al., 2018) are neglected and the slope is assumed constant and equal to the original one.

Flood lamination scenario

The first scenario describes the modification of the flow regime due to the construction of an upstream reservoir, having the effect to reduce the variability of flowing discharge. Notice that we consider no alteration of the sediment supply that would further modify the response of alternate bars (Venditti et al., 2012).

The modified flow regime can be modelled by considering the water volume conservation for a lake of area A_l and water level h:

$$A_l \frac{dh}{dt^*} = Q_{IN} - Q, \tag{7.4}$$

where Q_{IN} and Q indicate the input and output discharge respectively, the former being known on the basis of the existing hydrological record.

We then assume that the output discharge follows an efflux law of the type:

$$Q = B\, c_Q \sqrt{2g}\, h^a, \tag{7.5}$$

where $c_Q \simeq 0.41$ and a is an exponent that for a rectangular weir of width B equals $3/2$.

Inverting eq. (7.5) and substituting into (7.4) gives, after some algebraic manipulations:

$$\frac{A_l}{\left(B\, c_Q \sqrt{2g}\right)^{\frac{1}{a}}} \frac{dQ}{dt^*} = \frac{Q_{IN} - Q}{Q^{1-\frac{1}{a}}}. \tag{7.6}$$

At this point it is convenient to express discharge in dimensionless form $Q_d = Q/Q_m$ when the discharge scale Q_m is the mean input discharge:

$$K \frac{dQ_d}{dt^*} = \frac{Q_{d,IN} - Q_d}{(Q_d)^{1-\frac{1}{a}}}, \tag{7.7a}$$

$$K := \frac{A_l}{\left(B\, c_Q \sqrt{2g}\right)^{\frac{1}{a}}} Q_m^{1-\frac{1}{a}}. \tag{7.7b}$$

It is worth noting that all the dimensions of the reservoir are grouped in the single parameter K, which represents a characteristic time scale of the response of the system, here set to 200 h.

Climate change scenario

Climate change is expected to be one of the main causes of increased flooding risk in the future, mainly due to the effect that higher temperature has on flooding peaks (te Linde et al., 2011). Since we are interested in a qualitative analysis of the effect that climate change has on the evolution of bar amplitude in a river reach, we do not look for a precise climate change model able to reproduce in detail the variations of the hydrological flow series, but rather we simply apply the overall expected modification to the natural series. Therefore, according with the predictions of Middelkoop et al. (2001) and Brunner et al. (2019), for who the global worming determines a decrease in snow accumulation and a consequent increase of flowing discharge in winter and a reduction in summer, we set a function that varies seasonally to modify the actual flow series. Specifically, a sinusoidal function c_f is considered, with a maximum variation of the discharge of $\pm 20\,\%$ at the half of January and half of July respectively:

$$c_f = 1 + 0.2 \cos(2\pi t), \tag{7.8}$$

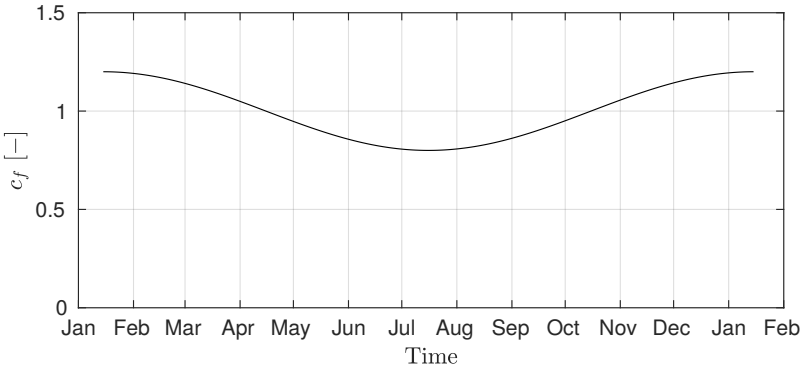

Figure 7.1. Simplified function describing a seasonal variation of the flow discharge due to climate change. Such function provides a variation of the actual flow series with an increment of discharge in winter and a decrement in summer, with a maximum variation of $\pm 20\,\%$ at the half of January and July respectively.

in which t is a dimensionless time variable ranging between 0 to 1 in the period between the 15^{th} of January of two consecutive years (see Fig. 7.1).

7.2.3 *Statistical approach to analyse the variation of bar amplitude*

The application of the morphological model to the flow series provides a function of bar amplitude in time $A^*(t^*)$ whose analysis allows for investigating the capability of each flood event in modifying bar amplitude.

First we identify the different flood events by considering the discharge stages between two consecutive discharge values that do not allow for bar evolution (i.e. between two consecutive instantaneous fully-wet conditions). In this way, the flood event is not necessarily identified by each peak of the flow series, but rather by a range of discharges in which more than one peak can potentially occur, depending on the discharge capability to allow for bar evolution.

Then, we statistically analyse the signal of bar amplitude in time by considering that the evolution of bar amplitude is affected by magnitude and duration of flood events. To do this, we define Q_{max} and T_f as two random variables collecting peak values and

duration of the flood events identified in the flow sequence. Their effect has been accounted for in the following dimensionless form:

$$\widetilde{\Delta Q}_{max} = \frac{Q_{max} - mean(Q_{max})}{std(Q_{max})}, \tag{7.9a}$$

$$\widetilde{\Delta T}_f = \frac{T_f - mean(T_f)}{std(T_f)}. \tag{7.9b}$$

where $mean$ and std represent the mean and standard deviation operations respectively. A dimensionless bar amplitude A is obtained by scaling A^* with its long-term mean value A^*_{as}. Different metrics can be implemented to analyse the modification of bar amplitude, depending on the aim of the investigation.

To quantify the net effect that flood events have on varying bar amplitude, we compute the difference between final (A^*_f) and initial (A^*_0) bar amplitude, ΔA^*_{f0}. This quantity can be positive or negative, depending on the flood capacity to increase or decrease the amplitude of bars.

This metric does not provide information about how much bar amplitude varies during the flood event. To do that we compute the difference between the bar amplitude at the beginning of the flood event (A^*_0) with the minimum value (A^*_{min}) reached during the event, ΔA^*_{0m}. By theoretical and experimental works (Tubino, 1991; Welford, 1994), it was found that the major damping of bar amplitude occurs during the rising limb of the flood, therefore we relate this metric to the time needed to achieve the peak of the flood event, $T_{f,r}$, which in a dimensionless form is:

$$\widetilde{\Delta T}_{f,r} = \frac{T_{f,r} - mean(T_{f,r})}{std(T_{f,r})}. \tag{7.10}$$

In Fig. 7.2 an idealized flood event and the respective evolution of bar amplitude are shown in order to identify the variables considered in the analysis (i.e. Q_{max}, T_f and $T_{f,r}$) and the metrics describing bar amplitude modification (i.e. ΔA^*_{f0} and ΔA^*_{0m}).

Finally, the overall influence of Q_{max} and T_f on the bar amplitude evolution (ΔA) is investigated by a univariate linear regression method, in which flood peak and duration are considered as predictors:

$$\Delta A = a_0 + a_1 \widetilde{\Delta \xi} + \mu, \tag{7.11}$$

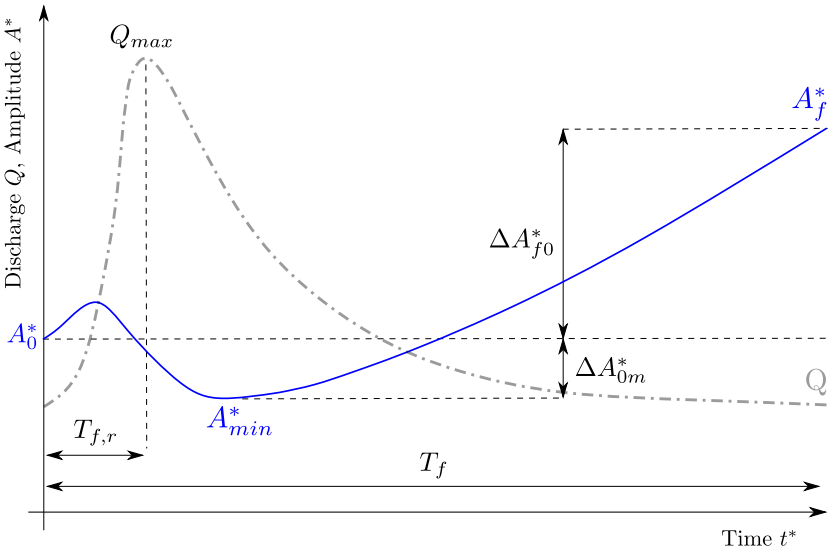

Figure 7.2. Sketch of an idealized flood event with the respective bar amplitude. Flood magnitude (Q_{max}) and duration (T_f and $T_{f,r}$) are the hydrological characteristics of floods considered to analyse the modification of bar amplitude in terms of total variation ($\Delta A^*_{f0} = A^*_f - A^*_0$) and the modification during each flood event ($\Delta A^*_{0m} = A^*_0 - A^*_{min}$).

where ΔA summarizes all dimensionless metrics of bar amplitude variation, $\widetilde{\Delta\xi}$ generically indicated the flood characteristic under investigation (i.e. $\widetilde{\Delta Q}_{max}$, $\widetilde{\Delta T}_f$ and $\widetilde{\Delta T}_{f,r}$) and μ includes all the residual terms of the model. To analyse the influence of magnitude and duration with respect to the bar amplitude variation, a bivariate analysis is performed by extending eq. (7.11) to both the variable:

$$\Delta A = a_0 + a_1 \widetilde{\Delta Q}_{max} + a_2 \widetilde{\Delta T}_f + \mu. \tag{7.12}$$

In the following, dimensionless metrics for bar amplitude variation are identified by means of the same symbol without the asterisk (*).

7.3 RESPONSE OF BAR AMPLITUDE EVOLUTION IN TIME

7.3.1 *Results of the unsteady model of Colombini et al. (1987) applied step-by-step*

The proposed model of Colombini et al. (1987) applied step-by-step (hereinafter CST-SbS) allows us to follow the evolution of bar amplitude in time due to the variation of discharge in the flow series. With respect to the Tubino (1991) model, CST-SbS does not treat the unsteadiness of the flow by means of a linearized process around a reference state, but rather models the flow regime as a sequence of steady states in which at each stage of discharge a value of bar amplitude is computed. Such value of bar amplitude is then the initial condition for the next one. We then assume that, provided the time step is taken conveniently small, the variation of flow discharge is sufficiently slow to allow for neglecting the derivatives of D_0^* and ϵ with respect to the discharge in the computation of coefficients in eq. (7.2).

Fig. 7.3 shows how bar amplitude evolves in $27\,\mathrm{years}$ of flood events in the upstream reach of the Alpine Rhine River, starting from an initially flat bed. It is evident that after the first period in which bar amplitude exclusively grows, the system oscillates around an average state ($A_{as}^* = 1.40\,\mathrm{m}$) because of the modification caused by single flood events. It is a clear picture of a river reach which is likely to form alternate bars, whose amplitude is able to evolve depending on the actual flow conditions. The signal of bar amplitude is characterised by long horizontal lines, which are related to discharge values that are not able to modify the actual bar amplitude of the river (i.e. the discharge is lower than the instantaneous fully-wet threshold).

A different response is observed for the downstream reach of the Alpine Rhine River (Fig. 7.4), for which the same period of flow record is available, where the unsteady model provides a highly oscillating bar amplitude A^*, ranging from a maximum value around $1.2\,\mathrm{m}$ to zero. Such response indicates the incapability of the system to choose a unique equilibrium state, but rather the possibility to observe alternate bars or, alternatively, to have a flat bed configuration in the river reach.

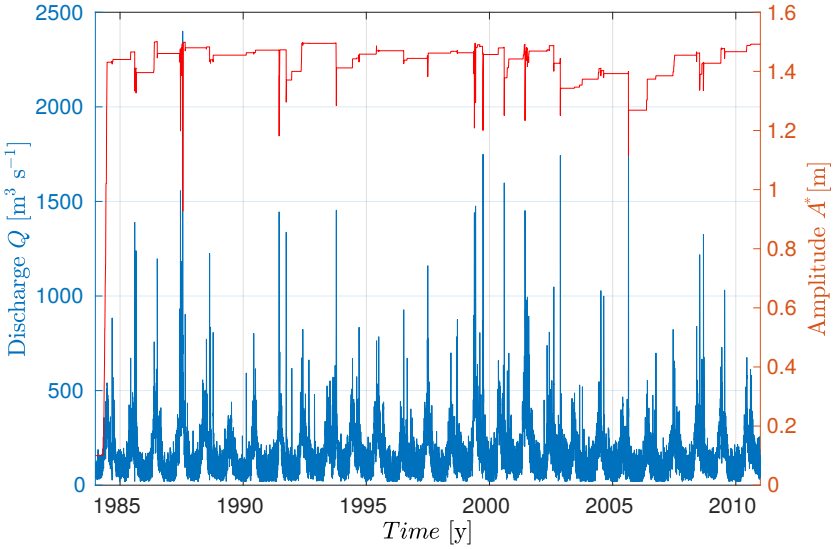

Figure 7.3. Evolution of bar amplitude in time predicted by means of CST-SbS model (right axis) due to the hydrological flow sequence of the upstream reach of the Alpine Rhine River between 1984 to 2010 (left axis). Horizontal lines in bar amplitude signal identify discharge values lower than the fully-wet threshold (i.e. which are not able to allow for bar evolution).

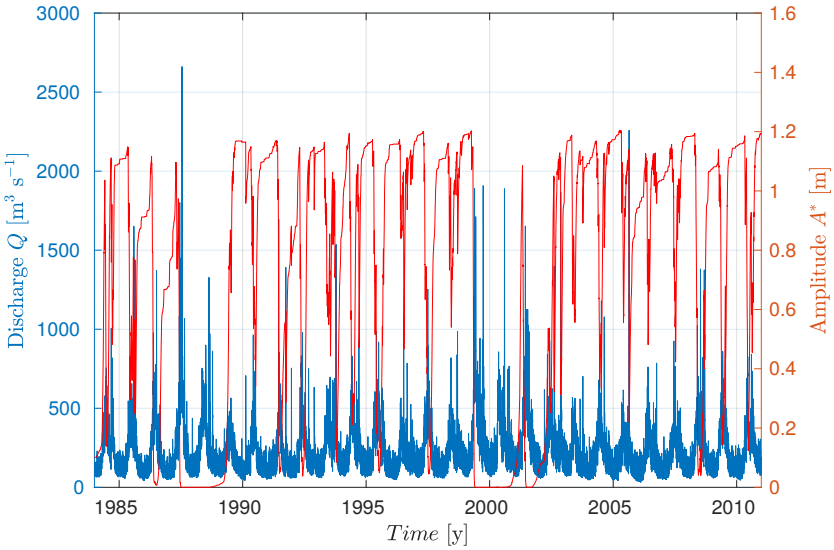

Figure 7.4. Evolution of bar amplitude in time predicted by means of CST-SbS model (right axis) due to the hydrological flow sequence of the downstream reach of the Alpine Rhine River between 1984 to 2010 (left axis). The oscillating variation of bar amplitude from 1.2 m to zero shows that two possible regime configurations are available.

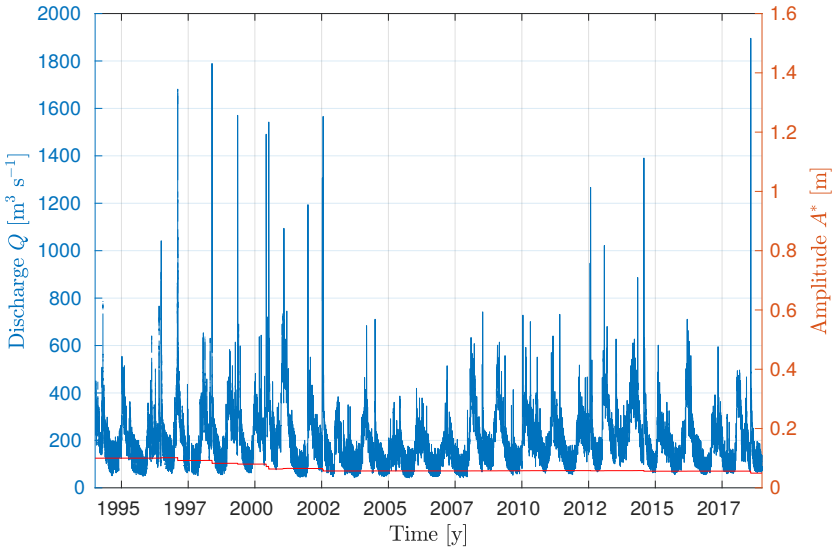

Figure 7.5. Evolution of bar amplitude in time predicted by means of CST-SbS model (right axis) due to the complex flow regime (left axis) for the reach of the Adige River (Trento, Italy). The absence of bars observed by field measurements is confirmed by the present numerical simulation.

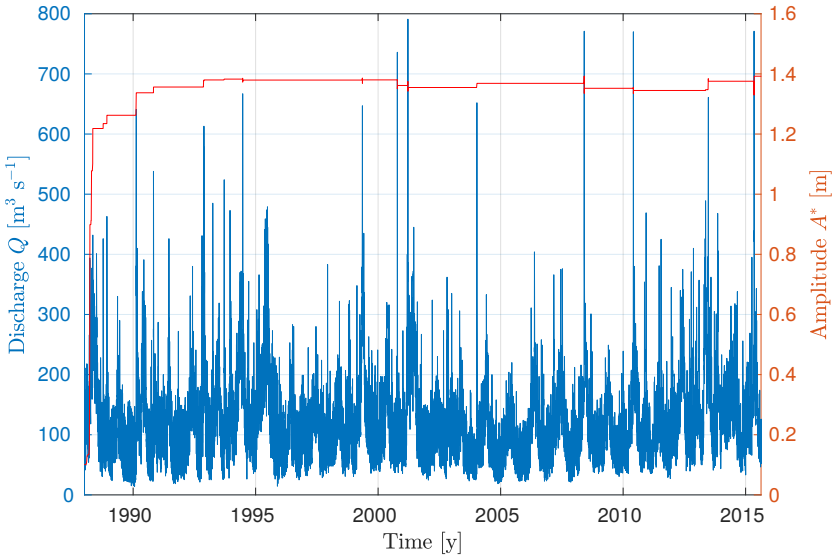

Figure 7.6. Evolution of bar amplitude in time predicted by means of CST-SbS model (right axis) due to the complex flow regime (left axis) for the reach of the Isère River (Montmèlian, France).

In Fig. 7.5 the response of bar amplitude evolution for the Adige River is reported, considering the 30 min-data of the flow series from June 1994. The simulation clearly shows no evolution of the riverbed, with a weak effect of largest floods to damp the almost vanishing bar amplitude.

Finally, Fig. 7.6 shows the simulation result for the hourly data of the flow series of the Isère River from 1988 to 2015. Similarly to the upstream reach of the Alpine Rhine River, bar amplitude achieves an equilibrium configuration ($A^*_{as} = 1.37\,m$) that is maintained almost constant for all the time. We observe that only the largest floods are able to slightly modify the amplitude of bars, which remains almost constant for all the simulated period.

A quantitative analysis of the average state achieved by the reaches of the study cases (except for the Adige River, where no evolution is observed) is proposed in terms of distribution of bar amplitude, f_A (Fig. 7.7). Left panels show the yearly distribution of bar amplitude, computed considering all values predicted by the model, so as to provide a measure of the probability of observing a certain value of bar amplitude in the reach during a typical reference period. Right panels show the distribution of bar amplitude considering only the active events, namely when the discharge is larger than the instantaneous fully-wet threshold. The latter metric is representative of the values of bar amplitude achieved by the river reach during flood events. The distributions of bar amplitude are characteristics of the different response of the river reaches to flow discharge variations and are analysed in the following by considering their shape, width and mean value.

Focussing on left panels of Fig. 7.7 we identify two different shapes of the yearly bar amplitude distributions: a modal distribution is found for the upstream reach of the Alpine Rhine River and the Isère River (panels a and e, respectively) with a clear peak, while a bi-modal one for the downstream reach of the Alpine Rhine River (panel c), in which the highest and lowest values of bar amplitude result to be the most frequent. The shape of bar amplitude distributions reflects the different response of the three river reaches. Specifically, in the upstream reach of the Alpine Rhine River and in the Isère River, where a regime state is achieved, the mean bar amplitude is representative of such regime state and the excursion in bar amplitude due to flood

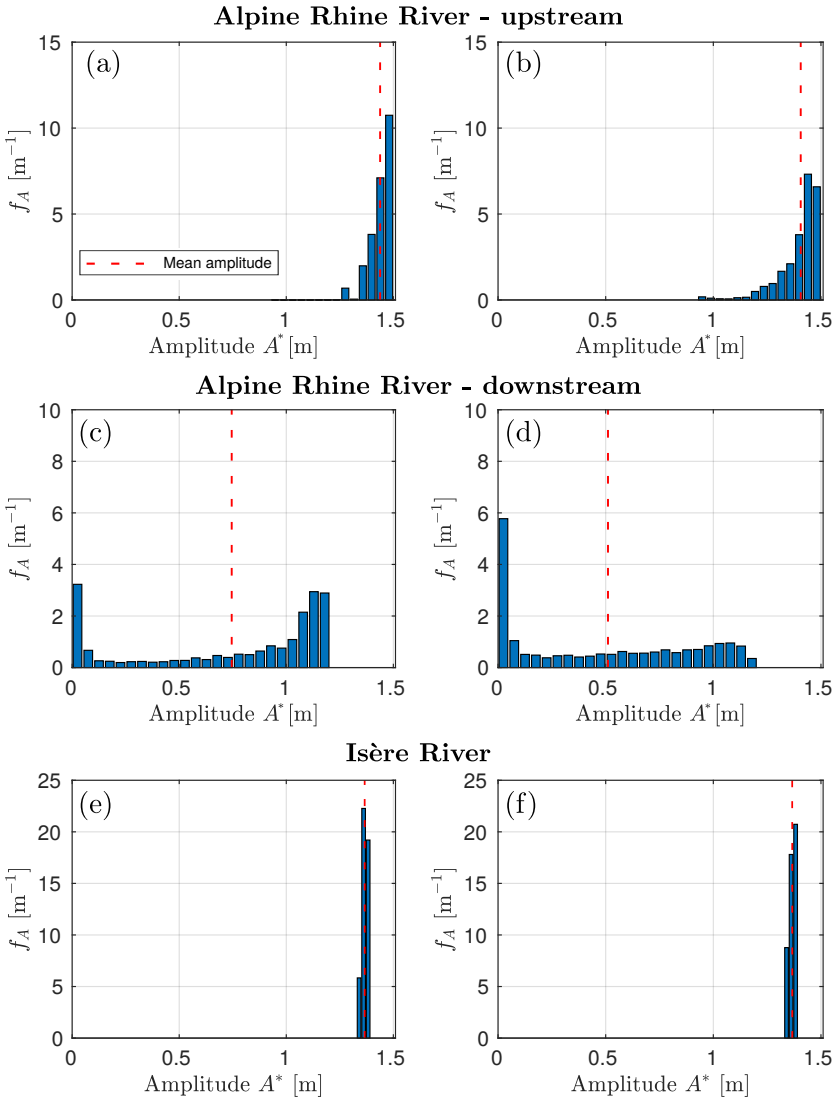

Figure 7.7. Distribution of bar amplitude for the Alpine Rhine River (panels a and b for the upstream reach and panels c and d for the downstream one) and the Isère River (panels e and f) predicted by the CST-SbS model. Left panels show the yearly distribution of bar amplitude; right panels show the distribution of bar amplitude related to the active events (i.e. when the discharge is larger than the instantaneous fully-wet value). Dashed vertical lines identify the average bar amplitude predicted by the unsteady model of CST-SbS.

events is relatively low. In the downstream reach of the Alpine Rhine River, the equilibrium configuration is not determined and the river makes experience of a large range of bar amplitude, whose mean value is not the most frequent.

Analysing the distributions obtained by excluding the periods of the flow sequence in which bars do not evolve because the emersion condition occurs (right panels of Fig. 7.7), we obtain a different result only for the downstream reach of the Alpine Rhine River. Indeed, the peak corresponding to the highest values of bar amplitude is reduced, while the peak related to the lowest values is increased, to the point that the most frequent state of bar amplitude during flood events is the flat bed. Moreover, all the values in Fig. 7.7d except the lowest ones show almost the same frequency, highlighting the incapability of the river reach to clearly identify a regime configuration.

7.3.2 *The long-term response of alternate bars*

In Chapter 6 we propose a method to predict the expected, long-tem bar amplitude in a river reach. Such average value of bar amplitude derives from the balance between bar-forming and bar-suppressing events occurring in the flow regime, which are accounted for by their probability density function. The application of Colombini et al. (1987) model step-by-step to the same flow series of the four study reaches allows us to compare the predicted long-term value of bar amplitude with the mean value derived by the actual magnitude and sequence of flow events. In the following we provide a brief summary of the main results of the bar-forming discharge method in order to proficiency discuss the results of the unsteady model.

Looking at Fig. 7.3 we observe that the unsteady model of CST-SbS shows the upstream reach of the Alpine Rhine River as a dynamic system in which flood events are able to modify bar amplitude, but such evolution always occurs in the neighborhood of the average state. Specifically, the mean bar amplitude results in the value of 1.40 m, computed excluding the initial transitory time required to achieve the regime configuration, with a standard deviation, SD^*_A, equal to 0.03 m. Similarly to the analysis performed in Chapter 5, the standard deviation is a good mea-

sure to quantify the magnitude of oscillations around the average state. The long-term bar amplitude predicted by the bar-forming discharge, A^*_{as}, is equal to 1.38 m, slightly lower than the mean bar amplitude predicted by the unsteady model. Nevertheless, the hypothesis that the average state of bar amplitude does not depend on the magnitude and sequencing of individual flood events is confirmed. Therefore, the probability density function results to be the key controlling parameter of the hydrological flow regime, enhancing the long-term result. By comparing the result of the unsteady model with the measured value of bar amplitude, we find that the average bar height ($H^*_{b,a}$) is 2.5 m with a maximum (H^*_b) of 3.8 m, which is coherent with the range $2.5 - 4$ m reported in Adami et al. (2016).

As concerning the downstream reach of the Alpine Rhine River, the oscillating response of bar amplitude between zero to 1.2 m (see Fig. 7.4) predicted by CST-SbS is perfectly consistent with the probability of bar occurrence, P_{form} around 50 % predicted by the bar-forming discharge method (see Section 6.4 for further details). Indeed, the simulation provides two possible configurations of the riverbed, with or without alternate bars (see also the bi-modal distribution of bar amplitude in Fig. 7.7c). Also in this case the mean bar amplitude of 0.73 m is larger than the long-term value of 0.37 m. The standard deviation of the bar amplitude is of the same order of magnitude of the mean value, providing a twofold implication: the average bar amplitude is far to be significant in describing the reach response, since it appears to rarely occur in the channel and (ii) the bar-forming discharge method, merely based on the probability density function of the flow series, is not able to capture the essential behaviour of the reach.

As result of the long-term analysis of bar amplitude in the Adige River and Isère River, we classified them as limit cases of the downstream and upstream reaches of the Alpine Rhine River respectively. Indeed, the former presents geometrical characteristics similar to the downstream reach of the Alpine Rhine River, with a riverbed morphology essentially flat, while the latter displays a stable sequence of high-relief bars (with average bar height $H^*_{B,a} = 3.5$ m) largely covered by vegetation (Serlet et al., 2018). The evolutionary model confirms the low propensity of

the bar amplitude to be modified by the flow regime, providing a response of bar amplitude consistent with field observations.

The flat bed configuration of the Adige River is clearly reproduced by the unsteady model (see Fig. 7.5), confirming the very low probability to observe bar occurrence predicted by the bar-forming discharge method. Indeed, the damping predicted by the unsteady model matches with the value of P_{form} much smaller than 50 %, making the criterion of bar formation suitable to describe the overall river reach response.

Finally, for the Isère River the bar presence is well-reproduced by the CST-SbS model, with a regime configuration that is essentially fixed, with slight modifications of bar amplitude due to the extreme values of the flow series (Fig. 7.6). Also in this case such response is consistent with the bar-forming discharge prediction. On the one hand, the probability of forming bars is of 100 % due to the fact that the critical discharge computed by the weakly nonlinear model of Colombini et al. (1987) is much larger than the maximum value within the flow record. On the other hand the evolution of bars is rare due to the large value of the fully-wet threshold. This allowed us to argue that once bars formed by means of the formative events, they can be hardly modified by the actual floods occurring in the river (the value of standard deviation is very low). The average bar amplitude of 1.37 m provides an average bar height of 2.7 m, which coincides with the long-term prediction of the bar-forming discharge method (see Tab. 6.2), letting us to conclude that both models are able to capture the essential behaviour of the reach.

Results on the average bar amplitude and standard deviation for the Alpine Rhine River and Isère River are summarized in Tab. 7.1.

7.3.3 *Analysis of initial conditions for bar amplitude evolution*

The above considerations can be deepened by analysing the hydrological conditions required to start bar evolution. To do that we computed the distribution ($f_{Q_{ev}}$) of discharge values at which the evolution of bar amplitude begins during each flood event (Q_{ev}), namely the instantaneous fully-wet condition. Specifically, for the upstream reach of the Alpine Rhine River

Table 7.1. Comparison of the average bar amplitude (A^*_{as}) computed by the bar-forming discharge method (BF) with the prediction of the evolutionary model of Colombini et al. (1987) applied step-by-step (CST-SbS) for the actual flow series and the hydrological scenarios. In the latter cases the average state is computed also excluded emerged conditions and a measure of the magnitude of oscillations is provided by means of the standard deviation (SD^*_A).

		Actual flow series		Lamination scenario		Climate change scenario	
		CST-SbS	BF	CST-SbS	BF	CST-SbS	BF
Alpine Rhine River up.							
A^*_{as} (yearly)	[m]	1.40	1.38	1.40	1.39	1.41	1.38
A^*_{as} (active)	[m]	1.37	–	1.38	–	1.38	–
SD^*_A	[m]	0.03	–	0.03	–	0.03	–
Alpine Rhine River down.							
A^*_{as} (yearly)	[m]	0.73	0.37	0.67	0.46	0.88	0.71
A^*_{as} (active)	[m]	0.52	–	0.47	–	0.73	–
SD^*_A	[m]	0.35	–	0.37	–	0.27	–
Isère River							
A^*_{as} (yearly)	[m]	1.37	1.37	1.38	1.38	1.36	1.36
A^*_{as} (active)	[m]	1.37	–	1.38	–	1.36	–
SD^*_A	[m]	0.01	–	0.01	–	0.02	–

and Isère River, we exclude the initial transitory phase needed to attain the regime response, while for the downstream reach of the Alpine Rhine River we consider all the flow series being the average configuration not achieved.

At the same time we compute the distribution ($f_{A_0^*}$) of the amplitude of bars presents in the channel when Q_{ev} occurs (A_0^*), in order to associate the magnitude of evolutionary events with the initial bar amplitude.

The distributions of instantaneous fully-wet condition and initial bar amplitude are shown in Fig. 7.8 for the Alpine Rhine River. Specifically, the upstream reach shows a unimodal distribution with a unique peak for both the instantaneous fully-wet condition (panel a) and the corresponding value of initial bar amplitude (panel b). The range of discharges responsible to start bar evolution is relatively narrow and falls in the neighborhood of the fully-wet threshold, Q_{fw}. Similarly, the initial bar amplitude ranges between 1.2 to 1.5 m, with the most frequent events slightly larger than the average state (A_{as}^*) predicted by the long-term analysis of the bar-forming discharge method.

Conversely, the downstream reach of the Alpine Rhine River presents a bi-modal distribution both for $f_{Q_{ev}}$ (panel c) and $f_{A_0^*}$ (panel d). Specifically, the initial value of discharge ranges from the threshold for motion and the fully-wet threshold and the initial bar amplitude from 0 to 1.2 m. These distributions highlight that the evolution of bar amplitude begins for the most of time (i) when the riverbed is almost flat by the action of flow stages just larger than the threshold for sediment motion or (ii) when bars are already formed and larger floods are responsible of the damping of bar amplitude. It is worth noticing that the average state of bar amplitude, A_{as}^*, does not remains for long in the reach, but it is a transitory value, mainly occurring during flood events.

The Isère River (Fig. 7.9) shows distributions similar to the upstream reach of the Alpine Rhine River, with a narrow range of both the instantaneous fully-wet condition (panel a, Q_{ev} ranges between 490 and 540 $m^3\ s^{-1}$) and the initial bar amplitude (panel b, A_0^* ranges between 1.34 to 1.39 m). Similarly to the Alpine Rhine the most frequent events that start the evolution of bars are slightly smaller than the fully-wet threshold.

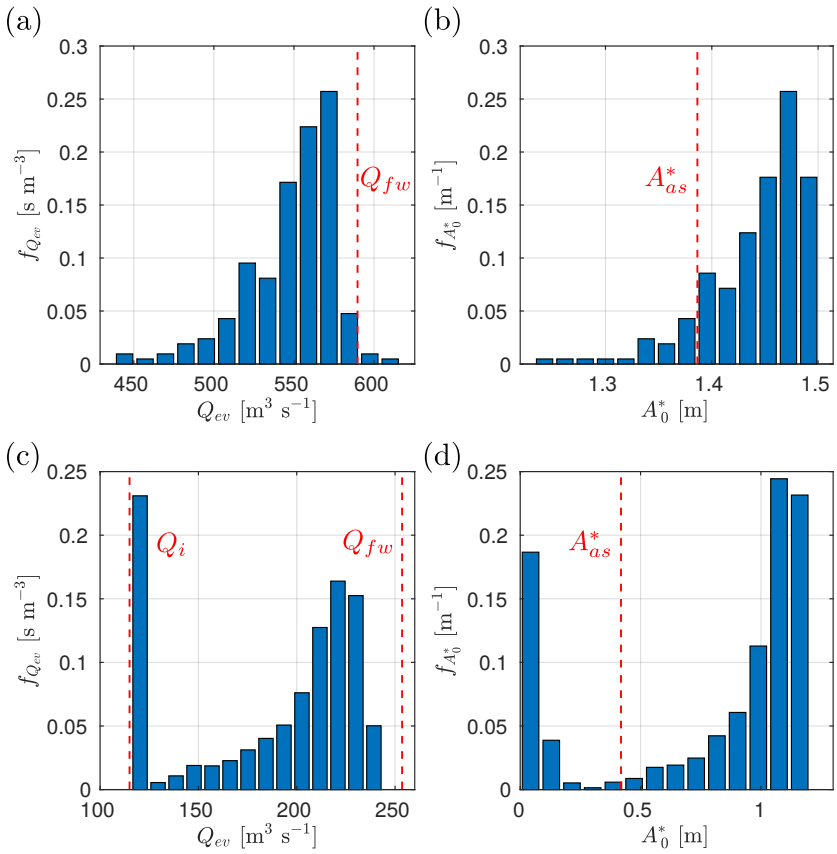

Figure 7.8. Distribution of discharge values that in flood events start the evolution of bar amplitude, Q_{ev} (panels a and c) and the corresponding initial stages of bar amplitude, A^*_0 (panels b and d) for the upstream and downstream reaches of the Alpine Rhine River (upper and lower panels respectively). The fully-wet threshold (Q_{fw}) and the long-term bar amplitude predicted by the bar-forming discharge method (A^*_{as}) are plotted as dashed lines.

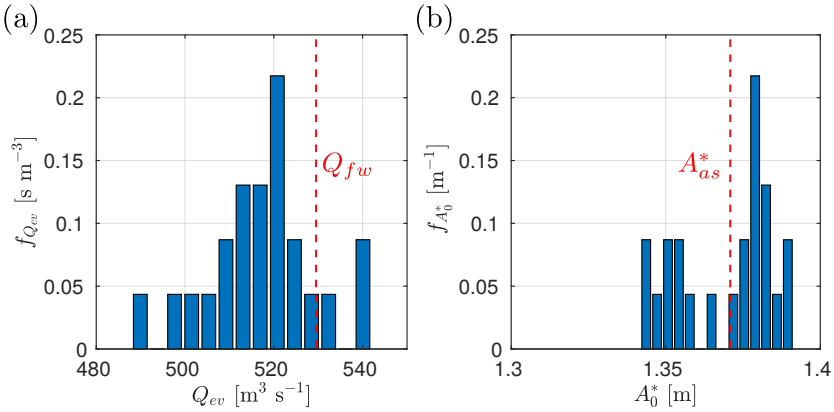

Figure 7.9. Distribution of discharge values that in flood events start the evolution of bar amplitude, Q_{ev} (a) and the corresponding initial stages of bar amplitude, A_0^* (b) for the Isère River. The fully-wet threshold (Q_{fw}) and the long-term bar amplitude predicted by the bar-forming discharge method (A_{as}^*) are plotted as dashed lines.

7.4 HYDROLOGICAL ALTERATION OF THE FLOW REGIME

The hydrological flow regime of a river is one of the key factors to determine its quality in terms of ecological health (e.g., Poff and Zimmerman, 2010). For this reason, the analysis of effects that human constructions or climate changes have in altering the hydrological flow regimes aroused interest in the scientific community (e.g., Bunn and Arthington, 2002; Yang et al., 2018), with particular focus on the interference with riverine ecosystems (Mittal et al., 2016).

However, not much work is available about the effect that hydrological alterations have on channel morphology, except for riparian corridors (Martínez-Fernández et al., 2018) and hydropeaking waves (Vanzo et al., 2016). The present analysis focusses on the effect that two simplified scenarios of flow series variation have on the long-term response of alternate bar amplitude. Specifically, the variation of flow regime has been investigated by simulating (i) the lamination of discharge provided by a reservoir and (ii) the modification of water flow due to climate change. Both scenarios modify the flow series by reducing the peak of larger floods and promoting low flows and moderate

floods, assuming that channel geometry and sediment supply do not change.

To investigate the effect that such scenarios have on the bar amplitude in a river reach, we apply the CST-SbS model to the altered flow series and compute the distribution of bar amplitude in order to compare results with the distribution obtained for the actual flow series.

7.4.1 *Distribution of bar amplitude*

In Figs. 7.10 and 7.11 results of the lamination (panels c and d) and climate change (panels e and f) scenarios are shown for the upstream and downstream reaches of the Alpine Rhine River respectively, in comparison with the actual flow regime (panels a and b). Similarly to the previous analysis, left panels identify the yearly distribution of bar amplitude, while the right panels show the distribution of bar amplitude during active events.

We observe that for the upstream reach the distributions of bar amplitude obtained for the two scenarios (panels c-f in Fig. 7.10) are almost the same that the ones obtained for the actual flow series (see panels a and b), with a slight variation in the average value (see Tab. 7.1 for values). Furthermore, the two metrics provide similar results in terms of bar amplitude distributions, meaning that the effect of single flood events does not significantly affect the overall response of the river reach.

Conversely, the downstream reach shows different responses to the hydrological scenarios. Specifically, while the lamination scenario does not have relevant influence on the distribution of bar amplitude, the climate change scenario is able to increase the frequency of occurrence of the highest bar amplitude values with respect to the flat bed configuration. Such evidence is found considering both the metric implemented to compute the distribution of bar amplitude.

It is worth noticing that the reduction of the peak during flood events occurs at different timescales in the two scenarios. Indeed, while the lamination scenario reduces all the flood events occurring in the flow series depending on the characteristics of the reservoir, the climate change scenario acts at a seasonal

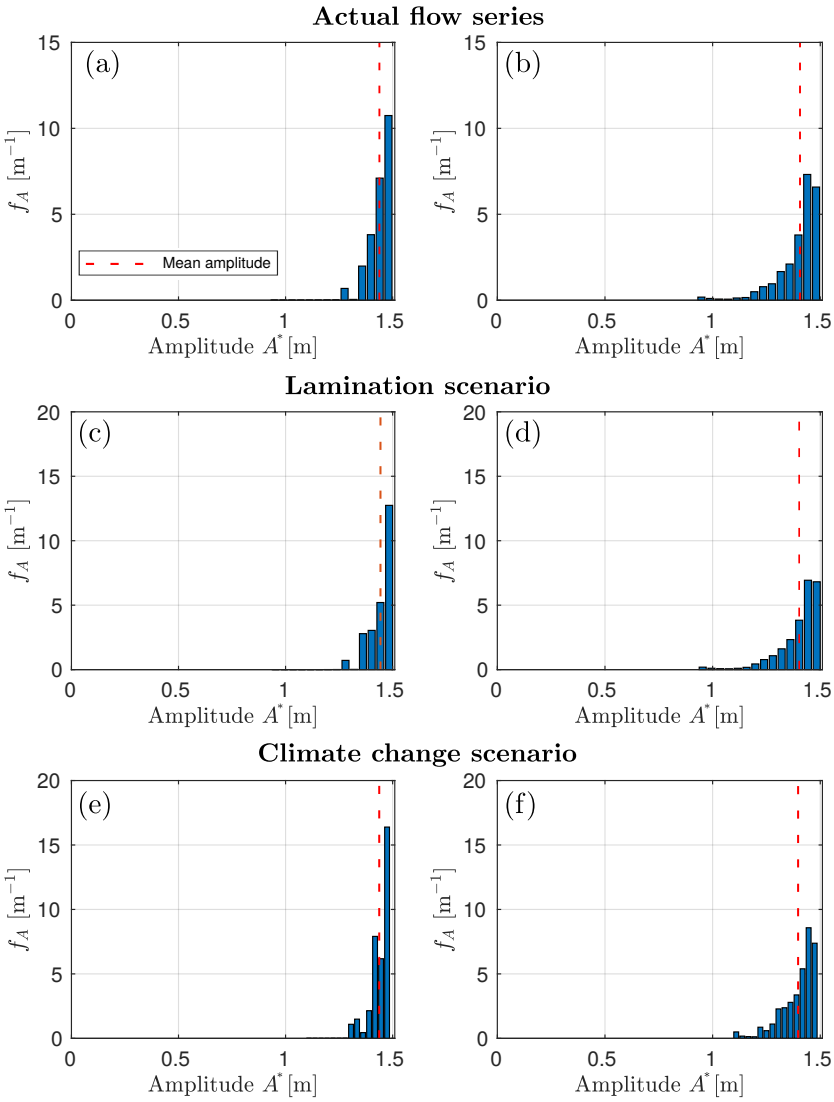

Figure 7.10. Frequency distribution of bar amplitude in the upstream reach of the Alpine Rhine River, predicted by the CST-SbS model when considering: (i) the actual flow series (panels a and b), (ii) the lamination scenario (panels c and d) and (iii) the climate change scenario (panels e and f). In left panels the yearly distribution of bar amplitude is reported, while in right panels the distribution are computed by considering only active events (i.e. when discharge exceed the instantaneous fully-wet threshold). Dashed vertical lines identify the average bar amplitude predicted by the unsteady model of CST-SbS.

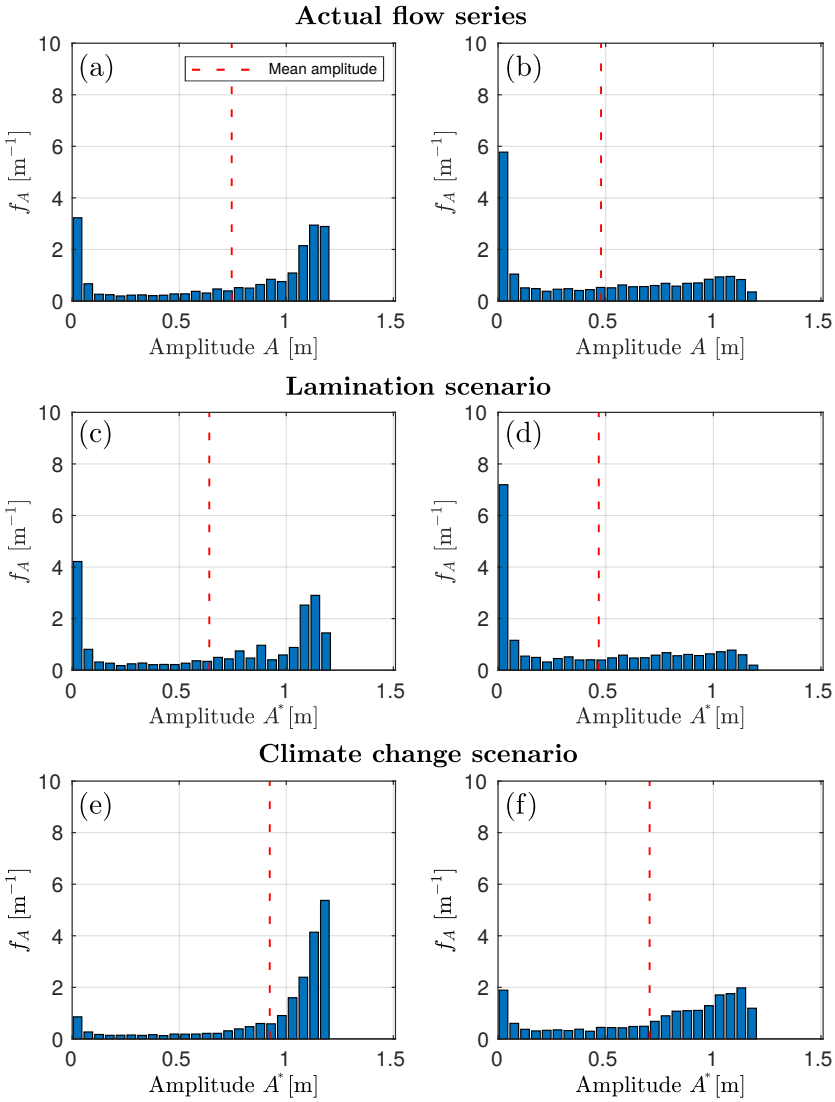

Figure 7.11. Frequency distribution of bar amplitude in the downstream reach of the Alpine Rhine River, predicted by the CST-SbS model when considering: (i) the actual flow series (panels a and b), (ii) the lamination scenario (panels c and d) and (iii) the climate change scenario (panels e and f). In left panels the yearly distribution of bar amplitude is reported, while in right panels the distribution are computed by considering only active events (i.e. when discharge exceed the instantaneous fully-wet threshold). Dashed vertical lines identify the average bar amplitude predicted by the unsteady model of CST-SbS.

timescale, by reducing or increasing flood peaks in summer and winter respectively.

Performing the same analysis to the Isère River we find that the amplitude of bars is almost constant during all the simulated period. The hydrological scenarios of flow regime alteration are not able to modify the response of the river reach, being the evolution of bars possible only with the largest floods. Nevertheless, we can reasonably suppose that the reduction of flow peaks due to both hydrological scenarios have the effect of reducing the already scarce propensity of the river reach to modify the amplitude of bars once they are formed.

7.4.2 *Effect of hydrological alteration in the long-term evolution of bar amplitude*

The different response of the river reaches to hydrological alteration can be predicted by performing the long-term analysis by means of the bar-forming discharge method. Specifically, the procedure to determine the average bar amplitude, A^*_{as}, is applied to the modified flow sequences, obtaining values reported in Tab. 7.1. For all the reaches the result is consistent with the mean value found by applying the CST-SbS method. Specifically, the upstream reach of the Alpine Rhine River and the Isère River are resistant to hydrological alteration, since the long-term bar amplitude does not change with respect to the value found for the actual flow series. Similarly, results of the downstream reach of the Alpine Rhine River are influenced only by the climate change scenario, with an increment of the average bar amplitude with respect to the actual flow series. Such different response to the overall similar effect of the two scenarios (i.e. the reduction of flood peaks) is due to the fact that the lamination scenario introduces variations in the hydrological regime at a shorter timescale with respect to the climate change scenario, in which a seasonal modification of the hydrological regime is imposed.

Moreover, the bar-forming discharge method provides a criteria to estimate how likely alternate bars are expected to form, depending on the scenario. The probability of bar occurrence, P_{form}, is computed for all the scenarios, confirming previous results on the average bar amplitude. In Fig. 7.12 the probability

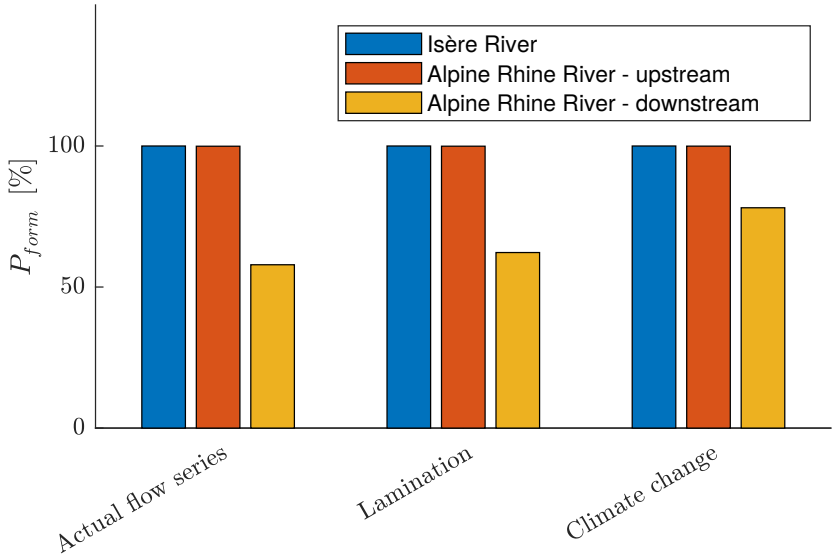

Figure 7.12. Probability of bar formation (P_{form}) computed with the bar-forming discharge method for the different scenarios of hydrological alteration in the study reaches of the Alpine Rhine River and Isère River.

of bar occurrence is shown in the three study cases noticing that the hydrological alteration affects exclusively the downstream reach of the alpine Rhine River. Indeed, the value of P_{form} around 50 % found for the actual flow series increases with both the hydrological scenarios, with a marked increment in case of the climate change.

Finally, the hydrological scenarios do not modify the magnitude of oscillations, providing a value of standard deviation SD^*_A overall similar to the value obtained by the actual flow series. Only the downstream reach of the Alpine Rhine River reduces the amplitude of oscillation with the climate change scenario, due to the increment of time in which the amplitude of the system is around the maximum value.

7.5 STATISTICAL ANALYSIS OF EVOLUTION OF BAR AMPLITUDE DURING FLOOD EVENTS

The capability of the unsteady model of CST-SbS to predict the evolution of bar amplitude in time by considering long se-

quences of actual flow events, allows us to investigate not only the distribution of bar amplitude, but also the response of bar amplitude to single flood events. Therefore, in addiction to the analysis of the long-term response of the river reach, we are able to investigate the effect that the actual sequence of different flood events has on the variation in bar amplitude. In this section we provide a statistical analysis on the response of the upstream reach of the Alpine Rhine River to the hydrological flow series, by relating the magnitude and duration of flood events with the metric of bar amplitude modification defined in Section 7.2.3 and illustrated in Fig. 7.2. Specifically, we investigate how (i) the net variation of bar amplitude due to each flood event (ΔA^*_{f0}) and (ii) the variation of bar amplitude during the flood (ΔA^*_{0m}) are affected by flood characteristics. These metrics are made dimensionless with the average state of bar amplitude.

7.5.1 *Identification of flood events*

To perform the statistical analysis on the influence of floods in the evolution of bar amplitude we need an objective criterion to identify individual flood events in the flow series. Observing the signal of bar amplitude in time we note that for most of the time bar amplitude does not evolve, since bars are emerged (low flows are the most frequent states in the flow series). Therefore, a suitable criterion to separate different flood events is to consider the portion of the flow series comprised between two consecutive horizontal segments (i.e. the contiguous portions of the flow record when all discharges are larger than the fully-wet threshold in Fig. 7.3). In this way we identify more than 200 floods in the flow series of the Alpine Rhine River, representing almost the 1.1 % of the total time. In Fig. 7.13 the sequence of flood events is reported, with dots summarizing the period of emersion between two consecutive floods.

At a first sight we observe that almost all discharge values lower than $500\,m^3\,s^{-1}$ are not able to modify the amplitude of bars, being lower than the instantaneous fully-wet condition. Moreover, the major variations of bar amplitude with respect to the average state is due to the largest floods that are not necessarily able to rebuild the initial value of bar amplitude, but

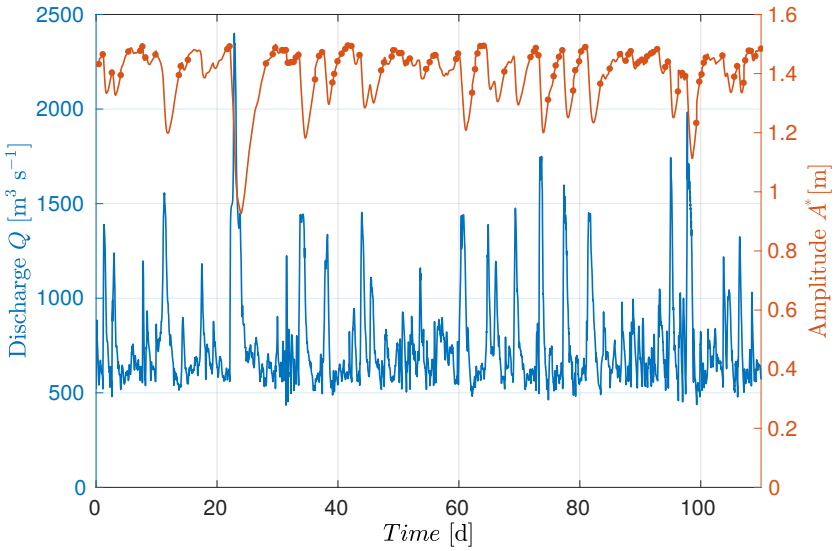

Figure 7.13. Evolution of bar amplitude (right axis) during the active events (left axis) in the upstream reach of the Alpine Rhine River. They are defined as the discharge values between two consecutive horizontal lines (i.e. the portion of the flow record for which the discharge is larger than the actual fully-wet threshold) and represent the 1.1 % of the whole flow series. Dots summarize the horizontal segments in Fig. 7.3.

Table 7.2. Mean and standard deviation of variables identified as significant to investigate the evolution of bar amplitude. Values are referred to flood events identified in the upstream reach of the Alpine Rhine River, due to its complex flow regime. Specifically, we consider the peak values (Q_{max}), the duration (T_f) and the time required to achieve the flow peak ($T_{f,r}$) of each flood event identified between two periods of no bar evolution.

		Mean	Standard deviation
Q_{max}	[m^3 s^{-1}]	730.31	290.95
T_f	[h]	13.82	22.26
$T_{f,r}$	[h]	4.83	7.22

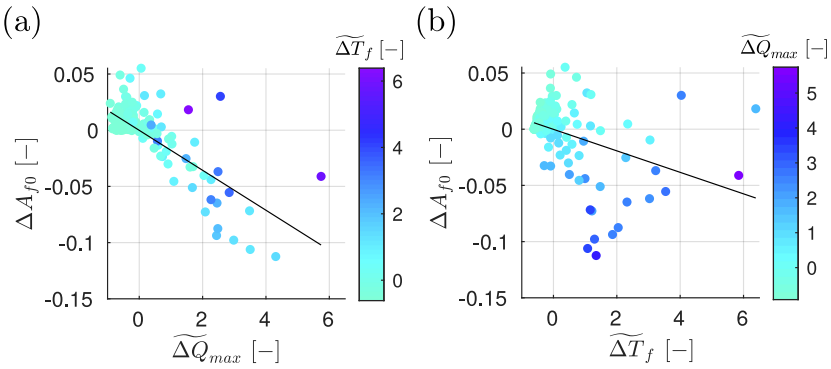

Figure 7.14. Variation of bar amplitude from the end and the beginning of floods, ΔA_{f0}, with respect to magnitude, $\widetilde{\Delta Q}_{max}$, (panel a) and duration, $\widetilde{\Delta T}_f$, (panel b) of events.

often require the action of subsequent moderate floods to recover the system around the average state.

For each flood event we compute the peak of the event (Q_{max}), the duration (T_f) and the time required to achieve the peak ($T_{f,r}$), obtaining three variables with mean and standard deviation reported in Tab. 7.2. From these variables we obtain the scaled quantities defined in Section 7.2.3, used for systematically investigating how floods are able to modify the amplitude of bars.

7.5.2 *Metrics describing the variation of bar amplitude*

The effect of floods on the net variation of bar amplitude is reported in Fig. 7.14, where the difference between final and initial bar amplitude ΔA_{f0} is plotted against the magnitude ($\widetilde{\Delta Q}_{max}$, panel a) and duration of events ($\widetilde{\Delta T}_f$, panel b). We note that variable ΔA_{f0} has a clear decreasing trend identified by the tendency lines in the plots, assuming values which are both positive and negative. Specifically, the overall effect of floods with a peak value in the neighborhood of the average value of Q_{max} are responsible of bar growth, while higher floods determine a bar damping. The role of time is different, being the longer the flood, the larger the recover of bar amplitude after the damping due to the peak.

However, it is convenient to split the sample of flood events on the basis of the global effect that they have on bar amplitude. In Fig. 7.15 upper and lower panels are referred to flood events responsible of bar growth ($\Delta A_{f0} > 0$) and decay ($\Delta A_{f0} < 0$) respectively. From these plots we can draw some considerations. First of all, the bar amplitude of the system increases mainly due to the effect of low and short flood events, which occur quite frequently being the most numerous in the sample of flood events. In these cases, i.e. panels (a) and (b) of Fig. 7.15, the tendency lines fitted by means of the linear model have low significance because of the scatter of points. This aspect is probably due to the fact that the effect of moderate floods with a relatively short duration is strongly influenced by the initial bar amplitude, which is an essential parameter to quantify the bar growth rate. In general, the lower the initial bar amplitude, the longer the time required to produce a significant increment of bar amplitude. A brief comment about the role of the initial bar amplitude is reported at the end of Section 7.5.3, when results of the bivariate analysis are discussed. Nevertheless, an increasing trend is found both with respect to the magnitude and duration of floods.

Conversely, flood events providing a net decrement of bar amplitude (panels c and d of Fig. 7.15) have a larger magnitude, which is at least twice the mean value of the sample. Indeed, the larger the flood peak, the larger the damping of bar amplitude, even though the duration is sufficiently short. We observe that the highest flood, which allows for a significant modification of bar amplitude, is long enough to allow the amplitude to recover a value similar to the beginning of flood event. On the other hand, floods in the range of $\widetilde{\Delta Q}_{max}$ between almost 2 to 4 have a lower duration and provide a larger variation in bar amplitude. This is evident by the fact that darker points are mainly above and below to the tendency line in panels (c) and (d) respectively. A marked trend for bar amplitude variation is observed both for the variables of peak discharge and flood duration, although the scatter with respect to the duration is larger.

In Fig. 7.16 the variation of bar amplitude between the initial value and the minimum achieved during the flood events, is shown with respect to peak values and the time required to achieve the peak. In the analysis we exclude flood events for

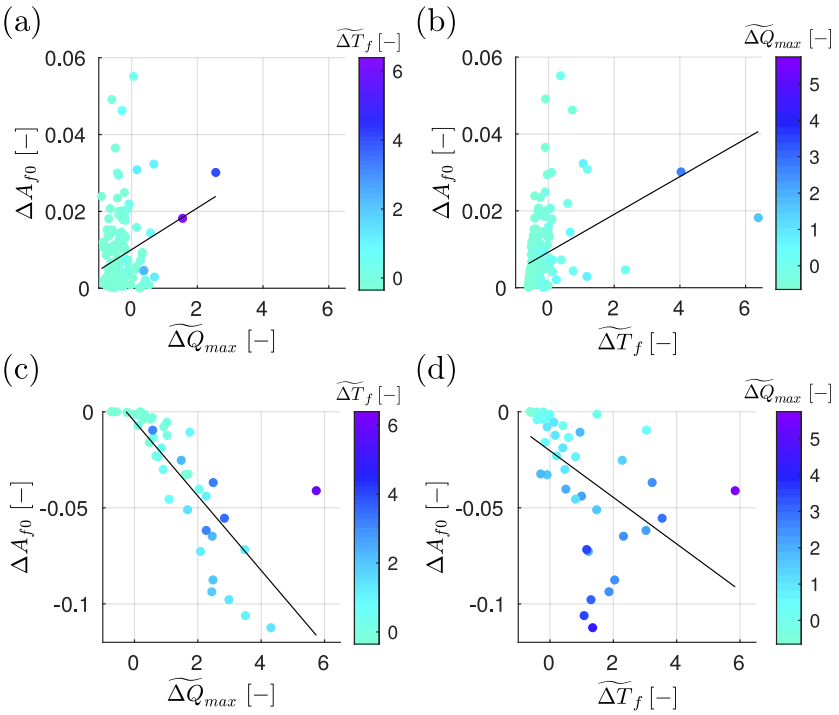

Figure 7.15. Variation of bar amplitude from the beginning to the end of floods, ΔA_{f0}, with respect to magnitude, $\widetilde{\Delta Q}_{max}$, (panels a and c) and duration, $\widetilde{\Delta T}_f$, (panels b and d) of events. Upper panels show floods producing an increment in bar amplitude, while lower panels a decrement. Dots represent sample values and their color indicate the value of the complementary variable; straight lines show the linear trend.

which this metric is zero, ΔA_{0m}, meaning that bar amplitude is only incremented during the event. The trend of ΔA_{0m} is positive with respect to both the investigated variables, with a larger scatter when the duration is chosen as parameter.

7.5.3 *Statistical analysis of the variation of bar amplitude*

In Tab. 7.3 the coefficients a_0 and a_1 of the univariate regression lines (see eq. 7.11) are summarized for the different metrics and the coefficient of determination R^2 is reported. We observe that the regression of bar amplitude variation is always better when the peak discharge is used as predictor (R^2 is larger), and

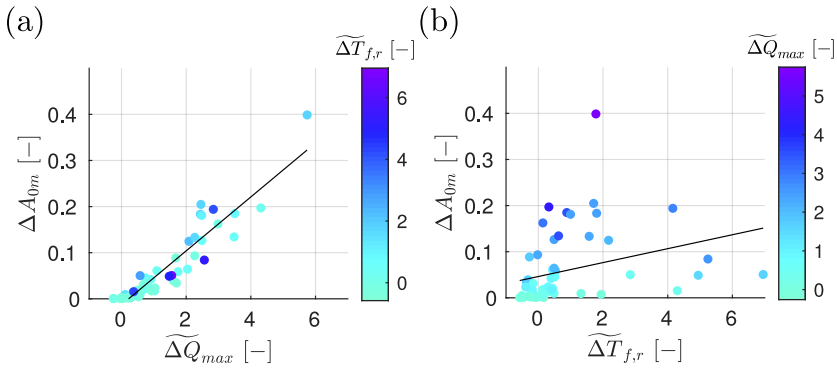

Figure 7.16. Variation of bar amplitude between initial and minima values, ΔA_{0m}, with respect to magnitude, $\widetilde{\Delta Q}_{max}$, (a) and duration before the peak, $\widetilde{\Delta T}_{f,r}$, (b) of events. Dots represent sample values and their color indicate the value of the complementary variable; straight lines show the linear trend.

the effect of flood peak is more relevant than flood duration in varying the amplitude of bars (i.e. the coefficient a_1 related to $\widetilde{\Delta Q}_{max}$ is always larger than the respective related to $\widetilde{\Delta T}_f$). Nevertheless, the duration of floods plays a clear role in the evolution of bar amplitude, since the longer the duration the higher the variation of bar amplitude.

However, the above univariate analysis does not allow for isolating the individual effect of magnitude and duration of floods on varying the amplitude of bars. Indeed, looking at Fig. 7.17 where each flood event is identified with respect to its magnitude and duration, we observe a correlation between $\widetilde{\Delta Q}_{max}$ and $\widetilde{\Delta T}_f$, which makes necessary a proper analysis to separate their contributions in modifying the amplitude of bars. Therefore, a bivariate analysis is proposed, in which the regression of bar amplitude variation is investigated as function of the two predictors, namely $\widetilde{\Delta Q}_{max}$ and $\widetilde{\Delta T}_f$. In Tab. 7.4 the coefficients a_0, a_1 and a_2 (see eq. 7.12) are reported for the different metrics investigated to quantify the variation of bar amplitude. It is worth noticing that, in defining the net variation of bar amplitude during flood events (ΔA_{f0}), magnitude and duration play an opposite role (i.e. coefficients a_1 and a_2 have opposite sign). Specifically, ΔA_{f0} shows a negative trend with respect to the magnitude of floods ($\widetilde{\Delta Q}_{max}$) and a positive trend with respect to the duration ($\widetilde{\Delta T}_f$),

Table 7.3. Coefficients of univariate linear model of eq. (7.11) used to fit the metrics implemented to quantify the evolution of bar amplitude with respect to the flood characteristics in the upstream reach of the Alpine Rhine River. Specifically, ΔA_{f0} represents the difference between final and initial bar amplitude and ΔA_{f0} the difference between the initial value of bar amplitude and the minimum value assumed during the flood. a_0 is the intercept, a_1 the slope of the line and R^2 the coefficient of determination.

		Univariate analysis		
		a_0	a_1	R^2
$\boldsymbol{\Delta A_{f0}}$				
$\widetilde{\Delta Q}_{max}$	[–]	−0.00012	−0.01777	0.577
$\widetilde{\Delta T}_f$	[–]	−0.00012	−0.00957	0.167
$\boldsymbol{\Delta A_{f0} > 0}$				
$\widetilde{\Delta Q}_{max}$	[–]	0.0101	0.0054	0.057
$\widetilde{\Delta T}_f$	[–]	0.0093	0.0049	0.144
$\boldsymbol{\Delta A_{f0} < 0}$				
$\widetilde{\Delta Q}_{max}$	[–]	−0.0051	−0.0194	0.657
$\widetilde{\Delta T}_f$	[–]	−0.0203	−0.0121	0.252
$\boldsymbol{\Delta A_{0m}}$				
$\widetilde{\Delta Q}_{max}$	[–]	−0.0130	0.0585	0.874
$\widetilde{\Delta T}_{f,r}$	[–]	0.0462	0.0151	0.095

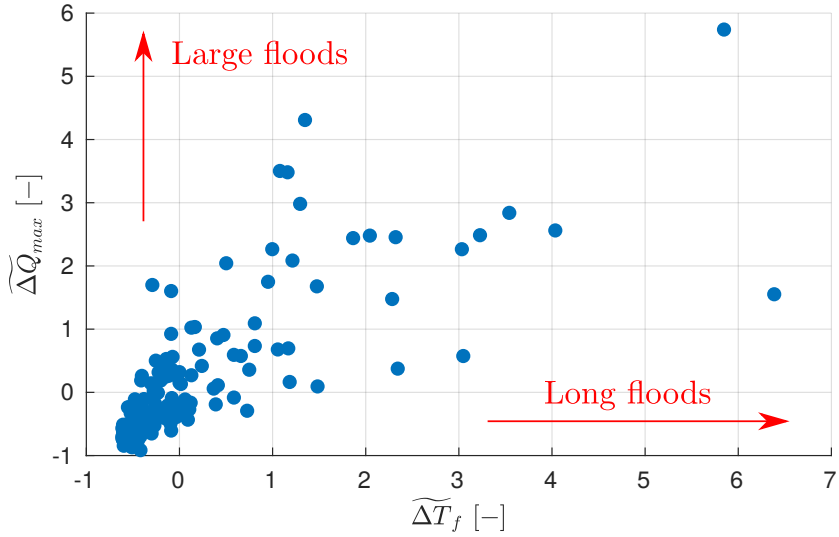

Figure 7.17. Correlation between flood events in the flow sequence of the Alpine Rhine River with respect to their magnitude ($\widetilde{\Delta Q}_{max}$) and duration ($\widetilde{\Delta T}_f$). Despite the scatter, there is an evident correlation. Therefore, the role of the two variables can not be studied independently, but a bivariate analysis is needed.

meaning that large floods tend to damp bar amplitude, while long floods tend to recover the initial configuration. A different response is observed for ΔA_{0m}, which shows a positive trend with respect to both the flood magnitude ($\widetilde{\Delta Q}_{max}$) and the time to reach the peak of the flood ($\widetilde{\Delta T}_{f,r}$). However, the dependence on time is much smaller than the dependence on magnitude, since the duration of flood is not able to significantly affect the damping of bar amplitude as the magnitude of the flood.

A final consideration is devoted to discuss how the instantaneous fully-wet bar amplitude, A_0^*, affects the evolution of bar amplitude during each flood event. Specifically, this contribution is hidden in the residual term of the bivariate regression (μ), which also includes all the "*other effects*" that can influence the evolution of bars, such as the shape of the hydrograph and the number of peaks in the flood event. The larger the residual, the lower the influence of flood magnitude and duration on the evolution of bar amplitude, meaning that the aforementioned other effects can play a significant role. Therefore, in order to

Table 7.4. Coefficients of the bilinear model of eq. (7.12), with reference to the variation of bar amplitude during flood events (i) between final and initial condition (ΔA_{f0}) and (ii) between the initial and the minimum value (ΔA_{0m}). a_0 is the intercept, while a_1 and a_2 are the regression coefficients with respect to flood magnitude ($\widetilde{\Delta Q}_{max}$) and duration ($\widetilde{\Delta T}_f$ or $\widetilde{\Delta T}_{f,r}$) respectively. Finally, R^2 is the coefficient of determination.

		Bivariate analysis			
		a_0	a_1	a_2	R^2
ΔA_{f0}	[–]	−0.0001	−0.0264	0.0110	0.664
$\Delta A_{f0} > 0$	[–]	0.0082	−0.0041	0.0068	0.156
$\Delta A_{f0} < 0$	[–]	−0.0044	−0.0232	0.0052	0.678
ΔA_{0m}	[–]	−0.0133	0.0581	0.0010	0.874

quantify the role of A_0^* we have computed the correlation between the residual obtained for the analysis of the net variation of bar amplitude, ΔA_{f0} and A_0^*/A_{as}^* obtaining the plot reported in Fig. 7.18 for bar forming and bar damping events.

Despite the large scatter, we can still identify a decreasing (increasing) trend of the residual in the case of bar-forming (-damping) floods, which seems to suggest that bar response also depends on the instantaneous value of the fully-wet bar amplitude. Specifically, considering that residuals mainly range between −0.04 to 0.04, we find a major influence of the initial bar amplitude for the bar-forming events, which exhibit a variation of bar amplitude of the same order of magnitude. Furthermore, we note a smaller scattering when $A_0^* \geqslant A_{as}^*$, which is probably due to the fact that the morphological evolution of highest bars can be significantly performed by more intense floods. Consequently, being clear the role of magnitude and duration of large floods to modify the amplitude of bars (see trends of ΔA_{f0} reported in Fig. 7.14), we deduce a minor influence of the initial bar amplitude on the resulting final value of bar amplitude.

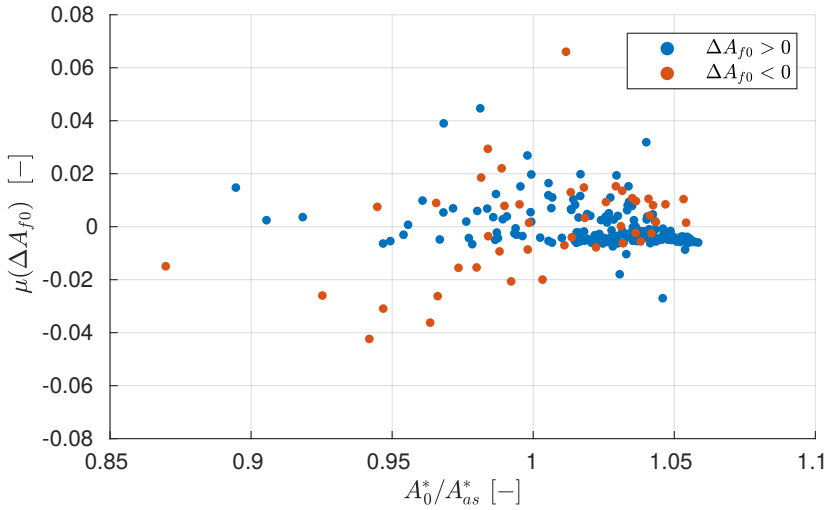

Figure 7.18. Correlation between the residual term of the bivariate analysis for the net variation of bar amplitude (ΔA_{f0}) and the instantaneous fully-wet bar amplitude (A_0^*) scaled with the average state of bar amplitude (A_{as}^*).

7.5.4 *Qualitative classification of floods*

The statistical analysis of the bar amplitude variation due to the characteristics of flood events which occur in the flow series allows for a qualitative classification of floods with respect to the effect that they have on bar amplitude. Indeed, the criterion we propose to identify different flood events on the basis of the emersion conditions, enables to group floods whose characteristics produces the same variation in bar amplitude.

Specifically, we found that the riverbed can be modified by flood events in three different ways depending on the relation between final and initial values of bar amplitude (A_f^* and A_0^* respectively). Specifically, we can distinguish three different types of floods:

- Type I: bar amplitude increases during all the flood event, without assuming smaller values than the initial one (i.e. $A_f^* > A_0^*$ and $A_{min}^* = A_0^*$);

- Type II: bar amplitude increases at the end of the flood event, but during the event it achieves values lower than the initial one (i.e. $A^*_f > A^*_0$ and $A^*_{min} < A^*_0$);
- Type III: the net variation of bar amplitude is negative and the final value achieved at the end of the flood is lower than the initial one (i.e. $A^*_f < A^*_0$).

As example of the different typologies, three flood events and the respective variation of bar amplitude are reported in Fig. 7.19 for the upstream reach of the Alpine Rhine River.

As already mentioned, the capability of a flood event to modify bar amplitude in a riverbed configuration with already-formed bars strongly depends on the initial value of bar amplitude, due to the emersion condition. So, we can suppose that the flood event in panel (a) of Fig. 7.19 would not be able to modify bar amplitude if the initial value was larger than the actual value (e.g. as in panel c). Nevertheless, peculiar characteristics of the three flood types can be identified. Specifically, events of the first type have a moderate magnitude without a clearly identified peak as in typical flood events. Conversely, floods of type II and III exhibit a larger peak, which is able to damp bar amplitude, with an excursion depending on the magnitude of the peak (i.e. the larger the peak, the larger the damping of bar amplitude). Considering the duration of floods, it is clear that the longer the falling limb, the higher the capability of the system to increase the amplitude of bars (floods of type I) or to recover the initial bar amplitude (floods of type II and III).

To extensively analyse the relation of magnitude and duration of flood events with their effect of bar amplitude, we relate magnitude and duration of flood events identifying the three typologies of floods (see Fig. 7.20). We found that floods of type I are characterised by magnitude and duration mainly lower than the average value of the flood peaks (see Tab. 7.2), with few points presenting a longer duration. Floods of type II have a magnitude just larger than the average value but a longer duration with respect to type I. Finally, floods of type III have a larger magnitude and a lower (or, at least equal) duration with respect to type II. The mechanism governing the classification of floods can be summarized as follows:

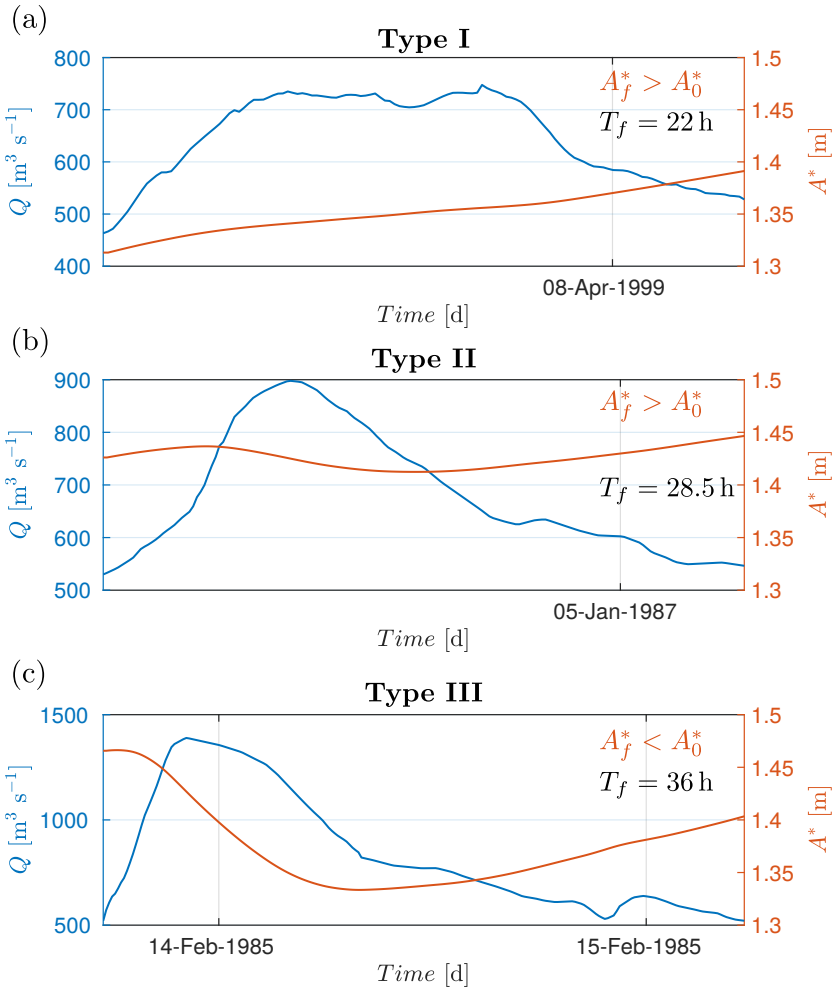

Figure 7.19. Example of different types of flood events depending on their effect on bar evolution for the upstream reach of the Alpine Rhine River. (a) flood event producing an increment of bar amplitude ($A_f^* > A_0^*$), (b) flood event producing a net increment of bar amplitude, but with a negative excursion with respect to the initial value and (c) flood event producing a net decrement of bar amplitude ($A_f^* < A_0^*$).

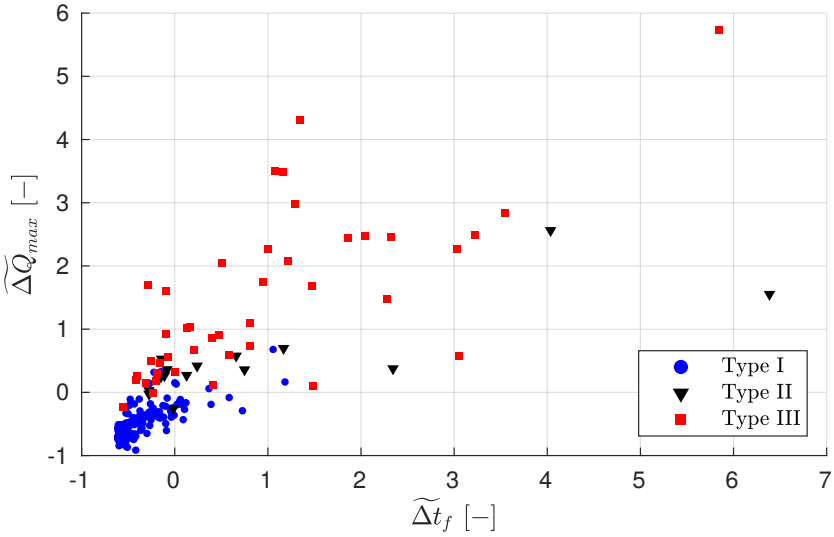

Figure 7.20. Classification of flood events in the plane of predictors $\widetilde{\Delta Q}_{max}$ and $\widetilde{\Delta T}_f$ with respect to the effect they have in bar amplitude evolution. Specifically, floods of type I produce exclusively an increment in bar amplitude, floods of type II produces a net increment, but during the event the amplitude is damped to values lower than the initial one and floods of type III produce a net decrement of bar amplitude.

- Moderate floods are the main driver of bar growth, being the largest values of the events sufficiently low to avoid a marked damping of bar amplitude (type I).
- The higher the peak of the flood, the lower the value of bar amplitude achieved during the flood event. Therefore, if the falling limb of the flood is sufficiently long to allow for the system to recover the initial bar amplitude, the flood is classified as of type II, otherwise it is of type III.
- Floods of type III are too short with respect to their magnitude to allow for an increment of bar amplitude at least equal to the damping.

The number of events (N_f) in each category of floods, their cumulative duration with respect to the total time of activity (T_{df}) and the cumulative variation of bar amplitude scaled with the average state (ΔA_{tot}) are summarized in Tab. 7.5. We note

Table 7.5. Number of flood events (N_f), cumulative duration with respect to the total time of activity (T_{df}) and total variation of bar amplitude (ΔA_{tot}) with respect of the average state for each typology of flood events.

		Type I	Type II	Type III
N_f	[–]	153	15	42
T_{df}	[%]	31.32	18.36	50.20
ΔA_{tot}	[–]	1.24	0.09	−1.35

that ΔA_{tot} caused by all the flood events of the flow sequence is almost zero, meaning that the system oscillates around the regime state in a sort of dynamic equilibrium.

7.6 CONCLUSIONS

The present analysis proposes an innovative application of the Colombini et al. (1987) weakly nonlinear model to predict the evolution of bar amplitude in time under variable flow conditions. With respect to numerical models, the computational time required to simulate how do bar evolve is negligible, since bar properties are assumed to be spatially uniform within the reach. Moreover, being the spatial solution of bar amplitude expressed as a superimposition of Fourier harmonics, the definition of a computational mesh in not necessary. Therefore, the numerical computation is reduced to the numerical integration of eq. (7.1), making fast the analysis of long flow sequences.

From a practical point of view, this model can be effectively used to simulate alterations in the hydrological flow regime, by investigating the variation of bar response due to human interventions or climate changes. We implemented two simplified scenarios simulating (i) the construction of a reservoir and (ii) the alteration of the hydrological cycle due to climate changes. Both scenarios act in modifying the peak of flood events, but the timescale of the alteration is different. Specifically, the lamination scenario reduces all the peaks of the flow series depending of the characteristics of the reservoir, while the climate change

scenarios modulates the variation of discharge with a seasonal recurrence (i.e. reducing flood peaks in summer and increasing flood peaks in winter). We found that hydrological alterations have major effects on systems with a not marked propensity to form alternate bars (e.g. the downstream reach of the Alpine Rhine River), in which a reduction of high floods is able to reduce the cumulative effect of bar damping, by increasing the probability of bar occurrence.

Furthermore, a suitable criterion is proposed to separate flood events in the flow series by considering the portion of hydrograph that allow for bar evolution. Specifically, the fully-wet condition for discriminating when bars are emerged has been considered following the approach of Redolfi et al. (2020). Such criterion allows us to identify more than 200 flood events in the flow series of the upstream reach of the Alpine Rhine River, obtaining a statistically significant sample to investigate how flood characteristics are responsible for bar amplitude evolution. We found that magnitude and duration of flood events play a clear role in increasing or damping the amplitude of bars. Specifically, moderate floods are responsible to bar formation, while higher floods provide a damping of bar amplitude, which is as lower as longer the duration. Such result is consistent with field observations of Welford (1994) and Eekhout et al. (2013).

Finally, we provide a qualitative classification of flood events depending on their net effect on bar amplitude. Specifically, moderate floods are mainly responsible to increase bar amplitude, which never decays below the initial value (floods of type I). Conversely, larger floods are able to damp bar amplitude during the different stages of the event, but they can provide a final value of bar amplitude larger (flood of type II) or lower than the initial one (flood of type III).

8

CONCLUSIONS

In the present PhD thesis we investigate the response of alternate bars to complex flow regime, with particular focus on the formative conditions that define the average bar amplitude of a river reach. By means of a theoretical analysis combined with experimental evidences, we observe that the response of bars to discharge variations presents peculiarities with respect to other morphological properties of a river, such as the average channel width or slope. Indeed, while such properties evolve at a timescale governed by the sediment transport (i.e. getting faster by increasing the discharge), alternate bars have a proper timescale of evolution governed by their growth rate. As a consequence, the classical approaches implemented to determine the dominant conditions and the average properties of a river reach are not suitable for the case of alternate bars. To overcome this limitation we propose a theoretically-based approach to predict whether bars are expected to form and which average value of bar amplitude they achieve. Our model provides a good interpretation of four study cases with different morphological responses in terms of alternate bars.

The purpose of this final chapter is to summarize the main results of the present work, providing a qualitative answer to the initial research questions.

In **Chapter 3** we investigate the equilibrium response of alternate bars to discharge variations by means of the Colombini et al. (1987) theory. To describe the response of a river reach, with constant geometrical characteristics (channel width and slope) and sediment size, we consider new appropriate dimensionless parameters in which the flow characteristics are isolated by the geometrical ones.

Starting from the Colombini et al. (1987) model, bar behaviour is found to be characterised by three distinctive discharge thresholds that allow us to provide a physical-based interpretation

of theoretical results. Specifically, in addition to the threshold for sediment motion, which is common to all morphological processes, the response of alternate bars is related to the critical aspect ratio for bar formation and to the condition of bar emersion.

As for the critical condition, being bar formation a threshold process governed by the channel aspect ratio β, the discharge value for which β equals the critical value β_{cr} defines the *critical threshold* for bars, representing an upper discharge value for which bars are expected to form. Such condition results from the opposite trends of β and β_{cr} with respect to the discharge: assuming a rectangular cross section, the former is a decreasing function and the latter an increasing one, crossing at the critical discharge value. As a consequence, since the bar height is proportional to the difference between β and β_{cr}, we find a decreasing trend with respect to flow discharge, until bar height vanishes at the critical condition.

From a mathematical point of view, the weakly nonlinear model of Colombini et al. (1987) is defined in the neighborhood of β_{cr}, which makes the theoretical prediction of bar amplitude no longer valid when the channel is far from such condition (i.e. $\beta \gg \beta_{cr}$). This leads the model to predict a bar height tending to infinity when flow discharge approaches the *threshold for sediment motion*. Furthermore, when the discharge is smaller than the so-called *fully-wet threshold* the predicted equilibrium elevation of the top of bars exceeds the water surface elevation, which makes the theoretical prediction no longer meaningful. Such physical condition of bar emersion poses a lower limit in the validity of the Colombini et al. (1987) weakly nonlinear model, since the model is defined for a simply connected domain, wherein the channel bed is fully submerged.

Moreover, the critical condition discriminates discharges that work to build bars from discharges that suppress them. Indeed, the linear growth rate of bars (i.e. valid for the firsts stages of bar evolution) is negative for discharges larger than the critical threshold, indicating the capacity of such discharge stages to dampen the initial bar amplitude. The recognition that the morphodynamical work acted on river bars by relatively low-flow stages can be reversed by high-flow stages represents the key

novelty of our approach in defining the formative conditions of alternate bars.

In **Chapter 4** we apply the analysis performed in Chapter 3 to a set of laboratory experiments conducted in a flume with constant geometrical characteristics and uniform grain size distribution, at different discharge conditions. Specifically, we provide a theoretical prediction of experimental observations by means of the Colombini et al. (1987) model, investigating the response of bar height, bar shape and bar migration rate to discharge variations.

The theory well reproduces the decreasing trend of bar height observed by the experiments, providing a quantitative and qualitative agreement for all the different metrics of bar height tested in the analysis. The fully-wet threshold is able to capture the condition of bar emersion occurring in the experiments conducted at low flows and the validity of the Colombini et al. (1987) theory is extended to discharge values lower than the fully-wet threshold by limiting the amplitude of bars to the emersion condition (i.e. by limiting the amplitude of bars to the value for which the minimum water depth is zero). In spite of its approximate derivation, the fully-wet limited bar amplitude seems to be able to capture the response of alternate bars for low flows. At the highest discharge values, we find that the transition between alternate bars and flat bed is not sharp, due to the occurrence of diagonal bars. Despite their clear alternate pattern, such kind of bedforms differ from alternate bars to the extent that they are shorter and display a faster migration rate.

The shape of bars is qualitatively reproduced by the theory, both considering the riverbed asymmetry and the amplitude of each component of the Fourier spectrum. In general, the bed topography predicted by the theory is more regular than the measured one, due to the fact that the weakly nonlinear approach cannot represent the highly nonlinear processes, mainly occurring at low discharges. Nevertheless, the predominant alternate pattern is captured by the model, being the first harmonic (i.e. a double sinusoidal bed deformation) larger than the second one for all discharge values. As for the second harmonic, the overall trend is captured by the theory, despite a bell-shape distortion

of the riverbed is preferred by actual bars with respect to the regular, periodic central bar pattern, predicted by the theory.

In **Chapter 5** the long-term effect of duration and sequencing of floods is investigated for a test case by applying the weakly nonlinear model of Tubino (1991), with the purpose of identifying which hydrological parameters mainly affect the response of alternate bars. We force the system with simplified flow sequences built (i) by interposing triangular floods or (ii) by means of the stochastic CPP process. Simulations are repeated modifying the duration of flood events and computing the average bar amplitude, the variation of bar amplitude with respect to the average state and the time required to achieve the equilibrium configuration for each duration. Indeed, as proposed by Tubino (1991) theory, the evolution of bar amplitude under unsteady flow conditions is possible only if the timescale of the floods and the timescale of bar amplitude have the same order of magnitude.

We find that the average state becomes independent of duration and sequencing of floods for sufficiently "short" events, making the probability density function the essential hydrological information to synthesize the flow regime. Conversely, for "long" events, the variation of bar amplitude has the same order of magnitude of the average state, while the system response depends also on the sequence of flood events. Therefore, the average bar amplitude does not describe the actual behaviour of the river reach.

Furthermore, the the analysis provides a quantification of a suitable timescale to characterise the flow regime. Indeed, Tubino (1991) investigated the evolution of bar amplitude due to a single flood event, whose timescale is related to its duration, while here we consider different sequences of flood events with different magnitude and duration. We observe that the integral scale of the flow series can be a good metric to take into account the duration and sequencing of flood events.

In **Chapter 6** we propose an innovative approach to quantify the long-term average bar amplitude in a river reach by taking into account the complexity of the flow regime. Moreover, we define a *"bar-forming"* discharge as the single discharge value able

to reproduce the same morphology of the actual flow sequence if applied steadily.

The model is inspired by the "effective discharge" method proposed by Wolman and Miller (1960) (in which the average characteristics of the channel are determined by the analysis of magnitude and frequency of flow events in terms of sediment transport), but implements all the peculiarities previously described that affect bar behaviour. The procedure includes two steps: the first is devoted to determining whether bars are expected to form, the second to determine their average amplitude if the first step is positively verified. Specifically, we compute the effectiveness of flood events by considering the evolutionary time of bars, which is the inverse of the linear bar growth rate, taking into account that discharge values can play an opposite role in bar evolution, depending on their position with respect to the critical threshold. Indeed, discharge stages lower than the critical threshold allow for bar formation, while the larger ones allow for bar suppression. The amplitude of bars is obtained by considering the nonlinear bar growth rate, which depends on the actual bar amplitude in the channel.

The model is applied to four study cases, with different morphological characteristics. Specifically, we focus on two reaches of the Alpine Rhine River, located upstream and downstream the confluence with the Ill River, which display a different morphological response, since the regular alternate bar pattern of the upstream reach disappear downstream the confluence (see Fig. 6.3a). The bar-forming discharge method is able to capture such different response, by predicting high-relief bars in the upstream reach and low-relief bars in the downstream one. Furthermore, the model is able to reproduce the two study cases of the Isère River and Adige River, which can be considered limit cases of the upstream and downstream reaches of the Alpine Rhine River respectively. Indeed, the former displays a stable sequence of alternate bars that can be hardly modified by the actual flow regime, while the latter presents an almost flat bed configuration.

In **Chapter 7** we adapt the Colombini et al. (1987) theory, originally defined to predict the amplitude of bars under steady flow conditions, to model the evolution of bar amplitude in

time due to a complex flow regime. In spite of its approximate formulation, such innovative application of the model allows us for modelling bar evolution due to long flow series with an almost negligible computational time.

We apply the model to the aforementioned study cases, simulating the evolution of bar amplitude for almost 30 years of hydrological records, obtaining results consistent with the bar-forming discharge method. Indeed, we find that bars evolve during flood events in the Alpine Rhine River, with different responses for the upstream and downstream reaches. Specifically, in the former bar amplitude slightly oscillates around the regime configuration, while in the latter the riverbed alternates periods with and without bars. Furthermore, no evolution of the riverbed is predicted for the Adige River, while, very low oscillation of bar amplitude around the regime state are simulated for the Isère River.

The ability of the model to simulate the evolution of bar amplitude for long flow series allows us to easily implement scenarios of hydrological alteration, e.g., due to flow lamination or climate changes. Specifically, we simulate two different scenarios: the first provides a reduction of flood peaks by means of the construction of a reservoir, the second modifies the hydrological sequence by reducing the discharge in summer (i.e. when the largest floods mainly occurs in snow-melting systems) and by increasing the discharge in winter. With reference to the same study cases, we observe that hydrological alterations have a significant impact (i) for those reaches where the effects of bar-forming and bar-suppressing events almost balance, namely the probability to form bars is similar to the probability of having flat bed, and (ii) if the hydrological alteration acts at a sufficiently long timescale, as the seasonal variation of the discharge in the climate change scenario. Indeed, a modification in bar response is found only for the downstream reach of the Alpine Rhine River, for which the climate change scenario would increase the tendency to form bars.

Finally, the possibility of modelling bar evolution for long flow series, allows for a statistical analysis of the effects that flood magnitude and duration have on bar amplitude. Considering the upstream reach of the Alpine Rhine River, we identify more than

200 flood events able to modify the amplitude of bars. Consistently with results of Tubino (1991), Welford (1994) and Eekhout et al. (2013), the growth of bars mainly occurs during the falling limb of the flood event. We find that moderate floods mainly produce an increase of bar amplitude, while larger floods are responsible for bar damping. Furthermore, the longer the flood duration, the higher the time required to recover the average state at the end of the event. Depending on their effect on modifying bar amplitude, we also provide a qualitative classification of flood events, identifying three types of floods. Specifically, floods of type I and II are bar-formative events, since they provide a net increasing of bar amplitude, while flood of type III are bar-suppressing events. Bar-formative events are mainly characterised by moderate peaks and sufficiently long duration to allow for bar growth. Conversely, bar-suppressing events are characterised by high peaks and duration too short to allow for the recovery of the initial bar amplitude.

9

ACKNOWLEDGMENTS

CHAPTER 4

This research has been supported by the Autonomous Province of Bozen-Bolzano (project no. 42, GLORI - Glaciers-to-Rivers Sediment Transfer in Alpine Basins), the Italian Ministry of Education, University and Research (MIUR) in the framework of the "Departments of Excellence" (grant no. L. 232/2016), and the "Agenzia Provinciale per le Risorse Idriche e l'Energia" (APRIE) of the Province of Trento (Italy).

We thank Chris Paola and Eric Prokocki for the stimulating comments and Marco Colombini for the interesting discussion.

CHAPTER 5

This work has been supported by the Italian Ministry of Education, University and Research (MIUR) in the frame of the "Departments of Excellence" Grant L. 232/2016. A MATLAB code for the computation of critical conditions (see Redolfi et al., 2019) is available at `https://bitbucket.org/Marco_Redolfi/bars_res-crit`.

CHAPTER 6

This research has been supported by the Italian Ministry of Education, University and Research (MIUR) in the framework of the "Departments of Excellence" (grant no. L. 232/2016). The MATLAB code for computing probability of bar formation, average bar height and bar-forming discharge depending on channel geometry, grain size and flow probability distribution, as well as data of the four study reaches, are made available at `https://doi.org/10.5281/zenodo.4277627`.

The paper has benefited from the insightful comments by Alessandra Crosato and two anonymous referees.

Appendices

A

STATISTICAL INTERPRETATION OF THE EFFECTIVE DISCHARGE METHOD

This chapter is based on the Supplementary Material of the paper: Carlin, M., M. Redolfi, and M. Tubino (2021), The long-term response of alternate bars to the hydrological regime, Water Resources Research, 57, e2020WR029314, https://doi.org/10.1029/2020WR029314.

In this section, we analyse the statistical meaning by the classic method of the effective discharge (Wolman and Miller, 1960). The method is based on the definition of the discharge value that gives the highest contribution to the transport of sediments. This contribution depends on the product between the sediment rating curve, which defines the capacity of each discharge to transport sediments, and the probability density function of the flow, which defines the frequency of occurrence of each discharge.

The meaning the product between the flow rating curve and the probability density function can be explained more precisely by following a probabilistic approach.

First, we need to assume that the flow rating curve $Q_s^*(Q)$ is a deterministic function that does not explicitly depend on time. Second, we divide the range of discharge in equally-spaced classes of width ΔQ and central value Q_c. For each discharge class, we can quantify the volume of sediment transported in a given reference period T_R^* (e.g., one year) as:

$$\Delta V_s = Q_s^*(Q_c)\,\Delta t^*, \tag{A.1}$$

where Δt^* indicates the time the flow stays in the flow interval ΔQ during the reference period.

In natural flow conditions, the value of Δt^* is clearly non constant, and it can be represented as a random variable whose probability distribution is different for each discharge class. However, for our purpose we do not need to know the distribution of Δt^* but only its expected value, namely:

$$E[\Delta V_s] = E[Q_s^*(Q_c)\,\Delta t^*] = Q_s^*(Q_c)\,E[\Delta t^*], \tag{A.2}$$

where the expected value of Δt^* can be computed by integrating the probability density function of the flow events f_Q:

$$E[\Delta t^*] = T_R^* \int_{\Delta Q} f_Q \, dQ = f_{Q_c} \, \Delta Q \, T_R^*, \tag{A.3}$$

where f_{Q_c} indicates the average probability density within the interval ΔQ.

By substituting eq. (A.3) into eq. (A.2) we find:

$$E[\Delta V_s] = Q_s^*(Q_c) \, f_{Q_c} \, \Delta Q \, T_R^*, \tag{A.4}$$

which, when divided by the constant values ΔQ and T_R^*, provides a definition of the product $Q_s^*(Q_c) \, f_Q$:

$$E\left[\frac{\Delta V_s}{\Delta Q \, T_R^*}\right] = Q_s^*(Q_c) \, f_{Q_c}. \tag{A.5}$$

Therefore, the product between the flow duration curve and the sediment transport rate for each discharge class can be interpreted as the expected value of the sediment volume normalized by the class width and the reference period. Taking the limit for $\Delta Q \to 0$, eq. (A.5) provides a continuous definition:

$$E\left[\frac{dV_s}{dQ} \, \frac{1}{T_R^*}\right] = Q_s^*(Q) \, f_Q. \tag{A.6}$$

The effective discharge, defined as the maximum point of the product $Q_s^*(Q) \, f(Q)$, can be interpreted as the discharge value that is expected to give the maximum contribution to the sediment transport in the reference (e.g., annual) period.

B

STEADY FLOW: COMPARISON OF COLOMBINI ET AL. (1987) AND TUBINO (1991) MODELS

B.1 INTRODUCTION

The morphological evolution of bar amplitude was found to be well predicted by Colombini et al. (1987) (CST) and Tubino (1991) (T91) weakly nonlinear models for steady and unsteady flow conditions respectively. The former provides a solution of the SWE system of equations by means of a perturbation approach for given geometrical characteristics of the channel and water discharge. The latter implement the flow unsteadiness by linearizing a flood event around a reference discharge value, for which the weakly nonlinear model of CST is solved; the parameters are then linearized to other discharge values.

Both models are strictly defined in the neighborhood of the critical threshold due to their weakly nonlinear derivation, which limits their validity to a sub-range of discharges between the threshold for sediment motion, Q_i, and the critical threshold for bars, Q_{cr}.

In Sections 3 and 4 we extensively discussed the CST model, by providing the widening of the validity range by means of the fully-wet limitation on bar amplitude. In this chapter we want to investigate the quasi-steady response of T91's model by comparing results with CST predictions. Specifically, we consider the range $Q_i - Q_{cr}$ and compare the linearized results of T91 with the weakly nonlinear prediction of CST.

B.2 METHOD

Let us consider as test case a straight rectangular channel with geometrical characteristics of width, W, and slope S equal to the reach upstream of the Alpine Rhine River. We assume the Engelund and Fredsoe (1982) friction formula to solve the uniform flow and we estimate the sediment rating curve by means of

Parker (1978) transport formula, assuming a relative submerged weight of sediment $R = 1.65$. Finally, sediment porosity p has been assumed 0.4 and the measure of the the effect of gravity on transverse transport has been accounted for by setting the empirical parameter r equal to 0.6. We compare the following quantities, extensively described in Chapter 2.

- *Channel aspect ratio*. The two models consider the following definition of β:

$$\beta = \frac{W}{2D_0^*}, \qquad \beta = \overline{\beta}\left[1 - \overline{\epsilon} D_{01}\right], \tag{B.1a,b}$$

  where over-lined variables are referred to the reference condition, $\overline{Q}$, and D_{01} is a parameter defined as function of the discharge in eq. (2.47).

- *Bar height*. The height of bars considered in the following is computed as H_{BM}, namely as the difference between maximum and minimum of bed topography, η. We compute η (eq. 2.34) by considering the equilibrium bar amplitude proposed by the models, meaning:

$$A_{eq} = \sqrt{-\frac{\alpha_{1R}}{\alpha_{2R}}}, \qquad A_T = \overline{A}_{eq}[1 - F\, q_{01}]^{\frac{1}{2}}, \tag{B.2a,b}$$

  for CST and T91 respectively, in which $\overline{A}_{eq}$ is the CST equilibrium bar amplitude at the reference condition, q_{01} is determined by means of eq. (2.61) and F is the parameter defined in eq. (2.58).

- *Bar migration rate*. The migration rate of bars was computed by dividing the nonlinear angular frequency, proposed in eqs. (2.40) and (2.63) for CST and T91 respectively, by the critical wavenumber λ_{cr}.

- *Linear bar growth rate*. The linear bar growth rate was defined in the two models as:

$$\Omega_0 = \epsilon \alpha_{1R}, \qquad \Omega_0 = \overline{\Omega}_0 + \overline{\epsilon}\, \overline{\alpha}_0 q_{01}, \tag{B.3a,b}$$

  for CST and T91 respectively.

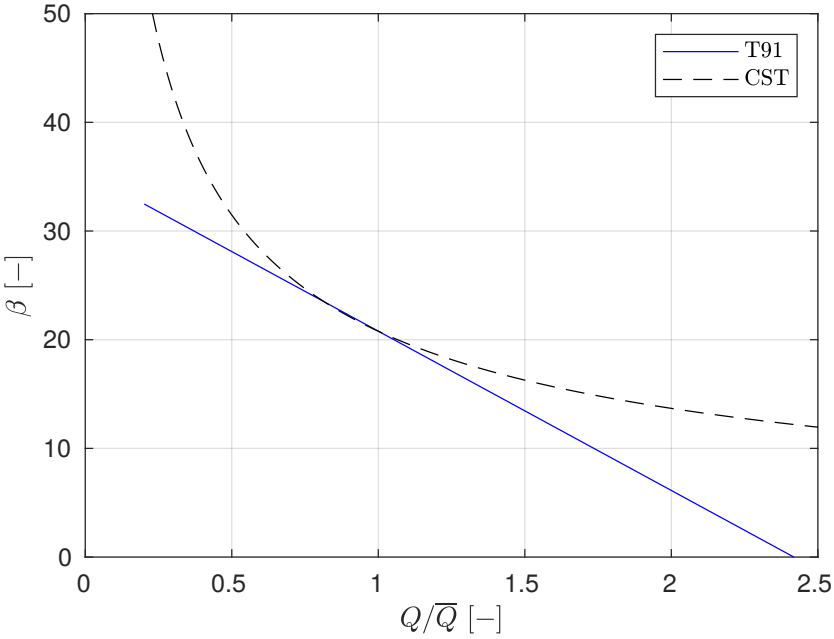

Figure B.1. Comparison of the channel aspect ratio, β, for the two models of Colombini et al. (1987) (CST) and Tubino (1991) (T91) for varying discharge values. The linearized result of T91 is largely lower for discharge values larger or lower than the reference discharge.

B.3 RESULTS AND DISCUSSION

In this section we provide results of the present analysis by scaling the quantities with the reference value of the T91 model.

The channel aspect ratio is the main parameter governing the behaviour of alternate bars being responsible of their formation and providing a measure of their amplitude if compared with the critical value β_{cr}.

Fig. B.1 shows the trend of the aspect ratio with respect to the discharge deriving from the models of CST and T91. The linearized model of T91 reproduces the decreasing trend described in Chapter 3, but largely underestimates the nonlinear response of low discharge values ($Q < \overline{Q}$). Similarly, when the discharge is larger than the reference state, the linear trend has a faster decrease, providing stability conditions for lower discharge values than CST.

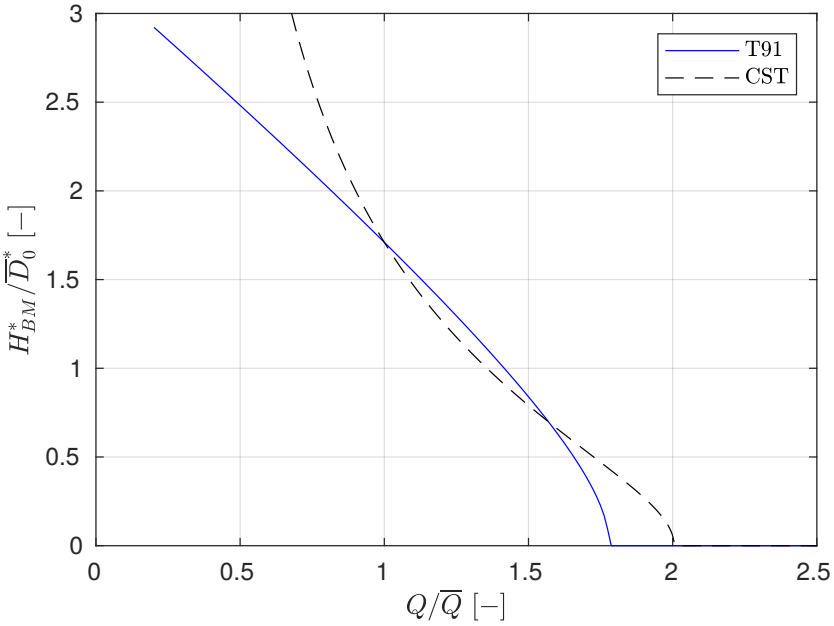

Figure B.2. Comparison of the bar height, H^*_{BM}, for the two models of Colombini et al. (1987) (CST) and Tubino (1991) (T91) for varying discharge values. The decreasing trend is well reproduced by the linearized model, providing a lower value of the critical threshold for bar formation.

These considerations allows us to better interpret the results of bar height shown in Fig. B.2. The linearized model of T91 well reproduces the decreasing trend of bar height, both qualitatively and quantitatively, providing an intrinsic limitation of the excessive increasing of bar height for low discharge value predicted by CST. Moreover, as we can expect by the trend of β, T91 provides a lower value of the critical threshold than CST.

Fig. B.3 shows that the migration rate of alternate with respect to the discharge is very similar for both the two models, being the response of CST almost linear in Q (see Fig. 3.9). Also in this case the nonlinearity related to discharge values near the threshold for motion is mitigated by considering fixed the value of bar amplitude (computed at the reference state).

Finally, for the linear growth rate of bars we observe the first important difference in the two models. In Fig. B.4, where curves are scaled with the hydrodynamic timescale referred to the

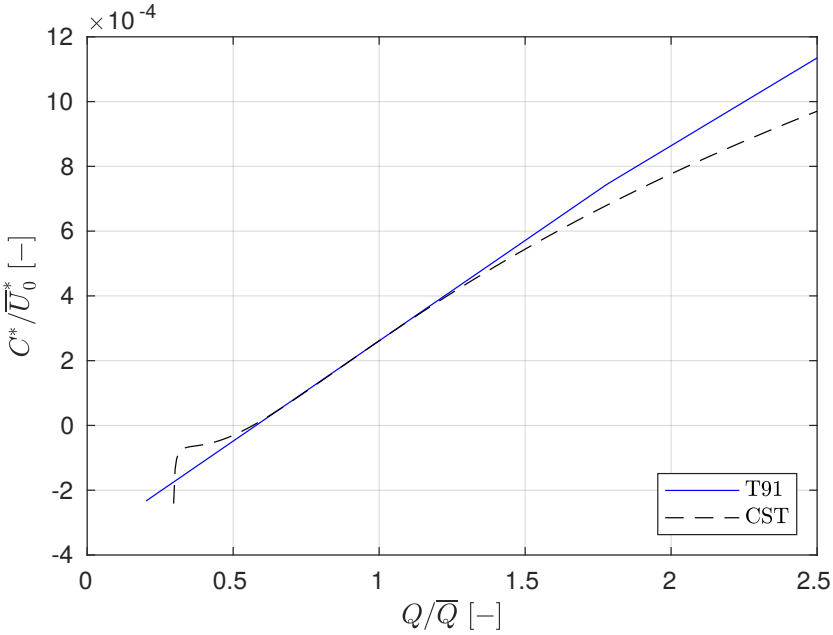

Figure B.3. Comparison of the bar migration rate, C^*, for the two models of Colombini et al. (1987) (CST) and Tubino (1991) (T91) for varying discharge values. The curve obtained by the CST model is almost linear in terms of water discharge and the linearized model of T91 well capture the trend.

reference conditions, $W/(2\,\overline{u}_0^*)$, we observe that the prediction of linear growth rate by CST is a curve with a maximum, similarly to the curves of Fig. 3.7. However, the linearized model of T91 is able to qualitatively reproduce only the decreasing limb of the CST curve, determining a large overestimation of the growth rate for low discharge values. Considering that actual flow series in rivers are characterised for the most of time by low flows, we can assume that the response of the T91 model to actual flow series largely promotes the formation and growth of bars.

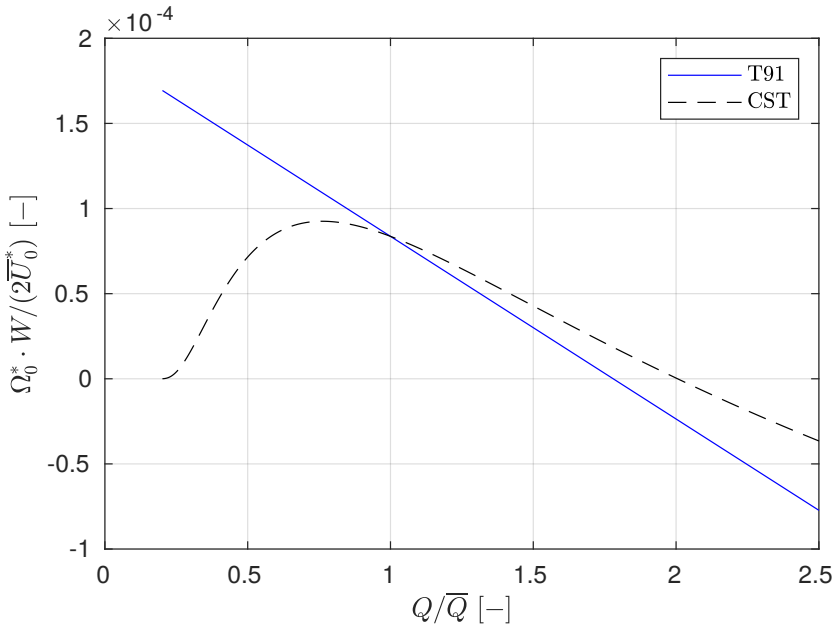

Figure B.4. Comparison of the bar growth rate, Ω_0^*, for the two models of Colombini et al. (1987) (CST) and Tubino (1991) (T91) for varying discharge values. The linear model is not able to capture the maximum trend, providing a large overestimation of bar growth for low discharge values.

BIBLIOGRAPHY

L. Adami. *Multi-decadal morphodynamics of alternate bars in channelized rivers: a multiple perspective*. PhD thesis, University of Trento, Italy, 2016.

L. Adami, W. Bertoldi, and G. Zolezzi. Multidecadal dynamics of alternate bars in the Alpine Rhine River. *Water Resources Research*, 52:8938–8955, 2016. doi:10.1002/2015WR018228.

E. D. Andrews. Effective and bankfull discharges of streams in the Yampa River basin, Colorado and Wyoming. *Journal of Hydrology*, 46:311–330, 1980. doi:10.1016/0022-1694(80)90084-0.

L. Arkesteijn, A. Blom, M. J. Czapiga, V. Chavarrías, and R. J. Labeur. The quasi-equilibrium longitudinal profile in backwater reaches of the engineered alluvial river: A space-marching method. *Journal of Geophysical Research: Earth Surface*, 124(11): 2542–2560, 2019. doi:10.1029/2019JF005195.

P. E. Ashmore and T. J. Day. Effective discharge for suspended sediment transport in streams of the Saskatchewan River Basin. *Water Resources Research*, 24(6):864–870, 1988. doi:10.1029/WR024i006p00864.

V. R. Baker. Stream-channel response to floods, with examples from central Texas. *Bulletin of the Geological Society of America*, 88(8):1057–1071, 1977.

J. J. Barry, J. M. Buffington, . P. Goodwin, M. Asce, J. G. King, and W. W. Emmett. Performance of Bed-Load Transport Equations Relative to Geomorphic Significance: Predicting Effective Discharge and Its Transport Rate. *Journal of Hydraulic Engineering*, 134(5):601–615, 2008. doi:10.1061/ASCE0733-94292008134:5601.

M. A. Benson and D. M. Thomas. A definition of dominant discharge. *International Association of Scientific Hydrology. Bulletin*, 11(2):76–80, 1966. doi:10.1080/02626666609493460.

M. B. Bertagni and C. Camporeale. Finite amplitude of free alternate bars with suspended load. *Water Resources Research*, 54(12):9759–9773, 2018. doi:10.1029/2018WR022819.

M. B. Bertagni, P. Perona, and C. Camporeale. Parametric transitions between bare and vegetated states in water-driven patterns. *Proceedings of the National Academy of Sciences*, 115(32): 8125–8130, 2018. doi:10.1073/pnas.1721765115.

W. Bertoldi, A. M. Gurnell, and N. A. Drake. The topographic signature of vegetation development along a braided river: Results of a combined analysis of airborne lidar, color air photographs, and ground measurements. *Water Resources Research*, 47(6):W06525, 2011. doi:10.1029/2010WR010319.

D. S. Biedenharn and C. R. Thorne. Magnitude-frequency analysis of sediment transport in the lower Mississippi river. *Regulated Rivers: Research & Management*, 9(4):237–251, 1994. doi:10.1002/rrr.3450090405.

A. Blom, E. Viparelli, and V. Chavarrías. The graded alluvial river: Profile concavity and downstream fining. *Geophysical Research Letters*, 43(12):6285–6293, 2016. doi:10.1002/2016GL068898.

A. Blom, L. Arkesteijn, V. Chavarrías, and E. Viparelli. The equilibrium alluvial river under variable flow and its channel-forming discharge. *Journal of Geophysical Research: Earth Surface*, 122(10):1924–1948, 2017. doi:10.1002/2017JF004213.

P. Blondeaux and G. Seminara. A unified bar–bend theory of river meanders. *Journal of Fluid Mechanics*, 157:449–470, 1985. doi:10.1017/S0022112085002440.

G. Botter, S. Basso, I. Rodriguez-Iturbe, and A. Rinaldo. Resilience of river flow regimes. *Proceedings of the National Academy of Sciences of the United States of America*, 110(32):12925–12930, 2013. doi:10.1073/pnas.1311920110.

M. C. Bowers, W. W. Tung, and J. B. Gao. On the distributions of seasonal river flows: Lognormal or power law? *Water Resources Research*, 48(5):W05536, 2012. doi:10.1029/2011WR011308.

A. C. Brayshaw. Bed microtopography and entrainment thresholds in gravel-bed rivers. *Geological Society of America Bulletin*, 96(2):218–223, 1985.

M. I. Brunner, D. Farinotti, H. Zekollari, M. Huss, and M. Zappa. Future shifts in extreme flow regimes in Alpine regions. *Hydrology and Earth System Science*, 23(11):12–19, 2019. doi:10.5194/hess-23-4471-2019.

S. E. Bunn and A. H. Arthington. Basic principles and ecological consequences of altered flow regimes for aquatic biodiversity. *Environmental Management*, 30(4):492–507, 2002. doi:10.1007/s00267-002-2737-0.

K. Bunte, S. R. Abt, K. W. Swingle, and D. A. Cenderelli. Effective discharge in rocky mountain headwater streams. *Journal of Hydrology*, 519:2136–2147, 2014.

R. A. Callander. Instability and river channels. *Journal of Fluid Mechanics*, 36(3):465–480, 1969. doi:10.1017/S0022112069001765.

M. Carlin, M. Redolfi, and M. Tubino. Effect of flow unsteadiness on the long-term evolution of alternate bars. In CRC Press, editor, *Proceedings of River Flow 2020*, pages 539–547, 2020. doi:10.1201/b22619-76.

M. Carlin, M. Redolfi, and M. Tubino. The long-term response of alternate bars to the hydrological regime. *Water Resources Research*, 57:e2020WR029314, 2021. doi:10.1029/2020WR029314.

P. Carling. The concept of dominant discharge applied to two gravel-bed streams in relation to channel stability thresholds. *Earth Surface Processes and Landforms*, 13(4):355–367, 1988. doi:10.1002/esp.3290130407.

A. Castellarin, G. Galeati, L. Brandimarte, A. Montanari, and A. Brath. Regional flow-duration curves: Reliability for ungauged basins. *Advances in Water Resources*, 27(10):953–965, 2004. doi:10.1016/j.advwatres.2004.08.005.

M. Church and R. I. Ferguson. Morphodynamics: Rivers beyond steady state. *Water Resources Research*, 51(4):1883–1897, 2015. doi:10.1002/2014WR016862.

M. Colombini and A. Stocchino. Three-dimensional river bed forms. *Journal of Fluid Mechanics*, 695:63–80, 2012. doi:10.1017/jfm.2011.556.

M. Colombini and M. Tubino. Finite amplitude free-bars: a fully nonlinear spectral solution. *Euromech*, 262:163–169, 1991.

M. Colombini, G. Seminara, and M. Tubino. Finite-amplitude alternate bars. *Journal of Fluid Mechanics*, 181:213–232, 1987. doi:10.1017/S0022112087002064.

R. Copeland, P. Soar, and C. Thorne. Channel-forming discharge and hydraulic geometry width predictors in meandering sand-bed rivers. In ASCE, editor, *Proceedings of the World Water and Environmental Resources Congress: Impacts of Global Change*, pages 1–12, Reston, Va., 2005. doi:10.1061/40792(173)568.

A. Crosato and E. Mosselman. Simple physics-based predictor for the number of river bars and the transition between meandering and braiding. *Water Resources Research*, 45(3):W03423, 2009. doi:10.1029/2008WR007242.

A. Crosato, F. B. Desta, J. Cornelisse, F. Schuurman, and W. S. J. Uijttewaal. Experimental and numerical findings on the long-term evolution of migrating alternate bars in alluvial channels. *Water Resources Research*, 48(6):W06524, 2012. doi:10.1029/2011WR011320.

D. W. Crowder and H. V. Knapp. Effective discharge recurrence intervals of Illinois streams. *Geomorphology*, 64(3-4):167–184, 2005. doi:10.1016/j.geomorph.2004.06.006.

A. Defina. Numerical experiments on bar growth. *Water Resources Research*, 39(4):1092, 2003. doi:10.1029/2002WR001455.

M. Diaz-Redondo, G. Egger, M. Marchamalo, S. Hohensinner, and E. Dister. Benchmarking Fluvial Dynamics for Process-Based River Restoration: the Upper Rhine River (1816–2014). *River Research and Applications*, 33(3):403–414, 2017. doi:10.1002/rra.3077.

P. W. Downs, P. J. Soar, and A. Taylor. The anatomy of effective discharge: The dynamics of coarse sediment transport revealed

using continuous bedload monitoring in a gravel-bed river during a very wet year. *Earth Surface Processes and Landforms*, 41(2):147–161, 2016. doi:10.1002/esp.3785.

M. W. Doyle, D. Shields, K. F. Boyd, P. B. Skidmore, and D. Dominick. Channel-Forming Discharge Selection in River Restoration Design. *Journal of Hydraulic Engineering*, 133(7):831–837, 2007. doi:10.1061/(ASCE)0733-9429(2007)133:7(831).

M. Dynesius and C. Nilsson. Regulation of river systems in the northern third of the world. *Science*, 266(5186):753–762, 1994. doi:10.1126/science.266.5186.753.

J. P. Eekhout, A. J. Hoitink, and E. Mosselman. Field experiment on alternate bar development in a straight sand-bed stream. *Water Resources Research*, 49(12):8357–8369, 2013. doi:10.1002/2013WR014259.

H. A. Einstein. The bed-load function for sediment transportation in open channel flows. Technical Bulletin 1026, U.S. Department of Agriculture, Washington, D. C, 1950.

W. W. Emmett and M. G. Wolman. Effective discharge and gravel-bed rivers. *Earth Surface Processes and Landforms*, 26(13): 1369–1380, 2001. doi:10.1002/esp.303.

F. Engelund. The motion of sediment particles on an inclined bed. *Tech. Univ. Denmark ISVA, Prog. No. 53*, pages 15–20, 1981.

F. Engelund and J. Fredsoe. Sediment Ripples and Dunes. *Annual Review of Fluid Mechanics*, 14:13–37, 1982. doi:10.1146/annurev.fl.14.010182.000305.

F. Engelund and E. Hansens. A monograph on sediment transport in alluvial streams. Technical report, Technical University of Denmark, Ostervoldgade 10, Copenhagen K., 1967.

B. Federici and G. Seminara. Effect of suspended load oil sandbar instability. *Water Resources Research*, 42(7):W07407, 2006. doi:10.1029/2005WR004399.

V. Ferro and P. Porto. Identifying a dominant discharge for natural rivers in southern italy. *Geomorphology*, 139-140:313–321, 2012. doi:10.1016/j.geomorph.2011.10.035.

A. Frascati and S. Lanzoni. Morphodynamic regime and long-term evolution of meandering rivers. *Journal of Geophysical Research: Earth Surface*, 114(F2):F02002, 2009. doi:10.1029/2008JF001101.

J. Fredsoe. Meandering and Braiding of Rivers. *Journal of Fluid Mechanics*, 84(4):609–624, 1978. doi:10.1017/S0022112078000373.

Y. Fujita and Y. Muramoto. Experimental study on stream channel processes in alluvial rivers. *Bulletin of the Disaster Prevention Research Institute*, 32:49–96, 1982.

Y. Fujita and Y. Muramoto. Studies on the Process of Development of Alternate Bars. *Bulletin of the Disaster Prevention Research Institute*, 35(3):55–86, 1985.

D. J. Furbish. Irregular bed forms in steep, rough channels. *Water Resources Research*, 34(12):3635–3648, 1998.

M. Garcia and Y. Niño. Dynamics of sediment bars in straight and meandering channels: experiments on the resonance phenomenon. *Journal of Hydraulic Research*, 31(6):739–761, 1993.

G. A. Garcia Lugo, W. Bertoldi, A. J. Henshaw, and A. M. Gurnell. The effect of lateral confinement on gravel bed river morphology. *Water Resources Research*, 51:7145–7158, 2015. doi:10.1111/j.1752-1688.1969.tb04897.x.

D. Gilvear and N. Willby. Channel dynamics and geomorphic variability as controls on gravel bar vegetation; River Tummel, Scotland. *River Research and Applications*, 22(4):457–474, 2006. doi:10.1002/rra.917.

D. Gilvear, R. Francis, N. Willby, and A. Gurnell. 26 Gravel bars: a key habitat of gravel-bed rivers for vegetation. *Developments in Earth Surface Processes*, 11(07):677–700, 2007. doi:10.1016/S0928-2025(07)11154-8.

P. Goodwin. Analytical Solutions for Estimating Effective Discharge. *Journal of Hydraulic Engineering*, 130(8):729–738, aug 2004. doi:10.1061/(ASCE)0733-9429(2004)130:8(729).

P. Hall. Alternating bar instabilities in unsteady channel flows over erodible beds. *Journal of Fluid Mechanics*, 499:49–73, 2004. doi:10.1017/S0022112003006219.

T. B. Hoey and A. J. Sutherland. Channel morphology and bedload pulses in braided rivers: a laboratory study. *Earth Surface Processes and Landforms*, 16(5):447–462, 1991.

S. Hohensinner, G. Egger, G. Haidvogl, M. Jungwirth, S. Muhar, and S. Schmutz. Hydrological connectivity of a Danube river-floodplain system in the Austrian Machland: changes between 1812 and 1991. In Lavoisier SAS, editor, *Proceedings of the International Conference "European Floodplains 2002"*, pages 53–69, Strasbourg (France), 2007.

S. Ikeda. Lateral bed load transport on side slopes. *Journal of the Hydraulics Division*, 108(11):1369–1373, 1982.

S. Ikeda. Prediction of Alternate Bar Wavelength and Height. *Journal of Hydraulic Engineering*, 110(4):371–386, 1984. doi:10.1061/(ASCE)0733-9429(1984)110:4(371).

C. C. Inglis. *The behaviour and control of rivers and canals (with the aid of models)*. Yeravda Prison Press, Poona, India, Poona, 1949.

M. Jaballah, B. Camenen, L. Pénard, and A. Paquier. Alternate bar development in an alpine river following engineering works. *Advances in Water Resources*, 81:103–113, 2015. doi:10.1016/j.advwatres.2015.03.003.

M. N. R. Jaeggi. Formation and Effects of Alternate Bars. *Journal of Hydraulic Engineering*, 110(2):142–156, 1984. doi:10.1061/(ASCE)0733-9429(1984)110:2(142).

M. Jäggi. *Alternierende kiesbanke (Alternate bars)*. PhD thesis, Swiss Federal Institute of Technology Zurich, Diss. ETH, 1983.

J. P. Johnson. Gravel threshold of motion: A state function of sediment transport disequilibrium? *Earth Surface Dynamics*, 4 (3):685–703, 2016. doi:10.5194/esurf-4-685-2016.

C. Jourdain, N. Claude, P. Tassi, F. Cordier, and G. Antoine. Morphodynamics of alternate bars in the presence of riparian

vegetation. *Earth Surface Processes and Landforms*, 45(5):1100–1122, 2020. doi:10.1002/esp.4776.

R. Kinoshita. Investigation of channel deformation in Ishikari River. *Report of Bureau of Resourcess, Dept. Science and Technology, Japan*, 174, 1961.

M. A. Knaapen, S. J. Hulscher, H. J. De Vriend, and A. Van Harten. Height and wavelength of alternate bars in rivers: Modelling vs. laboratory experiments. *Journal of Hydraulic Research*, 39(2): 147–153, 2001. doi:10.1080/00221680109499815.

S. Lanzoni. Experiments on bar formation in a straight flume 2. Graded sediment. *Water Resources Research*, 36(11):3351–3363, 2000a. doi:10.1029/2000WR900161.

S. Lanzoni. Experiments on bar formation in a straight flume: 1. Uniform sediment. *Water Resources Research*, 36(11):3337–3349, 2000b. doi:10.1029/2000WR900160.

S. Lanzoni and G. Seminara. On the nature of meander instability. *Journal of Geophysical Research: Earth Surface*, 111(F4):F04006, 2006. doi:10.1029/2005JF000416.

S. Lanzoni and M. Tubino. Grain sorting and bar instability. *Journal of Fluid Mechanics*, 393:149–174, 1999. doi:10.1017/S0022112099005583.

L. B. Leopold and M. G. Wolman. *River channel patterns: braided, meandering, and straight*. US Government Printing Office, 1957.

F. Lièbault, S. Lallias-Tacon, M. Cassel, and N. Talaska. Long profile responses of alpine braided rivers in se france. *River Research and Applications*, 29:1253–1266, 2013. doi:10.1002/rra.

P. E. Lisenby, J. Croke, and K. A. Fryirs. Geomorphic effectiveness: a linear concept in a non-linear world. *Earth Surface Processes and Landforms*, 43(1):4–20, 2018. doi:10.1002/esp.4096.

M. Mähr, D. Schenk, M. Schatzmann, and A. Meng. Alpine rhine project (section river Ill-lake constance). In *Proceedings of the International Conference on Fluvial Hydraulics, River Flow 2014*, pages 39–47, 2014.

V. Martínez-Fernández, M. Van Oorschot, J. De Smit, M. González del Tánago, and A. D. Buijse. Modelling feedbacks between geomorphological and riparian vegetation responses under climate change in a Mediterranean context. *Earth Surface Processes and Landforms*, 43(9):1825–1835, 2018. doi:10.1002/esp.4356.

E. Meyer-Peter and R. Muller. Formulas for bed-Load Transport. In *IAHSR 2nd meeting*, Stockholm, 1948. IAHR.

H. Middelkoop, K. Daamen, D. Gellens, W. Grabs, J. C. Kwadijk, H. Lang, B. W. Parmet, B. Schädler, J. Schulla, and K. Wilke. Impact of climate change on hydrological regimes and water resources management in the Rhine basin. *Climatic Change*, 49: 105–128, 2001. doi:10.1023/A:1010784727448.

N. Mittal, A. G. Bhave, A. Mishra, and R. Singh. Impact of human intervention and climate change on natural flow regime. *Water Resources Management*, 30:685–699, 2016. doi:10.1007/s11269-015-1185-6.

F. Molle. River-basin planning and management: The social life of a concept. *Geoforum*, 40(3):484–494, 2009. doi:10.1016/j.geoforum.2009.03.004.

F. Monegaglia, M. Tubino, and G. Zolezzi. Interaction between curvature-driven width oscillations and channel curvature in evolving meander bends. *Journal of Fluid Mechanics*, 876: 985–1017, 2019. doi:10.1017/jfm.2019.574.

E. Mosselman, M. Tubino, and G. Zolezzi. The overdeepening theory in river morphodynamics: two decades of shifting interpetations. In R. Ferreira, E. Alves, J. Leal, and A. Cardoso, editors, *Proceedings River Flow 2006*, pages 1175–1181, Lisbon, Portugal, 2006. Taylor & Francis.

D. B. Nash. Effective Sediment-Transporting Discharge from Magnitude-Frequency Analysis. *The Journal of Geology*, 102(1): 79–95, 1994.

J. M. Nelson. The initial instability and finite-amplitude stability of alternate bars in straight channels. *Earth Science Reviews*, 29 (1-4):97–115, 1990. doi:10.1016/0012-8252(0)90030-Y.

P. A. Nelson and J. A. Morgan. Flume experiments on flow and sediment supply controls on gravel bedform dynamics. *Geomorphology*, 323:98–105, 2018.

P. A. Nelson and G. Seminara. A theoretical framework for the morphodynamics of bedrock channels. *Geophysical Research Letters*, 39(6):1–5, 2012. doi:10.1029/2011GL050806.

P. A. Nelson, M. Bolla Pittaluga, and G. Seminara. Finite amplitude bars in mixed bedrock-alluvial channels. *Journal of Geophysical Research: Earth Surface*, 119(3):566–587, 2014. doi:10.1002/2013JF002957.

C. Nilsson, C. A. Reidy, M. Dynesius, and C. Revenga. Fragmentation and flow regulation of the world's large river systems. *Science*, 308(5720):405–408, 2005. doi:10.1126/science.1107887.

K. W. Olesen. Alternate bars in and meandering of alluvial rivers. Communication on Hydraulic, Report 83-1, Delft University of Technology, 1983.

G. Parker. On the cause and characteristic scales of meandering and braiding in rivers. *Journal of Fluid Mechanics*, 76(3):457–480, 1976. ISSN 0022-1120. doi:10.1017/S0022112076000748.

G. Parker. Self-formed rivers with equilibrium banks and mobile bed. Part 2. The gravel river. *Journal of Fluid Mechanics*, 89(1): 127–146, 1978.

G. Parker. Surface-based bedload transport relation for gravel rivers. *Journal of Hydraulic Research*, 28(4):417–436, 1990. doi:10.1080/00221689009499058.

G. Parker, P. R. Wilcock, C. Paola, W. E. Dietrich, and J. Pitlick. Physical basis for quasi-universal relations describing bankfull hydraulic geometry of single-thread gravel bed rivers. *Journal of Geophysical Research: Earth Surface*, 112(F4):F04005, 2007. doi:10.1029/2006JF000549.

G. Pickup and R. F. Warner. Effects of hydrologic regime on magnitude and frequency of dominant discharge. *Journal of Hydrology*, 29(1-2):51–75, 1976. doi:10.1016/0022-1694(76)90005-6.

N. L. Poff and J. K. Zimmerman. Ecological responses to altered flow regimes: A literature review to inform the science and management of environmental flows. *Freshwater Biology*, 55(1): 194–205, 2010. doi:10.1111/j.1365-2427.2009.02272.x.

A. Prins. Dominant discharge. Technical Report S 78-III, Waterloopkundig Laboratorium Delft, Netherlands, 1969.

H. Qian, Z. Cao, H. Liu, and G. Pender. Numerical modelling of alternate bar formation, development and sediment sorting in straight channels. *Earth Surface Processes and Landforms*, 42(4): 555–574, 2017.

M. Redolfi, G. Zolezzi, and M. Tubino. Free and forced morphodynamics of river bifurcations. *Earth Surface Processes and Landforms*, 44(4):973–987, 2019. doi:10.1002/esp.4561.

M. Redolfi, M. Welber, M. Carlin, M. Tubino, and W. Bertoldi. Morphometric properties of alternate bars and water discharge: a laboratory investigation. *Earth Surface Dynamics*, 8(3):789–808, sep 2020. doi:10.5194/esurf-8-789-2020.

S. Rodrigues, E. Mosselman, N. Claude, C. L. Wintenberger, and P. Juge. Alternate bars in a sandy gravel bed river: Generation, migration and interactions with superimposed dunes. *Earth Surface Processes and Landforms*, 40(5):610–628, 2015. doi:10.1002/esp.3657.

R. Schielen, A. Doelman, and H. E. De Swart. On the Nonlinear Dynamics of Free Bars in Straight Channels. *Journal of Fluid Mechanics*, 252:325–356, 1993. doi:10.1017/S0022112093003787.

V. Scorpio, S. Zen, W. Bertoldi, N. Surian, M. Mastronunzio, E. Dai Prá, G. Zolezzi, and F. Comiti. Channelization of a large Alpine river: what is left of its original morphodynamics? *Earth Surface Processes and Landforms*, 43(5):1044–1062, 2018. doi:10.1002/esp.4303.

M. J. Selby. Dominant geomorphic events in landform evolution. *Bulletin of the International Association of Engineering Geology-Bulletin de l'Association Internationale de Géologie de l'Ingénieur*, 9 (1):85–89, 1974.

G. Seminara. Fluvial sedimentary patterns. *Annual Review of Fluid Mechanics*, 42:43–66, 2010. doi:10.1146/annurev-fluid-121108-145612.

G. Seminara and M. Tubino. Alternate Bars and Meandering: Free, Forced and Mixed Interactions. In S. Ikeda and G. Parker, editors, *River Meandering*, chapter 10, pages 267–320. American Geophysical Union (AGU), Washington, D.C., 1989. doi:10.1029/WM012p0267.

G. Seminara, G. Zolezzi, M. Tubino, and D. Zardi. Downstream and upstream influence in river meandering. part 2. planimetric development. *Journal of Fluid Mechanics*, 438:213–230, 2001. doi:10.1017/S0022112001004281.

A. J. Serlet, A. M. Gurnell, G. Zolezzi, G. Wharton, P. Belleudy, and C. Jourdain. Biomorphodynamics of alternate bars in a channelized, regulated river: An integrated historical and modelling analysis. *Earth Surface Processes and Landforms*, 43(9): 1739–1756, 2018. doi:10.1002/esp.4349.

J. S. Sholtes and B. P. Bledsoe. Half-yield discharge: Process-based predictor of bankfull discharge. *Journal of Hydraulic Engineering*, 142(8):04016017, 2016.

A. Siviglia, G. Stecca, D. Vanzo, G. Zolezzi, E. F. Toro, and M. Tubino. Numerical modelling of two-dimensional morphodynamics with applications to river bars and bifurcations. *Advances in Water Resources*, 52:243–260, 2013. doi:10.1016/j.advwatres.2012.11.010.

P. J. Soar and C. R. Thorne. Channel restoration design for meandering rivers. Technical report, Engineer Research and Development Center, Coastal and Hydraulic Lab., Vicksburg, MS, 2001.

N. Struiksma, K. W. Olesen, C. Flokstra, and H. J. De Vriend. Bed deformation in curved alluvial channels. *Journal of Hydraulic Research*, 23(1):57–79, 1985.

N. Sukegawa. Study on meandering of streams in straight channels. *Report of Bureau of Resourcess, Dept. Science and Technology, Japan*, pages 335–363, 1971.

N. Surian, L. Mao, M. Giacomin, and L. Ziliani. Morphological effects of different channel-forming discharges in a gravel-bed river. *Earth Surface Processes and Landforms*, 34(8):1093–1107, 2009. doi:10.1002/esp.1798.

A. H. te Linde, P. Bubeck, J. E. C. Dekkers, H. de Moel, and J. C. J. H. Aerts. Future flood risk estimates along the river Rhine. *Natural Hazards and Earth System Sciences Future*, 11:459–473, 2011. doi:10.5194/nhess-11-459-2011.

M. Tubino. Growth of alternate bars in unsteady flow. *Water Resources Research*, 27(1):37–52, 1991. doi:10.1029/90WR01699.

M. Tubino and G. Seminara. Free–forced interactions in developing meanders and suppression of free bars. *Journal of Fluid Mechanics*, 214:131–159, 1990.

M. Tubino, R. Repetto, and G. Zolezzi. Free bars in rivers. *Journal of Hydraulic Research*, 37(6):759–775, 1999. doi:10.1080/00221689909498510.

D. Vanzo, G. Zolezzi, and A. Siviglia. Eco-hydraulic modelling of the interactions between hydropeaking and river morphology. *Ecohydrology*, 9(3):421–437, 2016. doi:10.1002/eco.1647.

F. Vautier. *Dynamique geomorphologique et végétalisation des cours d'eau endigues: l'exemple de l'Isère dans le Grésivaudan*. PhD thesis, Université Joseph Fourier, Grenoble, 2000.

J. G. Venditti, P. A. Nelson, J. T. Minear, J. Wooster, and W. E. Dietrich. Alternate bar response to sediment supply termination. *Journal of Geophysical Research: Earth Surface*, 117(2):1–18, 2012. doi:10.1029/2011JF002254.

A. Vianello and V. D'Agostino. Bankfull width and morphological units in an alpine stream of the dolomites (Northern Italy). *Geomorphology*, 83(3-4):266–281, 2007. doi:10.1016/j.geomorph.2006.02.023.

G. Vignoli and M. Tubino. Le condizioni di emersione di macro forme di fondo in alvei in ghiaia. In *Atti 29° Convegno Nazionale di Idraulica e Costruzioni Idrauliche*, pages 563–570, Trento, 2004. Editoriale Bios.

R. M. Vogel, J. R. Stedinger, and R. P. Hooper. Discharge indices for water quality loads. *Water Resources Research*, 39(10):1273, 2003.

M. R. Welford. A field test of tubino's (1991) model of alternate bar formation. *Earth Surface Processes and Landforms*, 19(4): 287–297, jun 1994. doi:10.1002/esp.3290190402.

P. R. Wilcock and B. T. DeTemple. Persistence of armor layers in gravel-bed streams. *Geophysical Research Letters*, 32(8):L08402, 2005. doi:10.1029/2004GL021772.

G. P. Williams. Bank-full discharge of rivers. *Water Resources Research*, 14(6):1141–1154, 1978. doi:10.1029/WR014i006p01141.

G. M. Wolman and J. P. Miller. Magnitude and frequency of forces in geomorphic processes. *The Journal of Geology*, 68(1): 54–74, 1960.

M. Wong and G. Parker. Reanalysis and Correction of Bed-Load Relation of Meyer-Peter and Müller Using Their Own Database. *Journal of Hydraulic Engineering*, 132(11):1159–1168, 2006. doi:10.1061/(ASCE)0733-9429(2006)132:11(1159).

Y. Yang, Z. Yang, X. an Yin, and Q. Liu. A framework for assessing flow regime alterations resulting from the effects of climate change and human disturbance. *Hydrological Sciences Journal*, 63(3):441–456, 2018. doi:10.1080/02626667.2018.1430897.

D. A. Zema, G. Bombino, P. Denisi, M. E. Lucas-Borja, and S. M. Zimbone. Evaluating the effects of check dams on channel geometry, bed sediment size and riparian vegetation in mediterranean mountain torrents. *Science of the Total Environment*, 642: 327–340, 2018. doi:10.1016/j.scitotenv.2018.06.035.

Q. Zeng, L. Shi, L. Wen, J. Chen, H. Duo, and G. Lei. Gravel bars can be critical for biodiversity conservation: A case study on Scaly-sided Merganser in South China. *PLoS ONE*, 10(5):1–13, 2015. doi:10.1371/journal.pone.0127387.

G. Zolezzi and G. Seminara. Downstream and upstream influence in river meandering. Part 1. General theory and application

overdeepening. *Journal of Fluid Mechanics*, 438(13):183–211, 2001. doi:10.1017/S002211200100427X.

G. Zolezzi, M. Guala, D. Termini, and G. Seminara. Experimental observations of upstream overdeepening. *Journal of Fluid Mechanics*, 531:191–219, 2005. doi:10.1017/S0022112005003927.

G. Zolezzi, R. Luchi, and M. Tubino. Morphodynamic regime of gravel bed, single-thread meandering rivers. *Journal of Geophysical Research: Earth Surface*, 114(F1):F01005, 2009. doi:10.1029/2007JF000968.